HSP90-stabilized proteins as therapeutic targets in cancer

Dissertation

for the award of the degree

"Doctor rerum naturalium"

of the Georg-August-University Göttingen

within the doctoral program Molecular Medicine

of the Georg-August University School of Science (GAUSS)

submitted by

Luisa Klemke

from Hessisch Lichtenau, Germany

Göttingen 2021

Thesis Committee

PD Dr. Ramona Schulz-Heddergott, Institute of Molecular Oncology, University Medical Center Göttingen (UMG)

Prof. Dr. Holger Reichardt, Institute for Cellular and Molecular Immunology, University Medical Center Göttingen (UMG)

Prof. Dr. Argyris Papantonis, Institute of Pathology, University Medical Center Göttingen (UMG)

Members of the Examination Board

1st Referee: PD Dr. Ramona Schulz-Heddergott, Institute of Molecular Oncology, University Medical Center Göttingen (UMG)

2nd Referee: Prof. Dr. Holger Reichardt, Institute for Cellular and Molecular Immunology, University Medical Center Göttingen (UMG)

Further members of the Examination Board

Prof. Dr. Argyris Papantonis, Institute of Pathology, University Medical Center Göttingen (UMG)

Prof. Dr. Heidi Hahn, Institute of Human Genetics, University Medical Center Göttingen (UMG)

Dr. Shiv Singh, Department of Gastroenterology, Gastrointestinal Oncology, and Endocrinology, University Medical Center Göttingen (UMG)

Dr. Nico Posnien, Department of Developmental Biology, Georg-August-University Göttingen

Date of oral examination: 8th June 2021

This thesis is dedicated to my family.

TABLE OF CONTENTS

LIST OF FIGURES

ABBREVIATIONS

°C	degree celsius
17AAG (Tanespimycin)	17-(allylamino)geldanamycin
ADP	adenosine diphosphate
AHA1	activator of 90 kDa heat shock protein ATPase homolog 1
AKT	RAC-alpha serine/threonine-protein kinase
AMPK	5'-AMP-activated protein kinase catalytic subunit alpha-1
AOM	azoxymethane
AP1	activating protein 1
APC	adenomatosis polyposis coli
ATP	adenosine triphosphate
BAX	BCL2 associated X protein
CCL2	C-C motif chemokine ligand 2
CCL5	C-C motif chemokine ligand 5
CCND1	cyclin D1
CD3	cluster of Differentiation 3
CD31	cluster of Differentiation 31
CD44	cluster of Differentiation 44
CD68	cluster of Differentiation 68
CD74	cluster of Differentiation 74
CDC37	cell division cycle 37
CDKN1A	cyclin dependent kinase inhibitor 1A
CDKN2A	cyclin dependent kinase inhibitor 2A
CHIP	c-terminus of Hsc70-interacting protein
CHX	cycloheximide
cJUN	AP1 transcription factor subunit
Co-IP	co-immunoprecipitation
con	control
CRC	colorectal cancer
cre	cyclization recombinase

CRISPR/Cas9	Clustered regularly interspaced palindromic repeats/CRISPR-associated protein 9
CTNNB1	catenin beta-1
CXCR2	C-X-C motif chemokine receptor 2
CXCR4	C-X-C motif chemokine receptor 4
CXCR7	C-X-C motif chemokine receptor 7
DAPI	4′,6-diamidino-2-phenylindole
DBD	DNA binding domain
DMSO	dimethylsulfoxide
DNA	deoxyribonucleic acid
DSS	dextran sodium sulfate
ERK	extracellular regulated MAP kinase
ERT2	estrogen receptor 2
FDA	Food and Drug Administration
Fig	figure
fl	floxed allele
GADD45A	growth arrest and DNA damage inducible 45 alpha
Ganet	Ganetespib
GC	glucocorticoid
GOF	gain-of-function
H2AX	histone variant 2A.X
HER2	human epidermal growth factor receptor 2
HHSEC	human hepatic sinusoidal endothelial cells
HIF1α	hypoxia inducible factor 1 subunit alpha
HOP	HSP70/HSP90 organizing protein
hrs	hours
HSC70	heat shock cognate 71 kDa protein
HSE	heat shock element
HSF1	heat shock factor 1
HSP40	heat shock protein 40
HSP70	heat shock protein 70
HSP90	heat shock protein 90
HSR	heat shock response

HUVEC	human umbilical vein endothelial cells
IBD	inflammatory bowel disease
IL-6	interleukin 6
IL-8 (CXCL8/Kc)	Interleukin-8
JAB1	JUN-activation domain-binding protein 1
JAK2	janus kinase 2
kDa	kilodalton
Ki67 (MKI67)	marker of proliferation Ki-67
KIP1/p27 (CDKN1B)	cyclin dependent kinase inhibitor 2A
KRAS	kirsten rat sarcoma viral oncogene homolog
LOF	loss-of-function
LOH	loss-of-heterozygosity
MAPK	mitogen-activated protein kinase
MDM2	mouse double minute 2 homolog
MIF	macrophage migration inhibitory factor
MKP1	mitogen-activated protein kinase phosphatase 1
mL	milliliter
MPO	myeloperoxidase
mRNA	messenger RNA
mutp53	mutant p53
ng	nanogramm
nM	nanomolar
NOS2	nitric oxide synthase 2
NOXA/PMAIP1	phorbol-12-myristate-13-acetate-induced protein 1
NP-40	Nonidet® P 40
ns	not significant
Onales	Onalespib
OSM	oncostatin M
oxMIF	oxidized MIF
p38 MAPK	p38 mitogen-activated protein kinase
PDAC	pancreatic ductal adenocarcinoma
PGE2	prostaglandin E2
PI3K	phosphoinositide 3 kinase

PLA2	phospholipase A2
pSTAT3	phosphorylated signal transducer and activator of transcription 3
PTGS2/COX2	prostaglandin-endoperoxide synthase 2/ cyclooxygenase 2
PUMA	p53 upregulated modulator of apoptosis
R	pearson correlation coefficient
Rad21	double-strand-break repair protein rad21 homolog
rhMIF	recombinant human MIF
RNA	ribonucleic acid
scr	scrambled siRNA
SDS	sodium dodecyl sulphate
SHP2	src homology 2 (SH2) domain-containing phosphatase 2
siRNA	small interfering RNA
SMAD4	mothers against decapentaplegic homologue 4
SRC	non-receptor tyrosine kinase
TAM	tamoxifen
TF	transcription factor
TNFa	tumor necrosis factor alpha
TP53	tumor protein 53
TP63	tumor protein 63
TP73	tumor protein 73
Tris	trisamine
VEGF	vascular endothelial growth factor
wks	weeks
WT	wildtype
µg	microgram
µl	microliter
µm	micrometer
µM	micromolar

1 ABSTRACT

Although cancer is among the most common causes of death worldwide, successful treatment options for most cancer entities remain elusive, raising the need for novel therapies. One attractive target of current drug candidates is the stress-inducible heat shock protein 90 (HSP90) chaperone machinery. Its normal chaperoning function is subverted in tumors to protect numerous mutated and overexpressed proteins from misfolding and degradation. Hence, it is playing a central role in oncogenic signaling. The addiction of cancer cells to the HSP90 chaperone machinery provides opportunities for targeting the stability of HSP90-dependent oncoproteins (clients).

To dissect the importance of the HSP90 chaperone machinery in tumor progression, we investigated two HSP90-stabilized proteins: the macrophage migration inhibitory factor (MIF) in colorectal cancer (CRC) and mutant p53 (mutp53) in pancreatic ductal adenocarcinoma (PDAC). Both proteins were shown to be elevated in cancer cells *via* the HSP90 chaperone machinery, correlating with worse prognosis for cancer patients.

MIF is a pro-inflammatory cytokine which is known to promote tumor progression in various cancer entities. Indeed, we demonstrate that loss of HSP90-stabilized MIF in CRC results in reduced tumor growth. This effect was accompanied by decreased macrophage recruitment and angiogenesis in established CRC tumors. Our data suggest that MIF acts *via* the CD74/MAPK axis and is indeed a cancer-relevant HSP90 client in CRC.

The tumor suppressor p53 (p53) is mutated in approximately 50% of all human cancers. We found that the mutp53^{R248W} variant is highly stabilized by the HSP90 chaperone machinery in pancreatic ductal adenocarcinoma (PDAC) cells. Furthermore, we identified a unique gain-of-function role of this p53^{R248W} mutant on cell migration. Mechanistically, mutp53^{R248W} specifically interacts with the phosphorylated transcription factor STAT3 and thus contributes to the aggressiveness of pancreatic cancer.

Our results further corroborate HSP90 as an attractive target to counteract tumor development, and we identified two HSP90 clients as cancer drivers, outlining additional target structures for cancer therapy.

2 INTRODUCTION

Cancer is one of the leading causes of death in the world, with rising incidence every year [1, 2]. It is considered a 'disease of change', marked by broad genetic and phenotypic heterogeneity and plasticity [3]. Remarkable efforts and advances have been made trying to understand the complexity of this disease. However, clinical trials for cancer therapies are the least successful compared to major other diseases [4, 5]. To address this issue, researchers from all over the world are focusing on targeted therapy and personalized oncology in order to develop tailor-made and specialized treatments for cancer patients [3, 5]. In this respect, it is particularly important to identify cancer-relevant biomarkers to increase the success rates of clinical trials [4, 5]. Several driver mutations have been identified to be essential for tumor initiation, providing a selection advantage for mutated cells [6-8]. However, throughout tumor development, cancer cells acquire genetic and epigenetic mutations as well as molecular alterations [9, 10]. Together with environmental factors such as nutrient/oxygen starvation and oxidative stress, these mutations and alterations induce different stress responses in cancer cells [11-15]. One of these responses is the heat shock response (HSR), leading to the induction of stress proteins such as heat shock protein 90 (HSP90) [14-16]. By assisting in the stabilization and activation of many proteins (termed clients), in particular oncogenes, HSP90 constitutes a suitable target for cancer therapy [16, 17]. Given the plethora of stabilized oncogenes, HSP90 inhibitors provide a possibility to overcome resistance mechanisms of cancer cells towards conventional chemotherapy [18-21].

2.1 HSP90 CHAPERONE MACHINERY

2.1.1 HSP90 chaperone machinery in normal cells

Heat shock proteins (HSPs) are a highly conserved ubiquitous family [16, 22-24]. Since their first discovery in 1962 [25], these proteins have been extensively studied and classified according to their molecular weights [26, 27]. Through assisting in the regulation of turnover, cellular localization and trafficking as well as activity of various proteins, HSPs can regulate growth, survival and differentiation of cells [16, 23, 28-30].

One of the most abundant stress proteins is the molecular chaperone HSP90 [24, 31, 32]. For HSP90, two major cytoplasmic isoforms have been identified: the inducible HSP90α isoform and the constitutive HSP90β isoform [24, 33]. HSP90 predominantly exists as homodimer of either isoform; however, monomers and heterodimers have also been reported [24, 33, 34]. Both isoforms consist of a C-terminal domain as well as a middle and N-terminal domain which are connected *via* a charged linker [23, 33]. The C-terminal domain is necessary for the interaction of two HSP90 monomers in order to form a functional dimer [35-37]. In contrast, the N-terminal domain is required for binding and hydrolysis of ATP molecules [35]. Importantly, assembly with other co-chaperones is necessary to form the full functional HSP90 chaperone machinery [29, 38]. An ATP-dependent chaperone cycle contains various steps of temporary and dynamic protein interactions, posttranslational modifications and conformational changes [23, 38] (**Figure 1**). In this manner, HSP90 can affect structure and functionality of its client proteins [38, 39]. For proper maturation, the chaperones HSP40 and HSP70 are the first to bind to the nascent polypeptide chain, forming the *early complex* [23, 39, 40]. HSP70 of the *early complex* can bind to HSP90 *via* the adaptor protein HOP (HSP70/HSP90 organizing protein), allowing the client to be transferred to HSP90 (*intermediate complex*) [23, 39-43]. If a polypeptide chain cannot be formed properly, the presence of co-chaperones such as the E3 ubiquitin-protein ligase CHIP (C-terminus of Hsc70-interacting protein) target the client peptide for proteasomal degradation [43, 44]. In contrast, proper maturation of clients are achieved by binding of ATP to HSP90, resulting in a transition into a 'closed and twisted' conformation, which is characterized by the interaction of the middle and N-terminal domains [45]. At this stage, binding of the other co-chaperones triggers the dislocation of HOP, HSP70 and HSP40 to form the *late complex* [29, 39]. After hydrolysis of ATP, the mature protein is released. Dissociation of ADP reinstates the initial open conformation of HSP90, thus allowing binding of new clients [38, 39].
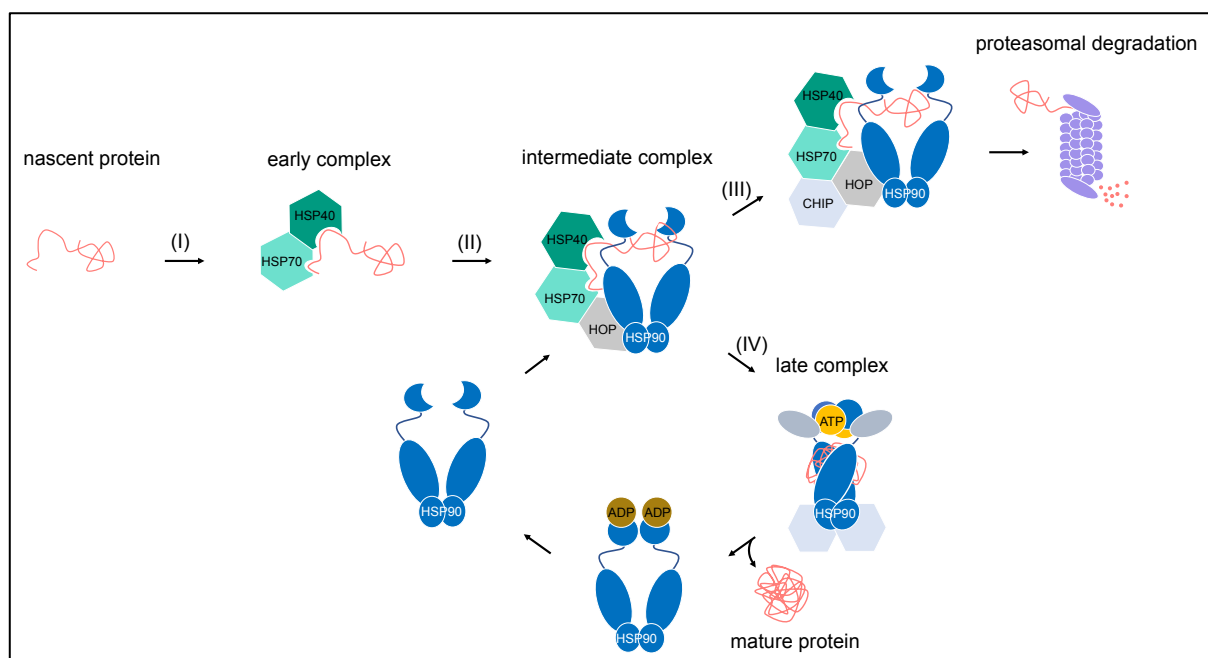
Figure 1: ATPase cycle of the HSP90 chaperone machinery. (I) Nascent polypeptide chains are being captured by HSP90 co-chaperones HSP70, HSP40 to form the *early complex*. (II) Binding of HSP70 to HSP90 *via* HOP allows translocation of the nascent polypeptide chain from the *early complex* to the HSP90 chaperone (*intermediate complex*). (III) Binding of the co-chaperone CHIP or other E3 ubiquitin protein ligases mark nascent proteins for proteasomal degradation. (IV) In contrast, binding of ATP to the N-terminal domain of HSP90, results in its transition into the 'closed and twisted' conformation, which is characterized by interaction of its middle and N-terminal domains. Other co-chaperones displace HSP70/HSP40 and HOP and assist in stabilizing the conformation of the *late complex*. After hydrolysis of ATP, the mature protein is released, and dissociation of ADP reverts HSP90 into its initial open conformation.

To this date, the mechanism behind how HPS90 recognizes its client proteins remains elusive, since no common patterns have been discovered thus far [23]. In the past decades, more than 20 co-chaperones have been identified, exhibiting different molecular functions [23, 39]. Additionally, a variety of post-translational modifications of HSP90 such as acetylation, phosphorylation and nitrosylation are known to regulate the activity of the protein and modulate its specificity to other co-chaperones or clients [17, 23, 46]. Therefore, the exact composition of co-chaperones and the dynamics of the ATPase cycle highly depend on the molecular context, the presence of post-translational modifications and the client to be processed [23, 45, 47, 48].

Among the main transcriptional regulators of HSPs are the members of the heat shock factor (HSF) family [49]. In vertebrates, the most important regulator of HSPs is the heat shock factor 1 (HSF1) [49, 50]. Under physiological conditions, inactive

monomeric HSF1 is bound to HSP90 [51-54]. However, cellular stress can trigger the accumulation of unfolded proteins which activates HSP90 [23, 51]. Unfolded proteins are captured by HSP70 and HSP40, for further translocation of the unfolded protein to HSP90 [42, 51]. The unfolded or misfolded proteins are further processed as described more detailed in **section 2.1.1** to form a mature protein. This process leads to the displacement of HSF1 from HSP90, allowing the formation of an active trimeric HSF1 complex [49, 53] (**Figure 2**). The trimeric HSF1 molecule translocates to the nucleus to act as a transcription factor [49, 51]. It binds to heat shock elements (HSE), a promotor region upstream of the HSP genes to initiate the expression of heat shock proteins such as HSP90 and HSP70 [49, 50].
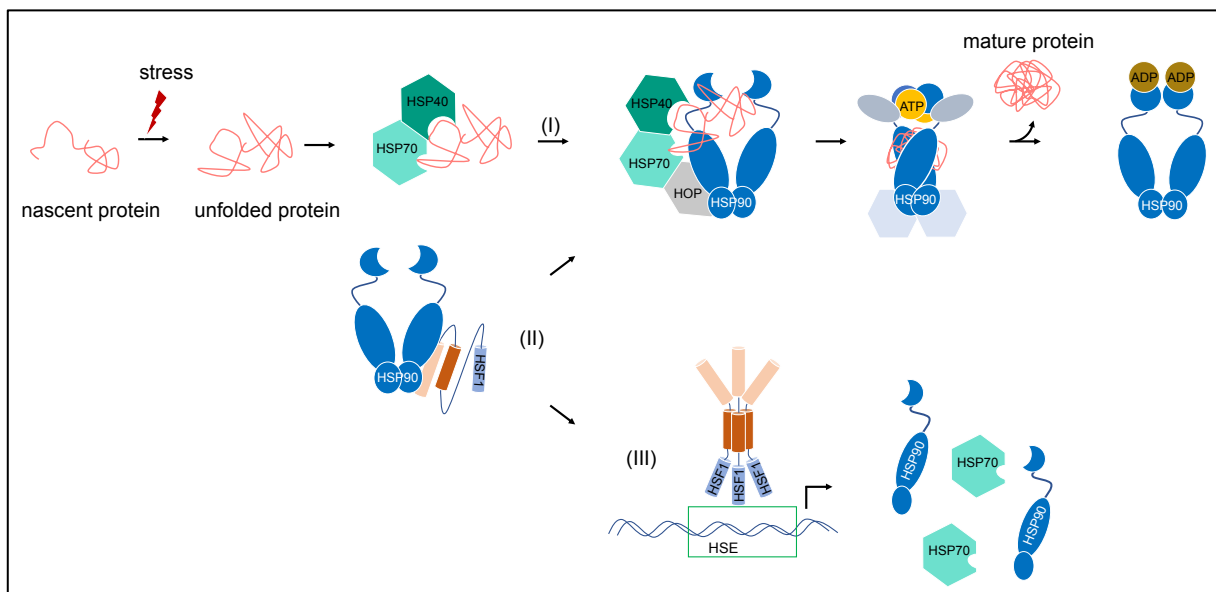
Figure 2: Transcriptional regulation of HSPs in normal cells. Nascent polypeptide chains accumulate to unfolded or misfolded proteins due to cellular stress. (I) HSP40 and HSP70 capture these unfolded proteins for translocation to HSP90. (II) Under physiological conditions, inactive monomeric HSF1 is bound to HSP90. Under stressed conditions, HSF1 dissociates from HSP90, resulting in its trimerization and transcriptional activation. (III) In the nucleus, HSF1 binds to heat shock elements (HSE) upstream of the heat shock protein genes such as *HSP90* and *HSP70*.

According to the updated list by the Picard Lab, more than 800 HSP90 client proteins have been identified thus far [21]. Given the plethora of clients, it is not surprising that heat shock proteins can contribute to the development and progression of many pathological conditions such as cancer, neurodegenerative or infectious diseases [30, 38, 42, 43, 55]. Two HSP90-stabilized clients which have been associated with tumor progression are the macrophage migration inhibitory factor (MIF) and mutant p53 (mutp53) [56, 57].

2.1.2 HSP90 response in cancer

The elevated expression of HSP90 and other co-chaperones have been reported previously for many different cancer entities [17, 58], such as breast [59, 60], colorectal [61, 62] or pancreatic cancers [63, 64]. In most cases, the overexpression of chaperones in general and HSP90 in particular, correlates with decreased survival of cancer patients [59, 61, 62]. Cancer cells are rapidly proliferating cells, with a high demand for newly synthesized proteins [13, 15]. The extensive amount of cytotoxic stress, caused by the high mutational load, oxygen and nutrient starvation, can give rise to an accumulation of unfolded or misfolded proteins [15, 16, 23, 51, 65]. In order to cope with this cellular stress, which could be detrimental and cytotoxic in the long run, cancer cells respond by inducing HSP expression [16, 66] (**Figure 2**). While HSF1 and HSP90 strongly co-regulate each other in normal cells [49], constant cellular stress in cancer cells results in a constitutive activation of HSF1 and HSF1-mediated chaperone expression, which can favor the formation of superchaperone complexes [67-71] (**Figure 3**).
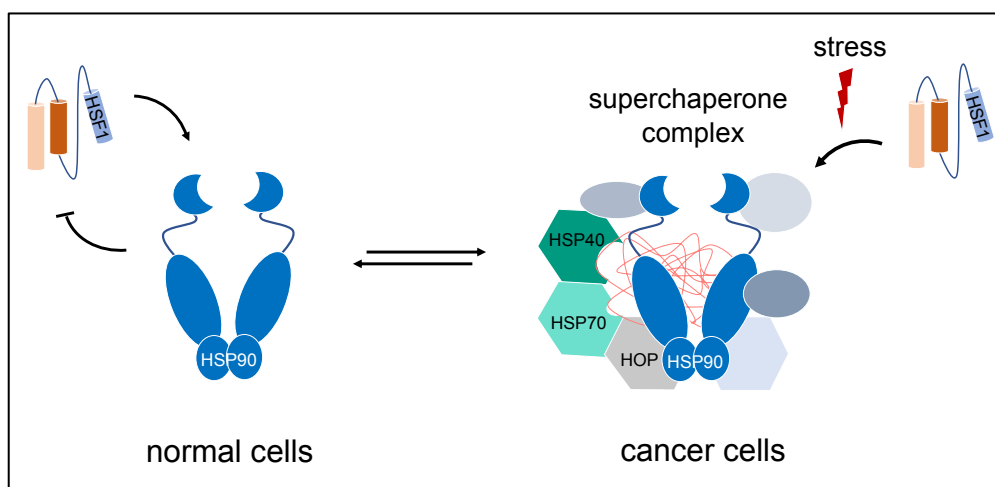
Figure 3: Native forms of HSP90 in normal compared to cancer cells. In normal cells, HSP90 exists as a transient dimer in order to assist in protein turnover and activity. Cellular homeostasis is achieved by counter regulation between HSF1 and HSP90. Due to high stress levels in cancer cells, HSF1 is constitutively active, resulting in increased expression of HSP90 and other chaperones. The association of multiple co-chaperones with HSP90 leads to the formation of *superchaperone complexes,* which in turn support increased stabilization and decreased degradation of its client proteins.

These superchaperone complexes further support tumor development by assisting in the proper maturation, stabilization and activity of a plethora of oncogenes (such as mutp53, AKT, v-SRC) [16, 56, 71, 72]. Thus, HSP90 helps to fulfill the hallmarks of

cancer defined by Hanahan and Weinberg, which includes increased proliferation, angiogenesis, invasion and metastasis [17, 73, 74].

In that context, several cancer-relevant HSP90 clients have already been identified across different cancer origins [72, 75]. In breast cancer for example, the human epidermal growth factor receptor-2 (HER2; ErbB2/Neu) was described as an important client of the HSP90 chaperone machinery [72, 76, 77]. Interestingly, a previous publication from our group found that HER2 overexpression regulates hyperactivation of HSF1, resulting in increased induction of the HSP90 chaperone machinery (**Figure 2**) and thus further stabilization of HSP90 clients, providing a positive feed-forward loop [76]. In comparison, the androgen receptor was identified as important HSP90 client relevant for prostate cancer progression [75, 78].

Because of its pleiotropic functions, the abundance of clients and large impact on tumor development and progression, HSP90 is considered a promising therapeutic target in cancer therapy [16, 72, 75].

2.1.3 HSP90 as therapeutic target

The aberrant activation of HSP90 within the superchaperone complexes results in higher ATPase activity of HSP90 in cancer cells compared to normal cells [68, 71, 79]. Consequently, HSP90 is considered a potential target to selectively affect cancer cells [71, 80]. In the past decades, several clinical trials have been performed using small molecules, which are able to bind and inhibit the N-terminal ATP binding pocket of HSP90, resulting in client degradation of cells with high ATPase activity such as cancer cells [71, 79, 81]. Unfortunately, first-generation inhibitors such as Tanespimycin (17AGG) showed low efficacy, high toxicity and reduced solubility [82, 83]. In order to address this issue, second-generation inhibitors such as Ganetespib (STA9090) and Onalespib (AT13387) have been developed and applied to clinical trials [20, 82, 84]. Using these inhibitors, several *in vivo* studies confirmed decreased tumor development for T-cell lymphomas [85], non-small cell lung cancers [86, 87] and breast cancers [88]. However, other studies in cancer entities such as colorectal cancer demonstrated low antitumor efficacy of HSP90 inhibition alone, with efficacy only observed in the presence of other chemotherapeutics [89, 90].

Even though second-generation inhibitors have shown lower cytotoxicity compared to first-generation inhibitors [20, 83],only limited efficacies have been reported in some *in vivo* studies and clinical trials [20, 84, 89, 90]. So far, none of the 18 HSP90 inhibitors in development have shown sufficient efficacy for FDA (Food and Drug Administration) approval [14, 89, 91]. The limited efficacy of these HSP90 inhibitors was thought to be caused by the activation of HSF1 [84, 92]. The HSF1 mediated heat shock response (HSR) results in increased expression and activation of HSPs such as HSP70 (**Figure 2**) which can diminish the effects of an HSP90 inhibitor [49, 92]. In order to reduce the HSR, inhibitors binding to the C-terminal domain or those that disrupt the HSP90 protein-protein interactions are currently investigated [67, 92-95]. Such inhibitors have shown encouraging results thus far, causing the degradation of client proteins with limited induction of the HSF1 response compared to the N-terminal inhibitors [67, 92, 94].

Taken together these results have further emphasized the need to investigate the molecular basis of the disease for targeted and personalized medicine and the need for predictive cancer-relevant biomarkers for HSP90 inhibitors. Because of that, we are investigating the role of two important HSP90 clients: the macrophage migration inhibitory factor (MIF) and mutant p53 (mutp53).

2.2 MACROPHAGE MIGRATION INHIBITORY FACTOR IN COLORECTAL CANCER

2.2.1 Colorectal Cancer

Colorectal cancer (CRC) is the third most common cancer worldwide, with rising incidence every year [96-98]. In the majority of cases, the disease is caused by sporadic mutations due to environmental factors like age or lifestyle factors such as improper diet and the lack of physical exercise [96, 99]. However, a minority of CRC cases occur as a result of inherited genetic mutations [96, 99]. As early as in the late 1980s, Vogelstein and colleagues demonstrated, that a series of oncogene mutations and loss of tumor suppressors are essential for the development and progression of sporadic CRC [100, 101]. Genetic alterations of *APC (adenomatosis polyposis coli), CTNNB1 (catenin beta-1), KRAS (Kirsten ras oncogene homolog), TP53 (tumor protein 53),* and *SMAD4 (mothers against decapentaplegic homologue 4)* are essential

drivers for the successive malignant degeneration of normal mucosa to carcinoma and metastasis [96, 99, 101]. Other important causative factors for colorectal cancer are inflammatory bowel diseases (IBD) such as ulcerative colitis and crohn's disease [96, 99, 102]. Due to the characteristic chronic and relapsing inflammation of these diseases, leading to inflammation-induced damage of the intestinal tissues, IBD patients are highly susceptible to developing CRC [99, 102].

To investigate a colitis-associated type of colorectal cancer, the AOM/DSS mouse model can be used [103-105]. This model entails a single injection of azoxymethane (AOM), a carcinogenic chemical agent causing DNA damage in the colon due to methylation of guanosine [103, 104]. After one week of rest, dextran sodium sulfate (DSS) is added to the drinking water, causing an acute inflammation in the intestine, due to the disruption of the epithelial barrier and infiltration of the microbiome into the tissue [103, 106]. After administration of both agents, rodents develop tumors in the colorectal part of the intestine, mimicking the human patient situation [103, 105].

In sum, inflammation can play a crucial role in the development of colorectal cancer. Due to the long symptom-free tumor growth and the broad range of occurring symptoms, most patients are diagnosed at later stages of the disease [107, 108]. Thus, preventive CRC screenings as well as development of predictive biomarkers are essential to allow earlier detection and better prognosis of these tumors [102, 107, 108].

It has been shown in various human cancer entities that elevated MIF levels in epithelial tumor cells correlated with poorer patient prognosis [109-112]. In a mouse model for breast cancer, we previously showed that elevated MIF levels are due to a stabilization through the HSP90 chaperone machinery, thus contributing to tumor progression [57, 80]. Hence, in the current study we investigated whether MIF is a tumor driver and can serve as potential drug target in CRC.

Before describing the role of MIF in cancer cells, the next section depicts the functions of the pro-inflammatory cytokine under physiological and inflammatory conditions.

2.2.2 Macrophage migration inhibitory factor – a pro-inflammatory cytokine under physiological and inflammatory conditions

Macrophage migration inhibitory factor (MIF) is a ubiquitous pro-inflammatory cytokine involved in inflammatory and immune responses [113-115]. First discovered in 1966, it was shown to inhibit random migration of peritoneal macrophages [116-118] and to function as a homotrimer [119, 120]. Besides its function as a pro-inflammatory cytokine, it was also reported to have enzymatic activity *via* its tautomerase domain [119-121]. MIF was shown to be involved in a plethora of disorders such as cardiovascular [122-124], neurodegenerative [125] and pulmonary diseases [126].

MIF can fulfil its pleiotropic functions either *via* receptor-mediated pathways by binding to CD74/CD44, CXCR2, CXCR4 and CXCR7 [113, 123, 127-130] or through receptor-dependent or independent endocytosis [113, 124, 131, 132] (**Figure 4**). By binding to transmembrane receptors extracellular MIF initiates various downstream signaling cascades and assists in diverse cellular functions [113, 123]. Depending on the cellular context, these receptors function individually or as heterocomplexes [124, 129, 130]. The exact signaling pathway for MIF highly depends on the cellular context, the expression of the receptors on different cell types as well as environmental factors such as the expression of ligands that compete with MIF for binding to non-cognate receptors [128-130]. Binding of MIF to the non-cognate receptors CXCR2 or CXCR4 actives G-proteins, whereas interaction with CXCR7 activates ß-arrestin which inhibits short term G-protein coupled receptor signaling and results in a long-lasting ERK1/2 (extracellular regulated MAP kinase) and PI3K (phosphoinositide 3 kinase) activation [130, 133]. Binding to the cognate CD74 receptor triggers its dimerization with CD44 and the activation of a downstream signaling cascade, for example *via* the tyrosine kinase SRC [127, 134]. The individual and combined activation of these pathways can result in the activation of MAP-kinases or PI3K/AKT, that results in cell proliferation, migration and angiogenesis [113, 124, 128, 129, 133, 134]. Furthermore, activation of ERK1/2 promotes induction of phospholipase A2 (PLA2) and cyclooxygenase 2 (COX2) resulting in transformation of arachidonic acid to prostaglandin E_2 (PGE$_2$), an essential driver of inflammatory responses [113, 135-137]. Simultaneously, MIF-mediated activation of COX2 is suggested to have an inhibitory impact on p53, resulting in decreased apoptosis and further supporting cellular survival and proliferation [113, 133, 138]. However, MIF can also enter cells *via* endocytosis [113,

124]. Intracellular MIF can for instance bind to JAB1 (JUN-activation domain-binding protein 1) resulting in its inactivation [139, 140]. The inactivation of JAB1 prevents activation of cJUN (AP1 transcription factor subunit), which functions as a co-activator of the activator protein 1 (AP1), known to be involved in the regulation of proliferative and inflammatory signals [113, 139-141]. Furthermore, MIF-JAB1 diminishes JAB1 induced degradation of the cyclin-dependent kinase inhibitor KIP1 (p27), resulting in increased cell cycle arrest [113, 139, 142, 143]. In this respect, high levels of intracellular MIF can counteract MIF-receptor induced pathways [122, 124].
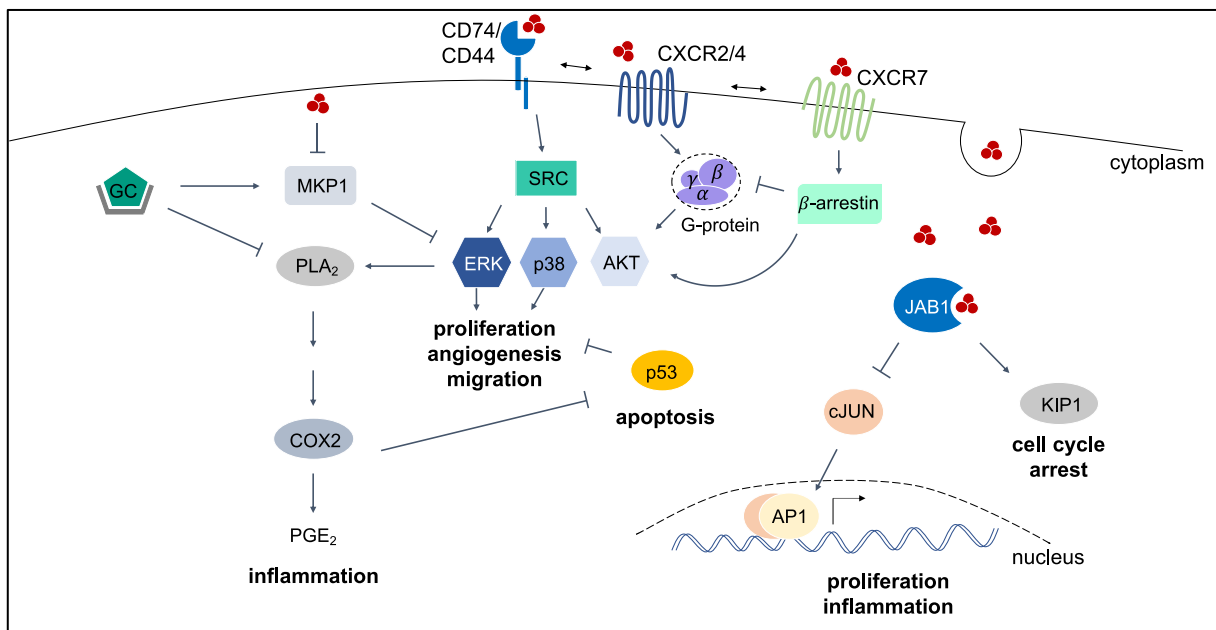
Figure 4: Pleiotropic MIF functions under physiological and inflammatory conditions. Macrophage migration inhibitory factor (MIF) acts in a receptor-dependent manner by binding to CD74/CD44, CXCR2/4/7 or can enter cells *via* endocytosis. Depending on the molecular context, the different MIF receptors can form heterocomplexes, which trigger downstream activation of MAPKs ERK1/2, p38 or PI3K/AKT supporting migration, proliferation, angiogenesis and inflammation of cells. MIF-induced activation of COX2 can have an inhibitory impact on p53, further promoting cellular survival by inhibiting apoptotic responses. High intracellular levels of MIF can counteract the receptor-induces pathways, caused by MIF-mediated inhibition of JAB1. This subsequently, leads to an induction of cell cycle arrest (*via* KIP1) and a reduction of inflammatory and proliferative signals (*via* cJun/AP1).

Counter regulatory activity has been reported between MIF and glucocorticoids (GC), hormones which are important anti-inflammatory players [113, 122, 144]. By inhibiting PLA$_2$ or inducing the expression of mitogen-activated protein kinase phosphatase 1 (MKP1, the main negative regulator of ERK), high levels of glucocorticoids, can hamper MIF-induced pathways [137]. Similarly, it has been reported that MIF is able to counteract glucocorticoids for example through inhibition of MKP1 [113, 137, 144].

Therefore, a balance between the pro-inflammatory cytokine MIF and the anti-inflammatory glucocorticoids is essential for proper cellular homeostasis in order to prevent the development of diseases [122, 130].

Taken together, there is an increasing amount of evidence over a number of years, that MIF is not just a pro-inflammatory cytokine involved in inflammatory responses but is also a potential driver of tumor development [145, 146].

2.2.3 Macrophage migration inhibitory factor – a tumor promotor under oncogenic conditions

It has been shown in various human cancer entities such as breast [109], prostate [110, 147], colon [111, 148] and hepatocellular carcinomas [112] that elevated MIF levels in epithelial tumor correlated with poorer patient prognosis.

Thus far, the role of MIF in intestinal cancer has been investigated *in vivo* by using *Apc^{min}* mice [149] or xenograft tumor models [111, 150, 151], confirming the tumor supportive role of MIF is this cancer entity. However, a causative *in vivo* model, mimicking the human patient situation remains elusive, since patients with malignant intestinal neoplasia mostly develop tumors in the distal part of the intestine (colon and rectum) [105]. Only a minority of tumors grow in the small intestine, as observed for the *Apc^{min}* mice [152]. Therefore, we have chosen to investigate the role of MIF as cancer-relevant HSP90 client in a more clinically relevant approach using the AOM/DSS mouse model to induce colitis-associated cancer [103].

In a recent study, our research group was able to show that MIF levels are elevated in breast cancer cells [57]. These high MIF levels (**Figure 5**) arise as a consequence of cellular stress induced activation of HSF1, triggering the expression of various chaperones [49, 57, 76, 80] (**Figure 2**). As a consequence, the formation of superchaperone complexes (**Figure 3**) leads to high stabilization of the MIF protein [57, 67, 76]. Furthermore, oxygen starvation in cancer cells triggers the activation of hypoxia inducible factor 1 alpha (HIF1α), a major transcription factor of *MIF* and pro-angiogenic genes such as *VEGF* [153-156]. In addition, extracellular MIF can bind to its receptors in an autocrine or paracrine fashion in order to trigger proliferation, angiogenesis, migration or apoptosis of cells *via* induction of the MAP kinases (p38, ERK1/2) or PI3K/AKT [111, 150, 151, 157-162]. In a positive feed-forward loop, these

proteins can further contribute to the activation of HSF1 and HIF1α to trigger MIF expression and stabilization [70, 76, 155, 163, 164]. In cancer cells, MIF can also contribute to inflammatory processes by activation of PLA$_2$ [159]. The inhibitory impact of COX2 on the tumor suppressor p53 contributes to decreased apoptosis, which further supports cancer cell survival and proliferation [138, 159, 165, 166].
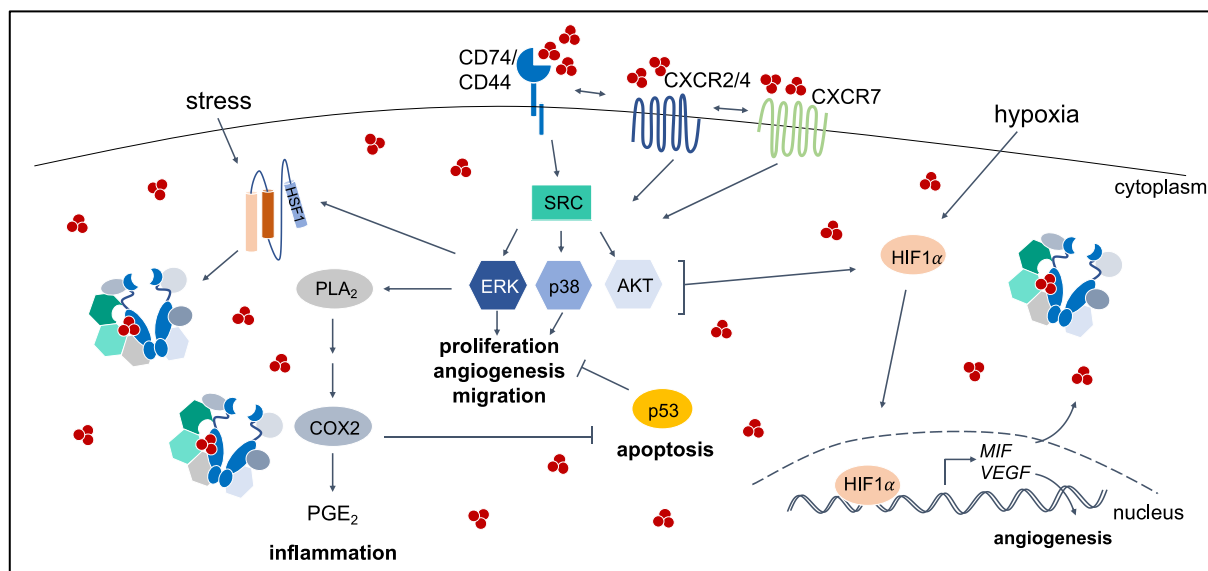
Figure 5: MIF stabilization and functions in cancer cells. Stabilization of MIF *via* HSP90 multichaperone complexes results in elevated MIF protein levels in cancer cells and serum. Furthermore, constant cellular stress and oxygen starvation induce constitutive activation of HIF1α and HSF1. HSF1 further promotes activation and expression of the HSP90 chaperone machinery. HIF1α can function as a transcription factor for MIF further promoting elevation of MIF levels on gene expression levels in cancer cells. Increased binding of MIF to its receptors enhances activation of downstream signaling pathways to promote proliferation, migration and inflammation to promote carcinogenesis.

Notably, the increased expression, stabilization and secretion of MIF from cancer cells and its chemokine like properties, can further contribute to the recruitment and activation of tumor promoting immune cells such as tumor associated macrophages [123, 154, 155, 167]. Constituents of the tumor microenvironment can support tumor progression, not just by expressing and secreting MIF themselves [148, 168], but also by producing and secreting various cytokines which can further promote tumorigenic proliferation and angiogenesis [167, 169, 170].

In cancer cells, MIF has also been shown to promote cellular resistance to stress or chemotherapeutics *via* regulation of MAPKs, STAT3 or AMPK, subsequently

promoting tumor cell survival [157, 171, 172]. Because of its pleiotropic functions associated with tumor progression, MIF has been considered a promising selective target for cancer therapy [80, 157, 159]. Targeting of MIF can be achieved by three main strategies:

(I) Direct binding of small molecules to the tautomerase domain, which is known to be important for the interaction with other proteins [173, 174].

(II) By using monoclonal antibodies against MIF or its cognate receptor CD74, resulting in a modulation of the downstream signaling cascades and interference with MIF induced tumorigenic pathways [175].

(III) Indirect inhibition through its destabilization using HSP90 inhibitors, resulting in decreased MIF levels in cancer cells and diminished MIF-induced tumorigenic functions [57, 76].

To exploit the potential of anti-MIF therapy in the field of oncology, a number of approaches have also been used in preclinical as well as some clinical trials supporting MIF's tumorigenic potential [159, 175]. However, additional research is necessary to fully understand the tumor promoting mechanism of action and the potential of using MIF as a biomarker for CRC.

2.3   MUTANT P53 IN PANCREATIC DUCTAL ADENOCARCINOMA

2.3.1 Pancreatic ductal adenocarcinoma

Pancreatic cancer is the seventh leading cause of cancer death worldwide, with rising fatalities every year [2, 98]. Of all pancreatic malignancies, pancreatic ductal adenocarcinoma (PDAC) occurs with a frequency of more than 90% and is considered as highly chemoresistent and poorly treatable due to limited medical and surgical options [176-179]. The late onset of symptoms combined with a high capability to metastasize and high plasticity of the cancer cells, make PDAC one of the most aggressive entities with a five-year survival rate of around 8% [176-178]. Due to the broad heterogeneity of PDAC, several efforts have been made in order to specify defined PDAC subtypes based on histological findings as well as transcriptome analysis. Taken together, it is suggested to distinguish between the epithelial-like

classical subtype and the more aggressive basal-like quasi-mesenchymal subtype [177, 180-183].

PDAC derives from pancreatic intraepithelial neoplasia which are categorized into three stages (PanIN1-3) and characterized by successive accumulation of genetic mutations and increasing desmoplasia [177, 184]. Whereas mutations in *KRAS* are sufficient for the initiation of PanINs, additional genetic hits in tumor suppressor genes such as *TP53* (*tumor protein p53*), *CDKN2A* (*cyclin-dependent kinase inhibitor 2A*), and *SMAD4* (*mothers against decapentaplegic homologue 4*) are required for PanIN-PDAC lineage [177, 184, 185]. A significant hallmark of PDAC is the presence of a dense stromal matrix, known as the tumor microenvironment, which accounts for up to 90% of the tumor bulk and has been shown to further promote PDAC progression [177, 179]. Unfortunately, targeting components of the tumor microenvironment using anti-stromal therapies to diminish PDAC progression has not been successful in clinical trials so far [179].

In CRC we previously demonstrated that mutp53$^{R248Q/W}$ is stabilized by the HSP90 chaperone machinery, contributing to tumor progression and aggressiveness [56]. In PDAC, approximately 70% of patients carry mutations in *TP53* which is mutated as a late genetic event during tumor development [177, 186, 187]. Thus, we aimed to investigate whether mutant p53 (mutp53) is also a cancer-relevant HSP90 client in PDAC. To understand the altered functions of p53 mutants in cancer cells, the next section describes the physiological functions of the tumor suppressor p53.

2.3.2 Wildtype p53 – a tumor suppressor

Since its first discovery in 1979, the tumor suppressor p53, referred to as the 'guardian of the genome', has been extensively studied [188-190]. The genetic structure of *TP53* was shown to be highly evolutionarily conserved across species [191, 192]. It consists of an N-terminal transactivation domain, followed by a core DNA-binding domain and a C-terminal oligomerization domain [191, 193]. Under physiological conditions, p53 levels are tightly regulated and kept low, by its major antagonist, the E3 ubiquitin ligase MDM2, targeting it for proteasomal degradation [194-196]. However, a variety of different stressors such as nutrient starvation, DNA damage or hypoxia result in post-translational modifications of both proteins, leading to an induction of p53 activity [193,

195, 197]. Proper tetramerization of p53 is required for DNA binding, post-translational modifications as well as protein-protein interactions [197]. Following nuclear translocation, active p53 can bind to its target genes, and prevents the accumulation of mutagenic DNA [193, 195, 198]. As a transcription factor p53 regulates the expression of a large variety of genes involved in cell cycle progression (such as *CDKN1A, GADD45A*) as well as cellular survival and apoptosis (such as *BAX, PUMA, NOXA*) [193, 197, 199]. In a negative feedback loop, p53 induces the expression of MDM2, resulting in increased MDM2-mediated degradation of p53 to ensure normal cellular homeostasis [194, 195, 199].

Because of its pleiotropic functions in cellular protection and tumor suppression, mutation or ablation of *TP53* is an essential step in human tumor development [188, 200, 201]. Indeed, *TP53* has been shown to be mutated in approximately 50% of all human cancers, making it the most frequently mutated gene in a variety of cancer entities [202, 203].

2.3.3 Mutant p53 – a tumor promoter

The majority of *TP53* mutations are missense mutations in the central region of the gene, the DNA binding domain (DBD) [202, 204-206]. Some of these mutations occur with high frequency among different cancer entities and are so called hotspot mutations [202, 205, 206]. These mutations in the DNA binding domain can be distinguished in two main groups: 'DNA-contact' mutants (e.g.: R273H, R248Q), directly affecting residues necessary for DNA binding or 'conformational' mutants harboring mutations which are causing structural changes (e.g.: R282W, R175H) [205, 207]. Most mutations in the DNA binding domain result in the loss of the DNA binding capacity, leading to a loss of wildtype (WT) p53 tumor suppressor function (loss-of-function, LOF) [202, 205]. Especially in early stages of tumor development, mutations of *TP53* due to genotoxic stress occur only on one allele [208]. This results in an intermediate stage, characterized by the presence of heterocomplexes between mutp53 and the remaining WTp53 [205, 208]. This interaction of mutp53 and WTp53 results in diminished WTp53 activity, known as the dominant-negative effect of the mutant on the wildtype protein [202, 205, 208]. However, as tumors progress, loss-of-heterozygosity (LOH) results in the loss of the remaining WTp53 allele, which is a prerequisite for stabilization of mutp53 in cancer cells [208, 209]. Most of the DBD

mutants have been shown to be highly unfolded or less structurally stable than WTp53 [210-212]. The stabilization of these mutants is achieved by increased binding to the aberrantly activated HSP90 chaperone machinery (**Figures 2 and 3**), preventing it from proteasomal degradation (**Figure 1**), which results in elevated mutp53 levels in cancer cells [16, 56, 85, 213-215]. However, mutation of p53 can result in the exposure of a hydrophobic aggregation sequence within the DNA binding domain contributing to the formation of oligomers and prion-like proteins [216-219]. Co-aggregation of mutp53 and WTp53 in these prion-like structures is thought to contribute to the dominant negative effect [219, 220].

We propose that stabilization of mutp53 by HSP90 is a requirement for the gain of new tumorigenic functions (gain-of-function, GOF), providing a selection advantage for cancer cells [56, 208, 221, 222]. DBD hotspot mutants can no longer bind to the DNA to activate the transcriptional machinery, but still maintain the N-terminal transactivation domain [210]. Therefore, several mechanisms have been described through which p53 mutants can still fulfil their transcriptional activity (**Figure 6**):

(I) Binding of mutp53 to other proteins and transcription factors can results in their enhanced functional or transcriptional activity (*hyperactivation*) [210, 223].

(II) Binding of mutp53 to other proteins or transcription factors (TF) can diminish their functional or transcriptional activity (*inactivation*) [223, 224].

(III) Interaction of mutp53 with other proteins and transcription factors may contribute to a change of existing signaling pathways (*reprogramming*) [210, 224].
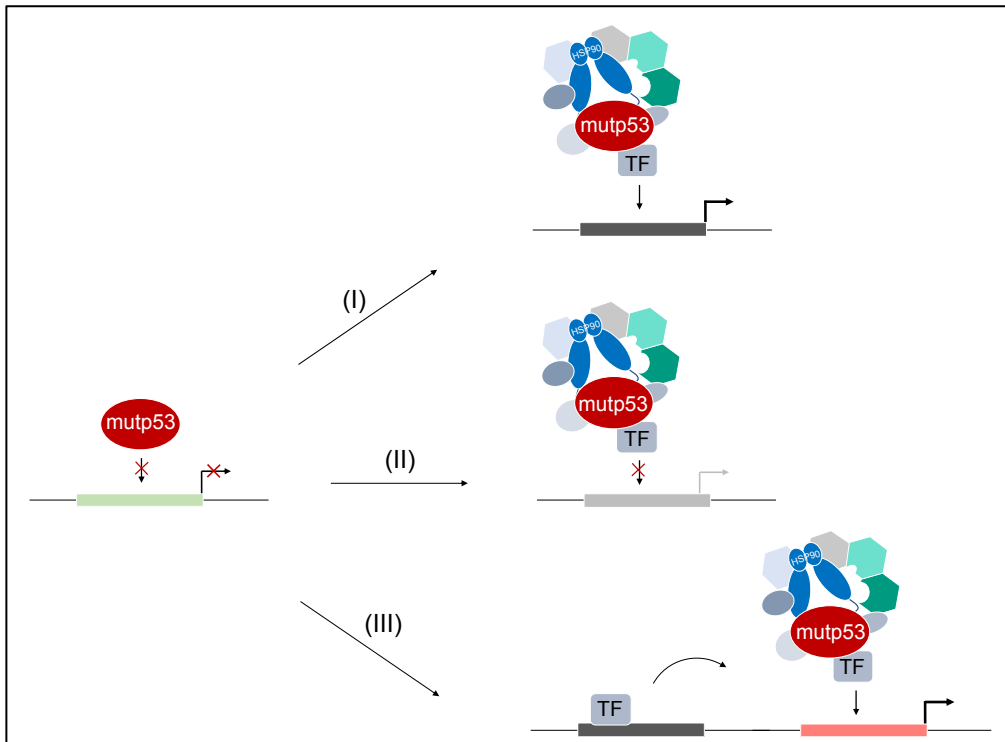
Figure 6: Gain-of-function of mutant p53 *via* interaction with other proteins. High stabilization of mutp53 *via* the HSP90 chaperone machinery is a prerequisite for gain-of-function (GOF). To fulfil its tumorigenic functions despite loss of DNA binding capacity, mutp53 interact with other proteins (such as co-factors) and transcription factors (TF). These interactions can trigger a *hyperactivation* (I), *inactivation* (II) or *reprogramming* (III) of these target proteins in order to drive tumor progression.

These mechanisms provide examples on how different p53 mutants (despite loss of DNA binding capacity) can gain new tumor promoting functions to support for example therapy resistance, invasion and metastasis of cancer cells [56, 210, 222, 224].

Because of the increasing network of mutp53 interactions with other proteins and regulation of pathways, several efforts have been made to target mutp53 in cancer therapy. In order to achieve this, two main strategies can be used:

(I)   Small molecules to restore WTp53 conformation and activity to induce cell cycle arrest and apoptosis in cancer cells and to prevent oligomerization of mutp53 proteins [225-228].

(II) Destabilization of mutp53 proteins by inhibition of the HSP90 chaperone complex [56, 85, 214, 226, 229].

The underlying mechanism of the gain of function is highly dependent on the mutant itself as well as the cellular context [204, 210]. Due to the different structures and functions caused by distinct mutations on p53, each mutant has to be considered as an individual protein [204]. Different mutp53 variants might result in unequal gain of new functions and show diverse tumor promoting activities and prognostic potentials [230, 231]. The existing controversies in the field of mutant p53 emphasize the necessity to further explore the exact mechanism of individual mutants and their relevance in tumor progression [231].

Thus, our research group investigates the specificity of the hotspot mutant p53$^{R248Q/W}$, its stabilization *via* the HSP90 chaperone system and its GOF to support cancer progression.

2.3.4 *Specific gain of new tumorigenic functions by mutp53$^{R248Q/W}$*

Mutp53$^{R248Q/W}$ is a hotspot missense mutant in the DNA binding domain (contact mutant), that has been shown to be elevated in cancer cells and to correlate with a worse prognosis in cancer patients [56, 209, 230].

In a murine model for colorectal cancer, our group has previously shown that mutp53$^{R248Q/W}$ is highly stabilized by the HSP90 chaperone machinery [56]. It exerts its gain-of-function on migration through interaction with the transcription factor pSTAT3, resulting in hyperactivation of the transcription factor STAT3 *via* displacement of its phosphatase SHP2 [56, 210] (**Figure 6**). Hence, mutp53$^{R248Q/W}$ leads to an increased transcriptional regulation of STAT3 target genes involved in proliferation and invasion [56]. Concomitantly, an ablation of mutp53 decreases pSTAT3 levels, and diminishes tumor promoting target gene expression [56] (**Figure 7**).
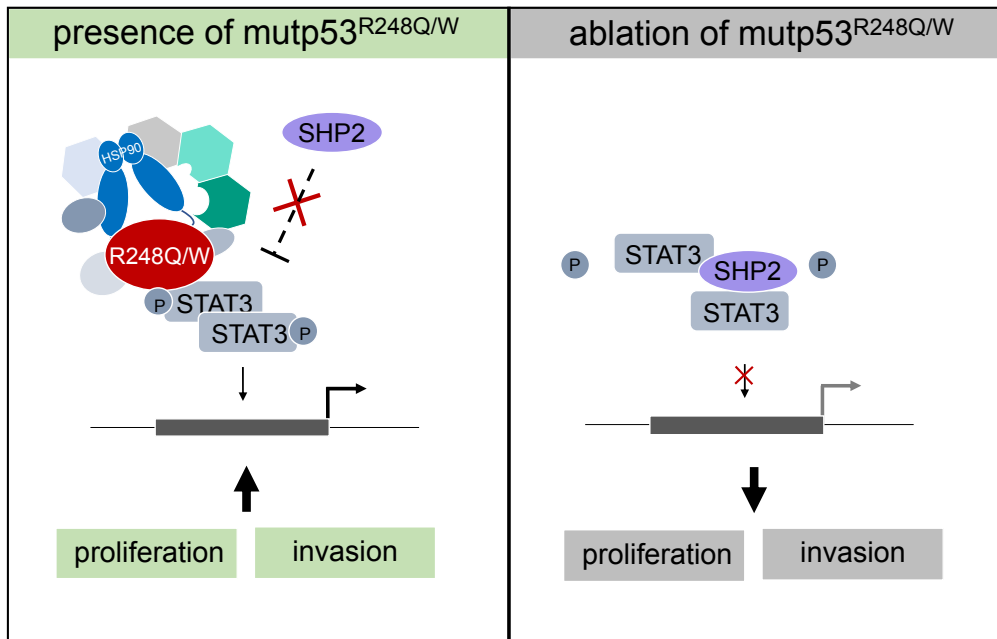
Figure 7: Gain-of-function of mutp53$^{R248Q/W}$ on proliferation and invasion through interaction with pSTAT3 in CRC. In CRC mutp53$^{R248Q/W}$ is highly stabilized *via* the HSP90 chaperone machinery, which is a known prerequisite for its gain-of-function (GOF) effects. mutp53$^{R248Q/W}$ binds to phosphorylated STAT3 (pSTAT3), resulting in a hyperactivation of the transcription factor *via* displacement of the phosphatase SHP2. The increased pSTAT3 level support expression of genes involved in proliferation and invasion. Ablation of mutp53$^{R248Q/W}$ strongly diminished pSTAT3 level and respective target gene expression.

Indeed, high levels of mutp53$^{R248Q/W}$ in colorectal cancer patients mostly correlated with high levels of pSTAT3 which was associated with poorer survival [56].

Importantly, the exact interaction partners of mutp53$^{R248Q/W}$ and the functional outcome (**Figure 6**) highly depend on the molecular and cellular context [204]. Besides colorectal cancer, mutp53$^{R248Q/W}$ has also been reported as potential tumor driver in breast cancer by upregulation of HER2 (human epidermal growth factor receptor 2) [232] or in ovarian cancer by inducing invasive gene expression *via* interaction with Rad21 [233]. In both cases, mutp53$^{R248Q/W}$ has been suggested to interact with other proteins to promote tumor progression and aggressiveness [232, 233].

Taken together these data suggest the need to further investigate the specificity of different p53 mutants in cancer entities based on the molecular context.

2.4   PROJECT SCOPE

The aim of this thesis is to investigate HSP90-stabilized proteins as therapeutic targets in cancer. We evaluated if the two HSP90 clients MIF and mutp53 are cancer-relevant HSP90 clients and thus, suitable drug targets in colorectal cancer and pancreatic ductal adenocarcinoma respectively.

2.4.1 Macrophage migration inhibitory factor in colorectal cancer

We aimed to investigate the role MIF in AOM/DSS induced colitis-associated tumor development (described in **section 2.2.1** in more detail). This chemically induced cancer model is known to mimic the human patient situation better than previously described *Apc^{min}* or xenograft mouse models [105, 149, 151]. To evaluate the impact of HSP90-stabilized MIF in CRC progression we made use of a conditional Mif knockout mouse as well as murine and patient-derived colonic tumor organoids. Our first and most important question was:

Are MIF levels elevated in AOM/DSS induced tumors and patient CRC samples?

To answer this question, mice were treated with AOM/DSS to induce tumor development. Mice were dissected 12 weeks after AOM injection and colon was prepared to evaluate the tumor burden and Mif level in CRC cells. By this approach, we were able to address the second most important question:

Are colorectal tumors dependent on MIF?

Since MIF as a pro-inflammatory cytokine is involved in immune and inflammatory responses, we first investigated the overall inflammation in established tumors (week 12 post-AOM) and during tumor initiation (3 days after DSS start: 'short' and 8 days after DSS stop: 'recovery'). Furthermore, we investigated tumorigenic mechanisms such as angiogenesis and proliferation in established tumors and recovering tissue.

To further clarify whether effects derive from epithelial cells or from stromal cells of the tumor bulk, *Mif*-depleted tumor organoids were prepared to assess tumorigenic MIF activity.

Additionally, different HSP90 inhibitors (first-generation inhibitor 17AAG; second-generation inhibitors Ganetespib and Onalespib) were used to evaluate susceptibility of tumor organoids harboring elevated Mif levels, compared to normal colon and small intestinal epithelia-derived organoids.

2.4.2 Mutp53^{R248W} specificity in pancreatic ductal adenocarcinoma

Using a panel of seven different cell lines, we wanted to elucidate the specificity of different mutp53 (mutant p53) variants in PDAC. Based on our results previously gained in a mouse model for colorectal cancer [56], we hypothesized that mutp53^{R248W} is stabilized through the HSP90 chaperone machinery resulting in a gain-of-function effect on proliferation and invasion *via* interaction with phosphorylated STAT3 (pSTAT3). Therefore, our most important question was:

Is mutant p53 stabilized via the HSP90 chaperone machinery in PDAC cells?

We evaluated the levels and stability of mutp53 in different PDAC cells. Using the two HSP90 inhibitors Gantespib and Onalespib, we investigated whether different mutp53 variants are stabilized by the HSP90 chaperone machinery. Using transwell migration and wound healing assays we elaborated on the functional role of different p53 mutants in migration. Next, we aimed to understand the underlying molecular mechanism, driving mutp53-dependent migration in PDAC.

Is mutp53-pSTAT3 complex formation necessary for migration in PDAC?

Therefore, co-immunoprecipitation experiments were performed to explore if different p53 mutants (and specifically R248W) are able to bind pSTAT3. To further analyze whether migration effects are due to a possible interaction with pSTAT3, migration assays were performed after STAT3 knockdown (siRNA) or STAT3 inhibition using the small molecule inhibitor Stattic.

3   RESULTS

3.1   PUBLICATION: MIF IN CRC

HSP90-STABILIZED MIF SUPPORTS TUMOR PROGRESSION VIA MACROPHAGE RECRUITMENT AND ANGIOGENESIS IN COLORECTAL CANCER

Luisa Klemke[1], Tiago De Oliveira[2], Daria Witt[1], Nadine Winkler[1], Hanibal Bohnenberger[3], Richard Bucala[4], Lena-Christin Conradi[2] and Ramona Schulz-Heddergott[1*]

[1] Institute of Molecular Oncology, University Medical Center Göttingen, Göttingen, Germany.

[2] Department of General, Visceral, and Pediatric Surgery, University Medical Center Göttingen, Göttingen, Germany.

[3] Institute of Pathology, University Medical Center Göttingen, Göttingen, Germany.

[4] Departments of Medicine, Pathology, and Epidemiology & Public Health, Yale School of Medicine and Yale Cancer Center, New Haven, CT, USA.

* Corresponding author: ramona.schulz@zentr.uni-goettingen.de

Own contribution:

Conducted experiments and data analysis for: Figures 2A-F, Figures 3B-D, Figures 4A-C, Figures 5A-C, E, G and H-J, Figures 6D-I, Figures 7A-D, Figures S1A-C, Figures S2A-C and G-I, Figures S3A-C and G-K, Figures S4A, B, Figures S5A-C. Data analysis for: Figures 1C, E, Figures 4E-G, Figures 5D, F, Figure 7E, Figure S2F, as well as preparation of additional supplemental material. Involved in the conceptualization, methodology, acquisition, analysis and interpretation of data, figure arrangement, writing and revising the manuscript.

Hsp90-stabilized MIF supports tumor progression via macrophage recruitment and angiogenesis in colorectal cancer

Luisa Klemke[1], Tiago De Oliveira[2], Daria Witt[1], Nadine Winkler[1], Hanibal Bohnenberger[3], Richard Bucala[4], Lena-Christin Conradi[2] and Ramona Schulz-Heddergott[1]

Abstract

Macrophage migration inhibitory factor (MIF) is an upstream regulator of innate immunity, but its expression is increased in some cancers via stabilization with HSP90-associated chaperones. Here, we show that MIF stabilization is tumor-specific in an acute colitis-associated colorectal cancer (CRC) mouse model, leading to tumor-specific functions and selective therapeutic vulnerabilities. Therefore, we demonstrate that a *Mif* deletion reduced CRC tumor growth. Further, we define a dual role for MIF in CRC tumor progression. *Mif* deletion protects mice from inflammation-associated tumor initiation, confirming the action of MIF on host inflammatory pathways; however, macrophage recruitment, neoangiogenesis, and proliferative responses are reduced in *Mif*-deficient tumors once the tumors are established. Thus, during neoplastic transformation, the function of MIF switches from a proinflammatory cytokine to an angiogenesis promoting factor within our experimental model. Mechanistically, *Mif*-containing tumor cells regulate angiogenic gene expression via a MIF/CD74/MAPK axis in vitro. Clinical correlation studies of CRC patients show the shortest overall survival for patients with high MIF levels in combination with CD74 expression. Pharmacological inhibition of HSP90 to reduce MIF levels decreased tumor growth in vivo, and selectively reduced the growth of organoids derived from murine and human tumors without affecting organoids derived from healthy epithelial cells. Therefore, novel, clinically relevant Hsp90 inhibitors provide therapeutic selectivity by interfering with tumorigenic MIF in tumor epithelial cells but not in normal cells. Furthermore, *Mif*-depleted colonic tumor organoids showed growth defects compared to wild-type organoids and were less susceptible toward HSP90 inhibitor treatment. Our data support that tumor-specific stabilization of MIF promotes CRC progression and allows MIF to become a potential and selective therapeutic target in CRC.

Introduction

Macrophage migration inhibitory factor (MIF), which was originally discovered as a secreted proinflammatory cytokine with a central role in immune and inflammatory responses, has also been identified as a tumor promoter[1,2].

MIF is known to exert effects in epithelial cancer cells, stromal fibroblasts, endothelial cells, and immune cells[3–10]. In tumors, the major source of MIF is the epithelial cells themselves[11–13], followed by a minor secretory contribution from constituents of the tumor microenvironment, such as stromal and inflammatory cells[5,14,15]. Therefore, tumor cells aberrantly elevate MIF expression via Hsp90-mediated protein stabilization[10,11,16]. The HSP90 chaperone machinery is a prerequisite for tumorigenesis because it stabilizes oncogenic and tumor-promoting proteins, protecting them from degradation[17,18]. We previously

Correspondence: Ramona Schulz-Heddergott
(ramona.schulz@zentr.uni-goettingen.de)
[1]Institute of Molecular Oncology, University Medical Center Göttingen, Göttingen, Germany
[2]Department of General, Visceral, and Pediatric Surgery, University Medical Center Göttingen, Göttingen, Germany
Full list of author information is available at the end of the article
Edited by M. Agostini

identified MIF as an Hsp90-stabilized protein in breast cancer cells[11].

Colorectal cancer (CRC) patients also present elevated MIF levels, which are associated with a worse prognosis[12,15,19–22]. Among cancers, CRC has the third highest incidence[23]. Previous in vitro studies in human CRC cells showed that MIF increases proliferation, angiogenesis, and migration[12,24,25]. Functionally, MIF can bind to its main receptor CD74 to activate p38, MAPKs, or PI3K/AKT, which induces the expression of angiogenic factors[4,12,24,26–28]. Furthermore, MIF regulates therapeutic resistance via regulation of STAT3, MAPKs, AMPK, or hypoxia-dependent mechanisms[28–31]. Other studies using CT26 allograft models support that MIF promotes CRC progression[12,24]. In vivo, it has been shown that MIF stimulates the early stages of small intestinal adenomas in Apc^{min} mice[27]. Although all these studies showed a positive correlation between aberrant MIF function and CRC growth, an in vivo model of causative and severe CRC that mimics the human CRC was not available.

In our study, we investigated whether MIF promotes tumor growth in an autochthonous colorectal azoxymethane (AOM)/dextran sodium sulfate (DSS) mouse model and whether MIF can serve as a potential drug target. Because of the tumor-specific Hsp90-mediated stabilization of MIF, this protein could be selectively targeted in CRC. Our data suggest that MIF increases CRC growth and supports tumor-specific macrophage recruitment, tumor cell proliferation, and neoangiogenesis without affecting overall inflammation in established tumors.

Strikingly, a recent study in a mouse model of chronic colitis-dependent CRC reported a tumor-protective role for MIF[32]. This phenomenon was not observed in neither the Apc^{min} mouse model[27] nor several other in vivo cancer studies, including myc-induced lymphoma, chronic lymphocytic leukemia, breast, prostate, bladder, and skin cancer[3,4,11,33–38]. An important difference between the previous work and our study is that we used a mouse model of acute colitis-associated CRC, which is more similar to human sporadic CRC[39]. Importantly, in our sporadic CRC model, MIF as a tumor-promoting factor is selectively targetable in tumor cells by inhibiting Hsp90, supporting a strong rationale for MIF as a potential therapeutic target in sporadic CRC.

Results

MIF supports tumor growth in a mouse model of CRC

Given the importance of MIF in cancer and to determine whether MIF supports CRC tumorigenesis, we used the severe CRC AOM/DSS mouse model, which includes one phase of acute colitis (Fig. 1A). After a recovery phase, mice exclusively develop tumors within 12 weeks in the large intestine[40]. At 5 weeks post-AOM, when the tumors were macroscopically visualized by colonoscopy, $Mif^{-/-}$

Fig. 1 MIF supports tumor growth in a CRC mouse model. A Schematic of the AOM/DSS CRC mouse model. Visualization of tumor burden started at week 5 by colonoscopy. At 12 weeks post-AOM injection, established tumors were analyzed. **B** Representative colonoscopy images of the colonic lumen of the indicated genotypes at week 5 post-AOM. Dashed lines indicate the tumor borders. **C** Average number of tumors (left) and tumor sizes (right) in $Mif^{+/+}$ and $Mif^{-/-}$ mice at 5 weeks post-AOM injection. Numbers were determined by colonoscopy in living mice. S1 = small tumors to S3 = larger tumors. **D** Representative H&E-stained colonic tissues with tumors from $Mif^{+/+}$ and $Mif^{-/-}$ mice at week 12 post-AOM injection. Scale bars, 600 μm. **E** Average number of tumors per mouse (left) and tumor sizes (right) of the indicated mice at 12 weeks post-AOM injection. **C**, **E** *n*, mouse numbers. Black lines, mean. Student's *t* test of indicated groups.

Fig. 2 MIF levels are elevated in CRC cells. A Relative *MIF* mRNA expression of individual human CRC patients (P1–P3). Matched pairs of adjacent epithelia ('N') and their tumors ('T') were evaluated by qRT-PCR, and RNA levels were normalized to those of *RPLP0* mRNA. Mean ± SD of four technical replicates. Student's *t* test was performed for comparison of indicated groups; ***$p \leq 0.001$. **B** MIF protein levels in matched pairs of tumor ('T') and adjacent epithelial ('N') tissues from three individual human CRC patients (P1–P3). Immunoblot analysis. Actin, loading control. MIF expression ratios (MIF/Actin) were calculated by densitometry, normalized to the loading control, relative to the respective epithelium ('N'). **C** Histological MIF staining in a colonic tumor from a human CRC patient. Scale bar, 200 µm. **D** Representative histological Mif staining in colonic tumors from *Mif*^{+/+} and *Mif*^{−/−} mice. *Mif*^{−/−} tumors served as negative control. Rectangles represent the area at a higher magnification. MM, muscularis mucosae; MP, muscularis propria. White arrows, tumor epithelial cells with elevated MIF levels. #, stromal cells of mucosa. Gray arrows, epithelial cells within the next surrounding colonic tissue layer. *, MM and MP of the next surrounding layer. Note that normal epithelial cells from untransformed regions of the colon show low MIF levels (gray arrow) compared to those in tumor cells (white arrow). Scale bars, 200 µm. **E** Mif protein levels in murine single tumor samples ('T') compared to matched normal epithelium ('N') from *Mif*^{+/+} mice. *Mif*^{−/−} tumors served as a negative staining control. Mif ratios were calculated as described in (**B**). **F** Mif mRNA level in single tumor samples ('T') of *Mif*^{+/+} and *Mif*^{−/−} mice compared to pooled normal epithelium ('N') of *Mif*^{+/+} mice (*n* = 2). mRNA levels were normalized to those of *Rplp0* mRNA. Means ± SD of four technical replicates.

mice showed a reduction in the tumor burden (Fig. 1B). Quantification of colonic tumors by a scoring system[41,42] revealed a reduction in tumor multiplicity in *Mif*^{−/−} mice (Fig. 1C). Moreover, at 12 weeks post-AOM, during which the CRC tumors are well established, MIF deficiency decreased tumor burden and numbers (Fig. 1D, E). In summary, MIF supports tumor growth in an acute colitis-associated CRC mouse model.

MIF levels are elevated in CRC cells

During tumorigenesis, MIF protein levels are increased[12,27]. Our data confirm elevated MIF levels in cancer cells from CRC patients (Figs. 2A–C, S1A). Compared to the moderate increase in *MIF* mRNA levels (Figs. 2A, S1A), MIF protein levels were strongly increased in tumors from patients (Fig. 2B, C). Similar to the patient tumors, established AOM/DSS-induced

tumors confirmed tumor-specific elevation of MIF expression (Fig. 2D). Intriguingly, epithelial cancer cells express high levels of MIF compared to those in the normal surrounding epithelium (Fig. 2D), indicating that the major source of MIF is tumor epithelial cells. Measurement of MIF expression in murine tumor lysates indicated increased MIF expression in tumors compared to normal colonic tissue (Figs. 2E, F and S1B, C). Taken together, these results confirm an enhanced tumor-specific increase in MIF occurrence within the epithelial tumor compartment.

A *Mif* deletion protects mice from inflammation-associated cancer initiation

As a proinflammatory cytokine, MIF regulates immune responses and is suggested to be a link between inflammation and cancer[1,2]. Therefore, we hypothesized that the

loss of *Mif* expression protects mice during the colitis-associated phase of tumor initiation. Indeed, during the recovery phase, colonic tissue damage and epithelial cell loss, as reflected by the inflammatory score, were increased in $Mif^{+/+}$ mice compared to $Mif^{-/-}$ mice and were accompanied by increased immune cell infiltration (Fig. 3A, B). To further examine the inflammatory response, we histologically analyzed the immune cell composition within the tumor microenvironment. Infiltrates from the colonic tissue of $Mif^{+/+}$ mice had higher percentages of CD3-positive (T-lymphocyte marker), MPO-positive (neutrophil/granulocyte marker), and FoxP3-positive (regulatory T-cell marker) cells than did colonic tissue from $Mif^{-/-}$ mice (Figs. 3C, S2A). Immune infiltrates and the inflammatory score showed a positive

correlation (Figure S2B). Interestingly, CD68-positive (monocyte/macrophage marker) cell infiltration was unchanged between the two mice groups (Fig. 3C, S2A). Similar to the changes in the inflammatory cell composition, the expression of inflammation-associated cytokines was downregulated in $Mif^{-/-}$ tissues during the recovery period, confirming a reduction in inflammation in the absence of Mif (Fig. 3D, S2C). Consistent with the protective effect of *Mif* deletion during recovery, $Mif^{-/-}$ mice showed a reduced overall inflammatory response under DSS administration (Figures S2D-G). Furthermore, since MIF inhibits p53 activity[11,43], we pursued whether MIF interferes with the DNA damage response and apoptosis in response to AOM treatment. Surprisingly, neither the levels of phosphorylated histone H2A.X
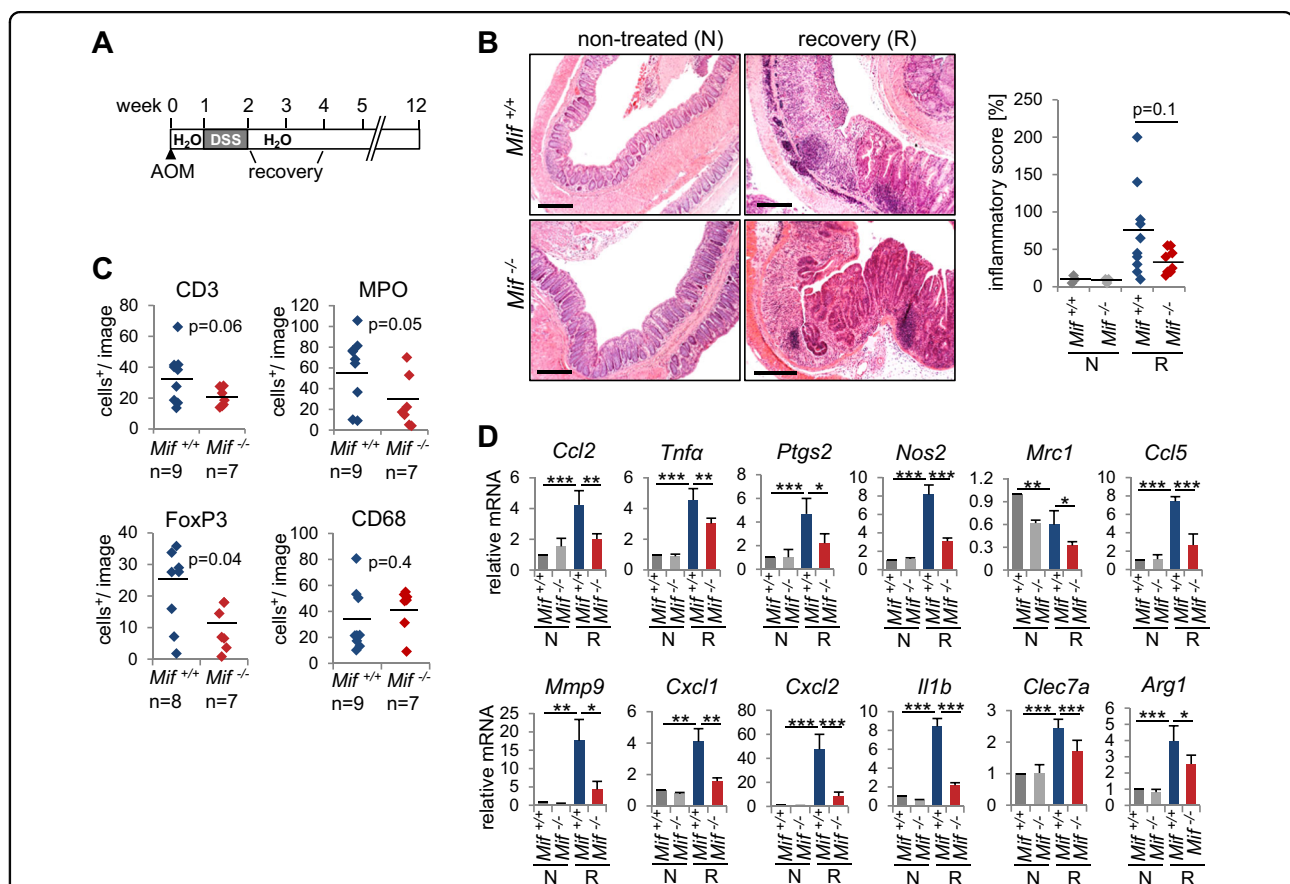
Fig. 3 A *Mif* deletion protects mice from inflammation-associated cancer initiation. A Schematic of the AOM/DSS mouse model. CRC was initiated by a single AOM injection, followed by one cycle of DSS administration. At 8 days of post-DSS treatment, mice were analyzed for recovery. **B** Representative H&E staining of colonic tissues from the indicated mice 8 days post-DSS (recovery = 'R') or from untreated control mice ('N'). Scale bars, 300 μm. (Right) The 'inflammatory score' was assessed based on tissue morphology and immune cell infiltration. (Left) Nontreated mice, $n = 3$/group; recovery $Mif^{+/+}$ mice, $n = 10$, $Mif^{-/-}$ mice, $n = 8$. Black lines, mean. p values were calculated with ANOVA Bonferroni's multiple comparison test; $p = 0.0455$. Indicated groups, calculated with Student's t test. **C** Quantification of the indicated histological staining of colonic tissues 8 days post-DSS ('recovery') in $Mif^{+/+}$ and $Mif^{-/-}$ mice. n, mouse numbers. Five to seven images (area = ×40 magnification) per mouse were analyzed for positively stained stromal cells. Black lines, mean. **D** mRNA levels of inflammatory genes in recovering ('R') and nontreated ('N') colonic tissues. Single samples from the indicated genotypes/groups were pooled (nontreated, $n \geq 3$; recovering tissue, $n \geq 4$). qRT-PCR was performed, and the expression levels were normalized to those of *Rplp0* mRNA. Means ± SD of ≥3 technical replicates/pools, each pipetted. **C**, **D** p values were calculated with Student's t test comparing the indicated groups. *$p \leq 0.05$, **$p \leq 0.01$, ***$p \leq 0.001$.

(a DNA damage marker) nor the expression of p53 target genes (*Mdm2, Cdkn1a, Ccnd1, Gadd45a,* and *Bax*) was altered in colonic tissues in *Mif*$^{-/-}$ mice compared to those in *Mif*$^{+/+}$ mice, suggesting that MIF failed to regulate an AOM-induced p53-dependent response in colonic epithelia (Figures S2H, I).

Overall, a *Mif* deficiency protected mice during the early phases of inflammation in the AOM/DSS model and demonstrated that during colitis-associated tumor initiation, MIF acts as a proinflammatory cytokine.

MIF supports CRC development via tumor-specific macrophage recruitment and angiogenesis without affecting overall inflammation

To determine whether MIF also acts as an inflammatory cytokine to support established tumors, we analyzed the expression of inflammatory markers at 12 weeks post-AOM. Interestingly, immunohistological staining (Figure S3A) and their corresponding quantifications (Fig. 4A) did not show any differences in the extent of infiltrating lymphocytes, regulatory T-cells or neutrophils/granulocytes within established tumors. In line with these findings, an assessment of inflammatory cytokines from tumor lysates failed to show major differences between *Mif*-expressing and *Mif*-deficient tumors, although all cytokines were upregulated in tumor samples ('T') compared to normal epithelium samples from untreated animals ('N') (Figure S3B). However, interestingly, CD68-positive macrophage/monocyte infiltration was decreased in *Mif*$^{-/-}$ tumors compared to *Mif*$^{+/+}$ tumors (Fig. 4B, upper panel), supporting the function of MIF as a chemokine to mediate macrophage recruitment[3,4,44]. To clarify whether elevated MIF expression in tumor cells mediates tumor-specific macrophage recruitment, we monitored the adjacent epithelium (Fig. 4B, lower panel). Indeed, macrophages specifically infiltrated tumors, suggesting that MIF regulates the chemotaxis of tumor-associated macrophages to promote CRC tumorigenesis. Tumor-associated macrophages are known to secrete tumor-promoting cytokines during cancer progression to stimulate tumor cell proliferation and angiogenesis[45,46]. Indeed, levels of Vegfa, an angiogenic cytokine known to be secreted by macrophages[46,47], are reduced in *Mif*$^{-/-}$ tumors (Figs. 4C, F, G, S3C). Moreover, in established CRC tumors, *Mif*$^{+/+}$ mice showed stronger vessel formation, as indicated by CD31-positive staining, compared to *Mif*$^{-/-}$ mice (Fig. 4D, E). Immunoblots confirmed increased activation of proangiogenic factors such as p38 and ERK in Mif-containing samples (Fig. 4F), an effect described previously[3,10,12,27,48]. MIF also affected tumor cell proliferation in AOM/DSS-induced tumors (Fig. 4H), which might explain the smaller tumors observed in *Mif*$^{-/-}$ mice (Fig. 1D, E).

Interestingly, Akt activity remained unchanged in *Mif*-deficient AOM/DSS tumors (Figure S3D), despite strong evidences that MIF activates PI3K/AKT in CRC[26] and other cancers[49,50].

Given that MIF also intrinsically regulates apoptosis via p53, e.g., in HER2-positive breast cancer or macrophages[11,51], we clarified whether the loss of MIF expression also activates p53 target genes in AOM/DSS tumors. In our CRC mouse model, *Mif* deficiency did not upregulate the expression of p53 target genes involved in apoptosis (e.g., *Bax, Bcl2l1, Bcl2,* and *Mcl1*) (Figure S3E). TUNEL staining confirmed the lack of altered apoptosis in *Mif*$^{-/-}$ tumors (Figure S3F). However, the expression of the cell cycle inhibitor *p21/Cdkn1a* was upregulated in *Mif*$^{-/-}$ tumors (Figure S3E), supporting the diminished proliferation upon MIF loss (Fig. 4H).

To assess whether angiogenesis and proliferation are affected during the recovery phase, we evaluated *Vegfa*, CD31, and Ki67 expression in colonic tissues at 8 days post-DSS (Figures S3G-K) and found that neither vessel formation and *Vegfa* expression nor proliferation was dependent on the presence of MIF during colonic tissue recovery.

Albeit our data confirmed that MIF supports inflammatory processes during colitis-associated tumor-initiating phases, we identified that in established tumors, MIF contributes to tumor-specific macrophage recruitment, tumor cell proliferation, and vessel formation without affecting overall inflammatory responses. Whether these infiltrated macrophages release proangiogenic cytokines[45,47] or whether MIF regulates angiogenic pathways in tumor cells themselves[52] must be further elucidated.

The CD74-MIF receptor complex facilitates the expression of proangiogenic factors in human CRC cells

MIF functions through CD74/CD44 and/or CXCR2/4 receptor complexes in proliferation, angiogenesis, and with its chemokine-like properties in monocyte and leukocyte recruitment[3,8,53–55]. The CD74 receptor is the main MIF receptor[53,56]. Since the expression of *Vegfa* is downregulated in *Mif*-deficient tumors (Figs. 4C, S3C), we examined whether tumor cells themselves are able to express angiogenic genes via MIF binding to CD74 to activate MAP kinases to induce *VEGF* and *IL8* expression[12,24,26–28]. First, we used the CD74-expressing (Fig. 5A) and MIF secreting HCT116 cell line[29,57]. Indeed, knockdown of either MIF or CD74 in HCT116 cells reduced *VEGFA* and *CXCL8/IL8* expression supporting a MIF-CD74 axis (Figs. S4A, 5B). Second, we used DLD-1 cells which do not express CD74 and are not shown to secrete MIF (Fig. 5A), thus, missing the prerequisites (secreted MIF and CD74) for a MIF-CD74 axis. As expected, in parental DLD-1 cells, depletion of MIF did not show any alterations in *VEGFA* and *CXCL8/IL8* expression (Figs. S4B, 5C). Moreover, supplementation of
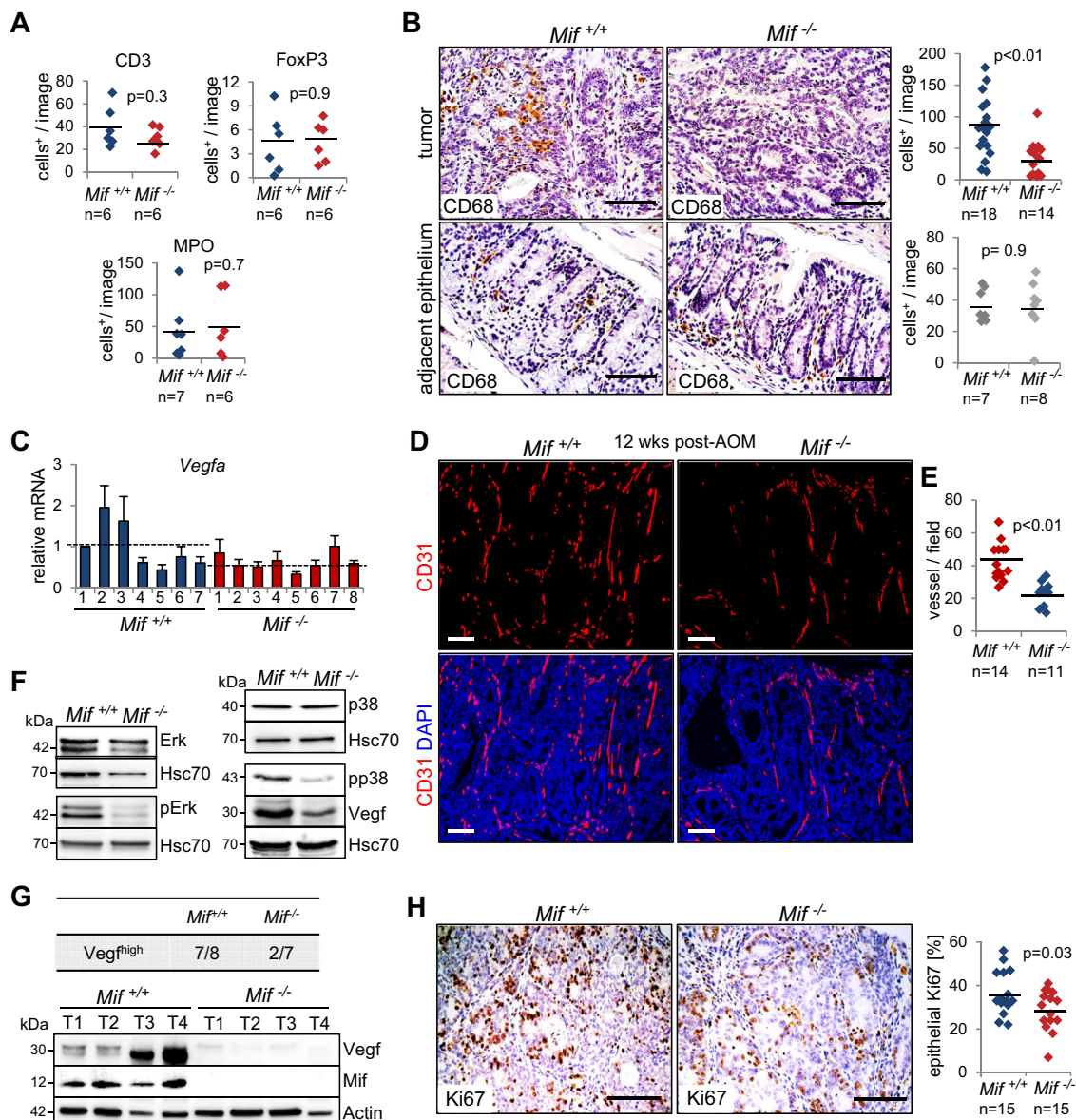
Fig. 4 MIF accelerates proliferation and angiogenesis in established colorectal tumors. A Quantification of the indicated histological staining of $Mif^{+/+}$ and $Mif^{-/-}$ tumors at 12 weeks post-AOM treatment. At least 2 images (area = ×40 magnification) per tumor were viewed for positive stromal cells. *n*, tumor number from 3 mice each. **B** Representative CD68 staining of indicted tumors and their corresponding adjacent normal epithelium at 12 weeks post-AOM injection. Scale bars, 100 μm. (Right) For each tumor, ≥3 images were taken, and positive staining was quantified. There were 18 tumors from 7 $Mif^{+/+}$ mice and 14 tumors from 8 $Mif^{-/-}$ mice. For adjacent epithelium, ≥5 images (area = ×40 magnification) per mouse were viewed and counted for positive stromal cells. *n*, mouse numbers. **C** mRNA levels of *Vegfa* in single tumors of different mice ($Mif^{+/+}$, *n* = 7; $Mif^{-/-}$ *n* = 8), relative to housekeeping gene, *Hprt1*. Means ± SD of four technical replicates. Black dashed line, mean. **D** Representative immunofluorescence for CD31 in tumors from $Mif^{+/+}$ and $Mif^{-/-}$ mice at 12 weeks post-AOM. DAPI, counterstaining. Scale bars, 100 μm. **E** Quantification of the vessel number from (**D**). Vessels from at least five images (area = ×40 magnification) per tumor were counted. A 'vessel' is defined as one separate fragment of CD31 staining. *n* = number of tumors out of 5 mice each. **F** Immunoblot analysis of $Mif^{+/+}$ and $Mif^{-/-}$ tumors at 12 weeks post-AOM with pooled samples (*n* ≥ 6 tumors per condition). Hsc70, loading control. **G** Summary of $Mif^{+/+}$ (*n* = 8) and $Mif^{-/-}$ (*n* = 7) tumors analyzed by immunoblot. (Bottom) Representative immunoblot analysis of single $Mif^{+/+}$ and $Mif^{-/-}$ tumors at 12 weeks post-AOM. Compared to a reference tumor (T1 of $Mif^{+/+}$), 'Vegf^high' means higher or same protein levels than the reference tumor. Actin, loading control. **H** Representative histological staining for Ki67 in tumors from $Mif^{+/+}$ and $Mif^{-/-}$ mice and quantification at 12 weeks post-AOM. Scale bars, 100 μm. Quantification of Ki67 staining counted within 2–4 images (area = ×40 magnification) per tumor. *n*, tumor number; both groups showed 15 tumors from 5 mice. **A**, **B**, **E**, **H** Black lines, mean. *p* values were calculated by Student's *t* test.
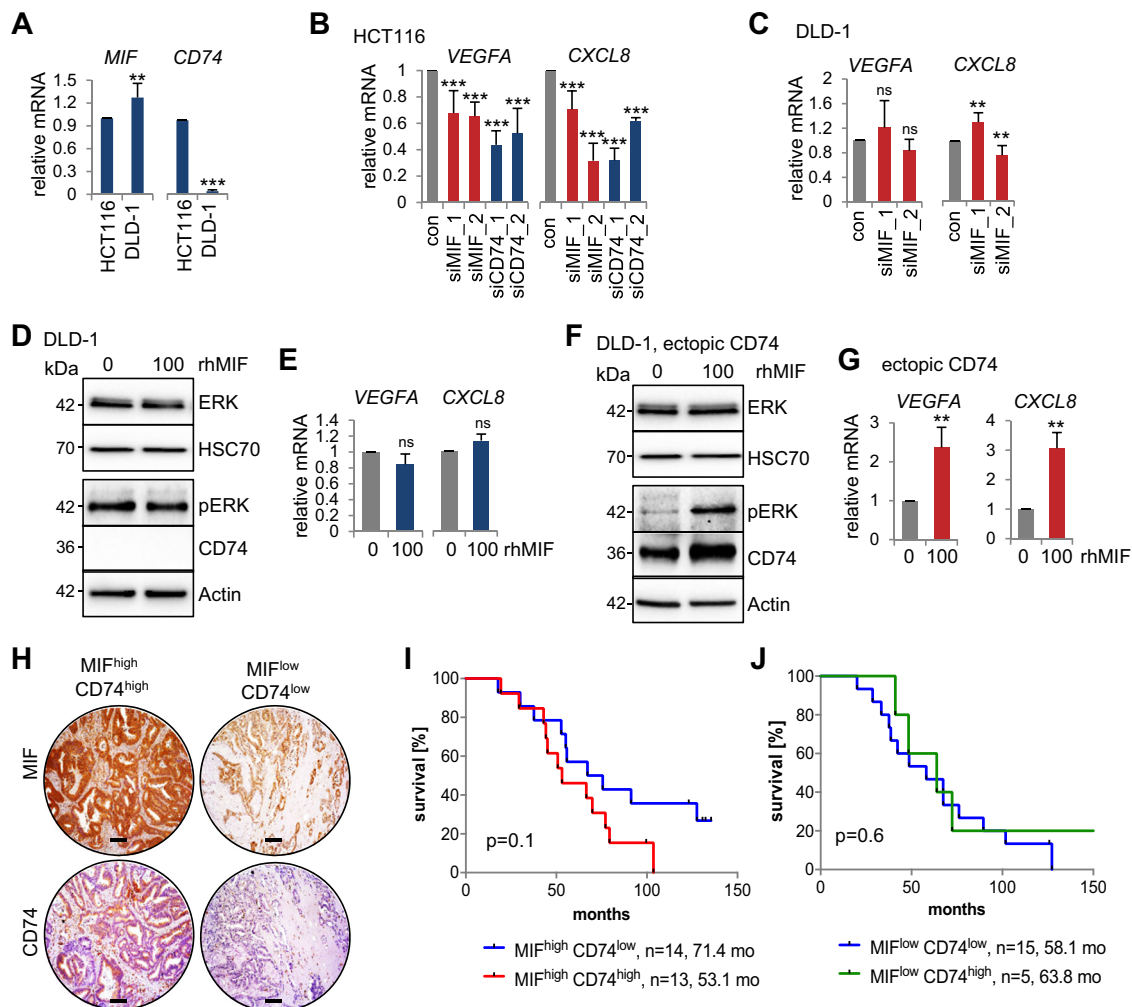
Fig. 5 The CD74-MIF receptor interaction facilitates the expression of angiogenic factors in CRC cells. A qRT-PCR analysis of the relative mRNA levels of *MIF* and *CD74* in HCT116 and DLD-1 CRC cells. Normalized to those of *RPLP0*. Means ± SD of 2 biological replicates with 3 technical replicates each. **B, C** Expression analysis of the indicated angiogenic genes in HCT116 (**B**) or DLD-1 (**C**) cells after siRNA-mediated knockdown of MIF or CD74 for 72 h; a scrambled siRNA served as the control ('con'). qRT-PCR were normalized to *HPRT1* or *RPLP0*, respectively. Means ± SD of ≥3 technical replicates from two biological replicates. **D, F** Angiogenic pathway analysis in CD74-deficient DLD-1 cells. 48 h after DLD-1 cells were transfected with an empty control (**D**) or CD74 overexpression plasmid (**F**), they were treated with 100 ng/mL recombinant human MIF (rhMIF) for 24 h. Immunoblots of CD74, pERK, and total ERK. Actin and Hsc70, loading controls. **E, G** Angiogenic marker expression (*VEGFA*, *CXCL8*). DLD-1 cells were treated as described in (**D, F**) followed by qRT-PCR. Expression of the indicated genes was normalized to that of *RPLP0*. Means ± SD of ≥3 technical replicates. **H** Representative images of serial sections from two human CRC patients stained for MIF and CD74 with different stabilization of MIF (MIF^{high}: stabilized, MIF^{low}: unstabilized) and expression levels of CD74 (CD74^{high}, CD74^{low}). Scale bars, 200 μm. **I, J** Correlation between patients with stabilized MIF (MIF^{high}) and CD74 levels (CD74^{high}, CD74^{low}) (**I**) and patients with unstabilized MIF (MIF^{low}) and CD74 levels (CD74^{high}, CD74^{low}) (**J**) on overall survival of patients. Log-rank (Mantel-Cox) test for comparison of indicated groups. **A, B, C, E, G** p values were calculated with Student's t tests for comparison of indicated groups; ns = not significant, *$p \le 0.05$, **$p \le 0.01$, ***$p \le 0.001$.

recombinant MIF (rhMIF) in DLD-1 cells to mimic MIF secretion, also failed to activate ERK or angiogenic gene expression (Fig. 5D, E). Importantly, supplementation of both, MIF by rhMIF and CD74 by plasmid-based ectopic expression, lead to ERK activation and increased *VEGFA* and *CXCL8/IL8* expression confirming that concomitant CD74 and secreted MIF are necessary for expression of angiogenic markers (Fig. 5F, G). To further investigate the MIF-CD74 axis, we performed clinical correlation studies based on MIF and CD74 expression levels of human CRC patients (Fig. 5H, I, J). Interestingly, simultaneous high levels of MIF and CD74 showed a trend for patient shortest survival (53.1 months) compared to stabilized MIF alone (71.4 months) (Fig. 5I). In contrast, CD74 status in patients with low MIF levels did not impact overall survival (Fig. 5J).

These findings underline the importance of MIF in cancer and support that MIF acts via CD74 in CRC.

MIF-driven CRC is vulnerable to Hsp90 inhibition

Next, we asked whether constitutive MIF stabilization in CRC cells creates vulnerabilities that can be therapeutically targeted. Since MIF is stabilized by Hsp90[11], we used the pharmacological Hsp90 inhibitor 17AAG. When $Mif^{+/+}$ and $Mif^{-/-}$ mice reached a defined tumor burden, they were treated with 17AAG (Fig. 6A). Hsp90 inhibition reduced MIF protein levels in AOM/DSS tumors (Fig. 6B) and showed a trend for decreased tumor burden in $Mif^{+/+}$ mice (Fig. 6C–E). Differences were not statistically significant but showed a trend in $Mif^{+/+}$ mice (Fig. 6D, E, left panels). By contrast, Hsp90 inhibition in $Mif^{-/-}$ mice failed to achieve tumor reduction (Fig. 6D, E, right panels).

To further support MIF as tumor-relevant Hsp90 client in CRC progression, we used genetically deleted MIF tumor organoid cultures. We observed a decreased growth in Mif-depleted organoids (Fig. 6F, G), further confirming, that MIF loss reduces tumor cell proliferation (Fig. 4H). Whether these growth defects arise from intracellular MIF functions and/or an MIF-CD74 axis remains elusive. Moreover, $Vegfa$ expression was reduced in those organoids (Fig. 6G). To further support MIF as a tumor-relevant Hsp90 substrate in CRC, we analyzed these Mif-depleted organoids after treatment with 17AAG (Fig. 6G, H). Indeed, a Mif depletion led to a decreased susceptibility toward 17AAG treatment compared to Mif-proficient organoids (Fig. 6H). Furthermore, apoptotic markers such as cleaved caspase-3 and Parp were only upregulated after 17AAG treatment in Mif-proficient organoids, but not in Mif-deficient organoids (Fig. 6I).

These data support a relevant point: Hsp90 inhibition seems to stronger target CRC tumors with elevated MIF, although the HSP90 system stabilizes innumerable oncogenes. These findings support that MIF is a tumor-relevant Hsp90 substrate in CRC.

MIF is a selective therapeutic target of Hsp90 inhibition in CRC-derived organoids

To exploit further therapeutically targeting of stabilized MIF, we administered Hsp90 inhibitors to healthy epithelial/mucosal-derived and tumor-derived murine colonic organoids from the same AOM/DSS-induced mice (i.e., matched pairs). Since organoids derived from mice with a 129S1/SvImJ background failed to grow in vitro in our laboratory (Figure S5A), we used C57BL/6 mice. Observation of the organoid morphology and the subsequent quantifications showed higher levels of cell death after 17AAG in tumor-derived organoids, compared to the epithelial-derived organoids (Fig. 7A). Immunoblot analysis confirmed strong reduction of Mif levels especially after treatment with 500 nM 17AAG (Fig. 7B). This prompted us to test Ganetespib and Onalespib, two clinically relevant second-generation HSP90 inhibitors that have been extensively tested in clinical trials and have a suitable toxicity profile[58–61]. Both inhibitors induced cell death to a far lesser extent in normal epithelial-derived organoids than in tumor-derived organoids (Fig. 7C) and showed promising specificity toward tumor organoids. Although Mif protein was degraded by Hsp90 inhibition in normal and tumor-derived organoids treated with either inhibitor (Fig. 7D), only tumor-derived organoids were morphologically disrupted upon Hsp90 inhibition (Fig. 7C), indicating that MIF plays a tumorigenic role rather than an essential function in normal epithelial cells. Importantly, and in line with our findings, we confirmed the enhanced Mif levels in tumor-derived organoids (Fig. 7B, D). Furthermore, in MIF-expressing patient-derived CRC organoids, Ganetespib markedly increased organoid death compared to that observed in the control organoids (Fig. 7E).

Therapeutic selectivity toward tumor cells plays an important role in therapy implementation. To further test whether Hsp90 inhibitors affect healthy tissues, we used organoids derived from the murine small intestine. Upon implementing the same treatment scheme as that used for colonic tumor-derived organoids, we discovered that 17AAG, Ganetespib, and Onalespib only exerted minor or no effects on the small intestine-derived organoids (Figure S5B). Indeed, Ganetespib failed to significantly degrade Mif protein in those organoids (Figure S5C), while another Hsp90 substrate, Stat3, was degraded. This confirms the selectivity of Hsp90 inhibition toward stabilized MIF in tumors. Even though immuno blot analysis also showed reduction of Mif levels after 17AAG treatment (Figure S5C), again depletion of unstabilized Mif in small intestinal organoids, did not impact morphology or survival of organoids (Figure S5B) as observed for normal colonic epithelia-derived organoids (Fig. 7A, B).

Thus, our findings highlight that MIF degradation via Hsp90 inhibition is a promising mechanism in CRC therapy. MIF acts not only as a critical driver in CRC but also as a selective target for Hsp90 inhibition in tumors.

Discussion

We used the immune-competent AOM/DSS mouse model, which mimics CRC progression in humans, to exploit the therapeutic potential of MIF. We demonstrated that MIF is specifically elevated in tumor cells and drives tumor growth in this acute colitis-associated ('sporadic') CRC model. Thus, in established tumors, stabilized MIF preferentially supports tumor-specific macrophage infiltration, vessel formation, and tumor cell proliferation.

Concomitantly, we also showed within this model that MIF regulates overall inflammatory signatures but especially during tumor initiation. Compared with $Mif^{+/+}$ mice, $Mif^{-/-}$ mice were protected against acute colitis-associated tumor initiation (Fig. 3), confirming the general function of MIF as a proinflammatory cytokine[3,10]. By

Fig. 6 MIF-driven CRC is vulnerable to Hsp90 inhibition. A Hsp90 inhibitor treatment timeline within the AOM/DSS mouse model. After tumors visualized via colonoscopy and scored as more than one S2/3 or three S1/2 tumors, mice were treated with the HSP90 inhibitor 17AAG for 3 weeks. **B** Representative histological Mif staining of tumor-bearing colonic tissue from $Mif^{+/+}$ mice after 3 weeks of 17AAG or vehicle treatment. White arrows indicate tumor epithelial cells with elevated Mif levels. Gray arrows indicate tumor cells with degraded Mif. #, normal epithelia of the next surrounding layer with low Mif levels. Scale bars, 100 µm. **C** Macroscopic overview of entire tumor-bearing colons from $Mif^{+/+}$ and $Mif^{-/-}$ mice after 3 weeks of treatment with 17AAG or vehicle. **D** Numbers of tumors per mouse as indicated in $Mif^{+/+}$ ($n = 5$ mice per group) and $Mif^{-/-}$ mice ($n = 3$ per group). Black lines, mean. p values with ANOVA, Bonferroni's multiple comparison test, $p = 0.212$. **E** Tumor sizes of mice from (D). Indicated groups, calculated with Student's t test. **F** Assessment of organoid growth in *Mif*-depleted organoids. $Mif^{fl/fl}$;*villincreERT2* mice with a defined tumor burden were treated with Tamoxifen (TAM) or respective vehicle control to generate *Mif*-deficient CRC tumors ($Mif^{\Delta/\Delta}$) to mimic a *Mif* epithelial-specific knockout. From those tumors, colonic tumor organoids were generated. Representative images and quantification of colonic tumor organoids (p 5) derived from oil ($Mif^{fl/fl}$) or TAM ($Mif^{\Delta/\Delta}$) treated mice. (right) At least 11 images were quantified from 10 different gel domes. Diameter of organoids was measured using ImageJ. Scale bars, 200 µm. Means ± SD from different images. **G** Expression analysis of *Mif* and *Vegfa* in $Mif^{fl/fl}$ or $Mif^{\Delta/\Delta}$ derived organoids. Via qRT-PCR, expression was co-normalized to *Rplp0* and *Hprt1*. Means ± SD of 4–5 technical replicates. **H** Imaging and quantification of organoid death of *Mif*-proficient (top) and *Mif*-deficient (bottom) organoids prepared as in (F) after 17AAG (500 nM) for 21 h. Scale bars, 200 µm. Quantifications based on organoid morphology. At least 5 images from ≥5 gel domes (×4 magnification each) per group were counted. The percentage of dead organoids was calculated to all organoids. Mean ± SD from ≥6 images. **I** Immunoblot of organoids of (**H**) at the endpoint of the experiment. Cc3 (cleaved caspase-3) and Parp (poly(ADP-ribose)-polymerase), apoptotic markers. Stat3 and Akt, further Hsp90 clients served as positive control for 17AAG functionality. Actin, loading control. **F**, **G**, **H** p values, *Student's* t tests for indicated groups.

contrast, established *Mif*-deficient tumors did not show reductions in overall inflammation (Fig. 4); rather, only tumor-associated macrophages significantly infiltrated $Mif^{+/+}$ tumors. Thus, MIF seems to lose its overall proinflammatory function once CRC tumors are

established. Proliferation, vessel formation and angiogenic cytokine expression were reduced in *Mif*-deficient tumors, an effect described previously[3,10,27,48].

Studies showing that human tumor cells themselves are able to activate MAPK-mediated *IL8* and *VEGF*
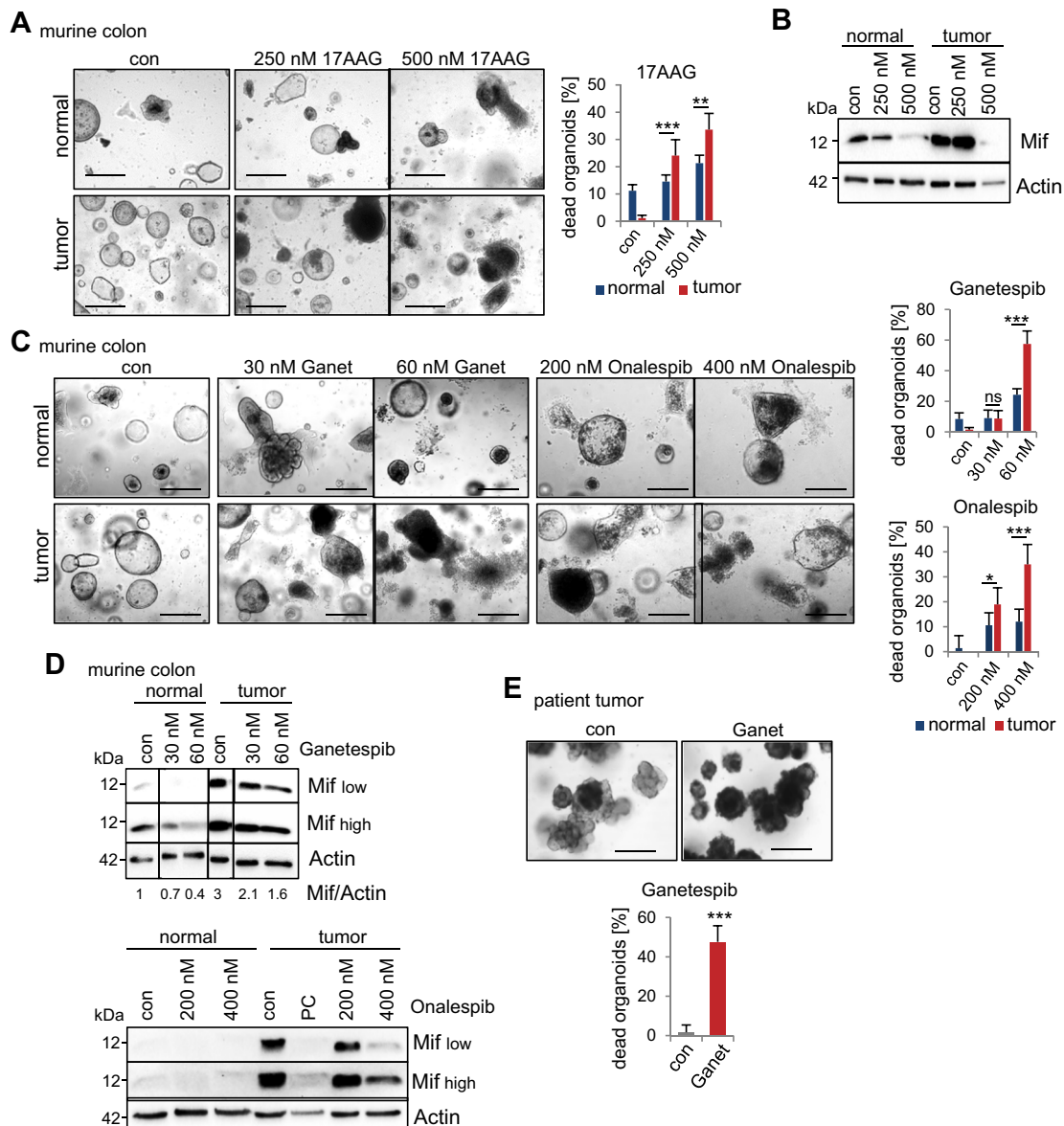
Fig. 7 MIF is an actionable and selective therapeutic target via Hsp90 inhibition in CRC-derived organoids. A, C Therapeutic selectivity of Hsp90 inhibitors. Representative images show colonic organoids derived from matched pairs of pooled $Mif^{+/+}$ tumors or their adjacent epithelium ('normal'). The indicated organoids were treated with DMSO ('con'), 17AAG (**A**), Ganetespib ('Ganet'), or Onalespib (**C**) at the indicated concentrations for 21 h. Scale bars, 200 µm. (Right) Quantifications based on organoid morphology. At least 6 images from ≥5 gel domes (×4 magnification each) per group were counted. For each group, number of dead organoids was calculated by the number of total organoids. The data are presented as the means ± SD from different images. **B, D** Hsp90 inhibitor treatment as described in (**A, C**) of matched pairs. Immunoblot analysis was performed to evaluate Mif degradation. 'Mif high' and 'Mif low' indicate exposure times during signal acquisition. Actin, loading control. PC, positive control. Mif/Actin, Mif expression ratios compared to Actin. **E** Representative images and quantification of organoids from patients with resectable CRC treated with 80 nM Ganetespib for 21 h. Scale bars, 200 µm. Quantification was performed as described in (**A**). Five images (×10 magnification) per condition were quantified. Means ± SD from different images. **A, C, E** Student's *t* test was performed for comparison of indicated groups; *$p ≤ 0.05$, **$p ≤ 0.01$, ***$p ≤ 0.001$.

expression by binding of MIF to its main receptor CD74[7,12,27,28,35,53] were confirmed within this study in human CRC cells (Fig. 5). Our data support that MIF can act in an autocrine MIF-CD74 manner in HCT116 CRC cells, resulting in accelerated expression of angiogenic factors. Furthermore, in DLD-1 cells, we supplemented recombinant MIF concomitantly with ectopic CD74 which mimics paracrine MIF-CD74 interactions to induce *VEGF* and *IL8*. In the in vivo CRC model, we assume that tumor epithelial cells do both, secrete MIF to recruit

macrophages to the tumor (which consequently secrete angiogenic factors) (Fig. 4B); and provide an autocrine MIF-CD74 interaction to induce the MAPK-VEGF axis (Fig. 5B and F), albeit we have not specifically tested it in this study. However, reduced expression of VEGF in *Mif*-deficient organoids (Fig. 6G), support the idea, that tumor cells themselves contribute to VEGF expression. Nevertheless, MIF is known to act as chemokine on tumor-specific macrophage recruitment and/or macrophage polarization, and macrophages are known to secrete angiogenic factors, further promoting CRC tumorigenesis[44,55]. In sum, tumor cells and tumor-associated macrophages might contribute to angiogenic factor expression but stabilized MIF in epithelial tumor cells provides the prerequisite for both scenarios.

To further test whether tumor epithelial cells with elevated MIF expression provide dual control over tumor growth, additional experimental models with inducible, tissue-specific *Mif* deletions are required. In principle, reduced chemotaxis of $Mif^{-/-}$ macrophages[62] or *Mif*-depleted fibroblasts within the tumor stroma[63] might also contribute to tumor reduction in $Mif^{-/-}$ mice.

The co-expression of MIF and CD74 seems to be important in tumorigenesis (Fig. 5), and either MIF or CD74 alone might not be strong tumor biomarkers. Our CRC patient study (Fig. 5H-J) as well as patient studies of lung cancer and colon carcinomatosis indicate that MIF/CD74 co-expression corresponds to an even worse prognosis[28,64]. Moreover, a recent mouse study revealed a strong upregulation of CD74 during colonic inflammation, promoting mucosal healing, and epithelial tissue recovery by enhanced cell proliferation[65]. While this study confirms the importance of a MIF/CD74 co-existence in proliferation, it also clarified that a CD74 deficiency alone massively increases overall inflammation with a reduced recovery rate[65]. In contrast, MIF deletion or ablation alone protects against inflammation, demonstrated in experimental models of gastrointestinal inflammation[66–68]. Why a CD74 single deletion intensifies inflammation remains speculative[65,69]. One explanation might be altered macrophage recruitment. $MIF^{-/-}$ macrophages exhibited reduced overall chemotaxis compared to wild-type macrophages, whereas $CD74^{-/-}$ macrophages showed random chemokinesis[62], leading to an accelerated inflammatory response. Moreover, receptors often co-regulate each other, and after CD74 loss, MIF might increase its affinity to CXCR2 and/or CXCR4 receptors driving inflammation instead of proliferation and angiogenesis[54,70]. Dual roles for ligand-receptor complexes are becoming increasingly evident in the context of active inflammation and mucosal recovery[69]. In sum, MIF/CD74 co-expression might be the major predictor for tumor growth in CRC.

MIF is mainly stabilized in tumors but not stromal or inflammatory cells (Fig. 2). MIF stabilization occurs via binding to Hsp90[16], which offers therapeutic approaches to target cancer cells via Hsp90 inhibition. We showed for the first time that clinically relevant Hsp90 inhibitors decreased MIF levels in CRC and subsequently reduced tumor growth (Figs. 6 and 7). Given the plethora of known Hsp90-stabilized oncogenes[18], it is interesting to see that Hsp90-mediated stabilization of MIF is critical for the survival of *Mif*-proficient murine colonic tumor-derived organoids (Fig. 6H). MIF reduced tumor-derived organoids show a reduced antitumor response to Hsp90 interference compared to that in *Mif*-proficient organoids, indicating that MIF is an important Hsp90-stabilized protein in CRC. Moreover, Hsp90 interference provides therapeutic selectivity toward tumor cells (Fig. 7). Since Hsp90 inhibitors exhibit fundamental differences in action[71], we focused on newly developed inhibitors such as Ganetespib and Onalespib.

In summary, since MIF stabilization is a crucial event, specifically in tumor cells, Hsp90 inhibition provides a potential approach to target MIF function in CRC. These findings support the tumor-promoting role of MIF in CRC and highlight the necessity to better understand the underlying MIF-induced tumorigenic mechanisms in CRC.

Materials and methods
Patient samples

Clinical samples (protein samples, RNA samples, PFA-fixed paraffin-embedded sections, patient tissue for cultivation) were provided by the Department of General, Visceral and Pediatric Surgery of the University Medical Center Göttingen (UMG, Germany).

Mouse models and genotyping

Mouse experiments were approved by state (Niedersächsisches Landesamt für Verbraucherschutz und Lebensmittelsicherheit, LAVES, Germany) and institutional (Göttingen University Medical Center) committees, which ensured that all experiments conformed to the relevant regulatory standards. Constitutive Mif knockout in the 129S1/SvImJ background has been described in detail in ref. [72]. DNA isolation and genotyping were performed using DirectPCR lysis Reagent and One-Taq®Quick-Load® MasterMix. Genotyping primers are specified in Supplemental Table 1. $Mif^{flox/flox}$ mice in C57BL/6NCrl background were described in detail[72,73]; and were used for the development of murine organoids. In brief, to remove floxed MIF alleles from colonic epithelial tissue, we crossed $Mif^{fl/fl}$ mice with *villinCreERT2*-harboring mice to generate $Mif^{fl/fl};villincreERT2$ transgenic mice. Mice were housed and handled under pathogen-free barrier conditions.

Murine CRC induction, colonoscopy, and treatment

For experiments, randomly selected 10-week-old female and male mice (>20 g) were used. For the induction of colorectal tumors, mice were treated with a single intraperitoneal injection of 10 mg/kg azoxymethane (AOM, Sigma-Aldrich) in 0.9% sodium chloride. After 1 week of rest, 1.5% (129S1/SvImJ background) or 2% (C57BL/6 background) DSS (MP-Biomedicals) was added to the drinking water for 6 consecutive days. Throughout the AOM/DSS phase, the body weights of the mice were continuously measured.

Five weeks after AOM induction, tumor development was monitored weekly by conducting a colonoscopy (Karl Storz GmbH) on anesthetized mice (1.5–2% isoflurane inhalation). Tumor sizes were determined according to the method described by Becker and Neurath[41] based on the colonic luminal perimeter as follows: S1 = just detectable, S2 = 1/8 of the lumen, S3 = 1/4 of the lumen, S4 = 1/2 of the lumen, and S5 > 1/2 of the lumen. For analysis of established tumors, we chose an endpoint study design, terminating the experiment at 12 weeks after AOM treatment to avoid losing mice to extraneous reasons such as intestinal obstruction and anal prolapse.

For pharmacological Hsp90 inhibitor analysis, tumors were visualized and validated by colonoscopy. Reaching a defined tumor burden, at least one S2/3 tumor and at least three S1/2 tumors when scored by colonoscopy, mice were treated with 17-allylamino, 17-demethoxygeldanamycin (17AAG, provided by the National Cancer Institute, NCI). Therefore, 17AAG was pre-dissolved in DMSO and further diluted in 10% DMSO/18% Kolliphor® RH40/3.6% Dextrose (Sigma-Aldrich) in H_2O. 60 mg/kg of 17AAG or vehicle were given by intraperitoneal injection for 5 days per week for 3 consecutive weeks. During 17AAG treatment, tumors were weekly visualized and monitored by colonoscopy.

At endpoints, mice were euthanized and the entire large intestine was harvested, longitudinally opened, and displayed. Tumor numbers were counted and sizes were measured with an electronic caliper. For subsequent analysis, single tumor biopsies were taken. Each large intestine was 'swiss rolled', fixed in 3.7% paraformaldehyde/PBS, processed for embedding and bisected. Both halves were placed into a mold for paraffin embedding.

For *Mif* depletion in vivo, AOM/DSS-treated *Mif*^{fl/fl} mice were used for Tamoxifen (TAM, Sigma-Aldrich) or respective vehicle control (oil). Reaching a defined tumor burden, at least one S2/3 tumor and at least three S1/2 tumors when scored by colonoscopy, mice were treated for 5 consecutive days, followed by 2 days of rest and another 3 days TAM/oil treatment. Twelve days after TAM-end, mice were dissected, and organoids were prepared (see section above).

All animal experiments were carried out in full agreement with the guidelines outlined above.

Human cell cultures, treatment, and transfection

The human CRC cell line DLD-1 was cultured in RPMI 1640 medium, whereas HCT116 CRC cells were cultured in McCoy's 5A modified medium. Media were supplemented with 10% FBS, Penicillin-Streptomycin, and L-glutamine (RPMI 1640). Cell lines were cultured at 37 °C and 5% CO_2 in a humidified atmosphere and were regularly tested for *Mycoplasma* contamination.

Knockdown of MIF or CD74 was achieved by siRNA transfection using Lipofectamine™3000 reagent according to the manufacturer's instructions. All siRNAs were purchased from Ambion and used according their guidelines; the sequences are listed in Supplemental Table 2. CD74 overexpression in DLD-1 cells was performed using Lipofectamine™3000 transfection reagent. In brief, 24 h after cell seeding, DLD-1 cells were cotransfected with 0.5 µg of GFP-containing plasmid and 1.5 µg of either pcDNA3.1-CD74 expression plasmid[56] or the corresponding pcDNA3.1/V5-His-TOPO control plasmid. Forty-eight hours post-transfection, cells were treated with recombinant human MIF as indicated.

HEK293T cell media conditioning for organoid culture medium

HEK293T cells expressing murine R-spondin-1 and Noggin or Wnt3a were cultivated in DMEM supplemented with 10% FBS, Penicillin-Streptomycin and Sodium Pyruvate in a humidified atmosphere at 37 °C with 5% CO_2. For HEK293T-mR-spondin-1 Zeocin and for HEK293T-mNoggin Geneticin were added to the medium during cultivation and expansion. For conditioning, medium was replaced by advanced DMEM/F12 medium supplemented with GlutaMAX™, Penicillin-Streptomycin, and 10 mM HEPES, and cells were cultivated for 1 week. For murine R-spondin-1-containing and Noggin-containing media, batch quality was examined using Dot-blot analysis. Murine colonic organoid culture medium contains advanced DMEM/F12 medium supplemented with 50% conditioned Wnt3a medium, 20% conditioned Noggin medium, 10% conditioned R-spondin-1 medium, N-2, B-27, 3.4 µg/mL ROCK inhibitor, 5 µM CHIR 99021, 500 nM A83-01, 10 mM Nicotinamide, 80 µM N-Acetyl-L-Cysteine, and 200 ng/mL rmEGF.

Preparation and cultivation of colonic and small intestinal organoids

Tumor-harboring large intestines of C57BL/6 mice were harvested. Three to four tumors per mouse and in parallel, parts of the normal epithelium were biopsied from the same mouse allowing generation of matched organoid pairs. Normal epithelial tissue was cut, washed,

and incubated in 4 mM EDTA/PBS for 30 min on ice. Pieces were thoroughly, mechanically dissociated in PBS. Tumor samples were digested with 2 mg/mL Collagenase type-I solution at 37 °C for 30 min. Normal crypts and tumor fragments were filtered using cell strainers. Cell pellets were washed, resuspended in cold Matrigel, and droplet-plated allowing Matrigel polymerization at 37 °C for 30 min. Organoids-containing domes were covered with organoid culture medium, cultivated at humidified 37 °C with 5% CO_2. Medium was exchanged every 2 to 3 days. Organoids splitting was performed once a week. For passaging, organoids were manually disrupted in ice-cold PBS, and cultured as described above.

Small intestinal tract starting from jejunum to the end of ileum were prepared from C57BL/6 mice, incubated in 5 mM EDTA/PBS for 30 min on ice, washed, and mechanically dissociated. Crypts were resuspended in cold Matrigel and cultured as colonic organoids, but with small intestinal organoid medium containing advanced DMEM/F12 supplemented with 20% conditioned mNoggin medium, 10% conditioned R-spondin-1 medium, N-2, B-27, 80 µM N-Acetyl-L-Cysteine, 50 ng/mL rmEGF.

Organoid treatments and morphological quantification

Experiment with matched pairs of normal epithelia-derived and tumor-derived colonic organoids, murine small intestinal organoids, and human organoids were performed between passage 2–7. HSP90 inhibitors 17AAG (National Cancer Institute, NCI), Onalespib and Ganetespib (Synta Pharmaceuticals) were dissolved in DMSO and used as indicated. For quantification of treatment response, light microscopy images of ≥5 Matrigel domes were taken from each condition. The amount of images was dependent on size and culture density as indicated. Based on morphology, dead organoids were defined as organoids with a partial or complete loss of outer epithelial barrier leading to disruption into clumps of dead cells or separation of dead cells[74]. The percentage of dead organoids was calculated relative to the total amount of organoids per image. For dead organoid quantification and measurement of organoid diameter ImageJ was used. For analysis of organoid lysates, Matrigel domes were disrupted using ice-cold PBS. Suspension was centrifuged and organoid-containing pellets were further washed and incubated with Cell Recovery solution (Corning) for complete removal of Matrigel. Organoids were resuspended in standard RIPA buffer for protein lysates and in TRIZOL for RNA isolation.

Histological analysis

Immunohistological stainings were performed with standardized protocols for formalin-fixed paraffin-embedded (FFPE) tissues. Following primary antibodies were used: MIF (Sigma-Aldrich, HPA003868), CD74 (Sigma-Aldrich, HPA010592), phospho-histone H2A.X (Ser139, Cell Signaling, #9718), Ki67 (Abcam, ab15580), Cluster of differentiation 31 (CD31 (SZ31), Dianova, DIA-310), Cluster of differentiation 3 (CD3 [SP7], Abcam, ab16669), Forkhead-box protein p3 (FoxP3, Abcam, ab54501), Myeloperoxidase (MPO, R&D Systems, AF3667). For CD68, two different antibodies were used to double-check staining (Abcam, ab53444 and eBioscience™, 14-0681-82). For detection of primary antibodies from rabbit and rat, ImmPRESS™ Reagent anti-Rabbit IgG and ImmPressTM Reagent anti-Rat IgG (both Vector Laboratories) were used. For antibodies from goat, the ABC detection system was used, entailing a biotinylated goat/sheep antibody (GE Healthcare) and ExtrAvidin®−Peroxidase (Sigma-Aldrich). As substrate for the horseradish peroxidases served 3,3′-Diaminobenzidine tetrahydrochloride (DAB, Roth). Counterstain of the nuclei was achieved using Mayers Hämalaun solution (Merck). Alexa Fluor®594-coupled secondary antibody was used as detection system for immunofluorescence with DAPI (Sigma-Aldrich) as counterstain for nuclei. Images were taken using a standard microscope (Carl Zeiss AG) with the ZEN imaging program from Zeiss. Figures were further prepared using Adobe Photoshop software. For quantification of staining, samples were blinded and positively stained cells were counted manually using CellCounter function of ImageJ. Percentage of epithelial Ki67-positive cells was determined relative to the total number of epithelial cells. For staining of CD31, CD68, CD3, FoxP3, and MPO, the number of positive cells was counted per image.

Hämalaun & Eosin G stained sections were used to determine the inflammatory score. The inflammatory score is based on morphological changes (grade of damage) of the tissue due to immune cell infiltration and epithelial layer disruption. Grade 0 = factor 0, no infiltration of immune cells, normal distribution of epithelia and amount of goblet cells; grade 1 = factor 1, minor infiltration of immune cells, epithelia is still intact and minor changes in goblet cell number; grade 2 = factor 2, moderate infiltration of inflammatory cells, epithelia is partly damaged and reduced number of goblet cells; grade 3 = factor 3, massive infiltration of immune cells, complete disruption/loss of epithelia and loss of goblet cells. For calculation, amount of tissue in percentage with respective grade of tissue damage was multiplied with the corresponding factor (factor 0–3). The obtained percentages were summed, resulting in a value for the inflammatory score (minimum 0−maximum 300) for each mouse. To ensure unbiased quantification, the inflammatory score was individually determined by one scientist and one pathologist.

TUNEL staining was used to detect DNA-strand breaks occurring during apoptotic cell death in established tumors. TUNEL reaction mix (Sigma-Aldrich) consists of TUNEL

enzyme solution and TUNEL label mix. The assay was performed according to manufactures guidelines. DAPI served as counterstaining, slides were mounted with Fluorescent Mounting Medium (DakoCytomation).

Quantitative immunohistochemistry on colon cancer patient samples

Section of a tissue micro array (TMA) for primary colonic tumors was kindly provided by the Department of Pathology of the University Medical Center Göttingen (UMG, Germany). According to described standard protocols for immunohistochemistry (see above), TMAs were stained for MIF (Sigma-Aldrich, HPA003868) and CD74 (Sigma-Aldrich, HPA010592). For CD74 staining tumors with more than 10% strongly positive stained cells or more than 40% overall stained cells with lower intensity were graded as high (CD74^{high}). For MIF staining, biopsis with high intensity in more than 70% of cells were graded as MIF^{high}. Biopsis with moderate or low intensity were graded as MIF[low].

Immunoblot analysis

For Whole lysates from human CRC cell lines and murine organoids were made with standard RIPA buffer (1% sodium deoxycholate, 10 mM EDTA, 1% Triton X-100, 0.1% SDS, 150 mM NaCl, 20 mM Tris-HCl pH 7.5, cOmplete[TM] mini protease inhibitor cocktail and phosphatase inhibitor mix consisting of 2 mM Imidazol, 1 mM sodium orthovanadate, and 1 mM sodium fluoride) was used. For protein extraction from human and murine samples, tissues were minced, lysed in RIPA buffer, and further processed by sonication. For determination of protein concentrations using BCA protein assay (Pierce), samples were centrifuged and supernatants were collected. Equal protein concentrations were separated by SDS gel electrophoresis and transferred onto nitrocellulose membranes (Amersham). After blocking with 5% milk (Roth), membranes were incubated with the following antibodies: MIF and CD74 (both Sigma-Aldrich); CDK4 and β-Actin (both Abcam); HSC70 [B-6], total AKT, phospho-AKT [D9E], phospho-p44/42 MAPK (ERK1/2), phospho-p38 MAPK [3D7], p38 MAPK, cleaved caspase-3, and PARP (all Cell Signaling); VEGF, STAT3, and ERK (all Santa Cruz). All primary antibodies were detected with HRP-conjugated secondary antibodies. Development of the signal was performed using Immobilion western chemiluminescent HRP substrate (Millipore/Merck) or Clarity Max™ Western ECL Substrate (BioRad). Detailed antibody information in Supplemental Table 2.

Quantitative real-time PCR (qRT-PCR)

RNA from human cell lines and colonic tissues and tumors was isolated using Trizol reagent (Invitrogen) according to manufacturer guidelines. Tissues and tumor pieces were shredded using a homogenizer (T10 basic ULTRA-TURRAX). After reverse transcription (M-MuLV Reverse Transcriptase from NEB) of equal amounts of mRNA, quantitative real-time PCR analysis was performed using a qPCR MasterMix (72 mM Tris-HCl pH 8.8 (Roth), 19 mM $(NH_4)_2SO_4$ (Roth), 0.01% Tween-20 (AppliChem), 3 mM $MgCl_2$, (Sigma-Aldrich), 1:80,000 SYBR Green (Invitrogen), 0.24 mM dNTPs, (dATP, dCTP, dGTP, dTTP, all dNTPs from Primetech), 19 U/ml Taq-polymerase (Primetech), 0.24% Triton X-100 (AppliChem), 300 mM Trehalose (Roth). Used primers are listed in Supplemental Table 1. For gene analysis, at least two different cDNAs (technical replicates) were used for qRT-PCR runs from one biological replicate. Biological replicates are independent experiments.

Quantification and statistical analysis

Statistics of each experiment such as number of animals, number of tumors, biological replicates, technical replicates, precision measures (mean and ±SD), and the statistical tests used for significance are provided in the figures and figure legends.

Densitometric measurements for quantification of immunoblot bands were done with the gel analysis software Image Lab™ (BioRad) and normalized to loading controls.

Pearson correlation factor R was used for analysis of immunohistochemical correlation studies on CRC tissue. GraphPad Prism was used for analysis of Kaplan–Meier survival curves with the Log-rank (Mantel-Cox) test.

The following designations for levels of significance were used within this manuscript: $*p \leq 0.05$; $**p \leq 0.01$; $***p \leq 0.001$; ns, not significant.

Author details
[1]Institute of Molecular Oncology, University Medical Center Göttingen, Göttingen, Germany. [2]Department of General, Visceral, and Pediatric Surgery, University Medical Center Göttingen, Göttingen, Germany. [3]Institute of Pathology, University Medical Center Göttingen, Göttingen, Germany. [4]Departments of Medicine, Pathology, and Epidemiology & Public Health, Yale School of Medicine and Yale Cancer Center, New Haven, CT, USA

Author contributions
Conceptualization: R.S.-H. and L.K.; methodology: R.S.-H., L.K., T.D.O., D.W., L.-C. C., N.W., and R.B.; acquisition of data: all authors; analysis and interpretation of

data: R.S.-H., L.K., D.W., and L.-C. C.; writing original draft: R.S.-H. and L.K.; writing, review, and editing: all authors; final approval: all authors; funding acquisition: R.S.-H.; supervision: R.S.-H.

Ethics approval
Patient samples (protein samples, RNA samples, PFA-fixed paraffin-embedded sections, patient tissue for cultivation) were provided by the Department of General, Visceral and Pediatric Surgery of the University Medical Center Göttingen (UMG, Germany) with approval from the ethics committee of UMG for the collection of CRC samples (approval numbers 9/8/08 and 25/3/17).

Conflict of interest
The authors declare that they have no conflict of interest.

References
1. Bucala, R. & Donnelly, S. C. Macrophage migration inhibitory factor: a probable link between inflammation and cancer. *Immunity* **26**, 281–285 (2007).
2. Conroy, H., Mawhinney, L. & Donnelly, S. C. Inflammation and cancer: macrophage migration inhibitory factor (MIF)—the potential missing link. *QJM* **103**, 831–836 (2010).
3. Gordon-Weeks, A. N., Lim, S. Y., Yuzhalin, A. E., Jones, K. & Muschel, R. Macrophage migration inhibitory factor: a key cytokine and therapeutic target in colon cancer. *Cytokine Growth Factor Rev.* **26**, 451–461 (2015).
4. Jankauskas, S. S., Wong, D. W. L., Bucala, R., Djudjaj, S. & Boor, P. Evolving complexity of MIF signaling. *Cell Signal* **57**, 76–88 (2019).
5. Mitchell, R. A. & Yaddanapudi, K. Stromal-dependent tumor promotion by MIF family members. *Cell Signal* **26**, 2969–2978 (2014).
6. Simons, D. et al. Hypoxia-induced endothelial secretion of macrophage migration inhibitory factor and role in endothelial progenitor cell recruitment. *J. Cell Mol. Med.* **15**, 668–678 (2011).
7. Amin, M. A. et al. Migration inhibitory factor mediates angiogenesis via mitogen-activated protein kinase and phosphatidylinositol kinase. *Circ. Res.* **93**, 321–329 (2003).
8. Asare, Y., Schmitt, M. & Bernhagen, J. The vascular biology of macrophage migration inhibitory factor (MIF). Expression and effects in inflammation, atherogenesis and angiogenesis. *Thromb. Haemost.* **109**, 391–398 (2013).
9. Lee, J. P. et al. Loss of autophagy enhances MIF/macrophage migration inhibitory factor release by macrophages. *Autophagy* **12**, 907–916 (2016).
10. O'Reilly, C., Doroudian, M., Mawhinney, L. & Donnelly, S. C. Targeting MIF in cancer: therapeutic strategies, current developments, and future opportunities. *Med. Res. Rev.* **36**, 440–460 (2016).
11. Schulz, R. et al. Inhibiting the HSP90 chaperone destabilizes macrophage migration inhibitory factor and thereby inhibits breast tumor progression. *J. Exp. Med.* **209**, 275–289 (2012).
12. He, X. X. et al. Macrophage migration inhibitory factor promotes colorectal cancer. *Mol. Med.* **15**, 1–10 (2009).
13. Hira, E. et al. Overexpression of macrophage migration inhibitory factor induces angiogenesis and deteriorates prognosis after radical resection for hepatocellular carcinoma. *Cancer* **103**, 588–598 (2005).
14. Maaser, C., Eckmann, L., Paesold, G., Kim, H. S. & Kagnoff, M. F. Ubiquitous production of macrophage migration inhibitory factor by human gastric and intestinal epithelium. *Gastroenterology* **122**, 667–680 (2002).
15. Morris, K. T., Nofchissey, R. A., Pinchuk, I. V. & Beswick, E. J. Chronic macrophage migration inhibitory factor exposure induces mesenchymal epithelial transition and promotes gastric and colon cancers. *PLoS ONE* **9**, e98656 (2014).
16. Schulz, R., Dobbelstein, M. & Moll, U. M. HSP90 inhibitor antagonizing MIF: The specifics of pleiotropic cancer drug candidates. *Oncoimmunology* **1**, 1425–1426 (2012).
17. Gomez-Pastor, R., Burchfiel, E. T. & Thiele, D. J. Regulation of heat shock transcription factors and their roles in physiology and disease. *Nat. Rev. Mol. Cell Biol.* **19**, 4–19 (2018).
18. Schopf, F. H., Biebl, M. M. & Buchner, J. The HSP90 chaperone machinery. *Nat. Rev. Mol. Cell Biol.* **18**, 345–360 (2017).
19. Chen, W. T. et al. Identification of biomarkers to improve diagnostic sensitivity of sporadic colorectal cancer in patients with low preoperative serum carcinoembryonic antigen by clinical proteomic analysis. *Clin. Chim. Acta* **412**, 636–641 (2011).
20. Lee, H. et al. Macrophage migration inhibitory factor may be used as an early diagnostic marker in colorectal carcinomas. *Am. J. Clin. Pathol.* **129**, 772–779 (2008).
21. Croner, L. J. et al. Discovery and validation of a colorectal cancer classifier in a new blood test with improved performance for high-risk subjects. *Clin. Proteom.* **14**, 28 (2017).
22. Yasasever, V. et al. Macrophage migration inhibitory factor in cancer. *Cancer Invest.* **25**, 715–719 (2007).
23. Marmol, I., Sanchez-de-Diego, C., Pradilla Dieste, A., Cerrada, E. & Rodriguez Yoldi, M. J. Colorectal carcinoma: a general overview and future perspectives in colorectal cancer. *Int. J. Mol. Sci.* **18**, https://doi.org/10.3390/ijms18010197 (2017).
24. Ogawa, H. et al. An antibody for macrophage migration inhibitory factor suppresses tumour growth and inhibits tumour-associated angiogenesis. *Cytokine* **12**, 309–314 (2000).
25. Shin, H. N., Moon, H. H. & Ku, J. L. Stromal cell-derived factor-1alpha and macrophage migration-inhibitory factor induce metastatic behavior in CXCR4-expressing colon cancer cells. *Int. J. Mol. Med.* **30**, 1537–1543 (2012).
26. Sun, B. et al. Induction of macrophage migration inhibitory factor by lysophosphatidic acid: relevance to tumor growth and angiogenesis. *Int. J. Mol. Med.* **12**, 633–641 (2003).
27. Wilson, J. M. et al. Macrophage migration inhibitory factor promotes intestinal tumorigenesis. *Gastroenterology* **129**, 1485–1503 (2005).
28. Bozzi, F. et al. MIF/CD74 axis is a target for novel therapies in colon carcinomatosis. *J. Exp. Clin. Cancer Res.* **36**, 16 (2017).
29. Cheon, S. K. et al. Macrophage migration inhibitory factor promotes resistance to MEK blockade in KRAS mutant colorectal cancer cells. *Mol. Oncol.* **12**, 1398–1409 (2018).
30. Russo, R. et al. Macrophage migration inhibitory factor is a molecular determinant of the anti-EGFR monoclonal antibody cetuximab resistance in human colorectal cancer cells. *Cancers* **11**, https://doi.org/10.3390/cancers11101430 (2019).
31. Yao, K. et al. Macrophage migration inhibitory factor is a determinant of hypoxia-induced apoptosis in colon cancer cell lines. *Clin. Cancer Res.* **11**, 7264–7272 (2005).
32. Pacheco-Fernandez, T. et al. Corrigendum to "Macrophage migration inhibitory factor promotes the interaction between the tumor, macrophages, and T cells to regulate the progression of chemically induced colitis-associated colorectal cancer". *Mediators Inflamm.* **2020**, 2195341, https://doi.org/10.1155/2020/2195341 (2020).
33. Hussain, F. et al. Human anti-macrophage migration inhibitory factor antibodies inhibit growth of human prostate cancer cells in vitro and in vivo. *Mol. Cancer Ther.* **12**, 1223–1234 (2013).
34. Martin, J. et al. Macrophage migration inhibitory factor (MIF) plays a critical role in pathogenesis of ultraviolet-B (UVB) -induced nonmelanoma skin cancer (NMSC). *FASEB J.* **23**, 720–730 (2009).
35. Choudhary, S. et al. Macrophage migratory inhibitory factor promotes bladder cancer progression via increasing proliferation and angiogenesis. *Carcinogenesis* **34**, 2891–2899 (2013).
36. Talos, F., Mena, P., Fingerle-Rowson, G., Moll, U. & Petrenko, O. MIF loss impairs Myc-induced lymphomagenesis. *Cell Death Differ.* **12**, 1319–1328 (2005).
37. Reinart, N. et al. Delayed development of chronic lymphocytic leukemia in the absence of macrophage migration inhibitory factor. *Blood* **121**, 812–821 (2013).
38. Nemajerova, A., Mena, P., Fingerle-Rowson, G., Moll, U. M. & Petrenko, O. Impaired DNA damage checkpoint response in MIF-deficient mice. *EMBO J.* **26**, 987–997 (2007).

39. De Robertis, M. et al. The AOM/DSS murine model for the study of colon carcinogenesis: from pathways to diagnosis and therapy studies. *J. Carcinog.* **10**, 9 (2011).

40. Tanaka, T. et al. A novel inflammation-related mouse colon carcinogenesis model induced by azoxymethane and dextran sodium sulfate. *Cancer Sci.* **94**, 965–973 (2003).

41. Becker, C., Fantini, M. C. & Neurath, M. F. High resolution colonoscopy in live mice. *Nat. Protoc.* **1**, 2900–2904 (2006).

42. Becker, C. et al. In vivo imaging of colitis and colon cancer development in mice using high resolution chromoendoscopy. *Gut* **54**, 950–954 (2005).

43. Hudson, J. D. et al. A proinflammatory cytokine inhibits p53 tumor suppressor activity. *J. Exp. Med.* **190**, 1375–1382 (1999).

44. Yaddanapudi, K. et al. Control of tumor-associated macrophage alternative activation by macrophage migration inhibitory factor. *J. Immunol.* **190**, 2984–2993 (2013).

45. Owen, J. L. & Mohamadzadeh, M. Macrophages and chemokines as mediators of angiogenesis. *Front Physiol.* **4**, 159 (2013).

46. Mehrad, B., Keane, M. P. & Strieter, R. M. Chemokines as mediators of angiogenesis. *Thromb. Haemost.* **97**, 755–762 (2007).

47. Corliss, B. A., Azimi, M. S., Munson, J. M., Peirce, S. M. & Murfee, W. L. Macrophages: an inflammatory link between angiogenesis and lymphangiogenesis. *Microcirculation* **23**, 95–121 (2016).

48. Nishihira, J. et al. Macrophage migration inhibitory factor (MIF): its potential role in tumor growth and tumor-associated angiogenesis. *Ann. N. Y Acad. Sci.* **995**, 171–182 (2003).

49. Lue, H. et al. Macrophage migration inhibitory factor (MIF) promotes cell survival by activation of the Akt pathway and role for CSN5/JAB1 in the control of autocrine MIF activity. *Oncogene* **26**, 5046–5059 (2007).

50. Oliveira, C. S. et al. Macrophage migration inhibitory factor engages PI3K/Akt signalling and is a prognostic factor in metastatic melanoma. *BMC Cancer* **14**, 630 (2014).

51. Mitchell, R. A. et al. Macrophage migration inhibitory factor (MIF) sustains macrophage proinflammatory function by inhibiting p53: regulatory role in the innate immune response. *Proc. Natl Acad. Sci. USA* **99**, 345–350 (2002).

52. Hanahan, D. & Weinberg, R. A. Hallmarks of cancer: the next generation. *Cell* **144**, 646–674 (2011).

53. Leng, L. et al. MIF signal transduction initiated by binding to CD74. *J. Exp. Med.* **197**, 1467–1476 (2003).

54. Zernecke, A., Bernhagen, J. & Weber, C. Macrophage migration inhibitory factor in cardiovascular disease. *Circulation* **117**, 1594–1602 (2008).

55. Yaddanapudi, K. & Mitchell, R. A. In *MIF Family Cytokines in Innate Immunity and Homeostasis* (eds Richard Bucala & Jürgen Bernhagen) 59–76 (Springer International Publishing, 2017).

56. Shi, X. et al. CD44 is the signaling component of the macrophage migration inhibitory factor-CD74 receptor complex. *Immunity* **25**, 595–606 (2006).

57. Hu, C. T. et al. MIF, secreted by human hepatic sinusoidal endothelial cells, promotes chemotaxis and outgrowth of colorectal cancer in liver prometastasis. *Oncotarget* **6**, 22410–22423 (2015).

58. Jhaveri, K. & Modi, S. Ganetespib: research and clinical development. *Onco Targets Ther.* **8**, 1849–1858, (2015).

59. Alexandrova, E. M. et al. Improving survival by exploiting tumour dependence on stabilized mutant p53 for treatment. *Nature* **523**, 352–356 (2015).

60. Do, K. et al. Phase I study of the heat shock protein 90 (Hsp90) inhibitor onalespib (AT13387) administered on a daily for 2 consecutive days per week dosing schedule in patients with advanced solid tumors. *Invest. N. Drugs* **33**, 921–930 (2015).

61. Graham, B. et al. The heat shock protein 90 inhibitor, AT13387, displays a long duration of action in vitro and in vivo in non-small cell lung cancer. *Cancer Sci.* **103**, 522–527 (2012).

62. Fan, H. et al. Macrophage migration inhibitory factor and CD74 regulate macrophage chemotactic responses via MAPK and Rho GTPase. *J. Immunol.* **186**, 4915–4924 (2011).

63. Petrenko, O., Fingerle-Rowson, G., Peng, T., Mitchell, R. A. & Metz, C. N. Macrophage migration inhibitory factor deficiency is associated with altered cell growth and reduced susceptibility to Ras-mediated transformation. *J. Biol. Chem.* **278**, 11078–11085 (2003).

64. McClelland, M., Zhao, L., Carskadon, S. & Arenberg, D. Expression of CD74, the receptor for macrophage migration inhibitory factor, in non-small cell lung cancer. *Am. J. Pathol.* **174**, 638–646 (2009).

65. Farr, L. et al. CD74 Signaling Links Inflammation to Intestinal Epithelial Cell Regeneration and Promotes Mucosal Healing. *Cell Mol. Gastroenterol. Hepatol.*, https://doi.org/10.1016/j.jcmgh.2020.01.009 (2020).

66. de Jong, Y. P. et al. Development of chronic colitis is dependent on the cytokine MIF. *Nat. Immunol.* **2**, 1061–1066 (2001).

67. Ohkawara, T. et al. Amelioration of dextran sulfate sodium-induced colitis by anti-macrophage migration inhibitory factor antibody in mice. *Gastroenterology* **123**, 256–270 (2002).

68. Wong, B. L. et al. Essential role for macrophage migration inhibitory factor in gastritis induced by *Helicobacter pylori*. *Am. J. Pathol.* **174**, 1319–1328 (2009).

69. Hoffmann, A., Zwissler, L. C., El Bounkari, O. & Bernhagen, J. Studying the pro-migratory effects of MIF. *Methods Mol. Biol.* **2080**, 1–18 (2020).

70. Schwartz, V. et al. A functional heteromeric MIF receptor formed by CD74 and CXCR4. *FEBS Lett.* **583**, 2749–2757 (2009).

71. Neckers, L. et al. Methods to validate Hsp90 inhibitor specificity, to identify off-target effects, and to rethink approaches for further clinical development. *Cell Stress Chaperones* **23**, 467–482 (2018).

72. Fingerle-Rowson, G. et al. The p53-dependent effects of macrophage migration inhibitory factor revealed by gene targeting. *Proc. Natl Acad. Sci. USA* **100**, 9354–9359 (2003).

73. Brocks, T. et al. Macrophage migration inhibitory factor protects from non-melanoma epidermal tumors by regulating the number of antigen-presenting cells in skin. *FASEB J.* **31**, 526–543 (2017).

74. Grabinger, T. et al. Ex vivo culture of intestinal crypt organoids as a model system for assessing cell death induction in intestinal epithelial cells and enteropathy. *Cell Death Dis.* **5**, e1228 (2014).

Supplemental material
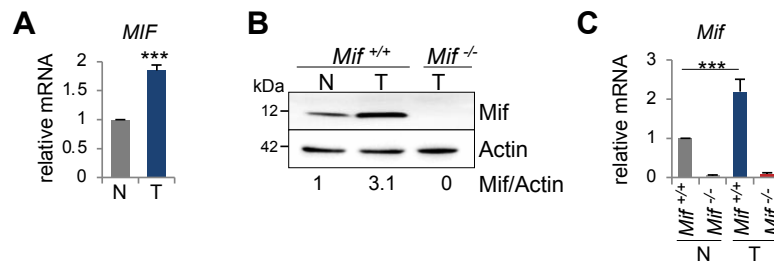
Supp Figure 1

Figure S1: Related to Figure 2. **MIF levels are elevated in colorectal cancer cells.** (A) Pooled cases of single patients (P1-P3), including tumor samples ('T') and their adjacent normal epithelium ('N') (n=3 each). qRT-PCRs normalized to *RPLP0* mRNA. *MIF* expression in tumor samples was calculated relative to respective adjacent epithelium. Mean ± SD of 3 technical replicates in duplicates. (B) Mif protein level in pooled samples of tumors ('T') and normal epithelium ('N') of *Mif*^{+/+} mice. *Mif*^{-/-} tumors serve as negative staining control. Mif ratios (Mif/Actin) were calculated by densitometry, normalized to loading control, relative to *Mif*^{+/+} epithelium ('N'). (C) Relative *Mif* mRNA levels of pooled normal ('N', n≥2) and tumor ('T', n=6) samples from *Mif*^{+/+} and *Mif*^{-/-} mice. Mean ± SD of 5 technical replicates in duplicates. (A, C) Student's t test used for comparison of indicated groups: ***p≤0.001.

A

B

C

D

E

non-treated (N)   short (S)

F

Supp Fig 2

G

H post-AOM treatment

I

Supp Fig 2 ext
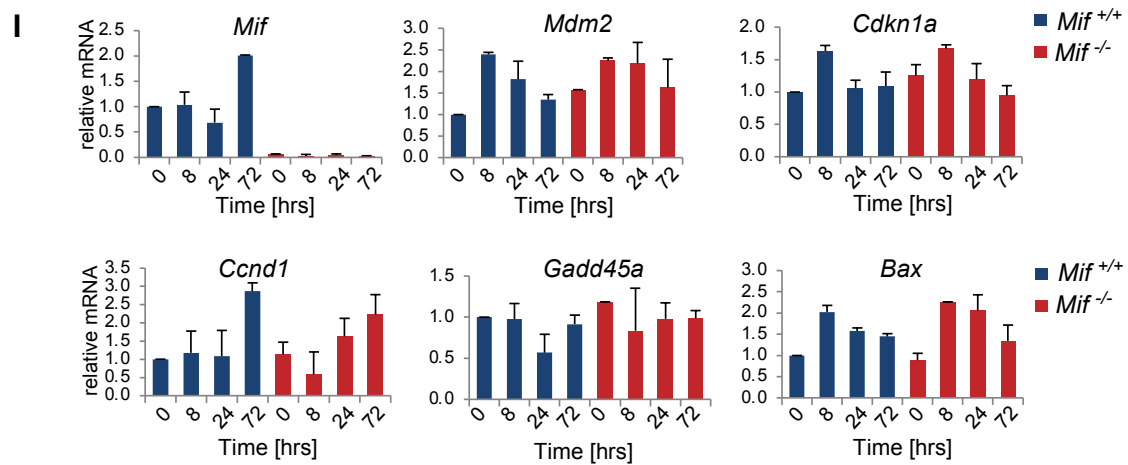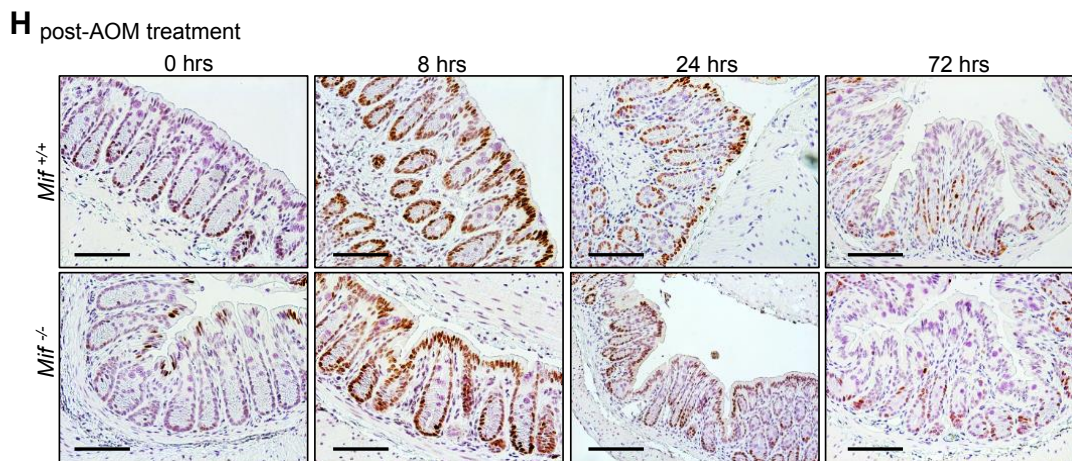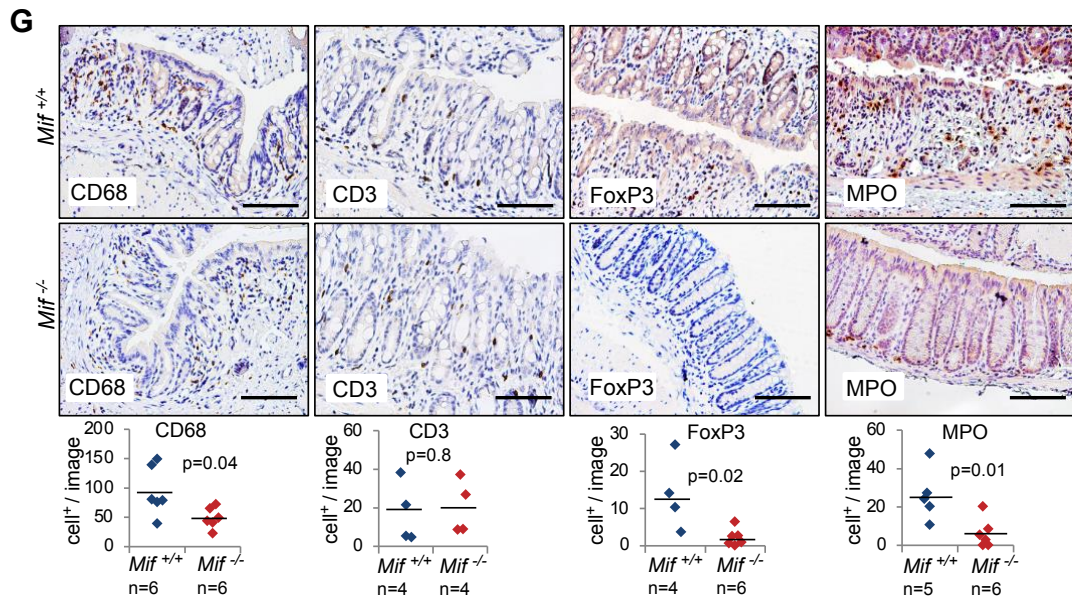
Figure S2: Related to Figure 3. **A MIF deletion protects mice from inflammation-associated cancer initiation.** (A) Histological staining of colonic tissues 8 days after DSS (recovery period) of indicated genotypes. Inflammatory marker CD68 (Cluster of Differentiation 68) for monocytes/macrophages, CD3 (Cluster of Differentiation 3) for T-lymphocytes, FoxP3 (Foxhead-box-protein P3) for regulatory T-cells and MPO (Myeloperoxidase) for neutrophils/granulocytes. Scale bars, 100 μm. (B) Correlation between the inflammatory score of $Mif^{+/+}$ and $Mif^{-/-}$ mice (Figure 3B) and the respective quantification of infiltrating immune cells (CD3, MPO and FoxP3 staining) in the recovery group from (Figure 3C). CD3, MPO and FoxP3 with $Mif^{+/+}$ n=6 and $Mif^{-/-}$ n=7. R, Pearson correlation factor. (C) mRNA expression of representative cytokines of individual mice from recovery group (8 days post-DSS) from single samples (4 mice per group). Via qRT-PCR, expression levels were normalized to those of *Rplp0*. Means $\pm$ SD of ≥2 technical replicates in duplicates. (D) Treatment scheme of the AOM/DSS colorectal cancer mouse model. Mice of the 'short' group were dissected at day 3 after starting DSS administration. (E) Representative H&E staining of colonic tissues of indicated genotype at day 3 after DSS start (short, 'S') or in untreated control tissue ('N'). Scale bar, 100 μm. (F) The inflammatory score of the 'short' DSS and control groups was assessed based on H&E stained tissue morphology in (E). Non-treated control n=3 mice per group, short n=6 mice per group. Black line, mean. p value with Student's t test. (G) Representative histology of inflammatory cells (CD68, CD3, FoxP3, MPO staining) in $Mif^{+/+}$ and $Mif^{-/-}$ colonic tissues at day 3 after DSS start. Scale bars, 100 μm. For quantifications of histological staining, 4-5 images (area=40x magnification) per mouse were counted for positive stained stromal cells. n, number of mice. Black line, mean. p values were calculated via Student's t test. (H) A MIF loss is dispensable for AOM-induced DNA damage response. Representative immunohistological phospho-Histone H2A.X staining after the initial AOM injection at indicated time points. Scale bars, 100 μm. (I) A MIF loss does not impair the AOM-induced p53 response. mRNA level of *Mif* and WTp53 target genes of indicated groups at different time points after a single AOM injection. Single colonic tissues of indicated time points and genotypes were pooled (n≥3 mice per group). qRT-PCRs normalized to *Rplp0* mRNA. Mean $\pm$ SD of 2 technical replicates, pipetted in duplicates.
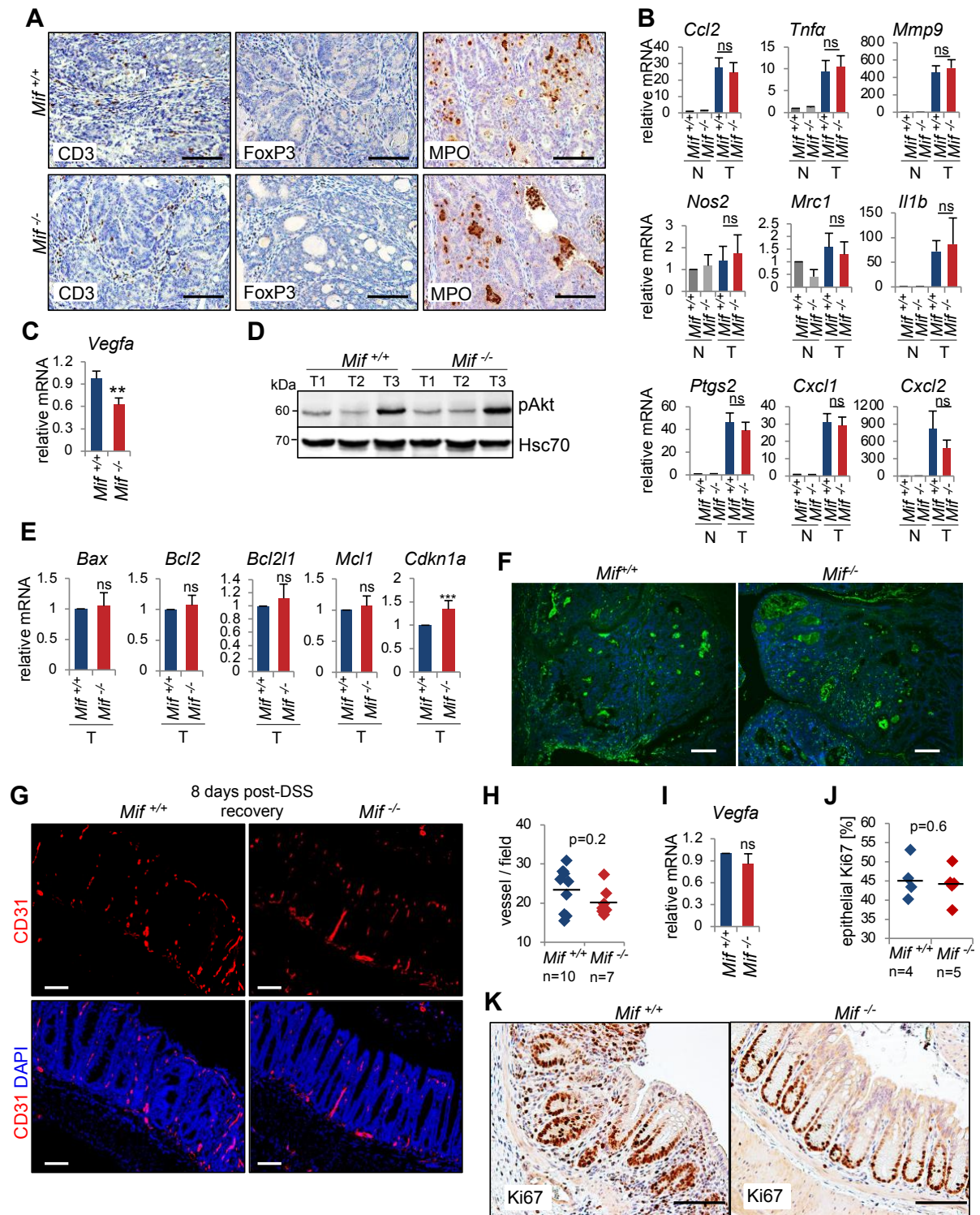
Supp Figure 3

Figure S3: Related to Figure 4. **MIF supports CRC tumor growth and macrophage infiltration without affecting overall inflammation.** (A) Representative histology of CD3, FoxP3 and MPO staining of $Mif^{+/+}$ and $Mif^{-/-}$ tumors. Scale bars, 100 µm. (B) mRNA expression of inflammatory genes in tumors ('T') and nontreated control tissues ('N') of indicated genotypes. Single colonic tissues (n≥2) or single tumors (n≥6) of indicated genotypes were pooled. qRT-PCR, expression levels were normalized to those of *Rplp0*. Means ± SD of 3-4 technical replicates in duplicate. Student's t test. (C) Relative expression of *Vegfa*, averaged from single tumor samples (7-8 mice) (Figure 4C). Means ± SD of 4 technical replicates. (D) Phospho (p)-Akt level of single tumors (T1-T3) of $Mif^{+/+}$ and $Mif^{-/-}$ mice. Hsc70, loading control. (E) Apoptotic gene expression of indicated tumors. Pooled single tumors (n≥6). qRT-PCR normalized to *Rplp0* mRNA. Mean ± SD of ≥5 technical replicates in duplicates. p value with Student's t test. ***p≤0.001; ns, not significant. (F) TUNEL staining in $Mif^{+/+}$ and $Mif^{-/-}$ tumors at 12 weeks post-AOM. Scale bars, 100 µm. (G, H) Representative immunofluorescence of $Mif^{+/+}$ and $Mif^{-/-}$ colonic tissue at 8 days post-DSS (recovery group), for CD31 (red) and DAPI (blue). Scale bars, 100 µm. Quantification of tumor vessel fragment density from (G). At least 6 images (area=40x magnification) per colonic tissue were counted and calculated. Black lines, mean. n, number of mice. p value with Student's t test. (I) Relative expression of *Vegfa* in recovering $Mif^{+/+}$ and $Mif^{-/-}$ colonic tissue (pool of 4-5 mice per group). Via qRT-PCR expression was calculated relative to those of *Rplp0*. Mean ± SD of 3 technical replicates in duplicates. p value with Student's t test. ns, not significant. (J, K) Quantification of epithelial Ki67 staining (J) and representative histology of recovering $Mif^{+/+}$ and $Mif^{-/-}$ colonic tissue at 8 days post-DSS (K). Ki67 positivity was performed using 6 images per mouse. n, number of mice. Normalization of positive epithelial cells to total number of epithelial cells. p value with Student's t test. Scale bars, 100 µm.
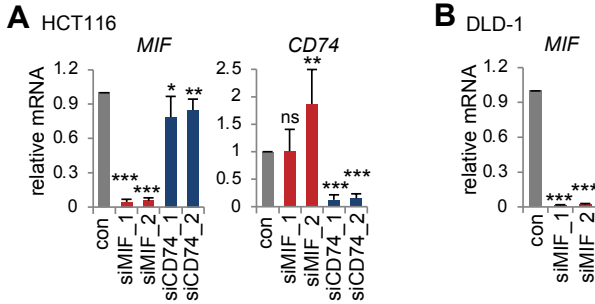
Supp Figure 4

Figure S4: Related to Figure 5. **Knockdown efficiency of MIF and CD74 by small interfering RNA (siRNA) in CRC epithelial cells.** (A, B) Expression of *MIF* and *CD74* in HCT116 (A) and DLD-1 (B) cells normalized to *RPLP0* or *HPRT1* respectively for evaluation of knockdown efficiency after 72 hrs siRNA transfection against *MIF*, *CD74* or respective scrambled control ('con'). Mean ± SD of 5-6 technical replicates in duplicates from 2 biological replicates. Student's t test: ns=not significant, *p≤0.05; **p≤0.01; ***p≤0.001.
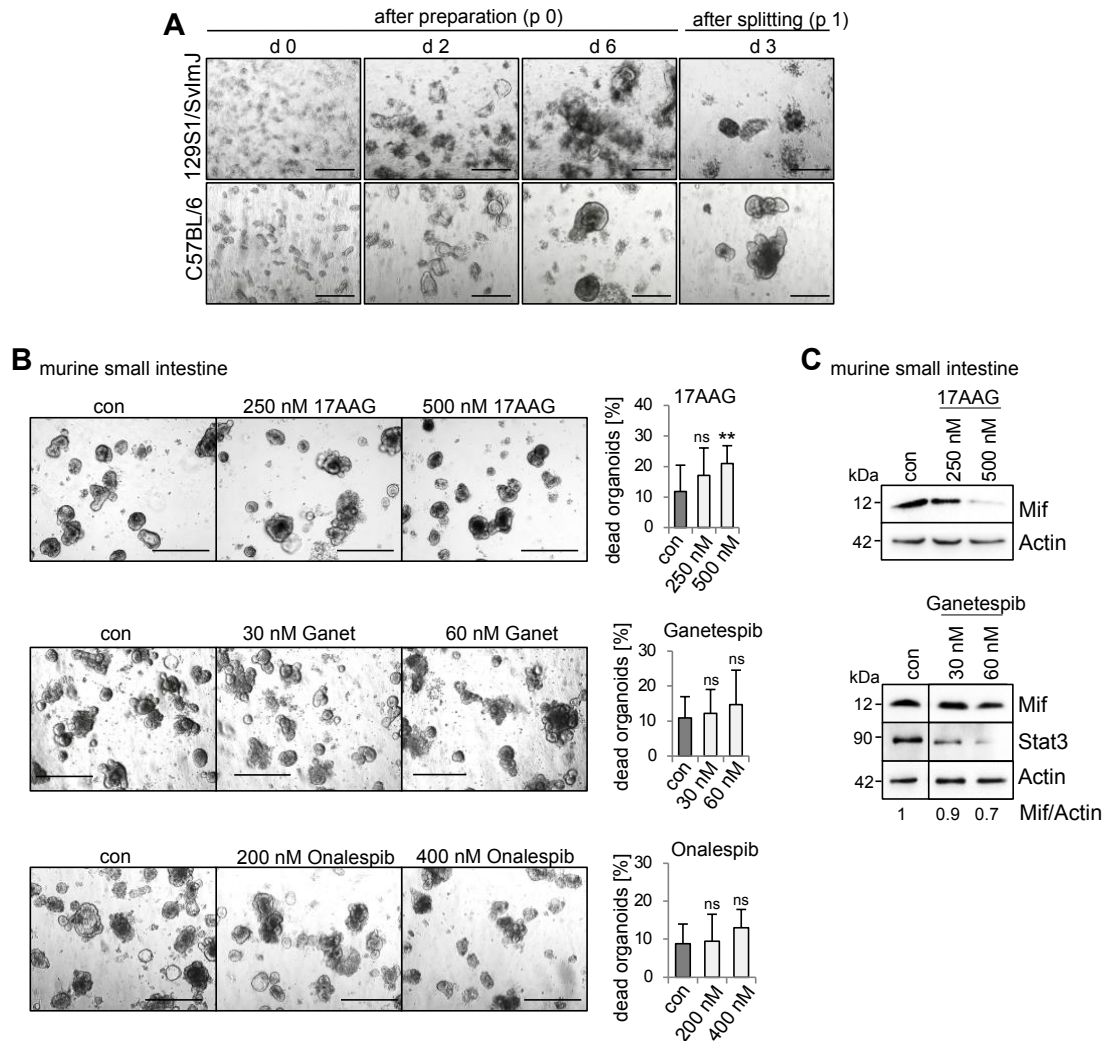
Supp Figure 5

Figure S5: Related to Figure 7. **MIF is an actionable and selective therapeutic target by Hsp90 inhibition in colorectal cancer-derived organoids.** (A) Representative images to evaluate growth and development of normal colonic organoids from two different mouse strains (129S1/SvImJ and C57BL/6). Images were taken at day of organoid preparation (d 0) as well as two (d 2) and six (d 6) days after preparation (p0=passage 0). Additional image taken three (d 3) days after splitting (p1=passage 1). Scale bars, 200 µm. (B) Representative images of murine normal small intestinal organoids after treatment with DMSO control ('con') and indicated concentrations of 17AAG, Ganetespib ('Ganet') or Onalespib for 21 hrs. Scale bars, 200 µm. Quantification reveal percentage of dead organoids relative to the total amount of organoids (≥9 images per condition from ≥5 gel domes). Mean ± SD from different images. p values in relation to control ('con'). *p≤0.05; ***p≤0.001. (C) Hsp90 inhibitor treatment as in (B) of matched pairs. Immunoblot analysis to evaluate Mif degradation. Well known Hsp90-stabilized protein Stat3 used as positive control for the treatment. Actin, loading control. Mif expression ratios (Mif/Actin) were calculated by densitometry, normalized to the loading control, vehicle control.

Supplemental Table 1: Primers

Gene	Origin	Forward	Reverse
Quantitative RT-PCR			
RPLP0 (36B4)	Human	5'-GATTGGCTACCCAACTGTTG	5'-CAGGGGCAGCAGCCACAAA
HPRT1	Human	5'-CCTGGCGTCGTGATTAGTGAT	5'-GGGCTACAATGTGATGGCCT
MIF_1	Human	5'-AGCAGCTGGCGCAGGCCAC	5'-CTCGCTGGAGCCGCCGAAGG
MIF_2	Human	5'-GCAGCTGGCGCAGGCCAC	5'-GGAGCCGCCGAAGGCCATGA
CD74	Human	5'-GGCAACATGACAGAGGACCA	5'-AGTGACTCTTTCGGTGGAGC
CXCL8 (IL8)_1	Human	5'-GCTCTGTGTGAAGGTGCAGTT	5'-AATTTCTGTGTTGGCGCAGT
CXCL8 (IL8)_2	Human	5'-ACACTGCGCCAACACAGAAA	5'-TTGCTTGAAGTTTCACTGGCAT
VEGFA	Human	5'-CTCCACCATGCCAAGTGGT	5'-GTCCACCAGGGTCTCGATTG
Rplp0 (36B4)	Mouse	5'-GCAGATCGGGTACCCAACTGTT	5'-CAGCAGCCGCAAATGCAGATG
Mif_1	Mouse	5'-TCCGTGCCAGAGGGGTTTCTGT	5'-ACGTTGGCAGCGTTCATGTCG
Mif_2	Mouse	5'-CTCCGTGCCAGAGGGGTTTCT	5'-GCACCACCGATCTTGCCGATG
Arg1	Mouse	5'-GAGCATGAGCTCCAAGCCAA	5'-TCTCTCACGTCATACTCTGTTTCT
Bax	Mouse	5'-GCTGATGGCAACTTCAACTGG	5'-TGATCAGCTCGGGCACTTTAG
Bcl2	Mouse	5'-GACTGAGTACCTGAACCGGC	5'-AGTTCCACAAAGGCATCCCAG
Bcl2l1	Mouse	5'-TCGCCGGAGATAGATTTGAATAACC	5'-TGGGCTCAACCAGTCCATTG
Ccl2	Mouse	5'-GTCCCTGTCATGCTTCTGGG	5'-GAGTAGCAGCAGGTGAGTGG
Ccl5	Mouse	5'-TCACCATATGGCTCGGACA	5'-TTCTCTGGGTTGGCACACAC
Ccnd1	Mouse	5'-GGAGCTGCTGCAAATGGAAC	5'-CAGTCCGGGTCACACTTGA
Cdkn1a (p21)	Mouse	5'-GTGGCCTTGTCGCTGTCTT	5'-GCGCTTGGAGTGATAGAAATCTG
Clec7a_1	Mouse	5'-AGGAAGCCGGGCTCCAT	5'-TACCACAAAGCACAGGATTCCTAAA
Clec7a_2	Mouse	5'-TGGGTGCCCTAGGAGGTTT	5'-AACCATGGCCCTTCACTCTG
Cxcl1 (Kc)	Mouse	5'-GCTGGGATTCACCTCAAGAA	5'-CTTGGGGACACCTTTTAGCA
Cxcl2	Mouse	5'-CTCTCAAGGGCGGTCAAAAG	5'-TTGGTTCTTCCGTTGAGGGAC
Gadd45a	Mouse	5'-AAGCTGCTCAACGTAGACCCC	5'-ATCCATGTAGCGACTTTCCCG
Il1b	Mouse	5'-AGCTTCCTTGTGCAAGTGTCT	5'-GACAGCCCAGGTCAAAGGTT
Mcl1	Mouse	5'-TAAGGACGAAACGGGACTGG	5'-AGTTTGGTGGCTGGAGCTTTA
Mdm2	Mouse	5'-GGTCCCTGTCCTTTGATCCG	5'-GCTCACTTACGCCATCGTCA
Mmp9	Mouse	5'-TCTGTCCAGACCAAGGGTACA	5'-GCCTTGGGTCAGGCTTAGAG
Mrc1	Mouse	5'-TTGGTGGCAATTCACGAGAG	5'-GGGAAGGGTCAGTCTGTGTTTG
Nos2	Mouse	5'-CCCTCCTGATCTTGTGTTGGA	5'-CAACCCGAGCTCCTGGAAC
Ptgs2	Mouse	5'-TCCTGACCCACTTCAAGGGA	5'-CTCCTTATTTCCCTTCACACCCA
Tnfa	Mouse	5'-AGGGATGAGAAGTTCCCAAATG	5'-TGTGAGGGTCTGGGCCATA
Vegfa_1	Mouse	5'-ACTGGACCCTGGCTTTACTG	5'-GATCCGCATGATCTGCATGG
Vegfa_2	Mouse	5'-CTGGACCCTGGCTTTACTGC	5'-TGAACTTGATCACTTCATGGGACT
Genotyping			
Mif A1	Mouse	5'-AGGTTAGTCACTCTACTGGCC	
Mif B1	Mouse	5'-TCTCACTGTTCTGGTGTGAGG	
Mif C1	Mouse	5'-GGCTCCTGGTCTCAGTCAGG	
Vil Cre	Mouse	5'-CGCGAACATCTTCAGGTTCT	
Vil Cre	Mouse	5'-CAAGCCTGGCTCGACGGCC	

Supplemental Table 2: Reagents and Resources

REAGENT or RESOURCE	SOURCE	IDENTIFIER (Cat#)
Antibodies		
Rabbit polyclonal anti-Akt	Cell Signaling	9272, RRID:AB_329827
Rabbit monoclonal anti-phospho-Akt (Ser473) [D9E]	Cell Signaling	4060, RRID:AB_2315049
Mouse polyclonal anti-beta-Actin	Abcam	ab6276, RRID:AB_2223210
Rabbit polyclonal anti-beta-Actin	Abcam	ab8227, RRID:AB_2305186
Rabbit monoclonal anti-CD3 [SP7]	Abcam	ab16669, RRID:AB_443425
Rat monoclonal anti-CD31 [SZ31]	Dianova	DIA-310, RRID:AB_2631039
Rat monoclonal anti-CD68 [FA-11]	Abcam	ab53444, RRID:AB_869007
Rat monoclonal anti-CD68 [FA-11]	eBioscience™	14-0681-82, RRID:AB_2572857
Rabbit polyclonal anti-CD74	Sigma-Aldrich	HPA010592, RRID:AB_1078482
Rabbit monoclonal anti-Cleaved Caspase-3 [5A1E]	Cell Signaling	9664, RRID:AB_2070042
Rabbit polyclonal anti-FoxP3	Abcam	ab54501, RRID:AB_880110
Rabbit monoclonal anti-Histone H2A.X, phospho (Ser139) [20E3]	Cell signaling	9718, RRID:AB_2118009
Mouse monoclonal HSC70 [B-6]	Santa Cruz	sc-7298, RRID:AB_627761
Rabbit polyclonal anti-Ki67	Abcam	ab15580, RRID:AB_443209
Rabbit polyclonal anti-p38 MAPK	Cell Signaling	9212, RRID:AB_330713
Rabbit monoclonal anti-phospho-p38 MAPK (Thr180/Tyr182) [3D7]	Cell Signaling	9215, RRID:AB_331762
Rabbit polyclonal anti-ERK	Santa Cruz	sc-94, RRID:AB_2140110
Rabbit monoclonal anti-phospho-p44/42 MAPK (Erk1/2) (Thr202/Tyr204) [D13.14.4E]	Cell Signaling	4370, RRID:AB_2315112
Rabbit polyclonal anti-MIF	Sigma-Aldrich	HPA003868, RRID:AB_1079290
Goat polyclonal anti-MPO	R&D system	AF3667, RRID:AB_2250866
Rabbit polyclonal anti-PARP	Cell Signaling	9542, RRID:AB_2160739
Rabbit polyclonal anti-STAT3	Santa Cruz	sc-482, RRID:AB_632440
Mouse monoclonal anti-VEGF [C1]	Santa Cruz	sc-7269, RRID:AB_628430
donkey anti-rat IgG (H+L) Alexa Fluor 594	Invitrogen	A-21209, RRID:AB_2535795
ExtrAvidin®−Peroxidase	Sigma-Aldrich	E2886, RRID:AB_2620165
biotinylated goat/sheep antibody	GE Healthcare	RPN1025-2ML, RRID:AB_1082105
ImmPRESS™ Reagent Anti-Rabbit IgG	Vector Laboratories	MP-7401, RRID:AB_2336529
ImmPRESS™ Reagent Anti-Rat IgG, mouse adsorbed	Vector Laboratories	MP-7444, RRID:AB_2336530
goat anti-rabbit IgG-HRP	Santa Cruz	sc-2004, RRID:AB_631746
goat anti-mouse IgG-HRP	Santa Cruz	sc-2005, RRID:AB_631736
Bacterial strains		
Bacteria: ElectroMAX DH10B cells	Invitrogen/Thermo Fisher Scientific	18290-015
Chemicals, Peptides and Recombinant Proteins		
0.9% sodium chloride	B. Braun	2001675
17AAG	Provided by NCI	N/A
3,3'-Diaminobenzidine tetrahydrochloride (DAB)	Roth	CN75.2
Ammonium sulfate $(NH_4)_2SO_4$	Roth	9218.1
AOM (Azoxymethane)	Sigma-Aldrich	A5486
BCA protein assay	Pierce	23227
Clarity Max™ Western ECL Substrate	BioRad	1705062
cOmplete™ mini protease inhibitor cocktail	Roche	11836170001
Cycloheximide	Sigma-Aldrich	C7698
DAPI	Sigma-Aldrich	D9542
dATP	Primetech	1202.4
dCTP	Primetech	1203.4

Dextrose	Sigma-Aldrich	D9434
dGTP	Primetech	1204.4
DirectPCR lysis Reagent	Peqlab	31-101-T
DSS (Dextran sodium sulfate)	MP Biomedicals	160110
dTTP	Primetech	1205.4
EDTA	Roth	8040.1
Eosin G	Roth	7089.1
Fluorescent Mounting Medium	DakoCytomation	S302380-2
Ganetespib	Provided by Synta Pharmaceuticals	N/A
Onalespib (AT13387)	Selleckem	S1163
HRP substrate	Millipore/Merck	WBKLS0500
Imidazole	Roth	3899.2
Isoflurane CP	CP-Pharma	1214
Kolliphor® RH 40	Merck	07076
Lipofectamine™ 3000 Transfection Reagent	Invitrogen	L3000015
M-MuLV Reverse Transcriptase	New England Biolabs	M0253S
Magnesium chloride (MgCl$_2$)	Sigma-Aldrich	M1028
Mayer's Hemalum solution	Merck	109249
Milk powder	Roth	T145.4
NaCl	Roth	3957.2
Sodium Fluoride	Applichem	A0401
nitrocellulose membranes	Amersham	GE10600001
OneTaq® Quick-Load® 2X Master Mix	New England Biolabs	M0486L
Phusion® High-Fidelity DNA Polymerase	ThermoFisher Scentific	F530
Recombinant human Macrophage migration inhibitory factor	Immunotools	11344263
Roti ® Histokitt II	Roth	T160.1
SDS	Roth	CN30.3
Sodium deoxycholate	Sigma-Aldrich	30970
Sodium orthovanadate	Sigma-Aldrich	S6508
SYBR Green	Invitrogen	S7567
Tamoxifen (TAM)	Sigma-Aldrich	T5648
Taq-polymerase	Primetech	1800.4
Trehalose	Roth	5151.3
Tris-HCl	Roth	4855.3
Triton X-100	AppliChem	A1388
TRIzol™ Reagent	Invitrogen	15596026
TUNEL enzyme solution	Sigma-Aldrich	11767305001
TUNEL Label mix	Sigma-Aldrich	11767291910
Tween-20	AppliChem	A4974
Reagents for Cell culture		
A83-01	Sigma-Aldrich	SML0788
Advanced DMEM/F12 medium	Gibco	12634010
B-27	Gibco	17504044
Cell Recovery solution	Corning	11543560
CHIR 99021	Axon Medchem	1386
Collagenase type I, powder	Gibco	17018029
DMEM	Gibco	61965059
FBS	Merck	S0615
Geneticin (G418)	InvivoGen	ant-gn-1
GlutaMAX™	Gibco	35050061
HEPES	Gibco	15630080
L-Glutamine	Gibco	25030123

Matrigel	Corning	354230
McCoy's 5A modified medium	Gibco	16600082
Mycoplasma Detection Kit	Lonza	LT07-318
N-2	Gibco	17502048
N-Acetyl-L-Cysteine	Sigma-Aldrich	A9165
Nicotinamide	Sigma-Aldrich	N3376
Penicillin-Streptomycin	Gibco	15140122
rmEGF	ImmunoTools	12343406
ROCK inhibitor (Y-27632)	Sigma-Aldrich	SCM075
RPMI 1640	Gibco	42401042
Sodium Pyruvate	Gibco	11360039
Zeocin	InvivoGen	ant-zn-05
Experimental models: Cell lines		
HEK293T Wnt3a	Robyn Laura Kosinsky	
HEK293T Noggin	Farin et. al, 2012	PMID: 22922422
HEK293T R-spondin I	Farin et. al, 2012	PMID: 22922422
HCT116	ATCC	ATCC® CCL-247™
DLD-1	DSMZ	ACC 278
Experimental models: Mouse strains		
Mif knock-out (129S1/SvImJ)	Fingerle-Rowson et al., 2003	PMID: 12878730
Mif^fl/fl (C57BL/6N)	Fingerle-Rowson et al., 2003, Brocks et al., 2017	PMID: 12878730, PMID: 27825106
Mouse: villin:CreERT2	N/A	RRID:IMSR_JAX:020282
C57BL/6NCrl	Charles River	RRID:IMSR_CRL:27
Oligonucleotides and Recombinant DNA		
Primers for qPCR and genotyping	this paper	Table 1
siRNA Silencer™ Select Negative Control No. 2 siRNA (src2)	Invitrogen	4390847
siRNA MIF Silencer™ Select	ThermoFisher Scientific	4390824, ID s8780
siRNA MIF Silencer™	ThermoFisher Scientific	AM51331, ID 11396
siRNA hCD74 Silencer™ Select	ThermoFisher Scientific	4392420, ID s2715
siRNA hCD74 Silencer™ Select	ThermoFisher Scientific	4392420, ID s225179
pcDNA3 GFP	Addgene	74165
pcDNA3.1/V5-His-TOPO vector	Shi et al., 2006	PMID: 17045821
pcDNA3.1-CD74	Shi et al., 2006	PMID: 17045821
Software and Algorithms		
Adobe Photoshop Software	Adobe	https://www.adobe.com/de/creative cloud/plans.html
GraphPad Prism	GraphPad	https://www.graphpad.com
ImageJ software	Open source	https://imagej.net/Welcome
Image Lab™ Software	Biorad	http://www.bio-rad.com/de-de/product/image-lab-software
ZEN	Zeiss	https://www.zeiss.de/mikroskopie/produkte/mikroskopsoftware/zen.html

3.2   MANUSCRIPT: MUTP53 IN PDAC

THE GAIN-OF-FUNCTION P53 R248W MUTANT PROMOTES MIGRATION BY STAT3 DEREGULATION IN HUMAN PANCREATIC CANCER CELLS

Luisa Klemke[1], Clara F Fehlau[1], Nadine Winkler[1], Felicia Toboll[1], Shiv K Singh[2], Ute M Moll[3] and Ramona Schulz-Heddergott[1*]

[1] Institute of Molecular Oncology, University Medical Center Göttingen, Germany.

[2] Department of Gastroenterology, Gastrointestinal Oncology, and Endocrinology, University Medical Center Göttingen, Germany.

[3] Department of Pathology, Stony Brook University, Stony Brook NY 11794, USA

* Corresponding author: ramona.schulz@zentr.uni-goettingen.de

RUNNING TITLE

Missense mutant p53 function in PDAC

Own contribution:

Conducted experiments and data analysis for: Figure 1A, Figures 2A, B, Figures 3C, D, Figures 4A, E-G, Figure 5A-D, Figures S1, Supp. Fig. 2B. Data analysis for: Figure 1B, Figures 4B-D, H, as well as preparation of additional supplemental material. Involved in the conceptualization, methodology, acquisition, analysis and interpretation of data, figure arrangement, writing and revising the manuscript.

** Figures and corresponding figure legends are located at the end of the manuscript

The gain-of-function p53 R248W mutant promotes migration by STAT3 deregulation in human pancreatic cancer cells

Luisa Klemke[1], Clara Friederike Fehlau[1], Nadine Winkler[1], Felicia Toboll[1], Shiv K Singh[2], Ute M Moll[3] and Ramona Schulz-Heddergott[1*]

[1] Institute of Molecular Oncology, University Medical Center Göttingen, Germany

[2] Department of Gastroenterology, Gastrointestinal Oncology, and Endocrinology, University Medical Center Göttingen, Germany

[3] Department of Pathology, Stony Brook University, Stony Brook NY 11794, USA

* Corresponding author: ramona.schulz@zentr.uni-goettingen.de

RUNNING TITLE

Missense mutant p53 function in PDAC

CORRESPONDING AUTHOR

Dr. Ramona Schulz-Heddergott

Institute of Molecular Oncology, Universitätsmedizin Göttingen (UMG)

Justus-von-Liebig-Weg 11, 37077 Göttingen, Germany

E-mail: ramona.schulz@zentr.uni-goettingen.de

Phone: +49 551 39 60780

Fax: +49 551 39 60747

AUTHOR CONTRIBUTIONS

Conceptualization R. S.-H., L. K.; Methodology R. S.-H., L. K., C. F. F., S. K. S.; Experimentation L. K., C. F. F, N. W., F. T.; Writing Original Draft L. K., U. M. M.; Writing Review & Editing: all authors; Funding Acquisition U. M. M, R. S.-H.; Supervision R. S.-H.

CONFLICT OF INTEREST

All authors declare to have no conflict of interests.

ABSTRACT

Missense p53 mutations (mutp53) occur in approx. 70% of pancreatic ductal adenocarcinomas (PDAC). Typically, mutp53 proteins are aberrantly stabilized by Hsp90/Hsp70/Hsp40 chaperone complexes. Notably, stabilization is a precondition for specific mutp53 alleles to acquire powerful neomorphic oncogenic gain-of-functions (GOFs) that promote tumor progression in solid cancers mainly by increasing invasion and metastasis. In colorectal cancer (CRC) we recently established that the common hotspot mutants mutp53^{R248Q} and mutp53^{R248W} exert GOF activities by constitutively binding to and hyperactivating STAT3. This results in increased proliferation and invasion in an autochthonous CRC mouse model and correlates with poor survival in patients.

Comparing a panel of p53 missense mutations in a series of homozygous human PDAC cell lines, we show here that similar to CRC the mutp53^{R248W} protein again undergoes a strong Hsp90-mediated stabilization and selectively promotes migration. Highly stabilized mutp53 is degradable by the Hsp90 inhibitors Onalespib and Ganetespib, and correlates with growth suppression, possibly suggesting therapeutic vulnerabilities to target GOF mutp53 proteins in PDAC.

In response to mutp53 depletion only mutp53^{R248W} harboring PDAC cells show STAT3 de-phosphorylation and reduced migration, again suggesting an allele-specific GOF in this cancer entity, similar to CRC. Moreover, mutp53^{R248W} also exhibits the strongest constitutive complex formation with phosphorylated STAT3. The selective mutp53^{R248W} GOF signals through enhancing the STAT3 axis, which was confirmed since targeting STAT3 by knockdown or pharmacological inhibition phenocopied mutp53 depletion and reduced cell viability and migration preferentially in mutp53^{R248W}-containing PDAC cells. Our results confirm that mutp53 GOF activities are allele specific and can span across tumor entities.

INTRODUCTION

Already in the early 1990s the tumor suppressor p53 was coined as 'guardian of the genome' (Lane, 1992; Zilfou and Lowe, 2009) and it was known that mutation of the *TP53* gene (tumor protein p53, HGNC:11998) is an essential step in human tumor development (Hollstein et al., 1991; Lane, 1992). Ever since scientists have tried to understand the influence of the *TP53* status within the mutational landscape in different cancer entities and to investigate the role of different variants in tumorigenic pathways. It became evident that some p53 mutant protein variants do not only abrogates tumor suppressor functions (loss-of-function, LOF), but also gain new tumorigenic functions (gain-of-functions; GOFs). Given that approx. 70% are missense mutations leading to amino acid substitutions mostly in the DNA binding domain, some alleles are selected and occur at a high frequency, termed hotspots. Most hotspot mutants gain neomorphic tumorigenic functions, particularly in invasion and metastasis of solid tumors (Brosh and Rotter, 2009; Oren and Rotter, 2010; Goh et al., 2011; Kim and Lozano, 2018; Sabapathy and Lane, 2018; Mantovani et al., 2019). A key prerequisite for GOFs of some missense p53 mutants (termed here 'mutp53') is protein stabilization through the Hsp90/Hsp70/Hsp40 (heat shock protein 90/70/40) chaperone machinery, resulting in protection from MDM2 (mouse double minute 2) and other E3 ligases and thus proteasomal degradation (Walerych et al., 2004; Walerych et al., 2009; Wiech et al., 2012; Parrales et al., 2016; Schulz-Heddergott and Moll, 2018; Wawrzynow et al., 2018; Mantovani et al., 2019).

Due to the heterogeneity of *TP53* point mutations, whose phenotype in addition are highly dependent on the cellular context, different missense mutants exert different cellular responses (Freed-Pastor and Prives, 2012; Lee et al., 2012; Gencel-Augusto and Lozano, 2020). Thus, it is important to consider the context- and allele-dependent specificity of different mutp53 proteins (Lee et al., 2012; Walerych et al., 2015; Ubby et al., 2019; Kadosh et al., 2020). To investigate the mutp53 specificity, different groups have dissected the impact of various mutp53 GOF alleles on tumorigenesis using autochthonous mouse models (Hanel et al., 2013; Alexandrova et al., 2015; Kim et al., 2015; Schulz-Heddergott et al., 2018; Zhang et al., 2018) or clinical correlation studies (Said et al., 2013; Xu et al., 2014; Alexandrova et al., 2017; Schulz-Heddergott et al., 2018). Recent results from our group highlight the GOF hotspot mutp53$^{R248Q/W}$ specificity in mouse and human colorectal cancer (CRC). mutp53$^{R248Q/W}$ binds to and deregulates phosphorylated STAT3 (signal transducer and activator of transcription 3) by protecting it from SHP2 phosphatase (*PTPN11*, protein tyrosine phosphatase non-receptor type 11), its major negative regulator. Thus,

3

depletion of mutp53$^{R248Q/W}$ inhibits STAT3 signaling and causes suppression of tumor invasion and proliferation (Schulz-Heddergott et al., 2018). The p53 R248 hotspot is the single most common variant in all *TP53*-altered tumor types occurring in 9%, of cases which translates to about 66,000 newly diagnosed cancer patients in the US per year harboring R248 variants. Of R248 substitutions, over 90% are either Q or W, with similar frequencies (The Cancer Genome Atlas Program – National Cancer Institute).

Here we asked whether mutp53^{R248W} also exhibits tumor-promoting functions affecting migration in pancreatic ductal adenocarcinoma (PDAC). Note, the *TP53*^{R248Q} allele is not available in established PDAC lines. PDAC is currently the fourth leading cause of cancer death worldwide with a rapidly ascending trajectory, and incidence is predicted to increase even further in the future (Orth et al., 2019; Siegel et al., 2020). PDAC, which constitutes around 90% of all pancreatic malignancies, is highly aggressive and chemoresistant and still has a dismal 5 year survival rate of only approx. 9% (Grasso et al., 2017; Smigiel et al., 2018; Orth et al., 2019; American-Cancer-Society, 2020).

In approx. 70% of PDAC patients *TP53* undergoes mainly missense mutations (www.cbioportal.org) as a late genetic event at the transition from high grade PanIN dysplasia to invasiveness during pancreatic cancer progression (Guo et al., 2016; Cicenas et al., 2017). Here we show in a panel of common human PDAC cell lines harboring different homozygous missense p53 mutants that mutp53 variants differ in their protein stability, with mutp53^{R248W} again accumulating the highest protein levels also in the pancreatic cell context. Importantly, comparing all PDAC lines only mutp53^{R248W} depletion strongly reduced migration capacity. In support, mutp53^{R248W} specifically showed the strongest binding to phosphorylated STAT3 under baseline and cytokine-stimulated conditions, forming a constitutive mutp53^{R248W}-pSTAT3 complex. Only mutp53^{R248W} depletion was able to reduce pSTAT3 levels. Consequently, targeting the tumor-promoting mutp53^{R248W}-pSTAT3 complex by pSTAT3 depletion or pharmacological inhibition diminished cell viability and migration in mutp53^{R248W} expressing, but not in mutp53^{R273H} or mutp53^{R282W} expressing PDAC cells. Our results support a GOF function of mutp53^{R248W} in pancreatic cancer cell lines, justifying future investigations in this tumor entity *in vivo.*

RESULTS

p53 missense mutants in human PDAC cell lines are stabilized via HSP90

Since different p53 mutants have different conformations and thus different tumorigenic functions that additionally depend on specific cellular/oncogenic context, each allele and tumor type constellation should be considered separately (Bullock et al., 2000; Freed-Pastor and Prives, 2012; Kim and Lozano, 2018; Schulz-Heddergott and Moll, 2018). To investigate the allele specificity of mutated *TP53* in pancreatic ductal adenocarcinoma (PDAC), we used homozygous human PDAC cell lines expressing different endogenous p53 hotspot and non-hotspot missense mutants. The panel included CAPAN-1 (p53^{A159V}), BXPC-3 (p53^{Y220C}), PANC-1 (p53^{R273H}), MIA-PACA-2 (p53^{R248W}), PA-TU-8902 (p53^{C176S}) and PA-TU-8988T (p53^{R282W}). L3.6pl harbors a truncating LOF mutation and served as p53null control. Unfortunately, an established PDAC line with a mutated *TP53*^{R248Q} allele is not available. The absence of wildtype p53 function was verified in all cases (Figure S1).

Comparative immunoblot analysis identified the highest steady state protein levels in MIA-PACA-2 cells expressing the R248W mutant (Figure 1A). The second highest levels were observed in C176S and R282W harboring PA-TU-8902 and PA-TU-8988T cells, respectively. The lowest level was seen in A159V expressing CAPAN-1 cells (Figure 1A). Cycloheximide chase experiments confirmed that the highest p53 steady state levels in cells harboring mutp53^{R248W}, mutp53^{C176S} and mutp53^{R282W} were also the most stable proteins with the longest half-lives, while mutant p53 protein with the lowest level (A159V) had the shortest half-life (Figure 1B).

A key prerequisite for the gain-of-function (GOF) of some missense p53 mutants is protein stabilization through the Hsp90 chaperone machinery. Importantly, the clinically relevant Hsp90 inhibitors Ganetespib or Onalespib provide therapeutic selectivity towards tumor epithelial cells but not normal cells, making them attractive for anti-cancer therapies (Klemke et al., 2021). Furthermore, in other cellular contexts such as lymphoma (Alexandrova et al., 2015), treatment with the Hsp90 inhibitors Ganetespib or Onalespib also downregulated mutp53 protein levels in most PDAC cells, except BXPC-3 cells (Figure 2A), indicating that mutp53 proteins are mainly stabilized in this context by the Hsp90 chaperone machinery. In line, PANC-1, MIA-PACA-2, PA-TU-8902 and PA-TU-8988T cells showed diminished cell growth by about 40%, while the other lines had less reduction (Figure 2B). These data reinforce that at least some mutp53 proteins in PDAC might also be targetable with Hsp90 inhibitors.

The p53^{R248W} mutant selectively promotes migration in PDAC cells

We previously established that a main GOF activity of the mutp53^{R248W} and mutp53^{R248Q} in colorectal cancer compared to p53 null is promotion of cell migration and invasion in tumors *in vivo* and *in vitro* (Schulz-Heddergott et al., 2018). To test whether this is also the case in PDAC we performed migration assays. Of note, transwell migration assays showed that only siRNA-mediated depletion of mutp53^{R248W} decreased the migration capacity of MIA-PACA-2 cells, while depletion of other alleles failed to do so (Figures 3A-D). Interestingly, PA-TU-8988T and PA-TU-8902 cells which also express high levels of stabilized mutp53^{R282W} or mutp53^{C176S} respectively (Figures 1A, B) did not show reduced migration after mutp53 depletion (Figure 3C) or were completely unable to migrate through the pores of the transwell membrane (Figure 3E). This remained even after treatment of PA-TU-8902 cells with the cytokines Interleukin-6 (IL-6) and Oncostatin M (OSM) (Figure 3E), known to induce migration and proliferation in numerous cell types (Natesh et al., 2015; Razidlo et al., 2018; Che et al., 2019). This suggests that high mutp53 stabilization per se is a necessary but not sufficient precondition for acquiring a GOF on migration.

To confirm the effects seen in migration assays, 3 cell lines were further analyzed by wound healing scratch assays. Again, specifically MIA-PACA-2 cells bearing the R248W mutation showed the strongest reduction in wound closing capacity upon mutp53 depletion (Figures 3F-H).

Mutp53^{R248W} selectively binds to phosphorylated STAT3 in PDAC cells

In colorectal carcinoma an important mechanism of tumor invasion is mediated by mutp53$^{R248Q/W}$-pSTAT3 signaling by forming a physical complex (Schulz-Heddergott et al., 2018). Reduced migration capacity of MIA-PACA-2 cells after mutp53^{R248W} depletion (Figures 3A, F) suggests a similar mechanism. Since the STAT3 pathway is also an important driver of PDAC tumorigenesis (Denley et al., 2013; Nagathihalli et al., 2015), we asked whether mutp53^{R248W}-regulated migration is similarly mediated through STAT3 signaling. The PDAC panel showed high constitutive levels of phosphorylated STAT3 (pSTAT3) in 5 of the 7 cell lines (Figure 4A). Only 2 cell lines, PA-TU-8902 and PA-TU-8988T, had very low levels of activated STAT3 (yet exhibited significant stabilization of mutp53). On the other hand, this immunoblot analysis which examines relative ratios of both proteins indicated that 4 lines with high pSTAT3 had very low or undetectable mutp53 levels. Importantly, MIA-PACA-2 cells, as the only cell line with dually high levels of both mutp53 and pSTAT3, seem to fulfill the best precondition to promote migration via this axis.

Thus, co-immunoprecipitations (CoIPs) were performed to test which of the various mutp53 proteins are able to bind STAT3. Indeed, R248W in MIA-PACA-2 cells showed the strongest binding to total STAT3 protein compared to BXPC-3 and PANC-1 cells, forming a constitutive endogenous signaling complex (Figure S2A). Since phosphorylation status is another important parameter for binding to STAT3, these cell lines with different mutp53 variants and stabilization levels were subjected to CoIPs with an antibody specific for phosphorylated STAT3. Among these mutants analyzed, mutp53^{R248W} in MIA-PACA-2 cells again showed the strongest binding to pSTAT3 (Figure 4B). CAPAN-1 cells with low mutp53 level showed a minor binding to pSTAT3 (Figure 4C) such as BXPC-3 and PANC-1 cells (Figure 4B) (yet exhibited moderate levels of mutp53 compared to CAPAN-1). However, PA-TU-8988T cells with intermediate mutp53 levels (lower than in MIA-PACA-2 but higher than in PANC-1 or BXPC-3 cells) again showed a strong binding of mutp53^{R282W} to pSTAT3 (Figure 4D). This confirms a point made in colorectal carcinoma that the ability of mutp53 to bind to pSTAT3 correlates with the degree of its stabilization (Schulz-Heddergott et al., 2018).

To investigate if the mutp53-pSTAT3 complex can directly regulate the phosphorylation status of STAT3 as shown in CRC (Schulz-Heddergott et al., 2018), we depleted mutp53 in MIA-PACA-2, PA-TU-8988T, PANC-1, BXPC-3 and PA-TU-8902 cells (Figures 4E, S2B). In MIA-PACA-2 and PA-TU-8988T cells, both with a strong mutp53-pSTAT3 complex formation, only mutp53^{R248W} regulated STAT3 activity in PDAC cells, as indicated by decreased STAT3 phosphorylation selectively in MIA-PACA-2 cells (Figure 4E). In all other cell lines tested, pSTAT3 level were not decreased after mutp53 depletion (Figures 4E, S2B). Why mutp53 binding to pSTAT3 failed to reduce STAT3 activity in PA-TU-8988T cells remains speculative but confirms the reduced migration capacity after mutp53 depletion exclusively in MIA-PACA-2 cells (Figures 3A-D). These data further underline the strong invasive GOF function of the mutp53$^{R248Q/W}$ allele reaching across cancer entities.

Although most PDAC cell lines already exhibited high constitutive levels of pSTAT3 at baseline (Figure 4A), treatment with Interleukin-6 (Figure 4F) or Oncostatin M (Figure 4G) further stimulated the STAT3 pathway and induced additional increase in phosphorylated STAT3. Thus, to further evaluate whether the mutp53 binding capacity to pSTAT3 increases with higher pSTAT3 levels, MIA-PACA-2, as well as PANC-1 and BXPC-3 cells (both with a low binding capacity) were treated with IL-6, OSM or solvent control. Interestingly, even after this strong induction of pSTAT3, the p53^{R248W} mutant showed by far the strongest binding to pSTAT3, again emphasizing allele selectivity (Figure 4H). These data suggest that it is not the level of pSTAT3 that predicts p53 binding in PDAC, but rather the nature of the mutp53 variant. In sum, mutp53^{R248W} shows a strong

ability for complexing with pSTAT3 and regulation of migration, independent of the levels of phosphorylated STAT3.

Mutp53^{R248W} selectively regulates STAT3 phosphorylation and activity in PDAC cells

The above findings led us to hypothesize that mutp53^{R248W} binds to and deregulates pSTAT3 in PDAC cells by forming an oncogenic complex. Since mutp53^{R248W} depletion also selectively suppressed phosphorylation and thus activation of STAT3 (Figure 4E), we next asked whether the R248W mutant can be functionally linked to STAT3 dependency for migration in PDAC cells. To this end we determined migration capacity after STAT3 ablation. Indeed, depletion of STAT3 suppressed migration ability in mutp53^{R248W} expressing MIA-PACA-2 cells (Figure 5A) but not in mutp53^{R273H} expressing PANC-1 cells (Figure 5B).

To confirm that phosphorylated STAT3 is critical for the oncogenic mechanism of the tumor-promoting mutp53^{R248W}-pSTAT3 complex, we used the small-molecule STAT3 inhibitor Stattic. Stattic selectively inhibits activation of STAT3 through interference with dimerization and nuclear translocation (Schust et al., 2006). It has been shown that Stattic substantially reduces STAT3 phosphorylation in colorectal, liver and breast cancer cells (Schust et al., 2006; Lin et al., 2011; Spitzner et al., 2014) as well as in PDAC cells such as MIA-PACA-2 and PANC-1 (Cardoso et al., 2012; Lin et al., 2016; Nagathihalli et al., 2018). Importantly, among the panel of PDAC cells, R248W expressing MIA-PACA-2 cells were again the most susceptible to pSTAT3 inhibition by Stattic with the lowest IC$_{50}$ value (8 µM) in cell viability assays (Figure 5C). Likewise, migration after Stattic treatment was strongly suppressed in MIA-PACA-2 cells (by ∼70%), but lower suppressed in PANC-1 (by ∼15%) or PA-TU-8988T cells (by ∼45%) cells (Figure 5D).

The mutp53^{R248W}-STAT3 complex might accelerate tumor progression in PDAC patients as we had previously seen in CRC patients (Schulz-Heddergott et al., 2018). Indeed, TCGA patient data support this notion since PDAC patients harboring *TP53^{R248Q}* or *TP53^{R248W}* mutations showed a trend for reduced survival compared to patients with loss-of-function NS+FS mutation (Figure 5E), supporting the mutp53^{R248W}-pSTAT3 complex as a potentially attractive target in PDAC.

In conclusion, targeting the tumor-promoting mutp53^{R248W}-pSTAT3 complex by STAT3 depletion or pharmacological inhibition diminished cell viability and migration in mutp53^{R248W} expressing, but not in mutp53^{R273H} expressing, PDAC cells.

DISCUSSION

The phenotype of p53 missense mutants is heterogenous and moreover depends on the cellular context (Freed-Pastor and Prives, 2012; Lee et al., 2012; Gencel-Augusto and Lozano, 2020). Here we analyze a panel of p53 missense mutants (mutp53) in a series of homozygous human PDAC cell lines and compare the impact of various mutants on protein properties and functions. We find that mutp53^{R248W} protein undergoes strong Hsp90-mediated stabilization and selectively promotes migration by engaging in the strong constitutive complex formation with phosphorylated STAT3 at baseline and upon cytokine stimulation. Our data in pancreatic cancer suggest a R248W allele-specific gain-of-function on migration via STAT3 deregulation. These data mirror our previous findings in colorectal cancer (Schulz-Heddergott et al., 2018) and further underline the necessity to investigate p53 missense mutants in a context and allele-dependent manner (Lee et al., 2012; Walerych et al., 2015; Ubby et al., 2019).

Interestingly, PA-TU-8902 cells expressing intermediate stabilized mutp53^{C176S} showed strong STAT3 pathway stimulation by OSM or IL-6 (Figures 4F, G) but did not migrate at all through the transwell assay (Figure 3E), indicating that STAT3 fails to impact migration in these cells. Furthermore, PA-TU-8988T cells harboring intermediate levels of mutp53^{R282W} showed a strong binding to pSTAT3 but failed to regulate pSTAT3 level (indicating STAT3 activity) (Figure 4E) and failed to influence the migratory capacity in transwell assays as seen in mutp53^{R248W}-containing MIA-PACA-2 cells (compare Figure 3A and 3C). However, in principle, the mutp53^{R282W}-pSTAT3 complex confirms a point made in our colorectal carcinoma study that the ability of mutp53 to bind pSTAT3 correlates with the degree of its stabilization (Schulz-Heddergott et al., 2018). The function which is acquired by the mutp53^{R282W}-pSTAT3 complex in PA-TU-8988T remains speculative. STAT3 is not just an important factor for PDAC migration (Cardoso et al., 2012; Patel et al., 2014; Nagathihalli et al., 2016), but is also involved in many other hallmarks of cancer to promote tumor progression (Siveen et al., 2014; Zou et al., 2020).

Thus, we find that different p53 mutants have different impacts on migration- and cell growth-associated STAT3 functions. Importantly, among *TP53* mutations, several other common alterations exist that drive PDAC (Bailey et al., 2016). We cannot exclude that molecular PDAC subtypes influence mutp53 GOF activities. Other mutations and alteration might also contribute to migratory differences after depletion of mutp53 variants. To address this question, an isogenic cell panel with various *TP53* mutations is necessary. Since the maintenance of the *TP53* copy

number is very crucial in relation to mutp53 protein stabilization, a CRISPR/Cas9-based isogenic cell panel might be most useful.

Mechanistically, the favored gain-of-function hypothesis is that the nuclear presence of highly abundant stabilized mutp53 proteins, which have lost specific DNA binding capacity on their own, results in hijacking of (by binding to) other transcription factors and their specific cofactors, thereby building a complex network to divert and oncogenically reprogram their transcriptional activity (Muller and Vousden, 2013; 2014; Kim et al., 2015; Walerych et al., 2015; Bellazzo et al., 2018; Kim and Lozano, 2018; Mantovani et al., 2019). Regarding co-factors, it is conceivable that the mutp53 protein also adds p53-specific coactivators into this illegitimate mix, and/or that the canonical coactivator specific for the partnering transcription factor might get displaced. Thus, interplay networks of mutp53 with co-regulation of various tumor drivers is essential for GOF mediated cancer progression (Oren and Rotter, 2010; Muller and Vousden, 2013; Kim et al., 2015; Kim and Lozano, 2018; Grzes et al., 2020). This concept could explain why the mutp53 status or the status of STAT3 phosphorylation alone is not yet a determinant for migration but depends on the specific missense mutation, resulting in specific mutp53-STAT3 complexes with mutp53 variant-specific transcriptional cofactors. In line, it is shown that mutp53^{R273H} and mutp53^{R175H} can regulate NF-ĸB activity in cancer cells (Weisz et al., 2007; Cooks et al., 2013). Interestingly, NF-ĸB and STAT3 also physically interact and coregulate transcriptional pathways in cancer (Grivennikov and Karin, 2010; Ji et al., 2019). Together with our finding that mutp53^{R273H} does not significantly bind to pSTAT3 in PANC-1 cells (Figures 4B) and does not regulate their migration (Figures 3B, G), it further emphasizes the allele specificity of oncogenic mechanisms. Other studies also show context-dependent mutp53 specificities (Freed-Pastor and Prives, 2012; Kim and Lozano, 2018). One example is mutp53^{R175H} which promotes aberrant self-renewal in leukemic cells through binding to FOXH1 as critical regulator of stem cell–associated genes (Loizou et al., 2019). Furthermore, mutp53^{R175H} or mutp53$^{R273H/C}$ form complexes with NF-Y and p300 proteins to override cellular failsafe programs thus, permitting tumor progression (Di Agostino et al., 2006). Mutp53 promotes invasion, e.g. via constitutive activation of EGFR/integrin signaling (Muller et al., 2009) and by antagonizing TAp63 (Adorno et al., 2009).

Mutp53 stabilization occurs via binding to Hsp90 (Alexandrova et al., 2015; Mantovani et al., 2019) which offers therapeutic approaches to target stabilized GOF mutp53 protein in cancer cells via Hsp90 inhibition. Thus, treatment with the HSP90 inhibitors Ganetespib and Onalespib diminished mutp53 levels in most analyzed PDAC cells (Figure 2A). However, in BXPC-3 cells, both Hsp90 inhibitors failed to destabilize Hsp90 clients (also see functional control AKT). Why

remains speculative but resistance mechanisms are known such as an UGT1A (UDP glucuronosyltransferase 1A) overexpression (Landmann et al., 2014). Importantly, in cells with a strong stabilization of mutp53 (MIA-PACA-2, PA-TU-8902 and PA-TU-8988T, Figure 1B), inhibition of HSP90 resulted in significant suppression of cell growth (Figure 2B). In CAPAN-1 cells with a low degree of mutp53 stabilization (Figures 1A, B), HSP90 inhibition did not substantially impact cell confluency (Figure 2B).

In sum, our preliminary *in vitro* results support a GOF of mutp53^{R248W} in pancreatic cancer, justifying future *in vivo* investigations on stabilized mutp53 as putative therapeutic target in this important tumor entity that is in dire need of new therapeutic concepts.

MATERIAL AND METHODS

All materials used and corresponding information are provided as supplemental Table 1.

Cell Culture

Homozygous mutant human pancreatic cancer cell lines MIA-PACA-2 (mutp53^{R248W}) (DZMS, RRID:CVCL_0428), PANC-1 (mutp53^{R273H}) (ATCC, RRID:CVCL_0480), BXPC-3 (mutp53^{Y220C}) (ATCC, RRID:CVCL_0186), and PA-TU-8902 (mutp53^{C176S}) (DSMZ, RRID:CVCL_1845) were grown in DMEM (Gibco) with 10% FBS (Merck). PA-TU-8988T (mutp53^{R282W}) (DSMZ, RRID:CVCL_1847) were grown in DMEM medium with 5% FBS. CAPAN-1 (mutp53^{A159V}) (ATCC, RRID:CVCL_0237) were grown in RPMI 1640 (Gibco) with 20% FBS, and L3.6pl cells (truncating frameshift p53 mutation) (Bruns et al., 1999; Herreros-Villanueva et al., 2013) were grown in RPMI 1640 with 10% FBS. All media were supplemented with Penicillin-Streptomycin (10,000 U/mL, Gibco) and L-Glutamine (Gibco). All cell lines were grown at 37°C at 5% CO_2 in a humidified atmosphere and tested for Mycoplasma contamination on a regular basis (Mycoplasma Detection Kit, Lonza). Cell line authentication certificates are provided as supplemental material.

Transfection with siRNA

Depletion of human *TP53* or *STAT3* mRNAs was achieved by siRNA transfection using Lipofectamine™ 3000 (Invitrogen) or Lipofectamine™ 2000 (Invitrogen) transfection reagents. siRNA sequences are listed in supplemental Table 1. Cells were reverse transfected in 6-well plates (Sarstedt) according to manufacturer guidelines. After 24 hrs supernatant was collected and replaced by fresh culture medium. 72 hrs post-transfection cells were harvested for analyses.

Immunoblot analysis

Cell lysates were prepared with RIPA buffer containing 20 mM Tris-HCl pH 7.5, 10 mM EDTA, 1% sodium deoxycholate, 150 mM NaCl, 1% Triton X-100, 0.1% SDS, phosphatase inhibitor consisting of 2 mM imidazol, 1 mM sodium orthovanadate and 1 mM sodium fluoride, and cOmplete™ mini protease inhibitor cocktail (Roche). Samples were lysed in RIPA buffer with sonication. Protein concentrations were determined by BCA protein assay (Pierce). Equal amounts of lysates were loaded (15-30 µg) and separated by SDS-polyacrylamide gel electrophoresis followed by transfer onto nitrocellulose membranes (Amersham). After blocking with 5% milk (Roth), membranes were incubated with the following antibodies: HSC70 [B-6] (Santa Cruz), beta-Actin (Abcam), total-AKT [D9E] (Cell Signaling), p53 [DO-1] or HRP-

conjugated p53 [DO-1] (Santa Cruz), phospho-Y705 STAT3 [EP2147Y] (Abcam), total STAT3 (Santa Cruz) or total STAT3 [79D7] (Cell Signaling), MDM2 [IF-2] (Calbiochem®/Millipore), p21 Waf1/Cip1 [12D1] (Cell Signaling). Primary antibodies were detected with HRP-conjugated secondary antibodies. Signal was developed using Clarity Max™ Western ECL Substrate (BioRad), SuperSignal™ West Femto Maximum Sensitivity Substrate (ThermoFisher Scientific) or Immobilion Western chemiluminescent HRP substrate (Millipore/Merck). For antibody details see Table 1.

Co-immunoprecipitation

For coIP cells were lysed in buffer containing 50 mM Tris-HCl, pH 7.5, 150 mM NaCl, 1% Nonidet™ P40, 10 µM MG-132, phosphatase inhibitor consisting of 2 mM Imidazol, 1 mM sodium orthovanadate and 1 mM Sodium Fluoride, and cOmplete™ mini protease inhibitor cocktail (Roche), followed by sonication. After centrifugation samples were precleared with protein G Sepharose (GE Healthcare) and equal amounts of protein were immunoprecipitated using antibodies against total STAT3 (Santa Cruz), phospho-Y705 STAT3 (Abcam) or control IgG antibody (Abcam). Precipitates were analyzed by immunoblotting. For coIPs, p53 was immunoblotted with an HRP-conjugated p53 antibody (Santa Cruz). 5% of each input was used as input control and stained with beta-Actin (Abcam) as loading control. To stimulate STAT3, cells were treated with 50 ng/mL IL-6 or OSM 24 hrs prior to performing the CoIP.

Cycloheximide chase

To evaluate the stability of different mutp53 proteins in the panel of PDAC cell lines Cycloheximide (CHX) chase experiments were performed. Cells were treated with 40 µg/mL Cycloheximide (Sigma-Aldrich) or ethanol vehicle control for 8 h and 24 hrs. Protein lysates were prepared with RIPA buffer as described in immunoblot analysis.

Treatment with Hsp90 inhibitors and STAT3 inhibitor

To investigate HSP90 chaperone dependent stabilization of different mutp53 proteins, cells were treated with Hsp90 ATPase inhibitors Ganetespib (Synta Pharmaceuticals) or Onalespib (Selleckchem). To investigate dependency on STAT3, small-molecule inhibitor Stattic (Santa Cruz) was used which prevents STAT3 phosphorylation and activation. Cells were seeded in 6-well plates (Sarstedt) and treated with the inhibitors or respective DMSO control for 24 hrs followed by harvesting protein lysates and immunoblot analysis. To determine cell confluency,

cells were seeded in 96-wells (Corning) and treated with Onalespib or Ganetespib for 24 hrs. Confluency was determined using the Celigo Imaging Cytometer (Nexcelom, Software v5.0.0.0).

Treatment with cytokines (IL-6, OSM)

To stimulate the STAT3 pathway, cells were seeded in 6-well plates (Sarstedt) and treated with Interleukin-6 (IL-6) or Oncostatin M (OSM 209a.a.) (both from Immunotools) or solvent control for 24 hrs and analyzed by immunoblots.

Cell viability assay after Stattic treatment

Cells were seeded in 96-well plates (Corning) and treated with increasing concentrations (0-80 µM) of Stattic or solvent control for 24 hrs. The CellTiter-Glo® Luminescent Cell Viability Assay (Promega), based on detectable ATP, was performed according to manufacturer's guidelines. Each biological replicate was measured in triplicates and viability was calculated relative to the solvent control for each cell line.

Wound healing assay

24 hrs after transfection with siRNAs or scrambled control, cells were incubated in serum-reduced media (1% FBS). 48 hrs post transfection, three scratches per well were made with a 1ml pipette tip or 200µl pipette tip as dublicates. 48 hrs after scratching, at least 5 images per scratch were taken, quantified, and averaged per experiment. The degree of wound healing was determined by measuring the scratched area per image using the 'polygon selection function' of Image J software. Wound healing rate was measured by averaging each scratch area after 48 hrs relative to the initial area at 0 hrs. Biological replicates are defined as independent experiments with cells at different passages and different days. For technical replicates cells from one experiment were seeded in two different wells (duplicates).

Transwell migration assay

Cells were either transfected with siRNA against *TP53* mRNA, *STAT3* mRNA or scrambled control, or treated with STAT3 inhibitor Stattic. 72 hrs after siRNA transfection, cells were trypsinized and seeded into transwell inserts (Corning) in serum-reduced media (1% FBS for MIA-PACA-2, PANC-1, BXPC-3 and PA-TU-8902; 0.5% FBS for PA-TU-8988T). Wells (Corning) were filled with the respective complete medium of each cell line.

To investigate migration potential upon Stattic treatment, cells were seeded in transwell inserts as described above. Different concentrations of Stattic or respective control were added to the cells 1-2 hrs after seeding, allowing cells to settle before treatment.

Final 24 hrs after seeding, cells that had migrated to the underside of the membrane were carefully washed with PBS, fixed in ice cold methanol for 10 min and stained with crystal violet (0.1% in 20% EtOH) for 20 min. After washing, remaining cells inside the insert were removed using a pre-wet Q-tip. Migrated cells were visualized by light microscopy and analyzed using Image J. Migration rate was calculated relative to scrambled siRNA or solvent control, respectively. Biological replicates are defined as independent experiments with cells at different passages and different days. For technical replicates cells from one experiment were seeded in two different transwell inserts (dublicates).

Attempting to induce migration of PA-TU-8902 cells, cells were seeded in 6-well plates (Corning) and treated with 50 ng/mL IL-6 or OSM (Immunotools). After 24 hrs pre-treatment, cells were transferred to transwell inserts, cytokines added again. And followed as described above.

Analysis of human patient TCGA data

Human genomic data including *TP53* gene mutation and clinical information was downloaded from cBioPortal (www.cbioportal.org). We used cBioportal Pancreatic ductal adenocarcinoma database in this analysis (Cerami et al., 2012; Gao et al., 2013). Two datasets were used to detect mutated samples and the clinical data, QCMG, Nature 2016, and TCGA, PanCancer Atlas (Bailey et al., 2016; Cancer Genome Atlas Research Network. Electronic address and Cancer Genome Atlas Research, 2017). *TP53* R248Q/W missense mutant group was sampled with *TP53* missense mutations (MS) with amino acid change R248, and *TP53* LOF group was sampled with frameshift (FS) and nonsense (NS) *TP53* mutations. R language (The R Project for Statistical Computing, https://www.r-project.org, version 4.0.2) and the package "survival" were used in the analysis, including calculating log-rank p-value and Kaplan-Meier curves.

Statistical analysis

The number of biological and technical replicates (mean ± SEM) is provided in the figure legends. For all experiments, an unpaired Student's t test was used to calculate p-values.

Acknowledgement

REFERENCES

Adorno, M., Cordenonsi, M., Montagner, M., Dupont, S., Wong, C., Hann, B., et al. (2009). A Mutant-p53/Smad complex opposes p63 to empower TGFbeta-induced metastasis. *Cell* 137(1)**,** 87-98. doi: 10.1016/j.cell.2009.01.039.

Alexandrova, E.M., Mirza, S.A., Xu, S., Schulz-Heddergott, R., Marchenko, N.D., and Moll, U.M. (2017). p53 loss-of-heterozygosity is a necessary prerequisite for mutant p53 stabilization and gain-of-function in vivo. *Cell Death Dis* 8(3)**,** e2661. doi: 10.1038/cddis.2017.80.

Alexandrova, E.M., Yallowitz, A.R., Li, D., Xu, S., Schulz, R., Proia, D.A., et al. (2015). Improving survival by exploiting tumour dependence on stabilized mutant p53 for treatment. *Nature* 523(7560)**,** 352-356. doi: 10.1038/nature14430.

American Cancer Society (2020). *Survival Rates for Pancreatic Cancer* [Online]. Available: https://www.cancer.org/cancer/pancreatic-cancer/detection-diagnosis-staging/survival-rates.html# [Accessed 10.12.2020].

Bailey, P., Chang, D.K., Nones, K., Johns, A.L., Patch, A.M., Gingras, M.C., et al. (2016). Genomic analyses identify molecular subtypes of pancreatic cancer. *Nature* 531(7592)**,** 47-52. doi: 10.1038/nature16965.

Bellazzo, A., Sicari, D., Valentino, E., Del Sal, G., and Collavin, L. (2018). Complexes formed by mutant p53 and their roles in breast cancer. *Breast Cancer (Dove Med Press)* 10**,** 101-112. doi: 10.2147/BCTT.S145826.

Brosh, R., and Rotter, V. (2009). When mutants gain new powers: news from the mutant p53 field. *Nat Rev Cancer* 9(10)**,** 701-713. doi: 10.1038/nrc2693.

Bruns, C.J., Harbison, M.T., Kuniyasu, H., Eue, I., and Fidler, I.J. (1999). In vivo selection and characterization of metastatic variants from human pancreatic adenocarcinoma by using orthotopic implantation in nude mice. *Neoplasia* 1(1)**,** 50-62. doi: 10.1038/sj.neo.7900005.

Bullock, A.N., Henckel, J., and Fersht, A.R. (2000). Quantitative analysis of residual folding and DNA binding in mutant p53 core domain: definition of mutant states for rescue in cancer therapy. *Oncogene* 19(10)**,** 1245-1256. doi: 10.1038/sj.onc.1203434.

Cancer Genome Atlas Research Network. Electronic address, a.a.d.h.e., and Cancer Genome Atlas Research, N. (2017). Integrated Genomic Characterization of Pancreatic Ductal Adenocarcinoma. *Cancer Cell* 32(2)**,** 185-203 e113. doi: 10.1016/j.ccell.2017.07.007.

Cardoso, A.A., Jiang, Y., Luo, M., Reed, A.M., Shahda, S., He, Y., et al. (2012). APE1/Ref-1 regulates STAT3 transcriptional activity and APE1/Ref-1-STAT3 dual-targeting effectively inhibits pancreatic cancer cell survival. *PLoS One* 7(10)**,** e47462. doi: 10.1371/journal.pone.0047462.

Cerami, E., Gao, J., Dogrusoz, U., Gross, B.E., Sumer, S.O., Aksoy, B.A., et al. (2012). The cBio cancer genomics portal: an open platform for exploring multidimensional cancer genomics data. *Cancer Discov* 2(5)**,** 401-404. doi: 10.1158/2159-8290.CD-12-0095.

Che, Q., Xiao, X., Liu, M., Lu, Y., Dong, X., and Liu, S. (2019). IL-6 promotes endometrial cancer cells invasion and migration through signal transducers and activators of transcription 3 signaling pathway. *Pathol Res Pract* 215(6)**,** 152392. doi: 10.1016/j.prp.2019.03.020.

Cicenas, J., Kvederaviciute, K., Meskinyte, I., Meskinyte-Kausiliene, E., Skeberdyte, A., and Cicenas, J. (2017). KRAS, TP53, CDKN2A, SMAD4, BRCA1, and BRCA2 Mutations in Pancreatic Cancer. *Cancers (Basel)* 9(5). doi: 10.3390/cancers9050042.

Cooks, T., Pateras, I.S., Tarcic, O., Solomon, H., Schetter, A.J., Wilder, S., et al. (2013). Mutant p53 prolongs NF-kappaB activation and promotes chronic inflammation and inflammation-associated colorectal cancer. *Cancer Cell* 23(5)**,** 634-646. doi: 10.1016/j.ccr.2013.03.022.

Denley, S.M., Jamieson, N.B., McCall, P., Oien, K.A., Morton, J.P., Carter, C.R., et al. (2013). Activation of the IL-6R/Jak/stat pathway is associated with a poor outcome in resected pancreatic ductal adenocarcinoma. *J Gastrointest Surg* 17(5)**,** 887-898. doi: 10.1007/s11605-013-2168-7.

Di Agostino, S., Strano, S., Emiliozzi, V., Zerbini, V., Mottolese, M., Sacchi, A., et al. (2006). Gain of function of mutant p53: the mutant p53/NF-Y protein complex reveals an aberrant transcriptional mechanism of cell cycle regulation. *Cancer Cell* 10(3)**,** 191-202. doi: 10.1016/j.ccr.2006.08.013.

Freed-Pastor, W.A., and Prives, C. (2012). Mutant p53: one name, many proteins. *Genes Dev* 26(12)**,** 1268-1286. doi: 10.1101/gad.190678.112.

Gao, J., Aksoy, B.A., Dogrusoz, U., Dresdner, G., Gross, B., Sumer, S.O., et al. (2013). Integrative analysis of complex cancer genomics and clinical profiles using the cBioPortal. *Sci Signal* 6(269)**,** pl1. doi: 10.1126/scisignal.2004088.

Gencel-Augusto, J., and Lozano, G. (2020). p53 tetramerization: at the center of the dominant-negative effect of mutant p53. *Genes Dev* 34(17-18)**,** 1128-1146. doi: 10.1101/gad.340976.120.

Goh, A.M., Coffill, C.R., and Lane, D.P. (2011). The role of mutant p53 in human cancer. *J Pathol* 223(2)**,** 116-126. doi: 10.1002/path.2784.

Grasso, C., Jansen, G., and Giovannetti, E. (2017). Drug resistance in pancreatic cancer: Impact of altered energy metabolism. *Crit Rev Oncol Hematol* 114**,** 139-152. doi: 10.1016/j.critrevonc.2017.03.026.

Grivennikov, S.I., and Karin, M. (2010). Dangerous liaisons: STAT3 and NF-kappaB collaboration and crosstalk in cancer. *Cytokine Growth Factor Rev* 21(1)**,** 11-19. doi: 10.1016/j.cytogfr.2009.11.005.

Grzes, M., Oron, M., Staszczak, Z., Jaiswar, A., Nowak-Niezgoda, M., and Walerych, D. (2020). A Driver Never Works Alone-Interplay Networks of Mutant p53, MYC, RAS, and Other Universal Oncogenic Drivers in Human Cancer. *Cancers (Basel)* 12(6). doi: 10.3390/cancers12061532.

Guo, J., Xie, K., and Zheng, S. (2016). Molecular Biomarkers of Pancreatic Intraepithelial Neoplasia and Their Implications in Early Diagnosis and Therapeutic Intervention of Pancreatic Cancer. *Int J Biol Sci* 12(3)**,** 292-301. doi: 10.7150/ijbs.14995.

Hanel, W., Marchenko, N., Xu, S., Yu, S.X., Weng, W., and Moll, U. (2013). Two hot spot mutant p53 mouse models display differential gain of function in tumorigenesis. *Cell Death Differ* 20(7)**,** 898-909. doi: 10.1038/cdd.2013.17.

Herreros-Villanueva, M., Zhang, J.S., Koenig, A., Abel, E.V., Smyrk, T.C., Bamlet, W.R., et al. (2013). SOX2 promotes dedifferentiation and imparts stem cell-like features to pancreatic cancer cells. *Oncogenesis* 2**,** e61. doi: 10.1038/oncsis.2013.23.

Hollstein, M., Sidransky, D., Vogelstein, B., and Harris, C.C. (1991). p53 mutations in human cancers. *Science* 253(5015)**,** 49-53. doi: 10.1126/science.1905840.

Ji, Z., He, L., Regev, A., and Struhl, K. (2019). Inflammatory regulatory network mediated by the joint action of NF-kB, STAT3, and AP-1 factors is involved in many human cancers. *Proc Natl Acad Sci U S A* 116(19)**,** 9453-9462. doi: 10.1073/pnas.1821068116.

Kadosh, E., Snir-Alkalay, I., Venkatachalam, A., May, S., Lasry, A., Elyada, E., et al. (2020). The gut microbiome switches mutant p53 from tumour-suppressive to oncogenic. *Nature* 586(7827)**,** 133-138. doi: 10.1038/s41586-020-2541-0.

Kim, M.P., and Lozano, G. (2018). Mutant p53 partners in crime. *Cell Death Differ* 25(1)**,** 161-168. doi: 10.1038/cdd.2017.185.

Kim, M.P., Zhang, Y., and Lozano, G. (2015). Mutant p53: Multiple Mechanisms Define Biologic Activity in Cancer. *Front Oncol* 5**,** 249. doi: 10.3389/fonc.2015.00249.

Klemke, L., De Oliveira, T., Witt, D., Winkler, N., Bohnenberger, H., Bucala, R., et al. (2021). Hsp90-stabilized MIF supports tumor progression via macrophage recruitment and angiogenesis in colorectal cancer. *Cell Death Dis* 12(2)**,** 155. doi: 10.1038/s41419-021-03426-z.

Landmann, H., Proia, D.A., He, S., Ogawa, L.S., Kramer, F., Beissbarth, T., et al. (2014). UDP glucuronosyltransferase 1A expression levels determine the response of colorectal cancer cells to the heat shock protein 90 inhibitor ganetespib. *Cell Death Dis* 5**,** e1411. doi: 10.1038/cddis.2014.378.

Lane, D.P. (1992). Cancer. p53, guardian of the genome. *Nature* 358(6381)**,** 15-16. doi: 10.1038/358015a0.

Lee, M.K., Teoh, W.W., Phang, B.H., Tong, W.M., Wang, Z.Q., and Sabapathy, K. (2012). Cell-type, dose, and mutation-type specificity dictate mutant p53 functions in vivo. *Cancer Cell* 22(6)**,** 751-764. doi: 10.1016/j.ccr.2012.10.022.

Lin, L., Jou, D., Wang, Y., Ma, H., Liu, T., Fuchs, J., et al. (2016). STAT3 as a potential therapeutic target in ALDH+ and CD44+/CD24+ stem cell-like pancreatic cancer cells. *Int J Oncol* 49(6)**,** 2265-2274. doi: 10.3892/ijo.2016.3728.

Lin, L., Liu, A., Peng, Z., Lin, H.J., Li, P.K., Li, C., et al. (2011). STAT3 is necessary for proliferation and survival in colon cancer-initiating cells. *Cancer Res* 71(23)**,** 7226-7237. doi: 10.1158/0008-5472.CAN-10-4660.

Loizou, E., Banito, A., Livshits, G., Ho, Y.J., Koche, R.P., Sanchez-Rivera, F.J., et al. (2019). A Gain-of-Function p53-Mutant Oncogene Promotes Cell Fate Plasticity and Myeloid Leukemia through the Pluripotency Factor FOXH1. *Cancer Discov* 9(7)**,** 962-979. doi: 10.1158/2159-8290.CD-18-1391.

Mantovani, F., Collavin, L., and Del Sal, G. (2019). Mutant p53 as a guardian of the cancer cell. *Cell Death Differ* 26(2)**,** 199-212. doi: 10.1038/s41418-018-0246-9.

Muller, P.A., Caswell, P.T., Doyle, B., Iwanicki, M.P., Tan, E.H., Karim, S., et al. (2009). Mutant p53 drives invasion by promoting integrin recycling. *Cell* 139(7)**,** 1327-1341. doi: 10.1016/j.cell.2009.11.026.

Muller, P.A., and Vousden, K.H. (2013). p53 mutations in cancer. *Nat Cell Biol* 15(1)**,** 2-8. doi: 10.1038/ncb2641.

Muller, P.A., and Vousden, K.H. (2014). Mutant p53 in cancer: new functions and therapeutic opportunities. *Cancer Cell* 25(3)**,** 304-317. doi: 10.1016/j.ccr.2014.01.021.

Nagathihalli, N.S., Castellanos, J.A., Lamichhane, P., Messaggio, F., Shi, C., Dai, X., et al. (2018). Inverse Correlation of STAT3 and MEK Signaling Mediates Resistance to RAS Pathway Inhibition in Pancreatic Cancer. *Cancer Res* 78(21)**,** 6235-6246. doi: 10.1158/0008-5472.CAN-18-0634.

Nagathihalli, N.S., Castellanos, J.A., Shi, C., Beesetty, Y., Reyzer, M.L., Caprioli, R., et al. (2015). Signal Transducer and Activator of Transcription 3, Mediated Remodeling of the Tumor Microenvironment Results in Enhanced Tumor Drug Delivery in a Mouse Model of Pancreatic Cancer. *Gastroenterology* 149(7)**,** 1932-1943 e1939. doi: 10.1053/j.gastro.2015.07.058.

Nagathihalli, N.S., Castellanos, J.A., VanSaun, M.N., Dai, X., Ambrose, M., Guo, Q., et al. (2016). Pancreatic stellate cell secreted IL-6 stimulates STAT3 dependent invasiveness of pancreatic intraepithelial neoplasia and cancer cells. *Oncotarget* 7(40)**,** 65982-65992. doi: 10.18632/oncotarget.11786.

Natesh, K., Bhosale, D., Desai, A., Chandrika, G., Pujari, R., Jagtap, J., et al. (2015). Oncostatin-M differentially regulates mesenchymal and proneural signature genes in gliomas via STAT3 signaling. *Neoplasia* 17(2)**,** 225-237. doi: 10.1016/j.neo.2015.01.001.

Oren, M., and Rotter, V. (2010). Mutant p53 gain-of-function in cancer. *Cold Spring Harb Perspect Biol* 2(2)**,** a001107. doi: 10.1101/cshperspect.a001107.

Orth, M., Metzger, P., Gerum, S., Mayerle, J., Schneider, G., Belka, C., et al. (2019). Pancreatic ductal adenocarcinoma: biological hallmarks, current status, and future perspectives of combined modality treatment approaches. *Radiat Oncol* 14(1)**,** 141. doi: 10.1186/s13014-019-1345-6.

Parrales, A., Ranjan, A., Iyer, S.V., Padhye, S., Weir, S.J., Roy, A., et al. (2016). DNAJA1 controls the fate of misfolded mutant p53 through the mevalonate pathway. *Nat Cell Biol* 18(11)**,** 1233-1243. doi: 10.1038/ncb3427.

Patel, K., Kollory, A., Takashima, A., Sarkar, S., Faller, D.V., and Ghosh, S.K. (2014). MicroRNA let-7 downregulates STAT3 phosphorylation in pancreatic cancer cells by increasing SOCS3 expression. *Cancer Lett* 347(1)**,** 54-64. doi: 10.1016/j.canlet.2014.01.020.

Razidlo, G.L., Burton, K.M., and McNiven, M.A. (2018). Interleukin-6 promotes pancreatic cancer cell migration by rapidly activating the small GTPase CDC42. *J Biol Chem* 293(28)**,** 11143-11153. doi: 10.1074/jbc.RA118.003276.

Sabapathy, K., and Lane, D.P. (2018). Therapeutic targeting of p53: all mutants are equal, but some mutants are more equal than others. *Nat Rev Clin Oncol* 15(1)**,** 13-30. doi: 10.1038/nrclinonc.2017.151.

Said, R., Hong, D.S., Warneke, C.L., Lee, J.J., Wheler, J.J., Janku, F., et al. (2013). P53 mutations in advanced cancers: clinical characteristics, outcomes, and correlation between progression-free survival and bevacizumab-containing therapy. *Oncotarget* 4(5)**,** 705-714. doi: 10.18632/oncotarget.974.

Schulz-Heddergott, R., and Moll, U.M. (2018). Gain-of-Function (GOF) Mutant p53 as Actionable Therapeutic Target. *Cancers (Basel)* 10(6). doi: 10.3390/cancers10060188.

Schulz-Heddergott, R., Stark, N., Edmunds, S.J., Li, J., Conradi, L.C., Bohnenberger, H., et al. (2018). Therapeutic Ablation of Gain-of-Function Mutant p53 in Colorectal Cancer Inhibits Stat3-Mediated Tumor Growth and Invasion. *Cancer Cell* 34(2)**,** 298-314 e297. doi: 10.1016/j.ccell.2018.07.004.

Schust, J., Sperl, B., Hollis, A., Mayer, T.U., and Berg, T. (2006). Stattic: a small-molecule inhibitor of STAT3 activation and dimerization. *Chem Biol* 13(11)**,** 1235-1242. doi: 10.1016/j.chembiol.2006.09.018.

Siegel, R.L., Miller, K.D., and Jemal, A. (2020). Cancer statistics, 2020. *CA Cancer J Clin* 70(1)**,** 7-30. doi: 10.3322/caac.21590.

Siveen, K.S., Sikka, S., Surana, R., Dai, X., Zhang, J., Kumar, A.P., et al. (2014). Targeting the STAT3 signaling pathway in cancer: role of synthetic and natural inhibitors. *Biochim Biophys Acta* 1845(2)**,** 136-154. doi: 10.1016/j.bbcan.2013.12.005.

Smigiel, J.M., Parameswaran, N., and Jackson, M.W. (2018). Targeting Pancreatic Cancer Cell Plasticity: The Latest in Therapeutics. *Cancers (Basel)* 10(1). doi: 10.3390/cancers10010014.

Spitzner, M., Roesler, B., Bielfeld, C., Emons, G., Gaedcke, J., Wolff, H.A., et al. (2014). STAT3 inhibition sensitizes colorectal cancer to chemoradiotherapy in vitro and in vivo. *Int J Cancer* 134(4)**,** 997-1007. doi: 10.1002/ijc.28429.

Ubby, I., Krueger, C., Rosato, R., Qian, W., Chang, J., and Sabapathy, K. (2019). Cancer therapeutic targeting using mutant-p53-specific siRNAs. *Oncogene* 38(18)**,** 3415-3427. doi: 10.1038/s41388-018-0652-y.

Walerych, D., Kudla, G., Gutkowska, M., Wawrzynow, B., Muller, L., King, F.W., et al. (2004). Hsp90 chaperones wild-type p53 tumor suppressor protein. *J Biol Chem* 279(47)**,** 48836-48845. doi: 10.1074/jbc.M407601200.

Walerych, D., Lisek, K., and Del Sal, G. (2015). Mutant p53: One, No One, and One Hundred Thousand. *Front Oncol* 5**,** 289. doi: 10.3389/fonc.2015.00289.

Walerych, D., Olszewski, M.B., Gutkowska, M., Helwak, A., Zylicz, M., and Zylicz, A. (2009). Hsp70 molecular chaperones are required to support p53 tumor suppressor activity under stress conditions. *Oncogene* 28(48)**,** 4284-4294. doi: 10.1038/onc.2009.281.

Wawrzynow, B., Zylicz, A., and Zylicz, M. (2018). Chaperoning the guardian of the genome. The two-faced role of molecular chaperones in p53 tumor suppressor action. *Biochim Biophys Acta Rev Cancer* 1869(2)**,** 161-174. doi: 10.1016/j.bbcan.2017.12.004.

Weisz, L., Damalas, A., Liontos, M., Karakaidos, P., Fontemaggi, G., Maor-Aloni, R., et al. (2007). Mutant p53 enhances nuclear factor kappaB activation by tumor necrosis factor alpha in cancer cells. *Cancer Res* 67(6)**,** 2396-2401. doi: 10.1158/0008-5472.CAN-06-2425.

Wiech, M., Olszewski, M.B., Tracz-Gaszewska, Z., Wawrzynow, B., Zylicz, M., and Zylicz, A. (2012). Molecular mechanism of mutant p53 stabilization: the role of HSP70 and MDM2. *PLoS One* 7(12)**,** e51426. doi: 10.1371/journal.pone.0051426.

Xu, J., Wang, J., Hu, Y., Qian, J., Xu, B., Chen, H., et al. (2014). Unequal prognostic potentials of p53 gain-of-function mutations in human cancers associate with drug-metabolizing activity. *Cell Death Dis* 5**,** e1108. doi: 10.1038/cddis.2014.75.

Zhang, Y., Xiong, S., Liu, B., Pant, V., Celii, F., Chau, G., et al. (2018). Somatic Trp53 mutations differentially drive breast cancer and evolution of metastases. *Nat Commun* 9(1)**,** 3953. doi: 10.1038/s41467-018-06146-9.

Zilfou, J.T., and Lowe, S.W. (2009). Tumor suppressive functions of p53. *Cold Spring Harb Perspect Biol* 1(5)**,** a001883. doi: 10.1101/cshperspect.a001883.

Zou, S., Tong, Q., Liu, B., Huang, W., Tian, Y., and Fu, X. (2020). Targeting STAT3 in Cancer Immunotherapy. *Mol Cancer* 19(1)**,** 145. doi: 10.1186/s12943-020-01258-7.

Figures/Figure Legends
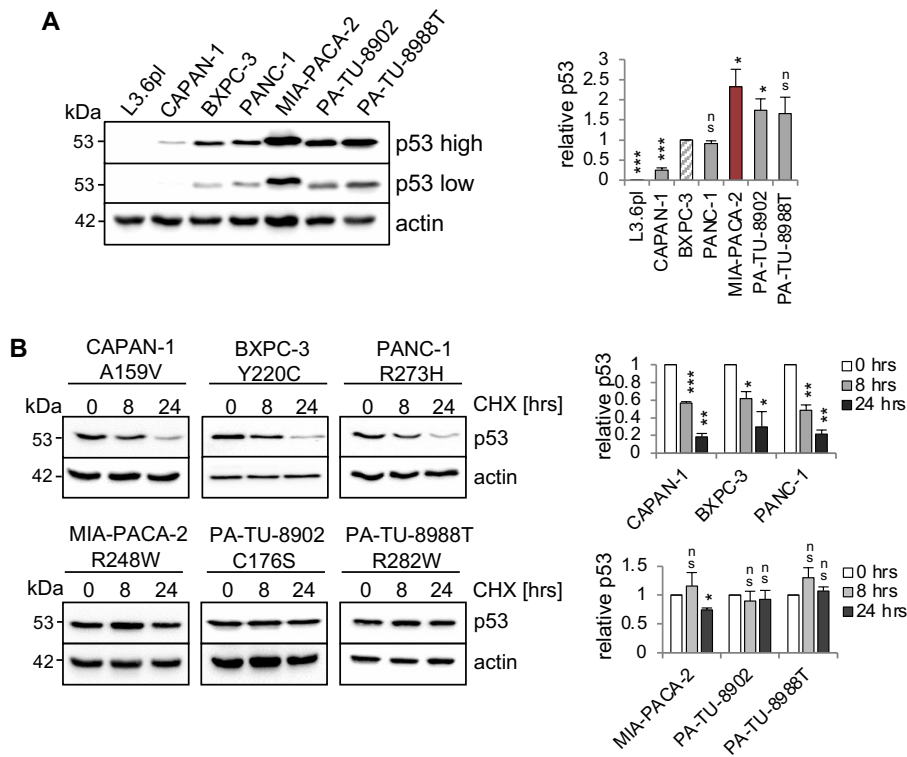
Figure 1

Figure 1: Stabilization of various missense p53 mutants in human PDAC cell lines. (A) Six PDAC cell lines harbouring various missense mutant p53 variants exhibit differential steady state protein levels. One representative immunoblot analysis out of 4 is shown. Actin as loading control. 'p53 high' and 'p53 low' mean exposure time. CAPAN-1 (mutp53^{A159V}), BXPC-3 (mutp53^{Y220C}), PANC-1 (mutp53^{R273H}), MIA-PACA-2 (mutp53^{R248W}), PA-TU-8902 (mutp53^{C176S}) and PA-TU-8988T (mutp53^{R282W}). L3.6pl cells harboring a truncating LOF mutation served as p53 null control. (right) Diagrams represent the means ± SEM of densitometric quantifications of two independent experiments with two technical replicates each (total n=4 immunoblots), normalized to actin or HSC70 and calculated relative to mutp53 level in BXPC-3 cells (patterned bar). (B) Differential half-lives of mutp53 proteins. Cycloheximide (CHX) chase experiment. Cells were treated with CHX for 8 and 24 hrs or vehicle control (0 hrs). One representative immunoblot. Actin, loading control. (right) Diagrams represent mutp53 protein levels as means ± SEM of densitometric quantifications of two independent experiments (n=2), normalized to actin or HSC70. Calculated relative to control treatment (0 hrs). (A, B) Student's t test. *p ≤ 0.05; **p ≤ 0.01; ***p ≤ 0.001; ns, not significant.
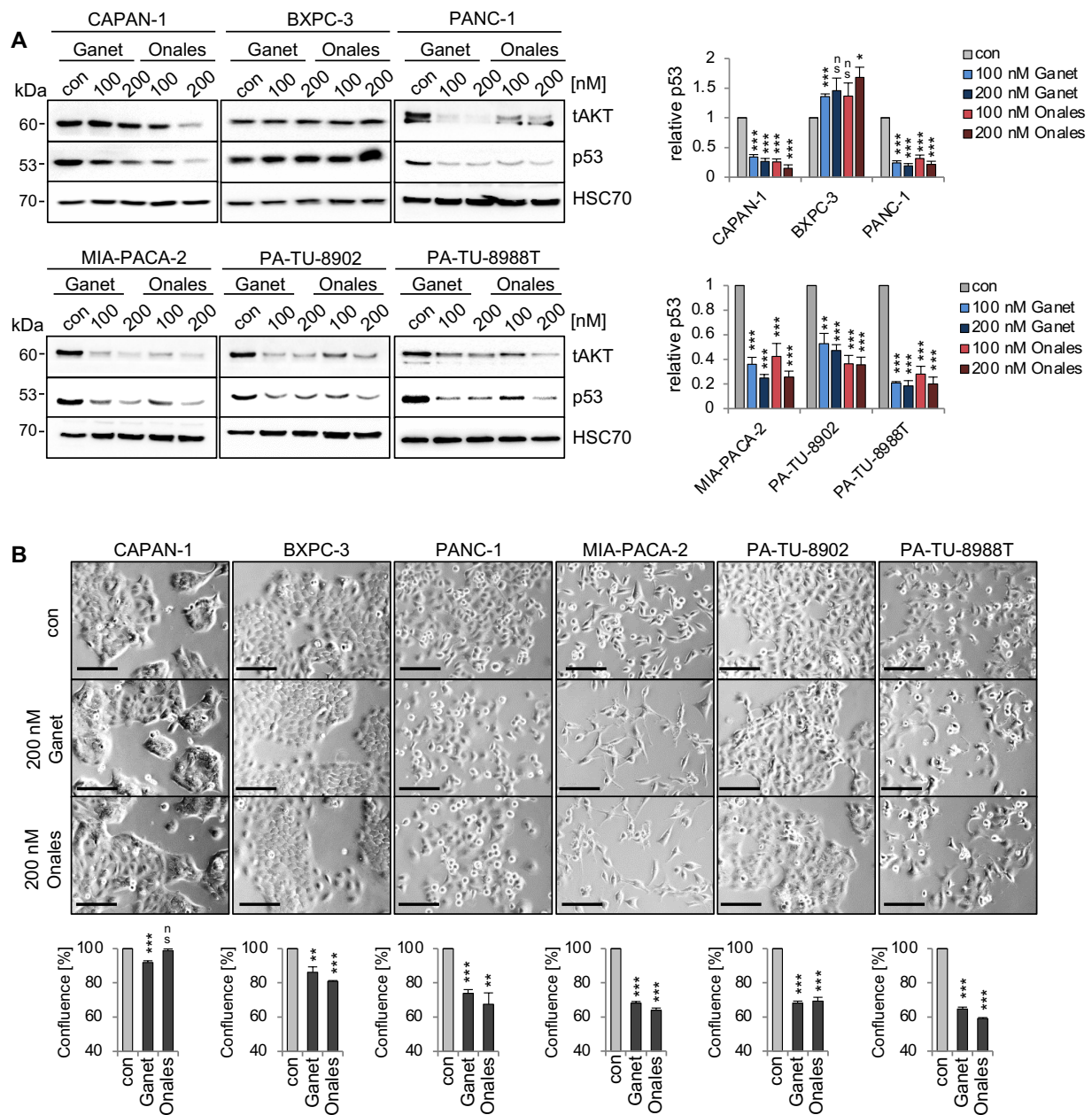
Figure 2

Figure 2: Missense p53 mutants in PDAC cells are stabilized by HSP90. (A) Hsp90 dependent aberrant stabilization of mutp53 proteins in PDAC cell lines. Cells were treated for 24 hrs with the indicated concentrations of Ganetespib, Onalespib or DMSO. One representative immunoblot out of 3 each is presented. HSC70, loading control. Total AKT ('tAKT', AKT serine/threonine kinase 1) as well-known Hsp90 client serves as functional control for an Hsp90 inhibition. (right) Diagrams represent the means ± SEM of densitometric quantifications of at least two independent experiments with technical replicates (total n≥3 immunoblots), normalized to HSC70. Calculated relative to control DMSO treatments (con). (B) Cell confluence determination. Representative images of cells after treatment with 200 nM Ganetespib, Onalespib or solvent control for 24 hrs. Cell confluency was analysed using a Celigo imaging cytometer. Scale bars, 100 μm. Confluence was calculated relative to their respective DMSO control from n=3 biological replicates. Student's t test. *$p ≤ 0.05$; **$p ≤ 0.01$; ***$p ≤ 0.001$; ns, not significant.
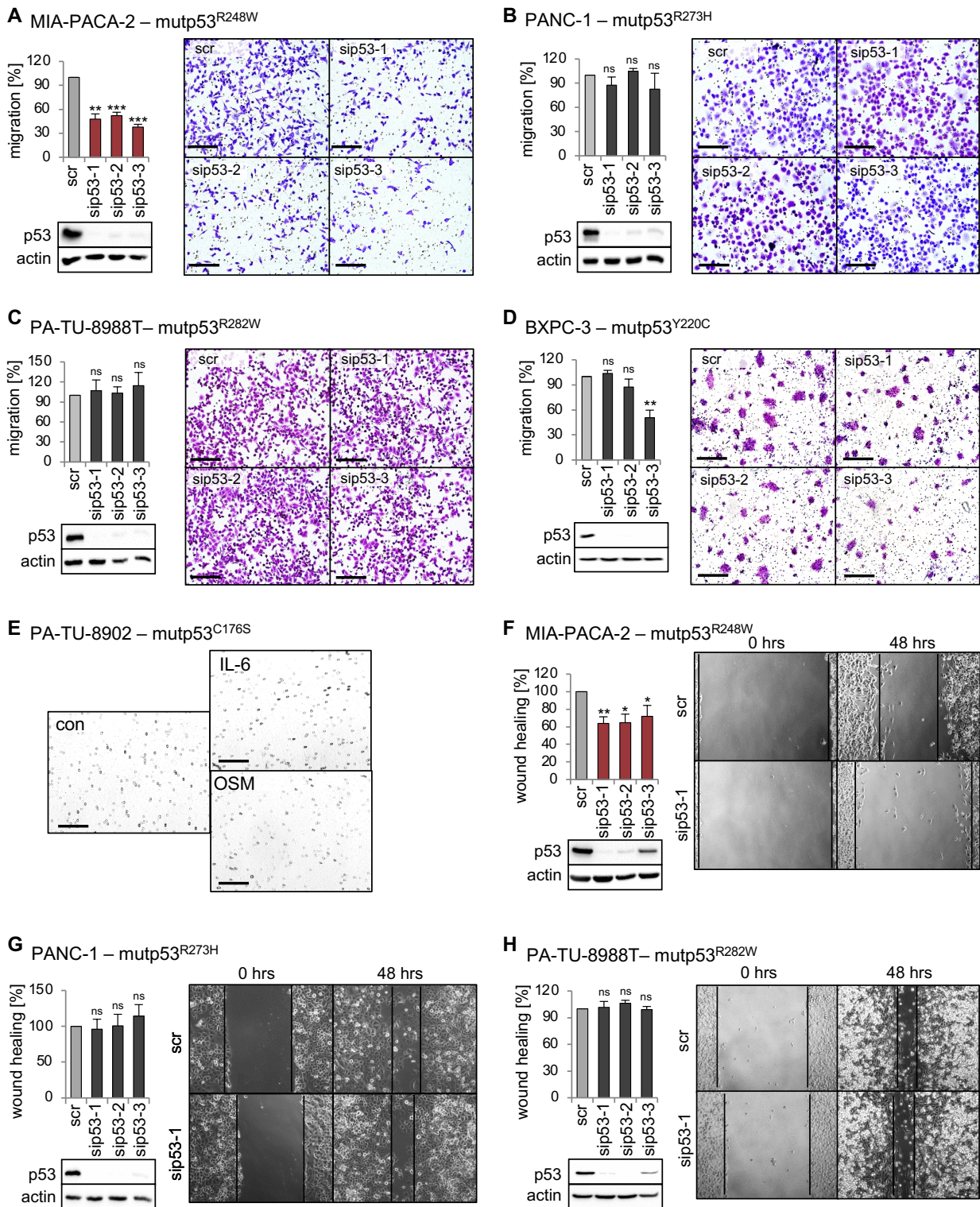
Figure 3

Figure 3: Mutp53^{R248W} selectively promotes migration in PDAC cells. (A-D) Transwell migration assays of MIA-PACA-2, PANC-1, PA-TU-8988Tand BXPC-3 cells to evaluate mutp53-dependent migration activity. mutp53 was depleted with three different siRNAs against *TP53* mRNA (sip53 1-3). 72 hrs post-transfection with siRNAs, cells were seeded into transwell inserts and migration to the membrane underside was determined after 24 hrs. MIA-PACA-2 cells: 3 biological replicates (n=3), PANC-1 cells: 2 biological replicates (n=2), PA-TU-8988T cells: 3 biological replicates (n=3), BXPC-3 cells: 3 biological replicates, one with a technical replicate (n=4). Note, siRNA 'sip53-3' reduced migration in BXPC-3 cells might be a consequence of siRNA off-target effects. Migration was calculated relative to scrambled control (scr, set as 100%). Representative images of membrane undersides are shown. Scale bars, 200 µm. Immunoblot analysis verifies knockdown of mutp53. Actin, loading control. (E) Transwell migration assay of PA-TU-8902. Representative images of stained transwells after 24 hrs of migration are shown. To induce migration cells had been stimulated for 24 hrs with 50 ng/mL Interleukin-6 (IL-6), Oncostatin M (OSM) or solvent control (con) prior to seeding into inserts, followed by additional cytokine treatment for another 24 hrs. Gray dots are pores of the membrane. Scale bars, 200 µm. (F-H) mutp53-dependent wound healing of MIA-PACA-2, PANC-1 and PA-TU-8988T cells. mutp53 knockdown for 48 hrs using three different siRNAs (sip53 1-3). 48 hrs post-transfection, scratch assays were performed for another 48 hrs. A minimum of 5 images were taken and quantified. MIA-PACA-2 cells: 3 biological replicates, 1 out of 3 with a technical replicate (n=4), PANC-1 cells: 2 biological replicates, 1 out of 2 with a technical replicate (n=3), PA-TU-8988T cells: 2 technical replicates (n=2). Wound healing capacity was calculated relative to scrambled control (scr). Representative images after 0 hrs and 48 hrs are shown. Solid lines represent edges of the scratch. Immunoblots verify knockdown of mutp53. Actin, loading control. (A-D, F-H) Diagrams represent the means ± SEM. Student's t test. *p ≤ 0.05; **p ≤ 0.01; ***p ≤ 0.001; ns, not significant.
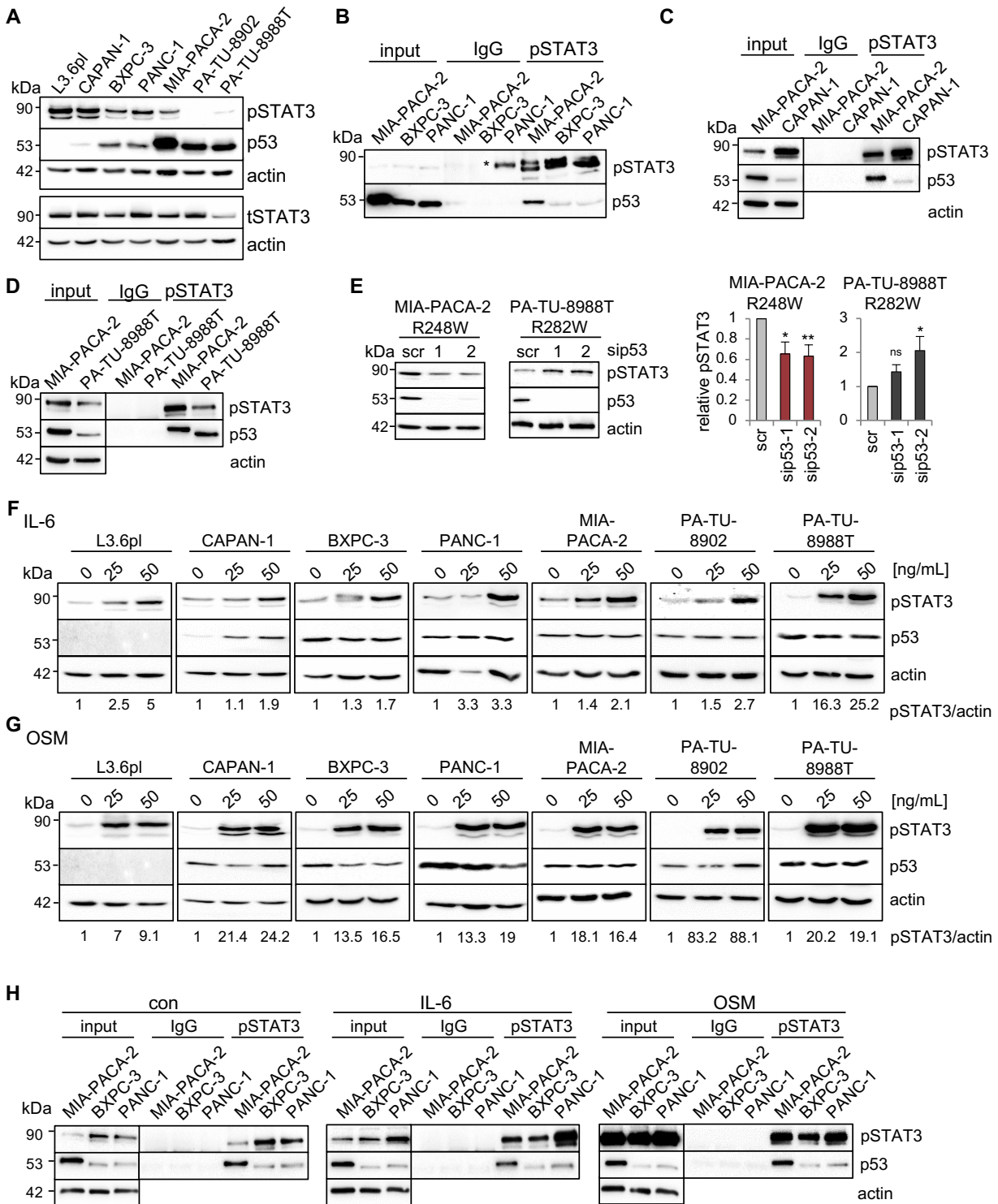
Figure 4

Figure 4: Mutp53^{R248W} selectively binds to phosphorylated STAT3 in PDAC cells. (A) Representative immunoblot analysis of seven different PDAC cell lines. pSTAT3, pTyr 705-STAT3 (Y705) and total STAT3 (tSTAT3). Actin, loading control. (B-D) Co-immunoprecipitations (CoIPs) of untreated MIA-PACA-2, PANC-1, BXPC-3 (B), CAPAN-1 (C) and PA-TU-8988T (D) cells using anti-pSTAT3 (Y705) or IgG antibodies followed by immunoblot analysis. MIA-PACA-2 cells were always used as positive control. Note, the pSTAT3 band marked by an asterisk in (B) is an artefact due to a leaky pocket from the neighbouring MIA-PACA-2 lane. (E) Knockdown of mutp53 in MIA-PACA-2, but not in PA-TU-8988T cells downregulates pSTAT3 levels. Cells were transfected with two different siRNA against *TP53* mRNA (sip53-1, -2) or scrambled control (scr) for 72 hrs followed by immunoblot analysis. Representative immunoblot out of 3 (MIA-PACA-2) and out of 4 (PA-TU-8988T). Actin, loading control. (right) Diagrams represent the means ± SEM of densitometric quantifications of three (MIA-PACA-2, n=3) or two (PA-TU-8988T, n=4) independent experiments, normalized to actin. Calculated relative to control scrambled siRNA (scr). Student's t test. *p ≤ 0.05; **p ≤ 0.01; ns, not significant. (F, G) Treatment of PDAC cell lines with the indicated concentrations of Interleukin-6 (IL-6, F), Oncostatin M (OSM, G) or respective solvent controls for 24 hrs. Representative immunoblot for pSTAT3 (Y705) induction is shown. Quantification by densitometry, normalized to actin loading control (pSTAT3/actin ratio) and calculated relative to solvent control. 'pSTAT3/actin', densitometric quantifications of the representative immunoblot, normalized to actin and relative to 0 ng/ml IL-6 or OSM treatments. (H) CoIPs of MIA-PACA-2, PANC-1 and BXPC-3 cells stimulated with 50 ng/mL IL-6, OSM or solvent control for 24 hrs. Immunoprecipitation using anti-pSTAT3 (Y705) or IgG antibodies, followed by immunoblot as indicated. Actin in unprecipitated input lysates, loading control. (B-D and H) 5% of input were used for input control.
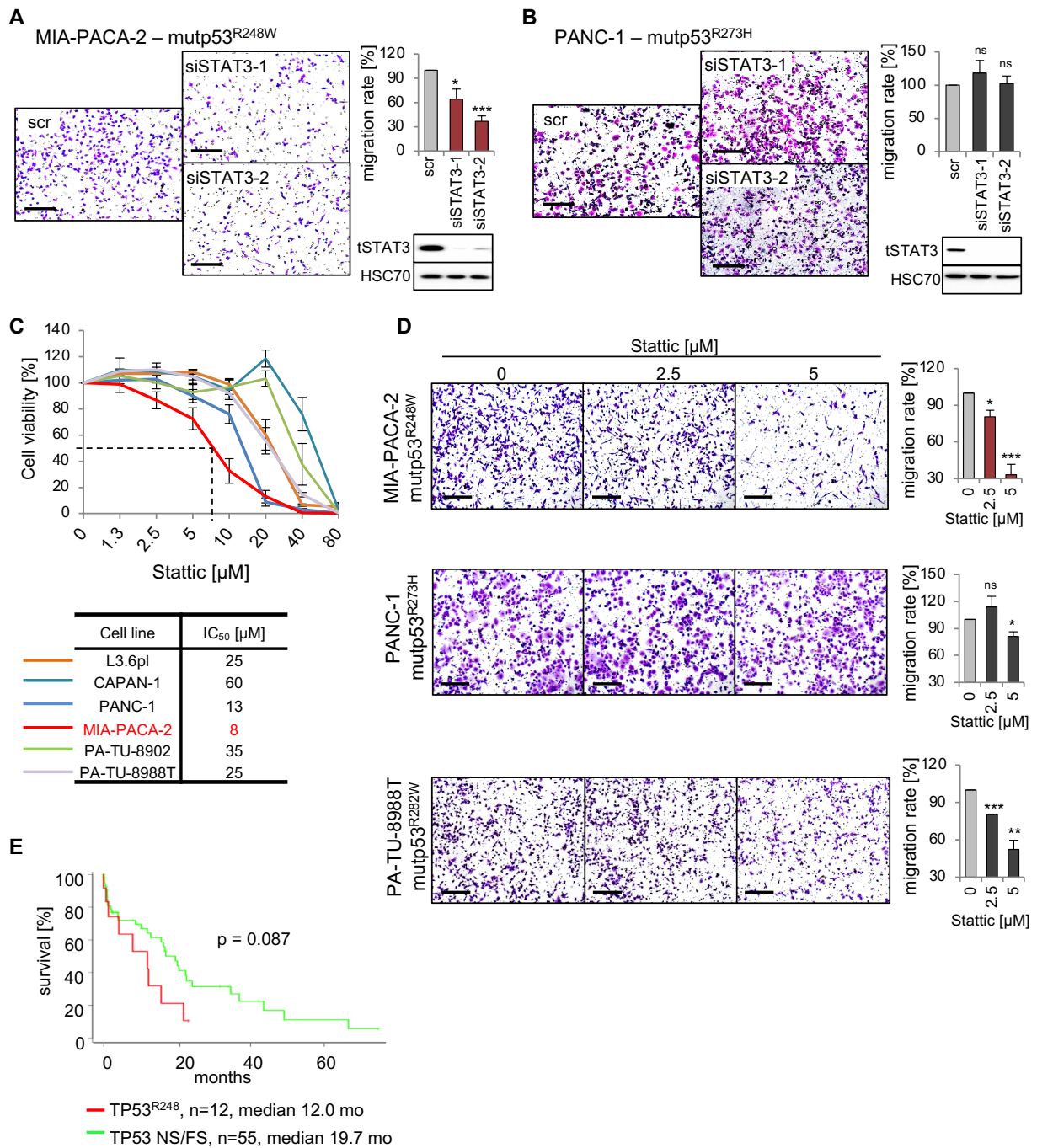
Figure 5

Figure 5: p53^{R248W} mutant selectively regulates STAT3 phosphorylation and activity in PDAC cells. (A, B) STAT3 knockdown phenocopies mutp53 knockdown in migration assays. MIA-PACA-2 (A) and PANC-1 (B) cells were transfected with two different siRNAs against *STAT3* mRNA (siSTAT3-1, -2) or scrambled control (scr). 72 hrs post-transfection cells were seeded into transwell inserts to assess their migration. After 24 hrs cells were fixed, stained and counted at the membrane underside. Scale bars, 200 μm. MIA-PACA-2 cells: 4 biological replicates (n=4), PANC-1 cells: 3 biological replicates, 2 out of 3 with 2 technical replicates (n=5). Cells were calculated relative to scrambled control. Immunoblot analysis to confirm knockdown of STAT3. HSC70, loading control. (C) Cell viability assays of the indicated PDAC cell lines. Dose response curve after treatment with increasing concentrations of the STAT3 inhibitor Stattic or solvent control for 24 hrs. For each cell line 3-4 biological replicates were measured. Diagram represents means ± SEM. From these curves IC$_{50}$ values were determined, indicated in the table. Of note, MIA-PACA-2 cells are the most sensitive to Stattic treatment, indicated by the dashed line. (D) STAT3 inhibition phenocopies mutp53 knockdown in migration assays. Transwell migrations assays of MIA-PACA-2, PANC-1 and PA-TU-8988T cells treated with the indicated concentrations of Stattic for 24 hrs. Scale bars, 200 μm. For all cell lines, quantification of 2 biological replicates, 1 of them with 2 technical replicates (n=3 total), calculated relative to 0 μM control treatment. (E) Survival curve of PDAC patients harboring TP53 R248 mutations versus patients harboring TP53 nonsense or frameshift (NS/FS) mutations. Number of patients and mean overall survival in months as indicated. TCGA data. Kaplan-Meier statistic, log-rank test. (A, B and D) Diagrams represent the means ± SEM. Student's t test. *p ≤ 0.05; **p ≤ 0.01; ***p ≤ 0.001; ns, not significant.

Supplemental material
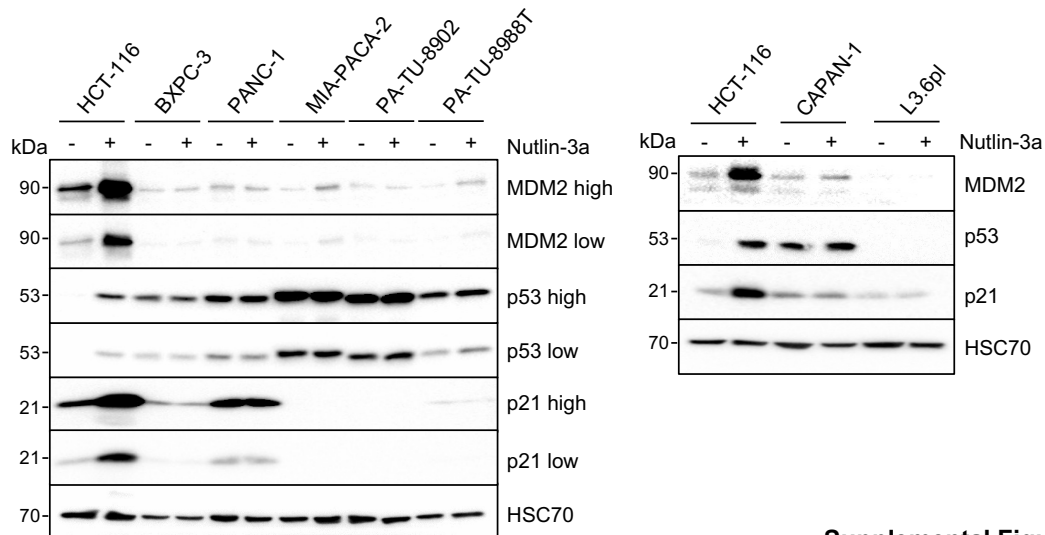
Supplemental Figure 1

Figure S1: Functional validation of missense p53 mutants in human PDAC cell lines. Representative immunoblots of seven PDAC cell lines harbouring various mutant p53 variants. Cells were treated with DMSO (-) or 10 μM Nutlin-3a (+) for 8 hrs. Wildtype p53 containing HCT 116 cells served as functional positive control for p53 activation. 'high' and 'low' mean exposure time. CAPAN-1 (mutp53A159V), BXPC-3 (mutp53Y220C), PANC-1 (mutp53R273H), MIA-PACA-2 (mutp53R248W), PA-TU-8902 (mutp53C176S) and PA-TU-8988T (mutp53R282W). L3.6pl cells harboring a truncating LOF mutation served as p53 null control. Note, all mutp53-containing cells failed to induce p53 targets p21 (CDKN1A, cyclin dependent kinase inhibitor 1A) and MDM2 (mouse double minute 2) after Nutlin-3a treatment.
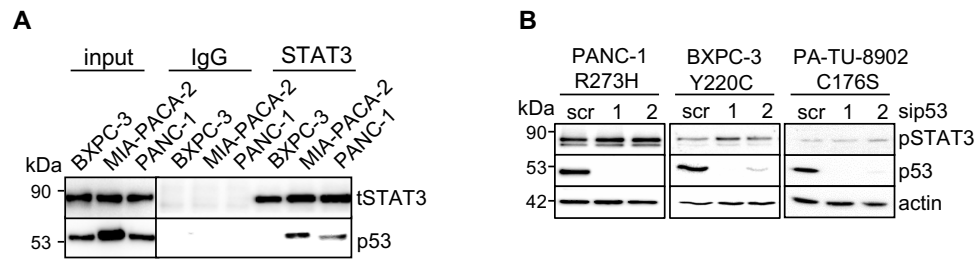
Supplemental Figure 2

Figure S2 related to Figure 4: Mutp53^{R248W} selectively binds to phosphorylated STAT3 in PDAC cells. (A) Co-immunoprecipitation (CoIP) of untreated BXPC-3, MIA-PACA-2 and PANC-1 cells to investigate mutp53 binding to total STAT3 (tSTAT3). Immunoprecipitation with anti-total STAT3 (STAT3) or immunoglobulin G (IgG) antibodies, followed by immunoblot analysis. (B) Knockdown of mutp53 in PANC-1, BXPC-3 or PA-TU-8902 cells does not downregulate pSTAT3 levels. Cells were transfected with two different siRNA against *TP53* mRNA (sip53-1, -2) or scrambled control (scr) for 72 hrs followed by immunoblot analysis. Representative immunoblots are shown. Actin, loading control.

Supplemental Table 1: Reagents and Resources

REAGENT or RESOURCE	SOURCE	IDENTIFIER		
Antibodies			**WB**	**Co-IP**
Rabbit monoclonal anti-Akt [D9E]	Cell Signaling	9272, RRID:AB_329827	1:1,000	
Mouse polyclonal anti-beta-Actin	Abcam	ab6276, RRID:AB_2223210	1:10,000	
Rabbit polyclonal anti-beta-Actin	Abcam	ab8227, RRID:AB_2305186	1:10,000	
Mouse monoclonal anti-HSC70 [B-6]	Santa Cruz	sc-7298, RRID:AB_627761	1:5,000	
Mouse monoclonal anti-MDM2 (Ab-1) [IF-2]	Calbiochem®/ Millipore	OP46, RRID:AB_2335867	1:300	
Rabbit monoclonal anti-p21 Waf1/Cip1 [12D1]	Cell Signaling	2947, RRID:AB_823586	1:1,000	
Mouse monoclonal anti-p53 [DO-1]	Santa Cruz	sc-126, RRID:AB_628082	1:10,000	
Mouse monoclonal anti-p53 [DO-1], HRP conjugated	Santa Cruz	sc-126 HRP, RRID:AB_628082	1:1,000	3µg
Rabbit monoclonal anti-phospho-Y705 STAT3 [EP2147Y]	Abcam	ab76315, RRID:AB_1658549	1:2,000	3µg
Rabbit polyclonal anti-STAT3	Santa Cruz	sc-482, RRID:AB_632440	1:1,000	
Rabbit monoclonal anti-STAT3 [79D7]	Cell Signaling	4904, RRID:AB_331269	1:1,000	3µg
Rabbit monoclonal anti-IgG [EPR25A]	Abcam	ab172730, RRID:AB_2687931		3µg
goat anti-rabbit IgG-HRP	Santa Cruz	sc-2004, RRID:AB_631746	1:10,000	
goat anti-mouse IgG-HRP	Santa Cruz	sc-2005, RRID:AB_631736	1:10,000	
Chemicals, Peptides and Recombinant Proteins				
BCA protein assay	Pierce	23227		
CellTiter-Glo® Luminescent Cell Viability Assay	Promega	G7571		
Clarity Max™ Western ECL Substrate	BioRad	1705062		
cOmplete™ mini protease inhibitor cocktail	Roche	11836170001		
Crystal violet (C.I. 42555)	Roth	T123.1		
Cycloheximide	Sigma-Aldrich	C7698		
Dimethyl sulfoxide (DMSO) Cell culture grade	AppliChem	A3672		
EDTA	Roth	8040.1		
Ethanol absolut	Chemsolute®/ Th.Geyer	2246		
Ganetespib	Provided by Synta Pharmaceuticals	N/A		
Imidazol	Roth	899.2		
Immobilion Western chemiluminescent HRP substrate	Millipore/Merck	WBKLS0500		

InSolution™ MG-132		Calbiochem®/ Merck		474791		
Interleukin-6		Immunotools		11340064		
Methanol		Roth		8388.3		
Milk powder		Roth		T145.4		
NaCl		Roth		3957.2		
NaF		AppliChem		A0401		
Nitrocellulose membranes		Amersham		GE10600001		
Nonidet™ P 40 Substitute		Sigma-Aldrich		74385		
Nutlin-3a		BOC Sciences		B0084-425358		
Onalespib		Selleckchem		S1163		
Oncostatin M (209a.a)		Immunotools		11344223		
Protein G Sepharose 4 Fast Flow		GE Healthcare		17061805		
SDS		Roth		CN30.3		
Sodium deoxycholate		Sigma-Aldrich		30970		
Sodium orthovanadate		Sigma-Aldrich		S6508		
Stattic		Santa Cruz		sc-202818		
SuperSignal™ West Femto Maximum Sensitivity Substrate		ThermoFisher Scientific		34095		
Tris-HCl		Roth		4855.3		
TritonX-100		AppliChem		A1388		
Tween-20		AppliChem		A4974		
Reagents for Cell culture						
DMEM		Gibco		31600091		
FBS		Merck		S0615		
L-Glutamine		Gibco		25030123		
Mycoplasma Detection Kit		Lonza		LT07-318		
Penicillin-Streptomycin		Gibco		15140122		
RPMI 1640		Gibco		42401042		
Lipofectamine™ 3000 Transfection Reagent		Invitrogen		L3000015		
Lipofectamine™ 2000 Transfection Reagent		Invitrogen		11668019		
TC treated 6 well plates		Sarstedt		83.3920		
TC treated 96 well plates		Corning		3903		
Falcon® Permeable Support for 24-well Plate with 8.0 µm Transparent PET Membrane		Corning		353097		
Falcon® 24-well TC-treated Cell Polystyrene Permeable Support Companion Plate		Corning		353504		
Experimental models: Cell lines						
			96 well	Transwell insert	6 well cmp	6 well transfection
L3.6pl	RRID:CVCL_0384	PMID: 23917223; PMID: 10935470	5,000	-	150,000	-
MIA-PACA-2	DSMZ, RRID:CVCL_0428	ACC 733	3,000	70,000	120,000	80,000

PANC-1	ATCC, RRID:CVCL_0480	CRL-1469	5,000	50,000	200,000	100,000
PA-TU-8988T	DSMZ, RRID:CVCL_1847	ACC 162	4,000	70,000	150,000	90,000
PA-TU-8902	DSMZ, RRID:CVCL_1845	ACC 179	4,000	70,000	150,000	100,000
BXPC-3	ATCC, RRID:CVCL_0186	CRL-1687	5,000	100,000	200,000	100,000
CAPAN-1	ATCC, RRID:CVCL_0237	HTB-79	10,000	-	300,000	-
						cmp, compound

Oligonucleotides and Recombinant DNA		
siRNA Silencer™ Select Negative Control No. 2 siRNA (scr)	Invitrogen	4390847
siRNA p53 Silencer™ Select No.1	ThermoFisher Scientific	4390824, siRNA ID s605
siRNA p53 Silencer™ Select No.2	ThermoFisher Scientific	4390824, siRNA ID s606
siRNA p53 Silencer™ Select No.3	ThermoFisher Scientific	AM51331, siRNA ID 106141
siRNA STAT3 Silencer™ Select No.1	ThermoFisher Scientific	4390824, siRNA ID s743
siRNA STAT3 Silencer™ Select No.2	ThermoFisher Scientific	4390824, siRNA ID s744
Software and Algorithms		
ImageJ software	Open source	https://imagej.net/Welcome
Image Lab™ Software	Biorad	http://www.bio-rad.com/de-de/product/image-lab-software
ZEN	Zeiss	https://www.zeiss.de/mikroskopie/produkte/mikroskopsoftware/zen.html
Image Lab™ Software	Biorad	http://www.bio-rad.com/de-de/product/image-lab-software
Adobe Photoshop Software	Adobe	https://www.adobe.com/de/creativecloud/plans.html
Celigo Imaging Cytometer	Nexcelom Bioscience	https://www.nexcelom.com/nexcelom-products/cellometer-and-celigo-image-cytometers/celigo-imaging-cytometer/

Supplemental cell lines authentication

Leibniz-Institut
DSMZ-Deutsche Sammlung von
Mikroorganismen und Zellkulturen GmbH

DSMZ

Leibniz-Institut DSMZ GmbH · Inhoffenstraße 7 B · 38124 Braunschweig

Georg-August-Universität Göttingen
Frau Luisa Klemke
Molekulare Onkologie
Justus-von-Liebig-Weg 11
37077 Göttingen

Leibniz
Gemeinschaft

| Ihr Zeichen/Your ref. | Unser Zeichen/Our ref.: WDi | +49(0)531-2616-166 | Datum/Date: 26.02.2021 |

Dear Ms. Klemke,

Thank you for your request for authentication of human cell lines and species verification of animal cell line samples. We performed DNA profiling using 17 different and highly polymorphic STR (Short Tandem Repeat) loci. In addition, we have tested your human samples for the presence of mitochondrial DNA sequences from rodent cells such as mouse, rat, Chinese and Syrian hamster.
Animal cell line samples have been subjected to the procedure of Cytochrome C Subunit I (COI) DNA Barcoding for identification of the species.
Results (table 1):

	sample	parental/reference line	comment/match
1	L3.6pl	Colo-357 (Kajiji SM et al., 1987)	full-matching STR profile of cell line COLO-357 in the reference database, authentic*
2	MIA-PACA-2	MIA-PACA-2 (DSMZ ACC 733)	full-matching STR profile of cell line MIA-PACA-2 in the reference database, authentic*
3	PANC-1	PANC-1 (DSMZ ACC 783)	full-matching STR profile of cell line PANC-1 in the reference database, authentic
4	BXPC-3	BXPC-3 (DSMZ ACC 760)	full-matching STR profile of cell line BXPC-3 in the reference database, authentic
5	CAPAN-1	CAPAN-1 (DSMZ ACC 244)	full-matching STR profile of cell line CAPAN-1 in the reference database, authentic
6	PA-TU-8902	PA-TU-8902 (DSMZ ACC 179)	full-matching STR profile of cell line PA-TU-8902 the reference database, authentic
7	HCT116 WT	HCT-116 WT (DSMZ ACC 581)	full-matching STR profile of cell line HCT-116 in the reference database, authentic*
8	RKO	RKO (ATCC CRL-2577)	full-matching STR profile of cell line RKO in the reference database, authentic*
9	LS174.T	LS174.T (DSMZ ACC 759)	full-matching STR profile of cell line LS174.T in the reference database, authentic*
10	SW480	SW-480 (DSMZ ACC 313)	full-matching STR profile of cell line SW-480 in the reference database, authentic
11	SW837	SW-837 (ATCC CRL-235)	fullmatching STR profile of cell line SW-837 in the reference database, authentic
12	SW620	SW-620 (ATCC CRL-227)	matching STR profile of cell line SW-620 in the reference database, authentic
13	DLD-1	DLD-1 (DSMZ ACC 278)	full-matching STR profile of cell line DLD-1 in the reference database, authentic
14	HT-29	HT-29 (DSMZ ACC 299)	full-matching STR profile of cell line HT-29 in the reference database, authentic
15	H1299	H1299 (ATCC CRL-5803)	full-matching STR profile of cell line H-1299 in the reference database, authentic*
16	SJSA	SJSA (ATCC CRL-2098)	full-matching STR profile of cell line SJSA in the reference database, authentic
17	Vero E6	Vero E6 (ATCC CRL-1033)	COI DNA Barcoding analysis revealed *Chlorocebus aethiops* species, species-specific
18	Calu-3 DPZ	Calu-3 DPZ (ATCC HTB-055)	full-matching STR profile of cell line CALU-3 in the reference database, authentic
19	Calu-3 ATCC	Calu-3 ATCC (ATCC HTB-055)	full-matching STR profile of cell line CALU-3 in the reference database, authentic
20	RPE WT	hTERT-RPE (ATCC CRL-4000)	full-matching STR profile of cell line hTERT-RPE in the reference database, authentic
21	HCC1806	HCC1806 (ATCC CRL-2335)	full-matching STR profile of cell line HCC1806 in the reference database, authentic

Leibniz-Institut
DSMZ-Deutsche Sammlung von
Mikroorganismen und Zellkulturen GmbH

DSMZ

The proof for rodent cells in all samples was negative: At a detection limit of $1:10^{-5}$ we could not detect mitochondrial sequences of *Mus musculus, Rattus norvegicus, Cricetulus auratus,* and *Cricetulus griseus*. Vice versa, sample 17 Vero E6 of *Chlorocebus aethiops* species is additionally free of human cells at a detection limit of 10^{-3}.

We have carried out a search of the generated STR profiles of your samples which showed predominantly full matches with the STR data sets of respective parental human cell lines. With the exception of animal sample 17, the human samples are of authentic origin as highlighted in green in table 1.

*Asteriks-marked samples of table 1 reveal either the phenomenon of Microsatellite Instability (MSI) or Loss of Heterozygosity (LoH) at STR loci, which are marked in green color in table 2 (allelic list enclosed). MSI and LoH are often observed in cell lines after bottlenecking selection procedures (e. g. immortalization, gene transfer experiments etc.) in combination with loss of DNA Mismatch Repair. As a consequence respective drifted or lost alleles can become visible without any impact on the status of authenticity. To ensure the STR results we have performed VNTR Typing which could confirm the predicted identities and are free of additional costs (gel documentation in excel sheet).

For authentication of animal cell line samples we have carried out DNA Barcoding by PCR amplification of the 5´-coding region of Cytochrome C Oxidase Subunit I and sequencing of the respective PCR product. Alignment of COI sequence revealed that sample Vero-E6 represents a cell culture of *Chlorocebus aethiops* (Green Monkey) indicating the correct species of primate cell line (table 1).

A further individualization of animal cell lines can often not be carried out because of the lack of suitable STR typing systems or is not possible in the case of rodent cells because of a lack of genetic variability by inbreeding.

The exclusion rate of the applied human STR system is indicating authenticity/uniqueness without any doubt, the matching probability of the system ranges from 1 in 1,114,000,000 for Caucasian and American.

Please find enclosed the documentation (STR electropherograms) and the allelic lists (tables 2 and 3).

Sincerely yours,

DSMZ

W. Dirks

Dr. Wilhelm Dirks
Abt. Menschliche und Tierische Zellkulturen
Leibniz-Institut DSMZ-Deutsche
Sammlung von Mikroorganismen
und Zellkulturen GmbH

Inhoffenstraße 7B • 38124 Braunschweig • Germany
wilhelm.dirks@dsmz.de • Tel.: +49-531-2616-166

References for cell line subclone L3.6pl:

COLO-357 (Morgan R.T., Woods L.K., Moore G.E., Quinn L.A., McGavran L., Gordon S.G. Human cell line (COLO 357) of metastatic pancreatic adenocarcinoma. Int. J. Cancer 25:591-598, 1980)

COLO357/FG (Kajiji S.M., Davceva B., Quaranta V. Six monoclonal antibodies to human pancreatic cancer antigens. Cancer Res. 47:1367-1376, 1987)

L3.1 (Vezeridis M.P., Tzanakakis G.N., Meitner P.A., Doremus C.M., Tibbetts L.M., Calabresi P. In vivo selection of a highly metastatic cell line from a human pancreatic carcinoma in the nude mouse. Cancer 69:2060-2063, 1992)

L3.2 (Vezeridis M.P., Tzanakakis G.N., Meitner P.A., Doremus C.M., Tibbetts L.M., Calabresi P. In vivo selection of a highly metastatic cell line from a human pancreatic carcinoma in the nude mouse. Cancer 69:2060-2063, 1992)

L3.3 (Vezeridis M.P., Tzanakakis G.N., Meitner P.A., Doremus C.M., Tibbetts L.M., Calabresi P. In vivo selection of a highly metastatic cell line from a human pancreatic carcinoma in the nude mouse. Cancer 69:2060-2063, 1992)

L3.6pl (Bruns C.J., Harbison M.T., Kuniyasu H., Eue I., Fidler I.J. In vivo selection and characterization of metastatic variants from human pancreatic adenocarcinoma by using orthotopic implantation in nude mice. Neoplasia 1:50-62, 1999)

Leibniz-Institut
DSMZ-Deutsche Sammlung von
Mikroorganismen und Zellkulturen GmbH

DSMZ

Identification Service
Submission Form

Institute/Company	Georg-August-Universität Göttingen
Name	Luisa Klemke
Department	Molekulare Onkologie
Street	Justus-von-Liebig-Weg 11
Postal code and City	37077 Göttingen
Country	Germany
E-mail	luisa.klemke@med.uni-goettingen.de
Telephone/Fax	0551-3960779
(PO no. for your invoice)	A-4501715941

Report language   English X   German ___

02/22/2021
_____
Date and signature

#	Sample Name	STR	COI	#	Sample Name	STR	COI	#	Sample Name	STR	COI
1	L3.6pl, 24.04.2018	x		8	RKO, 29.10.2020	x		15	H1299, 27.07.2020	x	
2	MIA-PACA-2, 13.11.2017	x		9	LS174.T, 06.06.2018	x		16	SJSA-1, 15.02.2021	x	
3	PANC-1, 13.11.2017	x		10	SW480, 28.08.2020	x		17	Vero E6, 16.10.2020		x
4	BXPC-3, 21.08.2017	x		11	SW837, 13.01.2021	x		18	Calu-3 DPZ, 08.12.2020	x	
5	CAPAN-1, 02.05.2018	x		12	SW620, 24.06.2020	x		19	Calu-3 ATCC, 25.05.2020	x	
6	PA-TU-8902, 28.01.2019	x		13	DLD-1, 28.08.2020	x		20	RPE htert WT, 10.05.2019	x	
7	HCT116 WT, 31.05.2019	x		14	HT-29, 06.08.2020	x		21	HCC1806, 21.09.2020	x	

Help   send e-mail   print form

Leibniz-Institut
DSMZ-Deutsche Sammlung von
Mikroorganismen und Zellkulturen GmbH

DSMZ

Leibniz-Institut
DSMZ-Deutsche Sammlung von
Mikroorganismen und Zellkulturen GmbH
Inhoffenstrasse 7b
D-38124 Braunschweig
Germany

Date:	11.07.2018
Your PO No.:	A - 4501481943
Our order No.:	A1807330-1
Contact:	Pia Palm

Material Transfer Agreement
Between the DSMZ and the Recipient of Cell Line(s)

PLEASE RETURN A SIGNED COPY OF THIS AGREEMENT by email to mutz@dsmz.de

All material listed will be made available subject to the following conditions:

1. The DSMZ provides cells as a service to the research community. These materials are solely for research purposes and not for use in humans. Cell lines and their products shall not be sold or used for commercial purposes or utilized in any other type of commercial activity.
2. Recipients herewith confirm (also on behalf of their institutions) that they are end users of materials supplied by the DSMZ. Materials shall not be passed on to third parties.
3. Appropriate reference shall be made in any ensuing publication(s), crediting the work of the original investigators which established the cell line(s) and the DSMZ as supplier. No alteration may be made to their DSMZ titles or acronyms.
4. It is understood that neither the DSMZ nor the depositor of the cells accept any liability whatsoever in connection with the receipt, handling, storage or use of the cell line(s).
5. Recipients accept (also on behalf of host institutions) all conditions of ordering, delivery and payment of the DSMZ.

ACC-No.	Name
162	PA-TU-8988T

I agree to the above restrictions:

Name of recipient: Dr. Ramona Schulz-Heddergott   Function: Gruppenleiterin

Company/University: Universitätsmedizin Göttingen   Institute/Department: Molekulare Onkologie

Complete Address: Justus von Liebig Weg 11, 37077 Göttingen

Date: 11.07.2018   Signature:

39

Leibniz-Institut
DSMZ-Deutsche Sammlung von
Mikroorganismen und Zellkulturen GmbH

DSMZ

Leibniz-Institut DSMZ GmbH • Inhoffenstraße 7 B • 38124 Braunschweig • GERMANY

Lieferadresse
Universitätsmedizin Göttingen
UMG - Molekulare Onkologie
Frau Magerhans
Justus von Liebig Weg 11
37077 GÖTTINGEN
DEUTSCHLAND
T.: 0551/39- 14128

Kundennr.: 30256

Rechnungsadresse
Georg-August-Universität Göttingen
Stiftung öffentlichen Recht
Universitätsmedizin
G3-1233 Kreditorenbuchhaltung
37099 GÖTTINGEN
DEUTSCHLAND

Kundennr.; 30419

Besteller:	**Herr Julian Kloth**
Bestellnr. :	A - 4501481943
Bestelldatum.:	11.07.2018
VAT Nr. :	
Rechnung vom:	18.07.2018
Unsere Ref.-Nr.:	A1807330-1
Versand:	18.07.2018
Ansprechpartner:	Pia Palm

Lieferschein 01807236-1

Pos.	Menge	Leistung	Bezeichnung	Risikogruppe	Zolltarif-Nr.
1	1	ACC 162	PA-TU-8988T	1	30 02 90 90

Bemerkungen:

Zollvermerk: Nettogewicht reine Biomasse: 0.9 g

Sämtliche Lieferungen und Leistungen erfolgen auf Basis der Allgemeinen Geschäftsbedingungen der DSMZ
(http://www.dsmz.de/terms.html)

Bitte beachten Sie unseren Begleitzettel.

Panel Genome Sequencing of human L3.6pl cells

Index	Gene	Transcript	Location	Pos.	Type	Nuc Change	Coverage	Cha	web Ref.	c. HGVS	p.	mu	m	TV	M	Weightin	Filter Step
1	GNAS	ENST0000037108	E1	-37411	[c C	G -> A (het)	22% (356) [22% (171) / 22% (185)]		rs74934823 (10	c.-37835G>A							distinct
2	MAPK4	ENST0000040038	E3	-10553	[c C	C -> T (homo)	100% (705) [100% (442) / 100% (263)]		rs7227230 (100	c.547-10553C>T							distinct
3	FAT4	ENST0000039432	E2	-4905	[ch C	T -> C (homo)	100% (759) [100% (524) / 100% (235)]		rs925243 (1000	c.5176-4905T>C							distinct
4	BRD2	ENST0000044908	E1	-3818	[ch C	G -> A (homo)	99% (427) [100% (348) / 96% (79)]		rs116656352 (1	c.-3976G>A							distinct
5	BRD2	ENST0000044908	E1	-3813	[ch C	C -> A (homo)	99% (466) [100% (379) / 97% (87)]		rs115634162 (1	c.-3971C>A							distinct
6	LMNA	ENST0000036830	E2	-778	[chr C	C -> G (homo)	100% (291) [99% (159) / 100% (132)]		rs665979 (1000	c.357-778C>G							distinct
7	LMNA	ENST0000036830	E2	-739	[chr C	T -> G (homo)	100% (306) [100% (137) / 100% (169)]		rs513043 (1000	c.357-739T>G	0/2 of 4						distinct
8	BRD2	ENST0000044908	E7	-232	[chr C	A -> G (homo)	99% (391) [100% (235) / 99% (156)]		rs3129307 (100	c.1060-232A>G							distinct
9	BRD2			-53..-51 /	D	CTT (homo)	93% (589) [95% (333) / 91% (256)]			c.1438-53_1438-51delCTT							distinct
10	KMT2D	ENST0000030106	E32	-46	[chr1 C	G -> A (het)	33% (378) [32% (202) / 33% (176)]			c.8047-46G>A							distinct
11	LMNA	ENST0000036830	E7	-43	[chr1 C	A -> G (het)	64% (656) [68% (273) / 62% (383)]		rs16837198 (10	c.1158-43A>G							distinct
12	SLIT2	ENST0000050415	E28	-42	[chr4 C	A -> G (het)	31% (267) [28% (104) / 33% (163)]		rs2290750 (100	c.2851-42A>G							distinct
13	SMARCA4	ENST0000045071	E10	-37..-36 /	Indel	TG -> CA (homo)	92% (898) [94% (421) / 91% (477)]		rs386806808 (d	c.762-37_1762-36delinsCA							distinct
14	MYCBP2	ENST0000035733	E42	-20	[chr1 C	A -> G (homo)	100% (320) [100% (233) / 100% (87)]		rs3742103 (100	c.6001-20A>G							distinct
15	SMARCA2	ENST0000034972	E9	-19	[chr9 C	G -> A (het)	36% (199) [33% (103) / 39% (96)]		rs141618610 (1	c.1522-19G>A							distinct
16	LRP1B	ENST0000038948	E36	-17 / 1bp	I (Dup)	T (het)	51% (207) [54% (168) / 43% (39)]		rs398104769 (d	c.5759-18dupT							distinct
17	FGFR2	ENST0000035848	E14	-17	[chr1 C	T -> G (het)	46% (203) [48% (143) / 44% (60)]		rs3135802 (100	c.1864-17T>G							distinct
18	LRP1B	ENST0000038948	E34	-17	[chr2 C	A -> G (homo)	100% (545) [100% (323) / 100% (222)]		rs7599219 (dbS	c.5501-17A>G							distinct
19	TLE4	ENST0000037655	E11	-16	[chr9 C	C -> T (homo)	100% (235) [100% (206) / 100% (29)]		rs73652238 (10	c.784-16C>T							distinct
20	MARK2	ENST0000040201	E18	-16	[chr1 C	C -> T (het)	25% (258) [24% (132) / 25% (126)]			c.1962-16C>T							distinct
21	KMT2C	ENST0000026218	E18	-15	[chr7 C	T -> C (het)	43% (178) [46% (120) / 39% (58)]		rs62481502 (db	c.2872-15T>C							distinct
22	SF3B1	ENST0000033550	E19	-15	[chr2 C	A -> T (homo)	100% (209) [100% (169) / 100% (40)]		rs788017 (1000	c.2719-15A>T							distinct
23	LRP1B	ENST0000038948	E45	-15	[chr2 C	C -> G (het)	57% (218) [61% (142) / 52% (76)]		rs11694934 (10	c.7388-15C>G							distinct
24	ROBO3	ENST0000039780	E3	-14	[chr1 C	A -> C (het)	69% (11) [100% (11) / 0% (0)]		rs11219820 (10	c.488-14A>C							forced,distinct
25	EGFR	ENST0000027549	E1	-14	[chr7 C	A -> C (homo)	100% (85) [100% (80) / 100% (5)]		rs712830 (1000	c.-191A>C							forced,distinct
26	BRD2	ENST0000044908	E2	-13 / 1bp	I (Dup)	T (homo)	93% (91) [93% (86) / 100% (5)]			c.-112-14dupT							forced,distinct
27	SLIT2	ENST0000050415	E12	-12	[chr4 C	T -> C (homo)	100% (235) [100% (154) / 100% (81)]		rs519813 (1000	c.1059-12T>C							distinct
28	SF3B1	ENST0000033550	E13	-11 / 2bp	I (Dup)	TT (homo)	86% (166) [86% (129) / 86% (37)]		rs397804827 (d	c.1720-13_1720-12dupTT							distinct
29	ROBO2	ENST0000048769	E2	-10	[chr3 C	C -> G (het)	79% (1972) [78% (1215) / 80% (757)]		rs9631539 (dbS	c.-13-10C>G							distinct
30	BRD2	ENST0000044908	E3	-10	[chr6 C	T -> C (homo)	99% (256) [99% (193) / 100% (63)]		rs635688 (1000	c.193-10T>C							distinct
31	MYCBP2	ENST0000035733	E13	-10 / 1bp	I (Dup)	T (het)	55% (126) [69% (101) / 30% (25)]		rs549452634 (d	c.1534-11dupT							distinct
32	KRAS	ENST0000025607	E6	-9	[chr12 C	T -> C (het)	37% (117) [38% (78) / 34% (39)]		rs12313763 (10	c.*5-9G>A							distinct
33	SLIT2	ENST0000050383	E9	-9	[chr4 g C	G -> T (het)	30% (191) [30% (105) / 30% (86)]		rs7695303 (100	c.776-9G>T							distinct
34	KMT2D	ENST0000030106	E11	-7 / 1bp	[D	C (homo)	96% (946) [96% (401) / 96% (545)]		rs112620957 (d	c.2798-7delC							distinct
35	BRAF	ENST0000028860	E1	-7	[chr7 g C	A -> C (het)	29% (7) [32% (7) / 0% (0)]			c.-68A>C							forced,distinct
36	LRP1B	ENST0000038948	E27	-7	[chr2 g C	T -> G (het)	51% (81) [53% (70) / 44% (11)]		rs12987572 (10	c.4335-7T>G							distinct
37	NARF	ENST0000030979	E9	-6	[chr17 C	T -> G (het)	74% (704) [73% (336) / 76% (368)]		rs12103494 (10	c.834-6T>G							distinct
38	ROBO1	ENST0000046423	E22	-6 / 1bp	I (Dup)	T (het)	83% (179) [88% (127) / 74% (52)]		rs369027577 (d	c.2883-7dupT							distinct
39	APC	ENST0000025743	E5	-4 / 1bp	[D	A (het)	74% (111) [82% (58) / 68% (53)]		COSM19338 (C	c.423-4delA							distinct
40	BRD2	ENST0000044908	E8	-4	[chr6 g C	G -> C (homo)	100% (981) [100% (597) / 100% (384)]		rs3097644 (100	c.1189-4G>C							distinct
41	FAT1	ENST0000044180	E3	-4	[chr4 g C	G -> C (homo)	100% (354) [100% (259) / 100% (95)]		rs172903 (1000	c.3266-4G>C							distinct
42	PBRM1	ENST0000039483	E11	-4	[chr3 g C	G -> A (het)	74% (287) [65% (104) / 81% (183)]		COSM4002750	c.996-4G>A							distinct
43	LRP1B	ENST0000038948		3 (1239)	[C	C -> T (het)	65% (77) [67% (74) / 38% (3)]	· V (413	rs1525579 (100	c.1239T>C	p.Val413=						forced,distinct
44	LRP1B	ENST0000038948	E50	5 (8031)	[C	A -> G (het)	32% (122) [31% (73) / 33% (49)]	Q (267	COSM4001201	c.8031A>G	p.Gln2677=						distinct
45	CDKN2A	ENST0000030449	E2	5 (155)	[c C	T -> A (homo)	100% (932) [100% (567) / 100% (365)]	> K (52	COSM13436 (C	c.155T>A	p.Met52Lys						distinct
46	LRP1B	ENST0000038948	E54	5 (8526)	[C	T -> C (het)	30% (123) [30% (78) / 30% (45)]	Y (2842	COSM3757652	c.8526T>C	p.Tyr2842=						distinct
47	ROBO3	ENST0000039780	E21	5 (2991)	[C	G -> A (homo)	100% (569) [100% (327) / 100% (242)]	· A (997	rs7933204 (100	c.2991G>A	p.Ala997=						distinct
48	MYCBP2	ENST0000035733	E55	8 (7778)	[C	A -> G (homo)	100% (542) [100% (316) / 100% (226)]	S (2593	rs34478844 (10	c.7778A>G	p.Asn2593Ser						distinct
49	EGFR	ENST0000027549	E23	8 (2709)	[C	T -> C (homo)	100% (1254) [100% (646) / 100% (608)]	· T (903	rs1140475 (100	c.2709T>C	p.Thr903=						distinct
50	SF3B1	ENST0000033550	E5	8 (423)	[c C	A -> G (homo)	100% (380) [100% (163) / 100% (217)]	· K (141	COSM1129389	c.423A>G	p.Lys141=						distinct
51	POLR3A	ENST0000037237	E23	9 (2997)	[C	G -> T (het)	55% (377) [59% (190) / 52% (187)]	· V (999	rs12241228 (10	c.2997G>T	p.Val999=						distinct
52	JAG1	ENST0000025495	E20	10 (2382)	[C	C -> T (het)	62% (318) [64% (223) / 60% (95)]	· S (794	rs56225585 (10	c.2382C>T	p.Ser794=						distinct
53	FAT4	ENST0000039432	E10	20 (11814)	C	A -> G (het)	68% (262) [70% (180) / 65% (82)]	S (3938	rs17009721 (10	c.11814A>G	p.Ser3938=						distinct
54	KMT2C	ENST0000026218	E7	22 (871)	[C	C -> T (het)	78% (538) [81% (387) / 71% (151)]	· F (291	rs56850341 (10	c.871C>T	p.Leu291Phe						distinct
55	POLR3A	ENST0000037237	E16	26 (2100)	C	C -> T (het)	67% (629) [67% (346) / 67% (283)]	· I (700	rs79793998 (10	c.2100C>T	p.Ile700=						distinct
56	FAT1	ENST0000044180	E11	26 (8904)	C	C -> T (homo)	100% (277) [100% (226) / 100% (51)]	A (296	rs1280099 (100	c.8904C>T	p.Ala2968=						distinct
57	SLC25A24	ENST0000056548	E1	27	[chr1 C	T -> G (het)	78% (101) [78% (100) / 100% (1)]	· UTR	rs662282 (1000	c.-194T>G							forced,distinct
58	U2AF1	ENST0000029155	E1	29	[chr21 C	A -> C (het)	49% (298) [48% (166) / 49% (132)]	· UTR	rs17115876 (10	c.-65A>C							forced,distinct
59	MYCBP2	ENST0000035733	E62	29 (10440)	C	G -> A (homo)	100% (236) [100% (139) / 100% (97)]	P (3480	rs34700794 (10	c.10440G>A	p.Pro3480=						distinct
60	FAT4	ENST0000039432	E16	30 (12846)	C	C -> T (het)	71% (280) [73% (187) / 67% (93)]	S (4282	rs17009819 (10	c.12846C>T	p.Ser4282=						distinct
61	ROBO2	ENST0000048769	E1	32 (19)	[c C	C -> A (het)	79% (1720) [78% (832) / 80% (888)]	-> S (7)	rs12171318 (db	c.19C>A	p.Arg7Ser						distinct
62	NARF	ENST0000030979	E9	34 (867)	[C	T -> C (het)	78% (726) [76% (307) / 80% (419)]	· R (289	rs3829567 (100	c.867T>C	p.Arg289=						distinct
63	MYCBP2	ENST0000035733	E46	37 (6520)	C	C -> T (homo)	100% (329) [100% (220) / 100% (109)]	L (2174	rs34982494 (10	c.6520C>T	p.Leu2174=						distinct
64	FGFR2	ENST0000035848	E1	38	[chr10 C	G -> A (homo)	100% (275) [100% (80) / 100% (195)]	· UTR	rs1047111 (100	c.-236G>A							distinct
65	SMARCC2	ENST0000055016	E5	39 (438)	[C	A -> G (homo)	99% (785) [99% (318) / 100% (467)]	· P (146	rs7136420 (100	c.438A>G	p.Pro146=						distinct
66	BANF1	ENST0000031217	E1	39 / 2bp	I (Dup)	AG (het)	42% (291) [41% (165) / 44% (126)]	· UTR		c.-472_-471dupAG							distinct
67	PIK3CA	ENST0000026396	E12	42 (1788)	C	A -> G (het)	62% (572) [65% (322) / 59% (250)]	· E (596	rs137902538 (1	c.1788A>G	p.Glu596=						distinct
68	TLE4	ENST0000037655	E18	42 (2028)	C	A -> C (homo)	100% (959) [100% (447) / 100% (512)]	· A (676	rs34566811 (10	c.2028A>C	p.Ala676=						distinct
69	KRAS	ENST0000025607	E2	46 (35)	[c C	G -> A (het)	48% (318) [48% (150) / 48% (168)]	> D (12	rs121913529 (C	c.35G>A	p.Gly12Asp						distinct
70	LRP1B	ENST0000038948	E32	47 (5256)	C	A -> G (homo)	100% (721) [100% (412) / 100% (309)]	S (1752	COSM4133144	c.5256A>G	p.Ser1752=						distinct
71	ARID2	ENST0000033434	E1	52	[chr12 C	G -> A (het)	46% (6) [50% (6) / 0% (0)]	· UTR		c.-121G>A							forced,distinct
72	SLC25A24	ENST0000057004	E1	53	[chr1 C	A -> T (homo)	100% (91) [100% (91) / 0% (0)]	· UTR	rs524504 (1000	c.-145A>T							forced,distinct
73	ROBO2	ENST0000048769	E2	55 (42)	[c C	A -> G (het)	79% (2134) [76% (893) / 82% (1241)]	> T (14)	rs62269817 (db	c.42A>G	p.Thr14=						distinct
74	SMARCA4	ENST0000045071	E5	56 (915)	[C	G -> A (het)	95% (485) [47% (21) / 100% (464)]	· P (305	rs149573400 (1	c.915G>A	p.Pro305=						distinct
75	LRP1B	ENST0000038948		58 (4392)	C	A -> G (het)	43% (180) [44% (118) / 41% (62)]	R (1464	rs79054985 (10	c.4392A>G	p.Arg1464=						distinct
76	KMT2C	ENST0000026218	E15	59 (2591)	C	A -> G (het)	35% (69) [41% (56) / 22% (13)]	· G (864	rs4024420 (dbS	c.2591A>G	p.Glu864Gly						distinct
77	POLR3A	ENST0000037237	E3	60 (240)	[C	A -> C (het)	74% (330) [76% (206) / 71% (124)]	> L (80)	rs12248310 (10	c.240A>C	p.Leu80=						distinct
78	PBRM1	ENST0000039483	E23	64 (3522)	C	A -> T (homo)	100% (904) [100% (389) / 100% (515)]	P (1174	COSM4002747	c.3522A>T	p.Pro1174=						distinct
79	BRD2	ENST0000044908	E2	64	[chr6 C	G -> A (homo)	100% (405) [100% (286) / 100% (119)]	· UTR	rs516535 (1000	c.-49G>A							distinct
80	LRP1B	ENST0000038948	E30	67 (5006)	C	A -> C (het)	65% (639) [67% (399) / 63% (240)]	A (1669		c.5006A>C	p.Glu1669Ala						distinct
81	SLIT2	ENST0000050415	E21	68 (2211)	C	C -> T (het)	28% (204) [28% (107) / 28% (97)]	· V (737	rs7690492 (100	c.2211C>T	p.Val737=						distinct
82	APC	ENST0000025743	E14	69 (1695)	C	A -> G (homo)	100% (241) [100% (102) / 99% (139)]	· E (565	rs77921116 (10	c.1695A>G	p.Glu565=						distinct
83	LRP1B	ENST0000038948	E8	69 (1082)	C	G -> A (het)	36% (279) [35% (131) / 36% (148)]	· Q (361	COSM1007086	c.1082G>A	p.Arg361Gln						distinct
84	SLC25A24	ENST0000056548	E1	70..76 / 7b	D	CCTGCGC (het)	65% (112) [65% (110) / 50% (2)]	· UTR	rs150513527 (1	c.-151_-145delCCTGCGC							forced,distinct
85	FAT1	ENST0000044180	E23	74 (12177)	C	G -> C (homo)	100% (641) [100% (300) / 100% (341)]	N (4059	rs1280097 (100	c.12177G>C	p.Lys4059Asn						distinct
86	RBM6	ENST0000026602	E21	75 (3321)	C	C -> T (homo)	100% (371) [100% (112) / 100% (259)]	Y (1107	rs34158172	c.3321C>T	p.Tyr1107=						distinct
87	CHD1	ENST0000028404	E26	77 (3648)	C	C -> T (homo)	100% (670) [100% (350) / 100% (320)]	S (1216	rs140751250 (1	c.3648C>T	p.Ser1216=						distinct
88	EGFR	ENST0000027549	E20	78 (2361)	C	G -> A (homo)	99% (821) [98% (427) / 99% (394)]	· Q (787	COSM1451600	c.2361G>A	p.Gln787=						distinct
89	LRP1B	ENST0000038948	E85	80 (13047)	C	G -> A (het)	22% (220) [24% (108) / 21% (112)]	T (4349	rs1386356 (100	c.13047G>A	p.Thr4349=						distinct

90	GNAS	ENST0000037108!	E5	81 (393)	[C	C -> T (het)	81% (740)	[82% (276) / 81% (464)]	· I (131)	COSM3758661	c.393C>T	p.Ile131=	distinct
91	SLC25A24	ENST0000056548!	E4	82 (480)	[C	G -> A (het)	28% (139)	[25% (62) / 31% (77)]	· E (160)	rs11185293 (10	c.480G>A	p.Glu160=	distinct
92	PIK3CA	ENST0000026396:	E6	84 (1143)	C	C -> G (het)	63% (491)	[61% (178) / 64% (313)]	· P (381	rs72561481 (10	c.1143C>G	p.Pro381=	distinct
93	ROBO2	ENST0000048769:	E2	86..88 (73. Indel	GTG -> ATC (het)	34% (891)	[32% (326) / 36% (565)]	> I (25)		c.73_75delinsATC	p.Val25Ile	distinct
94	KMT2C	ENST0000026218!	E18	87 (2958)	C	A -> G (het)	51% (269)	[53% (123) / 50% (146)]	· P (986	rs28439884 (db	c.2958A>G	p.Pro986=	distinct
95	CHD1	ENST0000028404:	E31	87 (4335)	C	G -> A (homo)	100% (305)	[100% (112) / 100% (193)]	E (1445	COSM4003637	c.4335G>A	p.Glu1445=	distinct
96	ROBO2	ENST0000048769:	E2	88 (75)	[c C	G -> C (het)	39% (977)	[36% (347) / 42% (630)]	> V (25)	rs62269818 (db	c.75G>C	p.Val25=	distinct
97	LRP1B	ENST0000038948:	E51	89 (8238)	C	C -> T (het)	65% (284)	[65% (127) / 65% (157)]	G (274	rs61732738 (10	c.8238G>A	p.Gly2746=	distinct
98	SLC25A24	ENST0000056548!	E1	89	[chr1:	C	A -> C (het)	75% (115)	[76% (113) / 50% (2)]	' UTR	rs554709 (1000	c.-132A>C		forced,distinct
99	KMT2C	ENST0000026218!	E18	92 (2963)	C	G -> T (het)	55% (256)	[56% (112) / 54% (144)]	· F (988	rs28522267 (db	c.2963G>T	p.Cys988Phe	distinct
100	BRD2	ENST0000044908:	E8	92 (1280)	C	C -> T (homo)	100% (807)	[100% (418) / 100% (389)]	· V (427	rs3918143 (100	c.1280C>T	p.Ala427Val	distinct
101	SLC25A24	ENST0000056548!	E2	93 (276)	[C	A -> G (het)	71% (195)	[70% (85) / 73% (110)]	> K (92)	COSM3750202	c.276A>G	p.Lys92=	distinct
102	BRD4	ENST0000026337:	E11	95 (2142)	C	C -> T (homo)	100% (968)	[100% (444) / 100% (524)]	· S (714	rs114723577 (1	c.2142C>T	p.Ser714=	distinct
103	KMT2C	ENST0000026218!	E7	97 (946)	[C	A -> T (het)	83% (821)	[83% (469) / 82% (352)]	· S (316	rs10454320 (db	c.946A>T	p.Thr316Ser	distinct
104	ATM	ENST0000027861:	E23	99 (3383)	C	A -> G (homo)	100% (523)	[99% (136) / 100% (387)]	R (1128	COSM1350830	c.3383A>G	p.Gln1128Arg	distinct
105	FAT1	ENST0000044180:	E26	101 (1310:	C	T -> C (homo)	100% (840)	[100% (404) / 100% (436)]	S (4367	COSM4158952	c.13101T>C	p.Ser4367=	distinct
106	SMARCA4	ENST0000045071:	E8	105 (1524:	C	T -> C (homo)	100% (955)	[100% (480) / 100% (475)]	· H (508	COSM4131184	c.1524T>C	p.ŀ [c.1524T>C]	distinct
107	SMAD4	ENST0000034298:	E9	112 (1067:	C	C -> T (homo)	100% (733)	[100% (368) / 100% (365)]	· L (356	COSM14049 (C(	c.1067C>T	p.Pro356Leu	distinct
108	FAT1	ENST0000044180:	E19	112 (1066:	C	T -> G (homo)	100% (779)	[100% (403) / 100% (376)]	A (3554	rs2637777 (100	c.10660T>G	p.Ser3554Ala	distinct
109	LRP1B	ENST0000038948:	E16	113 (2616:	C	C -> T (homo)	100% (160)	[100% (76) / 100% (84)]	· D (872	rs13007735 (10	c.2616C>T	p.Asp872=	distinct
110	FGFR2	ENST0000035848:	E1	117	[chr1:	C	A -> G (het)	44% (65)	[44% (23) / 44% (42)]	' UTR	rs41258305 (10	c.-157A>G		distinct
111	EGFR	ENST0000027549:	E15	117 (1839:	C	C -> T (homo)	100% (676)	[100% (311) / 100% (365)]	· A (613	rs17290169 (10	c.1839C>T	p.Ala613=	distinct
112	TLE4	ENST0000037655:	E15	118 (1458:	C	C -> T (homo)	98% (1502)	[98% (751) / 98% (751)]	· H (486	rs61742686 (10	c.1458C>T	p.His486=	distinct
113	SF3B1	ENST0000033550:	E24	118 (3657:	C	A -> G (homo)	100% (721)	[100% (271) / 100% (450)]	V (1215	COSM3757859	c.3657A>G	p.Val1219=	distinct
114	SLIT2	ENST0000050415:	E1	120	[chr4:	C	G -> T (het)	26% (10)	[26% (10) / 0% (0)]	' UTR	rs7655084 (100	c.-133G>T		forced,distinct
115	TP53BP2	ENST0000034353:	E6	121 (595)	C	G -> A (het)	60% (380)	[58% (165) / 61% (215)]	M (199	rs146703239 (1	c.595G>A	p.Val199Met	distinct
116	FAT1	ENST0000044180:	E13	122 (9351:	C	T -> C (homo)	100% (1066)	[100% (477) / 100% (589)]	D (311	COSM4003024	c.9351T>C	p.Asp3117=	distinct
117	SMARCC2	ENST0000055016:	E25	134 (2682:	C	C -> T (homo)	100% (291)	[100% (101) / 100% (190)]	· A (894	rs17852368 (10	c.2682C>T	p.Ala894=	distinct
118	FAT1	ENST0000044180:	E13	134 (9363:	C	C -> T (homo)	100% (1039)	[100% (413) / 100% (626)]	N (312	rs2249916 (100	c.9363C>T	p.Asn3121=	distinct
119	SF3B1	ENST0000033550:	E18	135 (2631:	C	T -> C (homo)	100% (412)	[100% (128) / 100% (284)]	· G (877	COSM3757860	c.2631T>C	p.Gly877=	distinct
120	BRD7	ENST0000039468:	E7	144 (846)	C	C -> T (het)	50% (356)	[51% (163) / 50% (193)]	· A (282	COSM3720984	c.846C>T	p.Ala282=	distinct
121	U2AF2	ENST0000045055:	E11	159 (1191:	C	C -> T (homo)	99% (507)	[99% (193) / 99% (449)]	· D (397	COSM1396639	c.1191C>T	p.Asp397=	distinct
122	TP53	ENST0000026930!	E4	171 (267)	, D	C (homo)	95% (635)	[91% (272) / 98% (363)]	۱ 122 R	COSM1180853	c.267delC	p.Ser90Profs*33	distinct
123	FAT1	ENST0000044180:	E5	176 (3818:	C	A -> G (homo)	100% (991)	[100% (478) / 100% (513)]	R (127:	rs328418 (1000	c.3818A>G	p.His1273Arg	distinct
124	FAT4	ENST0000039432:	E4	191 (5760:	C	T -> C (homo)	100% (627)	[100% (295) / 100% (332)]	D (192	COSM1131273	c.5760T>C	p.Asp1920=	distinct
125	FGFR1	ENST0000044771:	E1	192	[chr8:	C	C -> T (homo)	100% (13)	[100% (10) / 100% (3)]	' UTR	rs2445003 (100	c.-751C>T		distinct
126	FGFR2	ENST0000036905:	E17	196	[chr1:	C	A -> G (homo)	85% (23)	[0% (0) / 85% (23)]	' UTR	rs1649167 (100	c.*190A>G		forced,distinct
127	LRP1B	ENST0000038948:	E41	206 (6633:	C	A -> T (het)	32% (220)	[37% (102) / 29% (118)]	P (2211	rs13431727 (10	c.6633A>T	p.Pro2211=	distinct
128	FAT1	ENST0000044180:	E19	209 (1075:	C	T -> C (het)	63% (545)	[63% (259) / 63% (286)]	T (358(	rs115705222 (1	c.10757T>C	p.Met3586Thr	distinct
129	BRD3	ENST0000030340:	E6	222 (936)	C	A -> G (homo)	100% (933)	[100% (440) / 100% (493)]	· L (312	COSM4163507	c.936A>G	p.Leu312=	distinct
130	TGFBR2	ENST0000029575:	E1	255	[chr3:	C	C -> G (het)	76% (212)	[76% (192) / 83% (20)]	' UTR	rs2306856 (100	c.-128C>G		distinct
131	FAT4	ENST0000039432:	E9	257 (7701:	C	G -> C (homo)	100% (817)	[100% (399) / 100% (418)]	V (2567	rs988863 (1000	c.7701G>C	p.Val2567=	distinct
132	BANF1	ENST0000031217:	E1	260	[chr1:	C	G -> C (het)	50% (449)	[51% (255) / 49% (194)]	' UTR	rs1786171 (100	c.-249G>C		distinct
133	BANF1	ENST0000031217:	E3	275	[chr1:	C	C -> A (het)	52% (123)	[54% (19) / 52% (104)]	' UTR	rs144367403 (1	c.*128C>A		distinct
134	PBRM1	ENST0000039483:	E17	287 (2211:	C	A -> G (homo)	100% (879)	[100% (457) / 100% (422)]	· T (737	COSM1566683	c.2211A>G	p.Thr737=	distinct
135	SLIT2	ENST0000050415:	E37	293	[chr4:	C	G -> A (homo)	100% (809)	[100% (303) / 100% (506)]	I' UTR	rs1379659 (100	c.*51G>A		distinct
136	FGFR1	ENST0000044771:	E1	307	[chr8:	C	C -> T (het)	33% (10)	[35% (8) / 29% (2)]	I' UTR	rs3213849 (100	c.-636C>T		forced,distinct
137	LMNA	ENST0000036830:	E4	392	[chr1:	C	C -> T (het)	75% (6)	[67% (2) / 80% (4)]	I' UTR	rs74116489 (10	c.*365C>T		distinct
138	SETD2	ENST0000040979:	E3	470 (557)	C	C -> T (homo)	100% (590)	[100% (268) / 100% (322)]	· L (186	rs78759480 (10	c.557C>T	p.Pro186Leu	distinct
139	ACVR2A	ENST0000024141:	E1	472 / 1bp	I (Dup)	T (het)	33% (4)	[33% (4) / 0% (0)]	I' UTR		c.-166dupT		forced,distinct
140	BRD2	ENST0000037482:	E2	523	[chr6:	C	G -> T (homo)	100% (312)	[100% (57) / 100% (255)]	I' UTR	rs974357 (1000	c.-782G>T		distinct
141	MARK2	ENST0000040201:	E19	548	[chr1:	C	A -> C (het)	47% (28)	[0% (0) / 47% (28)]	I' UTR	rs182664 (1000	c.*187A>C		forced,distinct
142	RNF43	ENST0000040797:	E9	633 (1585:	C	C -> T (homo)	75% (1042)	[76% (639) / 74% (403)]	W (529	COSM191575 ((	c.1585C>T	p.Arg529Trp	distinct
143	MYC	ENST0000037797:	E2	708 (738)	C	G -> A (het)	55% (945)	[50% (303) / 58% (642)]	· P (246	rs2070582 (100	c.738G>A	p.Pro246=	distinct
144	MYC	ENST0000037797:	E2	708 (738)	C	G -> A (het)	55% (945)	[50% (303) / 58% (642)]	· P (246	rs2070582 (100	c.738G>A	p.Pro246=	distinct
145	FAT1	ENST0000044180:	E27	883	[chr4:	C	G -> A (het)	30% (9)	[0% (0) / 30% (9)]	I' UTR	rs7680937 (100	c.*254G>A		forced,distinct
146	LRP1B	ENST0000038948:	E1	895	[chr2:	C	C -> T (homo)	99% (705)	[99% (453) / 99% (252)]	I' UTR	rs1375610 (100	c.-78C>T		distinct
147	KMT2D	ENST0000030106:	E10	1025..105:	D	ATCTCCGCAGGCT	74% (366)	[55% (98) / 85% (268)]	L -> L (7	rs375538882 (di	ATCTCCGCAGGCTGAC(	p.Ala765_Gln77	distinct
148	KMT2D	ENST0000030106:	E10	1025..105:	D	ATCTCCGCAGGCT	74% (366)	[55% (98) / 85% (268)]	L -> L (7	rs375538882 (di	ATCTCCGCAGGCTGAC(	p.Ala765_Gln77	distinct
149	TLE4	ENST0000037655:	E1	1063 (45)	C	A -> G (homo)	100% (751)	[100% (291) / 100% (460)]	· P (15)	COSM4164047	c.45A>G	p.Pro15=	distinct
150	FAT1	ENST0000044180:	E2	1230 (121:	C	T -> G (het)	28% (257)	[30% (160) / 26% (97)]	· R (404	COSM4003044	c.1212T>G	p.Ser404Arg	distinct
151	FAT4	ENST0000039432:	E1	1371 (135:	C	A -> T (homo)	100% (1316)	[100% (665) / 100% (651)]	· L (453	COSM3760369	c.1358A>T	p.Gln453Leu	distinct
152	FAT1	ENST0000044180:	E2	1392 (883:	C	A -> G (het)	59% (484)	[59% (245) / 59% (239)]	V (2946	rs76048257 (10	c.8836A>G	p.Ile2946Val	distinct
153	FAT1	ENST0000044180:	E2	1462 (144:	C	G -> A (het)	29% (308)	[27% (134) / 31% (174)]	> I (482	rs3733413 (100	c.1444G>A	p.Val482Ile	distinct
154	FAT1	ENST0000044180:	E2	1503 (148:	C	C -> T (het)	28% (334)	[27% (174) / 30% (160)]	· N (495	COSM4003040	c.1485C>T	p.Asn495=	distinct
155	FAT4	ENST0000039432:	E17	1520 (145:	C	A -> G (het)	64% (560)	[67% (271) / 61% (289)]	R (486(	rs1014866 (100	c.14598A>G	p.Arg4866=	distinct
156	APC	ENST0000025743:	E16	1774 (373:	C	A -> G (homo)	100% (578)	[100% (242) / 100% (336)]	Q (124:	rs74380081 (10	c.3732A>G	p.Gln1244=	distinct
157	FAT4	ENST0000039432:	E17	1836 (149:	C	C -> T (het)	36% (193)	[40% (65) / 34% (128)]	S (4972	COSM4002932	c.14914C>T	p.Pro4972Ser	distinct
158	FAT1	ENST0000044180:	E2	1860 (184:	C	C -> G (het)	30% (216)	[30% (108) / 30% (108)]	· L (614	COSM4003038	c.1842C>G	p.Phe614Leu	distinct
159	FAT4	ENST0000039432:	E9	2426 (987:	C	G -> A (het)	63% (385)	[61% (169) / 65% (216)]	G (329(	rs115219562 (1	c.9870G>A	p.Gly3290=	distinct
160	FAT4	ENST0000039432:	E1	2433 (242:	C	C -> T (homo)	100% (968)	[100% (592) / 100% (376)]	· V (807	COSM3760371	c.2420C>T	p.Ala807Val	distinct
161	FAT1	ENST0000044180:	E2	2602 (258:	C	G -> C (het)	33% (376)	[33% (212) / 33% (164)]	· L (862	COSM4003037	c.2584G>C	p.Val862Leu	distinct
162	SETD2	ENST0000040979:	E3	2617 (270:	C	G -> C (homo)	100% (961)	[100% (526) / 100% (435)]	· Q (902	rs58906143 (10	c.2704G>C	p.Glu902Gln	distinct
163	FAT4	ENST0000039432:	E1	2824 (281:	C	G -> T (het)	26% (284)	[26% (136) / 26% (148)]	· N (937	rs112454576 (1	c.2811G>T	p.Lys937Asn	distinct
164	FAT4	ENST0000039432:	E1	2957 (294:	C	T -> C (homo)	100% (667)	[100% (345) / 100% (322)]	· L (982	rs2940779 (100	c.2944T>C	p.Leu982=	distinct
165	FAT1	ENST0000044180:	E2	3208 (319:	C	A -> G (homo)	100% (959)	[100% (479) / 100% (480)]	G (106(	COSM4003035	c.3190A>G	p.Arg1064Gly	distinct
166	FAT1	ENST0000044180:	E10	3988 (879:	C	A -> T (het)	71% (575)	[70% (256) / 73% (319)]	L (293:	rs1280098 (100	c.8798A>T	p.Gln2933Leu	distinct
167	FAT1	ENST0000044180:	E10	3988 (879:	C	A -> C (het)	29% (231)	[30% (111) / 27% (120)]	P (293:	COSM4005727	c.8798A>C	p.Gln2933Pro	distinct
168	FAT4	ENST0000039432:	E9	4038 (114:	C	A -> G (homo)	64% (611)	[63% (290) / 65% (321)]	E (3828	rs17009684 (10	c.11482A>G	p.Lys3828Glu	distinct
169	FAT4	ENST0000039432:	E9	4174 (116:	C	G -> A (homo)	100% (916)	[100% (454) / 100% (462)]	N (387:	rs12650153 (10	c.11618G>A	p.Ser3873Asn	distinct
170	FAT4	ENST0000039432:	E1	4318 (430:	C	C -> T (homo)	100% (1097)	[100% (536) / 100% (561)]	I (1435	COSM4003036	c.4305C>T	p.Ile1435=	distinct
171	LRP1B	ENST0000038948:	E55	+3	[chr2:|	C	A -> G (het)	24% (72)	[27% (20) / 23% (52)]		rs117225004 (1	c.8850+3A>G		distinct
172	ROBO1	ENST0000046423:	E26	+4	[chr3:|	C	T -> C (homo)	100% (679)	[100% (303) / 100% (376)]		rs7636043 (100	c.3875+4T>C		distinct
173	LRP1B	ENST0000038948:	E33	+5	[chr2:|	C	A -> G (homo)	100% (380)	[100% (144) / 100% (236)]		rs996361 (1000	c.5500+5A>G		distinct
174	PBRM1	ENST0000039483:	E29	+6 / 3bp	I	GAG (homo)	88% (469)	[91% (166) / 87% (303)]		rs71084187 (db	4576+5_4576+6insGAG		distinct
175	SF1	ENST0000037739:	E6	+6	[chr11:	C	C -> T (het)	48% (736)	[52% (424) / 42% (312)]		rs148875917 (1	c.663+6C>T		distinct
176	GATA6	ENST0000026921:	E6	+7	[chr18:	C	A -> G (homo)	100% (219)	[100% (53) / 100% (166)]		COSM4000377	c.1620+7A>G		distinct
177	LRP1B	ENST0000038948:	E19	+10	[chr2:	C	A -> C (homo)	100% (217)	[100% (78) / 100% (139)]		rs1429348 (100	c.2968+10A>C		distinct
178	LRP1B	ENST0000038948:	E49	+12	[chr2	C	A -> T (het)	63% (347)	[62% (101) / 64% (246)]		rs13404083 (10	c.8026+12A>T		distinct
179	LMNA	ENST0000036830:	E4	+13	[chr1	C	G -> T (het)	61% (576)	[57% (227) / 64% (349)]		rs11264444 (10	c.810+13G>T		distinct

42

180	LRP1B	ENST0000038948·E30	+14 / 1bp I	A (het)	87% (451) [79% (152) / 92% (299)]	rs78477398 (10.5114+13_5114+14insA	distinct
181	LRP1B	ENST0000038948·E34	+15 [chr2 C	A -> G (het)	71% (411) [72% (155) / 70% (256)]	rs13382825 (10	c.5626+15A>G	distinct
182	MYCBP2	ENST0000035733·E42	+15 / 1bp D	T (homo)	95% (242) [100% (33) / 95% (209)]	rs397840781 (d	c.6226+15delT	distinct
183	KMT2C	ENST0000026218·E7	+15 [chr7 C	G -> C (het)	24% (198) [23% (59) / 24% (139)]	rs201635031 (d	c.1012+15G>C	distinct
184	CHD1	ENST0000028404·E13	+16 [chr5 C	A -> G (homo)	100% (337) [100% (93) / 100% (244)]	rs17166428 (10	c.1991+16A>G	distinct
185	SLIT2	ENST0000050415·E28	+16 [chr4 C	A -> G (het)	23% (102) [25% (41) / 22% (61)]	rs12506323 (10	c.2948+16A>G	distinct
186	MARK2	ENST0000040201·E11	+16 [chr1 C	C -> T (het)	51% (405) [50% (114) / 51% (291)]	rs224174 (1000	c.1101+16C>T	distinct
187	SMARCA4	ENST0000045071·E31	+16 [chr1 C	G -> T (homo)	100% (565) [100% (282) / 100% (283)]	rs151265814 (1	c.4675+16G>T	distinct
188	NARF	ENST0000030979·E3	+17 [chr1 C	A -> T (het)	74% (577) [73% (149) / 74% (428)]	rs28401416 (10	c.252+17A>T	distinct
189	ROBO3	ENST0000039780·E4	+24 [chr1 C	T -> C (homo)	100% (793) [100% (417) / 100% (376)]	rs4936957 (100	c.766+24T>C	distinct
190	SF1	ENST0000037739·E6	+32 [chr1 C	A -> G (homo)	100% (1454) [100% (607) / 100% (847)]	rs484886 (1000	c.663+32A>G	distinct
191	POLR3A	ENST0000037237·E22	+42 [chr1 C	T -> C (het)	59% (449) [58% (226) / 60% (223)]	rs3815891 (100	c.2988+42T>C	distinct
192	BRD2	ENST0000044908·E9	+663 / 4bp I (Dup)	GTTT (het)	56% (76) [79% (55) / 32% (21)]	c.1700+659_1700+662dupGTTT	distinct
193	BRD2	ENST0000044908·E9	+672 [chr C	A -> T (het)	84% (97) [85% (52) / 82% (45)]	rs2395380 (100	c.1700+672A>T	distinct
194	BRD2	ENST0000044908·E9	+689 [chr C	G -> T (homo)	95% (109) [91% (52) / 98% (57)]	rs2082260 (100	c.1700+689G>T	distinct
195	BRD2	ENST0000044908·E9	+698 / 1bp I (Dup)	T (het)	40% (47) [40% (20) / 40% (27)]	c.1700+697dupT	distinct
196	SLIT2	ENST0000050415·E1	+1105 [ch C	G -> A (het)	28% (334) [29% (137) / 27% (197)]	rs1323066 (100	c.179+1105G>A	distinct
197	SMAD4	ENST0000034298·E4	+2088 [ch C	G -> C (homo)	100% (89) [100% (42) / 100% (47)]	rs7229678 (100	c.454+2088G>C	2/1 of 3	distinct
198	SMAD3	ENST0000032736·E1	+32698 / 1 D	T (homo)	98% (1802) [98% (797) / 97% (1005)]	c.206+32698delT	distinct
199	ATM	ENST0000027861·E1	275 [chr1 C	G -> A (homo)	100% (280) [100% (140) / 100% (140)]	' UTR rs189037 (1000	c.-111G>A	1/0 DP	distinct
200	BRCA1	ENST0000035765·E10	1942 (261: C	C -> T (homo)	100% (1429) [100% (679) / 100% (750)]	· L (871 rs2612C>T	c.2612C>T	p.F 32/ DP, POLY	distinct
201	ASCC3	ENST0000036916·E12	33 (1935) C	C -> T (homo)	100% (525) [100% (343) / 99% (182)]	· L (645 rs41288423 (10	c.1935C>T	p.L 88/ Ident-SN distinct
202	MMACHC	ENST0000040106·E3	45 (321) [C	G -> A (het)	29% (242) [28% (107) / 31% (135)]	· V (107 rs2275276 (100	c.321G>A	p.\ 77/ Ident-SN distinct
203	TPH2	ENST0000033385·E9	57 (1125) C	A -> T (homo)	100% (895) [100% (523) / 100% (372)]	· A (375 COSM3753489	c.1125A>T	p.\ 162 Ident-SN distinct
204	EDNRB	ENST0000044657·E4	30 (831) [C	A -> G (homo)	100% (499) [100% (286) / 100% (213)]	· L (277 COSM3753750	c.831A>G	p.L 156 Ident-SN distinct
205	GABRG3	ENST0000033374·E8	98 (963) [C	C -> T (het)	37% (629) [37% (366) / 36% (263)]	· T (321 rs140679 (1000	c.963C>T	p.T 100 Ident-SN distinct
206	GABRG3	ENST0000033374·E8	98 (963) [C	C -> T (het)	37% (629) [37% (366) / 36% (263)]	· T (321 rs140679 (1000	c.963C>T	p.T 100 Ident-SN distinct
207	ATP13A4	ENST0000039244·E6	10 (543) [C	A -> G (het)	29% (249) [30% (163) / 28% (86)]	M (181 COSM3759936	c.543A>G	p.I 55/ Ident-SN distinct
208	WDFY3	ENST0000022236·E6	32 (336) [C	A -> G (het)	66% (523) [67% (280) / 65% (243)]	· L (112 COSM4003176	c.336A>G	p.L 56/ Ident-SN distinct
209	MUT	ENST0000027481·E3	251 (636) C	G -> A (homo)	100% (435) [100% (226) / 99% (209)]	· K (212 rs2229384 (100	c.636G>A	p.K 151 Ident-SN distinct
210	MPDZ	ENST0000031921·E25	157 (3609 C	A -> G (het)	29% (168) [31% (69) / 27% (99)]	K (120: rs10756457 (10	c.3609A>G	p.L 47/ Ident-SN distinct
211	LMNA	ENST0000036830·E9	-41 [chr1 C	C -> T (homo)	100% (1131) [100% (705) / 99% (426)]	rs553016 (1000	c.1489-41C>T	2/5 POLY	distinct
212	SMARCA2	ENST0000034972·E33	-20 [chr9 C	T -> C (homo)	100% (123) [100% (82) / 100% (41)]	rs3818384 (100	c.4595-20T>C	0/2 POLY	distinct
213	CHD6	ENST0000037323·E14	-19 [chr2 C	G -> A (homo)	100% (974) [100% (600) / 100% (374)]	rs4812516 (100	c.1858-19G>A	0/1 POLY	distinct
214	PIK3CA	ENST0000026396·E6	-17 [chr3 C	C -> A (homo)	100% (785) [100% (497) / 100% (288)]	rs2699896 (100	c.1060-17C>A	67/ POLY	distinct
215	MEN1	ENST0000031204·E2	-16 [chr1 C	C -> G (het)	56% (98) [56% (96) / 50% (2)]	rs509606 (100	c.-23-16C>G	1/5 POLY	forced,distinct
216	BRAF	ENST0000028860·E18	-16 [chr7 C	C -> T (het)	82% (14) [100% (10) / 57% (4)]	rs368721021 (C	c.2128-16C>T	1/1 POLY	distinct
217	BRCA2	ENST0000054445·E17	-14 [chr1 C	T -> C (het)	100% (469) [100% (365) / 100% (104)]	rs9534262 (100	c.7806-14T>C	85/ POLY	distinct
218	PIK3CA	ENST0000026396·E12	-13 [chr3 C	T -> C (het)	52% (267) [57% (200) / 41% (67)]	rs41273619 (10	c.1747-13T>C	0/1 POLY	distinct
219	ATM	ENST0000027861·E24	-12 / 1bp I (Dup)	A (het)	85% (130) [80% (89) / 98% (41)]	ClinVar ben (Mu	c.3403-13dupA	38/ POLY	distinct
220	JAG1	ENST0000025495·E6	10 (765) [C	C -> T (het)	35% (310) [35% (144) / 35% (166)]	· Y (255 COSM3758428	c.765C>T	p.T 5/7 POLY	distinct
221	KMT2D	ENST0000030106·E11	29 (2826) C	C -> T (homo)	100% (833) [100% (421) / 100% (412)]	· I (942 COSM3753294	c.2826C>T	p.I 3/1 POLY	distinct
222	ATM	ENST0000027861·E40	30 (5948) C	A -> G (homo)	100% (97) [100% (44) / 100% (53)]	S (198: rs659243 (1000	c.5948A>G	p.A 272 POLY	distinct
223	SMARCA2	ENST0000034972·E2	32 [chr9: C	G -> A (het)	58% (199) [59% (127) / 58% (72)]	' UTR rs10964468 (10	c.-5G>A	0/3 POLY	distinct
224	KRAS	ENST0000025607·E5	33 (483) [C	G -> A (homo)	100% (947) [100% (422) / 100% (525)]	· R (161 rs4362222 (100	c.483G>A	p.\ 79/ POLY	distinct
225	APC	ENST0000025743·E12	50 (1458) C	T -> C (homo)	100% (723) [100% (337) / 100% (386)]	· Y (486 COSM1432175	c.1458T>C	p.T 3/2 POLY	distinct
226	LMNA	ENST0000036830·E5	51 (861) [C	T -> C (het)	32% (339) [30% (143) / 34% (196)]	· A (287 rs538089 (1000	c.861T>C	p.A 2/8 POLY	distinct
227	FGFR2	ENST0000035848·E6	72 (696) [C	A -> G (homo)	100% (1149) [100% (490) / 100% (659)]	· V (232 rs1047100 (10	c.696A>G	p.V 0/1 POLY	distinct
228	FGFR2	ENST0000047788·E4	94 [chr10 C	A -> G (homo)	100% (668) [100% (466) / 100% (202)]	' UTR rs2981437 (100	c.-109A>G	1/0 POLY	distinct
229	KMT2D	ENST0000030106·E39	96 (10836 C	G -> A (homo)	100% (827) [100% (365) / 100% (462)]	Q (361 COSM431202 ((	c.10836G>A	p.C 3/1 POLY	distinct
230	SMAD3	ENST0000032736·E2	103 (309) C	A -> G (homo)	100% (1004) [100% (623) / 100% (381)]	· L (103 rs1065080 (100	c.309A>G	p.L 12/ POLY	distinct
231	LMNA	ENST0000036830·E12	106 [chr1 C	G -> C (homo)	100% (503) [100% (191) / 100% (312)]	' UTR rs7339 (1000Ge	c.*79G>C	2/7 POLY	distinct
232	MEN1	ENST0000031204·E9	114 (1299) C	T -> C (homo)	100% (1269) [100% (670) / 100% (599)]	· H (433 rs540012 (1000	c.1299T>C	p.F 20/ POLY	distinct
233	**TP53**	**ENST0000026930·E4**	**119 (215) C**	**C -> G (homo)**	**100% (735) [100% (313) / 100% (422)]**	**> R (72 COSM3766192**	**c.215C>G**	**p.P 149 POLY**	**distinct**
234	ARID1B	ENST0000034608·E6	135 (2172) C	G -> A (homo)	100% (969) [100% (377) / 100% (592)]	· A (724 COSM1487405	c.2172G>A	p.A 4/1 POLY	distinct
235	BCORL1	ENST0000054005·E3	154 (331) C	T -> C (homo)	100% (698) [100% (404) / 100% (294)]	· L (111 rs4830173 (100	c.331T>C	p.L 1/0 POLY	distinct
236	KMT2D	ENST0000030106·E10	168 (1426) C	G -> A (homo)	98% (511) [94% (127) / 100% (384)]	· T (476 rs1064210 (10	c.1426G>A	p.A 0/3 POLY	distinct
237	KMT2D	ENST0000030106·E10	168 (1426) C	G -> A (homo)	98% (511) [94% (127) / 100% (384)]	· T (476 rs1064210 (10	c.1426G>A	p.A 0/3 POLY	distinct
238	LMNA	ENST0000036830·E7	181 (1338) C	T -> C (homo)	100% (216) [100% (80) / 100% (136)]	· D (446 rs505058 (1000	c.1338T>C	p.A 2/8 POLY	distinct
239	LMNA	ENST0000036830·E7	181 (1338) C	T -> C (homo)	100% (216) [100% (80) / 100% (136)]	· D (446 rs505058 (1000	c.1338T>C	p.A 2/8 POLY	distinct
240	SMARCA2	ENST0000034972·E25	216 (3672) C	G -> A (homo)	100% (537) [100% (269) / 100% (268)]	E (1224 COSM3763856	c.3672G>A	p.C 0/4 POLY	distinct
241	JAG1	ENST0000025495·E26	218 (3417) C	C -> T (homo)	100% (866) [100% (403) / 100% (463)]	Y (1139 COSM3758426	c.3417T>C	p.T 5/7 POLY	distinct
242	CHD1	ENST0000028404·E35	263..265 (! D	CCT (homo)	97% (1467) [97% (808) / 96% (659)]	(1684 COSM327350 ((c.5050_5052delCCT	c.5050_5052delCCT	p.P 0/1 POLY	distinct
243	MEN1	ENST0000031204·E10	271 (1621) C	A -> G (homo)	100% (1341) [100% (779) / 100% (562)]	· A (541 COSM255213 ((	c.1621A>G	p.T 20/ POLY	distinct
244	SMAD3	ENST0000032736·E1	296 [chr1 C	G -> A (het)	26% (66) [21% (38) / 36% (28)]	' UTR rs1061427 (100	c.-15G>A	0/8 POLY	distinct
245	RNF43	ENST0000040797·E9	300 (1252) C	C -> A (homo)	100% (2000) [100% (1063) / 100% (937)]	M (418 COSM4130449	c.1252C>A	p.L 13/ POLY	distinct
246	NF2	ENST0000033864·E1	332 [chr2 C	G -> C (homo)	95% (158) [95% (154) / 100% (4)]	' UTR rs1800540 (100	c.-110G>C	12/ POLY	forced,distinct
247	CASR	ENST0000049013·E7	512 (2244) C	G -> C (homo)	100% (2197) [100% (1122) / 100% (1075)]	· P (748 rs2036400 (100	c.2244G>C	p.P 3/1 POLY	distinct
248	KMT2C	ENST0000026218·E14	635 (2448) I (Dup)	A (het)	27% (195) [29% (68) / 27% (127)]	816 (R rs150073007 (d	c.2447dupA	p.T 0/1 POLY	distinct
249	KMT2D	ENST0000030106·E31	1245 (747: C	G -> T (homo)	100% (1035) [100% (679) / 99% (356)]	G (249: COSM3722550	c.7479G>T	p.C 3/1 POLY	distinct
250	KMT2D	ENST0000030106·E31	1245 (747: C	G -> T (homo)	100% (1035) [100% (679) / 99% (356)]	G (249: COSM3722550	c.7479G>T	p.C 3/1 POLY	distinct
251	CASR	ENST0000049013·E7	1299 (303: C	G -> C (homo)	100% (1268) [100% (577) / 100% (691)]	Q (1011 rs1801726 (100	c.3031G>C	p.C 3/1 POLY	distinct
252	CASR	ENST0000049013·E7	1565 [chr C	A -> T (homo)	100% (623) [100% (159) / 100% (464)]	' UTR rs4677948 (100	c.*60A>T	3/1 POLY	distinct
253	BRCA2	ENST0000054445·E11	2654 (456: C	A -> G (homo)	100% (544) [100% (280) / 100% (264)]	· L (1521 rs206075 (1000	c.4563A>G	p.L 65/ POLY	distinct
254	SETD2	ENST0000040979·E3	3378 (346: C	T -> C (homo)	100% (1061) [100% (579) / 100% (482)]	N (115: rs6767907 (100	c.3465T>C	p.A 1/6 POLY	distinct
255	APC	ENST0000025743·E16	3507 (546: C	T -> A (homo)	100% (345) [100% (152) / 100% (193)]	D (182: COSM3760871	c.5465T>A	p.V 4/1 POLY	distinct
256	BRCA2	ENST0000054445·E17	4604 (651: C	G -> C (homo)	100% (335) [100% (214) / 100% (121)]	V (2171 COSM4147689	c.6513G>C	p.V 301 POLY	distinct
257	CASR	ENST0000049013·E7	+15 / 1bp I (Dup)	A (het)	29% (22) [0% (0) / 29% (22)]	rs33974189 (Mt	c.*188dupA	0/2 POLY	forced,distinct
258	LMNA	ENST0000036830·E6	+16 [chr1 C	G -> A (het)	37% (422) [35% (184) / 38% (238)]	rs534807 (1000	c.1157+16G>A	2/8 POLY	distinct
259	LMNA	ENST0000036830·E6	+16 [chr1 C	G -> A (het)	37% (422) [35% (184) / 38% (238)]	rs534807 (1000	c.1157+16G>A	2/8 POLY	distinct
260	CASR	ENST0000049013·E3	+19 [chr3 C	C -> G (homo)	99% (373) [100% (10) / 99% (363)]	rs9869985 (100	c.492+19G>A	3/1 POLY	forced,distinct
261	TP53	ENST0000026930·E2	+38 [chr1 C	C -> G (het)	93% (240) [61% (30) / 100% (210)]	rs1642785 (100	c.74+38C>G	117 POLY	distinct
262	BRCA1	ENST0000035765·E1	+101 [chr C	C -> G (homo)	99% (307) [100% (230) / 99% (77)]	rs799905 (1000	c.-20+101C>G	1/0 POLY	distinct
263	KDM6A	ENST0000037796·E18	-5 / 1bp [D	T (het)	45% (35) [42% (16) / 48% (19)]	ExAC, ClinVar (I	c.2703-5delT	0/1 POLY (sel distinct
264	RNF43	ENST0000040797·E2	524 (139) C	A -> G (homo)	22% (396) [22% (188) / 21% (208)]	· V (47) rs3744093 (100	c.139A>G	p.II 14/ Poly	distinct
265	SMARCA2	ENST0000034972·E4	350..352 (: D	GCA (het)	36% (102) [36% (46) / 36% (56)]	2 (235..236)	c.705_707delGCA	p.C 0/4 Sequenz distinct
266	BRCA2	ENST0000054445·E14	390 (7397) C	T -> C (homo)	100% (282) [100% (91) / 100% (191)]	A (246(rs169547 (1000	c.7397T>C	p.V 302 Wildtyp distinct

4   DISCUSSION

To increase the success rate of clinical trials in the field of oncology, it is necessary to direct cancer research towards personalized medicine and precision oncology characterized by tailor-made treatments for individual patients [3]. In this study we investigated whether HSP90 clients such as MIF (macrophage migration inhibitory factor) and mutp53 (mutant p53) can serve as potential biomarkers and drug targets in colorectal cancer (CRC) or pancreatic ductal adenocarcinoma (PDAC):

(I)   Figures labeled with '**Publication**' can be found in the published paper (**section 3.1**): Klemke *et. al.* 2021, Cell Death & Disease [234].

(II) Figures labeled with '**Manuscript**' can be found in the provisionally accepted but not yet published manuscript (**section 3.2**), Klemke *et. al.* 2021, Frontiers in Oncology.

(III) Figures without any of the mentioned specifications can be found in the dissertation itself.

The results gained in these two subprojects, will be discussed in detail in the following sections.

4.1 MIF PROMOTES COLORECTAL CANCER PROGRESSION

Various efforts have been made to better understand the biological function of MIF. It was first discovered as a pro-inflammatory cytokine shown to inhibit random migration of immune cells [116]. However, as research progressed it became evident that it has a more complex biology than previously described. To date, MIF has not just been extensively described as a chemokine but also as a hormone and enzyme [159, 162]. Furthermore, with its pleiotropic functions it can regulate tumorigenic pathways by supporting all hallmarks of cancer [73, 235].

In our current CRC study (**Publication in section 3.1**) using the colitis-associated AOM/DSS mouse model, we investigated the role of MIF in CRC development. We showed that Mif levels are elevated in CRC cells and that a depletion of Mif results in decreased tumor burden (**Publication Figures 1, 2 and S1**). These findings are in line

with results gained in small intestinal tumors of *Apc^min* mice [149] and xenograft mouse models [111, 151] further supporting MIF as a tumor promoting protein in intestinal cancers.

To understand the core mechanism leading to altered tumor development, we were intrigued to answer the following questions:

(I)   *Does MIF already affect CRC development during tumor initiation?*

(II) *Is the tumorigenic effect of MIF limited to established tumors?*

Interestingly, we found that MIF is an important player in both phases of CRC tumor development.

To explore the underlying tumorigenic mechanism that could explain the decreased tumor burden after *Mif* depletion, established tumors were biopsied (**Publication Figure 1A**) and recovering tissue was prepared to investigate tumor initiation (**Publication Figure 3A**). The recovery group (representing tumor initiation), is characterized by DSS induced disruption of the intestinal epithelial barrier, causing massive infiltration of immune cells and disruption of the tissue (**Publication Figure 3B; section 2.2.1**). Within this phase of tumor development, we hypothesized that MIF promotes DSS-induced inflammation as a pro-inflammatory cytokine and Mif loss results in decreased inflammation and better tissue recovery. Therefore, we evaluated the infiltration of regulatory T-cells (FoxP3$^+$), neutrophil granulocytes (MPO$^+$) and T-lymphocytes (CD3$^+$) into the damaged tissue.

During initial stages, MIF acted as a pro-inflammatory cytokine on overall inflammation, particularly on the recruitment of regulatory T-cells, neutrophil granulocytes and T-lymphocytes (**Publication Figures 3B-D and S2A-C**). In contrast, this effect was not observed in established tumors (**Publication Figures 4A and S3A, B**). Interestingly, monocyte/macrophage infiltration was altered in established tumors but not in adjacent normal epithelium (**Publication Figure 4B)** or during tumor initiation ('recovery'; **Publication Figures 3C and S2A**). Furthermore, angiogenic (CD31, VEGF) and proliferative (Ki67) markers were specifically regulated in established tumors after *Mif*-depletion (**Publication Figures 4C-H**) but not during tumor initiation **(Publication Figure S3G-K**). Our *in vitro* (HCT116 and DLD-1; **Publication Figures 5A-G**) and *ex vivo* (*Mif*-depleted colon-derived tumor organoids; **Publication Figures 6F, G**) studies

confirm involvement of tumor cell-derived MIF in angiogenic pathways. Together with clinical patient correlation studies (**Publication Figure 5H-J**), these data showed that MIF acts in a CD74-dependent manner in CRC. Using matched pairs of colonic organoids (normal and tumor tissues from the same donor), we confirmed MIF as an important HSP90 client and demonstrated that stabilized MIF results in higher susceptibility of tumor cells towards HSP90 inhibition (**Publication Figures 6H-I, 7A-D, S5B, C**).

Taken together, these data suggest that MIF function switches from a pro-inflammatory cytokine during tumor initiation to a HSP90-stabilized protein driving tumorigenic mechanisms in established tumors (**Figure 8**).
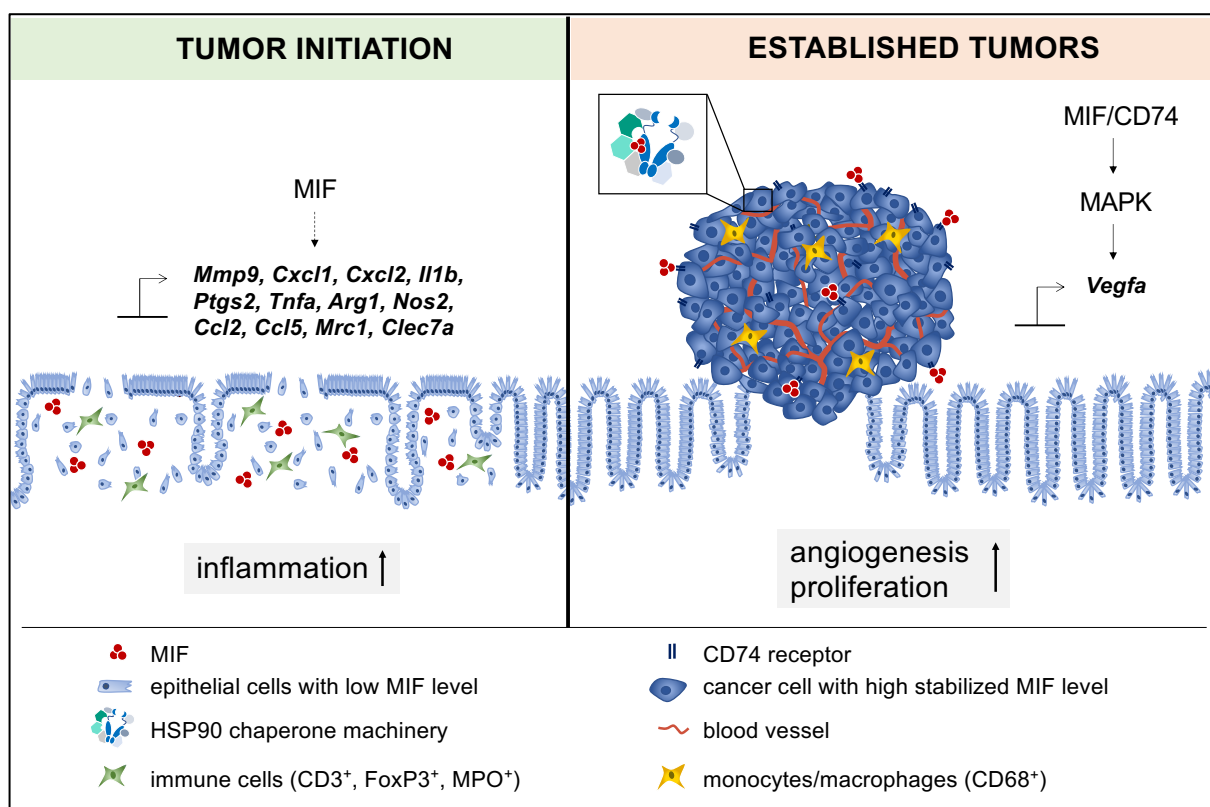
Figure 8: Functional switch of MIF during colorectal cancer progression. During tumor initiation MIF functions as a pro-inflammatory cytokine to regulate overall inflammation *via* recruitment of CD3^{+}, FoxP3^{+}, MPO^{+} immune cells and cytokine expression. In contrast, in established tumors MIF regulates the recruitment of tumor-associated macrophages and is involved in tumorigenic pathways such as proliferation and angiogenesis. Notably, MIF no longer regulates overall inflammation in established tumors.

4.1.1 MIF contributes to angiogenesis, but only in established tumors – a CD74-dependent mechanism

MIF has been described to promote colorectal tumorigenesis through regulation of angiogenesis [111, 149, 151, 236]. In established tumors of *Mif*-deficient mice, angiogenic markers (CD31 and Vegf) were downregulated compared to *Mif*-proficient mice (**Publication Figures 4C-G**). Furthermore, infiltration of tumor associated macrophages was reduced after Mif loss (**Publication Figure 4B**). From our *in vivo* study, we cannot conclude whether the MIF-dependent angiogenic effects are due to receptor mediated pathways in cancer cells themselves (**Figure 5**) or are a result of recruited tumor-associated macrophages, which are known to express and secrete angiogenic factors such as VEGF to support tumor progression [167, 170].

In this context, three different scenarios would be possible (**Figure 9**):

(I) Cancer cells harbor high levels of HSP90-stabilized MIF which is secreted into the surrounding stroma. The secreted MIF can act in an autocrine manner *via* the CD74 receptor to increase the expression and secretion of angiogenic factors such as VEGF and IL-8 from cancer cells [109, 111, 151, 155, 159].

(II) In a paracrine fashion, cancer cell-derived MIF also acts on constituents of the stromal compartment. MIF/CD74 interaction has been shown to be particularly important for chemotaxis of monocytes/macrophages [237]. In addition, tumor cell-derived MIF has been reported to contribute to the angiogenic potential of macrophages by inducing the expression of factors such as *VEGF* [161, 167, 238, 239]. Furthermore, tumor cell-derived MIF can promote neovascularization, by direct interaction with endothelial cells, resulting in their proliferation, migration and tube formation [162, 239].

(III) Stromal cells are also known to express and secrete MIF, which can act in an autocrine or paracrine fashion, further contribute to the expression of angiogenic factors [117, 167, 239-241]. Thus, the secretion of MIF from stromal cells can also contribute to neovascularization of tumors [167, 242].

In a tumor bulk, which consists of epithelial cancer cells and constituents of the tumor microenvironment, any combination of the three scenarios might contribute to vessel formation [168, 239]. However, scenarios (I) and (II) are most likely, since tumor cells

have high levels of stabilized MIF, hence being the major source of secreted MIF [57, 111].
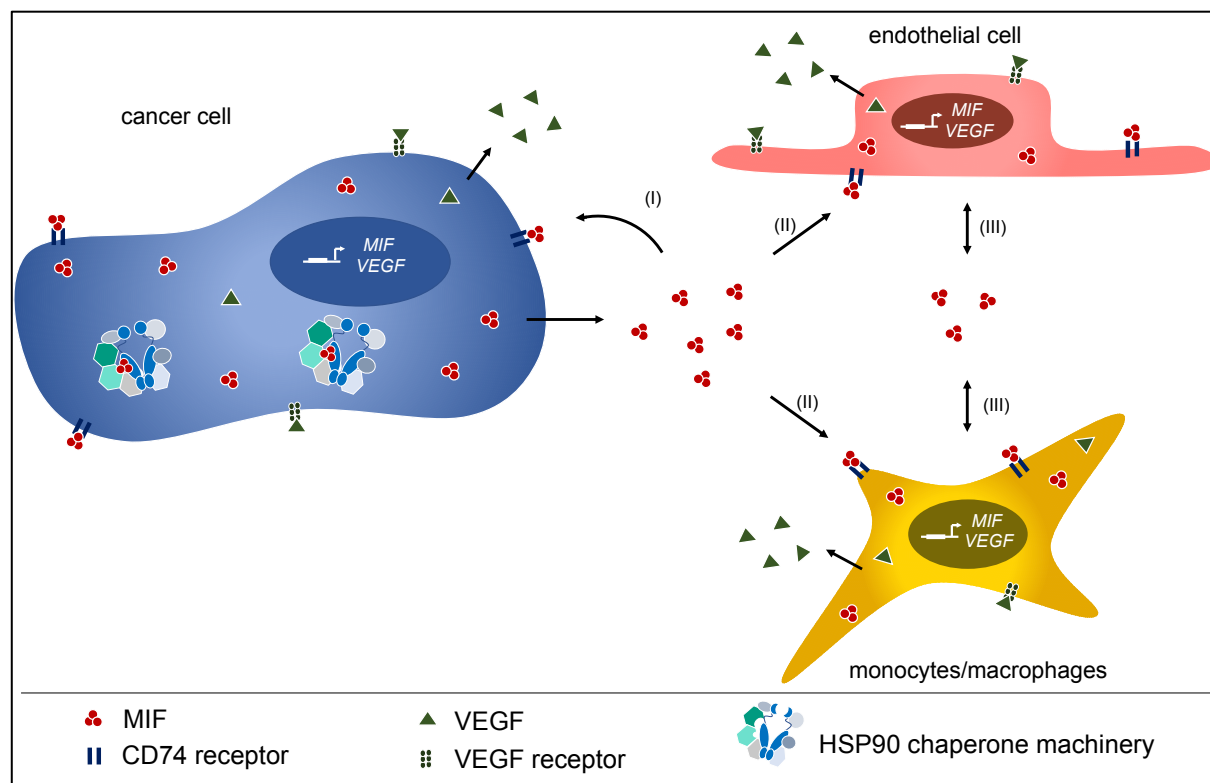
Figure 9: Possible scenarios on how MIF triggers angiogenesis in cancer. In cancer cells, MIF is highly stabilized by the HSP90 superchaperone machinery resulting in elevated MIF levels in cancer cells. (I) Secreted MIF acts in an autocrine loop, by binding to the CD74 receptor on cancer cells, promoting tumorigenesis *via* inducing expression and secretion of angiogenic factors (*VEGF*). (II) Moreover, tumor cell-derived MIF can act in a paracrine manner on monocytes/macrophages and endothelial cells which further promotes angiogenesis. (III) Macrophages/monocytes and endothelial cells also express and secrete MIF, which additionally triggers angiogenic responses by paracrine and autocrine loops.

Colorectal cancer cells have elevated MIF levels due to the stabilization *via* the HSP90 chaperone machinery (**Publication Figures 2, 6 and 7; Figure 5**), suggesting that most of the secreted MIF arises from these tumor cells themselves and contributes to angiogenesis. To prove this hypothesis, we used epithelial cell cultures to evaluate the expression of angiogenic factors. In *Mif*-deficient tumor organoids (**Publication Figure 6G**) as well as in human cancer cells (HCT116) (**Publication Figure 5B**), we found reduced expression of *VEGFA* or *IL8* after MIF loss, suggesting that HSP90-stabilized MIF in tumor cells themselves contributes to neovascularization in CRC *via* an autocrine loop. Of note, this effect was only observed in the presence of the cognate CD74 receptor (**Publication Figures 5A-G**).

Interestingly, we found that macrophage recruitment was specifically altered in established tumors, but not in adjacent normal tissue (**Publication Figure 4B**). MIF has been suggested to drive recruitment and activation of tumor-associated macrophages in a CD74-dependent manner, thereby promoting tumor progression *via* immunosuppression and angiogenesis [167, 168]. In line with these findings, Fan *et al.* demonstrated that *Mif-* and *CD74*-deficient murine macrophages displayed diminished chemotaxis [237]. The reduced chemotactic potential of macrophages in the absence of MIF might explain the lower number of macrophages observed in *Mif*-depleted tumors *in vivo* (**Publication Figure 4B**). In contrast to macrophages, other tested immune cells (neutrophil granulocytes, T-lymphocytes or regulatory T-cells) were not regulated in established tumors of *Mif*-deficient mice compared to wildtype mice. These immune cells are also known to contribute to tumor progression and to be regulated by MIF [161]. Indeed, the recruitment of T-cells [128, 243] and neutrophils [244, 245] has been mainly reported *via* the receptors CXCR2 and CXCR4. Taken together, the regulation of tumor associated macrophages but not neutrophil granulocytes, T-lymphocytes or regulatory T-cells (**Publication Figures 4A, B and S3A**), confirms the involvement of the MIF/CD74 axis in established CRC.

Further experiments are necessary to further investigate whether MIF in tumor cells or stromal cells (e.g., macrophages, fibroblasts, endothelial cells) constitutes the driving force of tumor progression. In that context, Hu *et al.* demonstrated that human hepatic sinusoidal endothelial cells (HHSECs) as well as human umbilical vein endothelial cells (HUVECs) cells were able to induce chemotaxis and migration in different CRC cell lines (SW480, HCT116) *via* secretion of MIF [246]. *Vice versa*, their study also showed, that MIF secreted from these cancer cells did not induce migration of endothelial cells [246]. In contrast, boyden chamber assays using HUVECs treated with recombinant MIF confirm its important role on neovascularization [241]. To further elaborate on the communication between cancer and endothelial cells, one could perform transwell and boyden chamber assays (with HUVECs) using the supernatant of *MIF*-proficient and *MIF*-depleted human epithelial cancer cells (e.g., HCT116) or matched pairs normal and tumor organoids from CRC patients.

However, additional preclinical proof-of-principal studies would help to understand the importance of cancer-derived MIF in the context of tumor development. Therefore, *Mif*$^{fl/fl}$*;villincre* mice can be used to specifically deplete *MIF* from colon epithelial cells,

while MIF expression in the tumor stroma remains unaltered [247]. These transgenic mice are characterized by the constitutive expression of the cre recombinase under regulatory control of the villin promotor [247]. The cre recombinase specifically recognizes loxP (floxed allele, fl) sequences allowing the recombination of defined target genes [247]. In *Mif^{fl/fl};villincre* mice, the *Mif* gene is flanked with two loxP sites, allowing the villincre recombinase to deplete Mif from intestinal epithelial cells.

By using this mouse strain in comparison to our constitutive *Mif* knockout mouse used in the current study, the following results would be expected:

(I) If MIF in cancer cells is the driving force of CRC development, an epithelial-specific depletion of MIF would result in decreased tumor burden.

(II) If MIF in stromal cells is the most important source for CRC development, we would not see any alteration of tumor growth after MIF loss in epithelial cells.

(III) If a combination of MIF in cancer and stromal cells results in the development of colorectal tumors, a milder reduction in tumor burden would be seen compared to that observed in the overall constitutive *Mif* knockout mice.

Evaluation of tumor burden, tumorigenic pathways and macrophage recruitment can reveal whether depletion of HSP90-stabilized MIF specifically in the intestinal epithelial cancer cells is the driver of tumor development in CRC.

An additional step would be to use a conditional *Mif* knockout mouse (*Mif^{fl/fl};villincreERT2)*. In these mice, the cre recombinase is fused with the mutated ligand-binding domain of the estrogen receptor ERT2 which interacts with HSP90 [247, 248]. Upon treatment with Tamoxifen HSP90 dissociates and the creERT2 fusion protein translocates into the nucleus to induce recombination of the target gene of interest [248]. This mouse model allows the depletion of genes at a defined time point. For the current study it would be of interest to use these conditional mice to investigate whether tumor cell-derived MIF is important for tumor maintenance. For those experiments, mice would be treated with AOM/DSS to induce tumor development. Then, *Mif* recombination is initiated using Tamoxifen at a particular tumor size. These approaches are especially important for clinical translation, since CRC patients are often diagnosed at a later stage of the disease [107, 108]. Therefore, most of these patients would already have established CRC tumors at the start of their treatment

[107]. Hence, the *Mif^{fl/fl};villincreERT2* mice would be a suitable model to investigate if MIF is essential for CRC maintenance and can serve as a suitable biomarker for treatment in the clinic.

Furthermore, these mice provide the possibility of co-cultures between *Mif*-proficient and *Mif*-deficient colonic tumor organoids together with isolated peritoneal *Mif*-proficient macrophages. These approaches enable the analysis of macrophage recruitment and activation dependent on the MIF status of the tumor cell. A few other groups have recently started using *Mif^{fl/fl}* mice to investigate effects of tissue-specific *Mif*-depletion on renal inflammation [249] or nonmelanoma skin cancer development [250]. Thus far, *in vivo* data from a mouse model for colorectal cancer remain elusive, which raises the need for further research.

To better understand whether tumor cell-derived MIF plays a role in mediating tumorigenesis, we investigated the underlying molecular mechanism by which MIF contributes to angiogenesis and proliferation. Analysis of ERK and p38 activity in *Mif*-deficient tumors revealed decreased phosphorylation of both MAPKs (**Publication Figure 4F**). Both factors are downstream of MIF's cognate CD74 receptor and are involved in proliferation and angiogenesis [127, 134, 159], which is supported by decreased VEGF levels after Mif loss in *vivo* (**Publication Figures 4C, F, G; Figure 5**). Concomitantly, in human CRC cells (HCT116, RKO), the regulation of ERK activity and downstream angiogenic genes were dependent on the presence of MIF and its cognate receptor CD74 (**Publication Figures 5A-G**). Accordingly, human patient correlation studies revealed that high levels of MIF in CRC cells along with high levels of CD74 correlated with reduced overall survival of patients compared to high MIF levels alone (**Publication Figures 5H, I**). In contrast, presence of CD74 in the absence of high MIF levels (MIF^{low}) did not impact patient survival (**Publication Figure 5J**). Taken together, these findings suggest that MIF acts on angiogenesis and proliferation in a CD74-dependent manner in CRC. Research from other groups confirm the importance of MIF and CD74 interaction in tumor progression throughout different cancer origins [157, 251, 252].

In sum, we found that HSP90-stabilized Mif in established colorectal cancer cells acts in a CD74-dependent manner, contributing to angiogenesis via regulation of MAPKs ERK and p38.

4.1.2 MIF contributes to overall inflammation, but only during tumor initiation – a CD74-independent mechanism?

We next aimed to investigate, whether MIF is already important for tumor initiation ('recovery'). Interestingly, angiogenic and proliferative factors, which were regulated in a CD74-dependent manner in established tumors (**section 4.1.1**) remained unchanged in $Mif^{-/-}$ mice during tumor initiation (**Publication Figures S3G-K**) which hints towards CD74-independent mechanisms of MIF. Indeed, the complexity of MIF receptors is evolving, since CD74/CD44 and non-cognate receptors (CXCR2, CXCR4, CXCR7) can signal individually, but have also been reported to form heterodimers [124, 128, 130, 159] (**section 2.2.2 and 2.2.3**).

Following DSS administration, massive tissue damage was observed in all animals of the recovery group; this effect was even more pronounced in Mif-proficient than Mif-deficient mice (**Publication Figure 3B**). We hypothesized that MIF loss might result in better recovery of the tissue due to decreased inflammatory processes, which led us to investigate some major players of the inflammatory pool. A variety of different hematopoietic cells such as neutrophils, macrophages and T-cells are essential drivers of a rapid wound healing response [253]. Neutrophils (MPO[+]) are the main immune cell population in human blood protecting the host from various infections [245, 254]. Bacterial infiltration into the tissue (e.g., by DSS administration, **section 2.2.1**), causes massive infiltration of neutrophils into the damaged area [245]. However, the exact role of neutrophils has been controversially discussed and is highly context dependent [254]. Besides their role in promoting tissue recovery, neutrophils act against the infiltrated microbiome by secreting proteases and reactive oxygen species (ROS) which might also contribute to further damage of host tissue and might result in delayed regeneration [245, 255]. T-Lymphocytes (CD3^{+}) are known to be potentially harmful for tissue recovery [256]. They secrete pro-inflammatory cytokines such as TNFα , which can trigger inflammatory responses and decrease tissue regeneration [256, 257]. Regulatory T-cells (FoxP3^{+}) are also important drivers of inflammation and tissue repair by modulating the infiltration of other immune cells such as neutrophils and T-lymphocytes [256]. Last but not least, macrophages have also been shown to play an important role in tissue repair and regeneration by secreting chemokines and matrix metalloproteinases [253].

Indeed, we found overall inflammation to be downregulated in *Mif*-deficient mice during tumor initiation (**Publication Figures 3C, D and S2A-C**). Importantly, T-cell and neutrophil recruitment were altered upon Mif loss, while recruitment of CD68 positive monocytes/macrophages remained unchanged (**Publication Figures 3C and S2A**). As it has been reported that *Mif* and *CD74* deficient murine macrophages display diminished chemotaxis [237], it was interesting to see that Mif loss did not alter macrophage recruitment during tumor initiation. In contrast, neutrophils which have so far been reported in the literature to be CD74 negative [133, 258, 259] showed diminished infiltration in the absence of Mif.

These data further suggest that CD74-independent mechanisms could be involved in the recruitment of immune cells during tumor initiation. Notably, the MIF-mediated recruitment of T-cells and neutrophils have been reported to occur mainly *via* CXCR2 and CXCR4 [124, 128, 161, 162, 243]. These results hint towards the binding of MIF to these receptors, to drive overall inflammation during tumor initiation. In accordance, Farr *et al.* reported that CD74 loss *in vivo* results in increased inflammation-induced tissue damage, caused by decreased tissue recovery [260]. One reasonable explanation for this observation could be the shift of MIF towards interaction with its non-cognate receptors CXCR2 and CXCR4 [128, 243, 260]. Consequently, due to the co-regulation of receptors and the possible shift of ligands/receptor binding, knockout or overexpression experiments in this context might not be ideal. Though out of scope of our current study, it would be of importance to understand the dynamics of these MIF receptors to further understand the role of MIF during CRC initiation.

Taken together we deduce that the reduction of tumor burden in *Mif*$^{-/-}$ mice might be a combination of: (I) decreased inflammation and better recovery during tumor initiation and (II) diminished proliferation and angiogenesis in established tumors.

4.1.3 HSP90-stabilized Mif contributes to tumor cell survival

Next, we aimed to investigate how Mif levels are elevated in colorectal cancer cells and whether it can serve as a drug target in CRC. In established tumors, *MIF* levels were upregulated at mRNA level (approx. 2.5-fold in mouse and human samples; **Publication Figures 2A, F and S1A, C**), which could be due to increased activation of its transcription factor HIF1α [155, 261] (**Figure 5**). However, using immunoblot

analysis, we found that MIF was even more strongly upregulated on protein levels (up to 5.1-fold in mouse and up to 8.5-fold in human samples; **Publication Figures 2B, E and S1B**). We previously showed that this protein elevation is due to increased stabilization of Mif through the HSP90 chaperone machinery in a mouse model for breast cancer [57, 76]. In our current study, we confirm elevation of Mif in CRC cells to be driven by stabilization *via* HSP90 (**Publication Figures 6 and 7**), thus raising the question:

Is MIF also a targetable, cancer-relevant HSP90 client in colorectal cancer?

To answer this question, mice were treated with the HSP90 inhibitor 17AAG to assess tumor burden. Interestingly, reduction of tumor growth was more pronounced in *Mif*-proficient than *Mif*-deficient mice (**Publication Figures 6B-E**), suggesting MIF as an important HSP90 client in CRC. In line with these results, *Mif*-depleted colonic tumor organoids were less susceptible towards HSP90 inhibitor treatment (17AAG) than *Mif*-proficient tumor organoids (**Publication Figures 6G-I**). Furthermore, we used matched pairs of colonic organoids (normal and tumor material derived from the same mouse), allowing us to investigate tumor-specificity and toxicities of HSP90 inhibitors *ex vivo*. Importantly, tumor-derived organoids, containing stabilized Mif, showed increased death after HSP90 inhibitor treatment compared to matched pairs of normal epithelial-derived organoids, containing unstabilized Mif (**Publication Figures 7A-D**). Even though immunoblot analysis reveals degraded Mif in both normal- and tumor-derived organoids, only degradation of tumor-derived, stabilized Mif resulted in increased organoid death. Again, these results confirm tumor promoting functions of MIF due to epithelial-specific stabilization through the HSP90 chaperone machinery.

Taken together, we propose that the combination of novel HSP90 inhibitors (reducing HSF1 response, **section 2.1.3**) together with anti-MIF agents might provide a possible way to selectively target tumor cells and increase anti-tumor effects. Furthermore, the combination treatments could provide a mechanism to bypass cancer resistance [19, 80].

In that respect, inhibition of MIF function can be achieved by using small molecules or antibodies against MIF itself or its cognate receptor CD74 [159, 175]. Small molecules against the tautomerase domain of MIF like ISO-1 have been extensively studied in preclinical trials for different cancers [175, 262, 263]. However, clinical trials were mostly conducted using antibodies against MIF or its cognate receptor CD74 [175].

Early phase clinical trials using BAX69 (Imalumab, anti-MIF) or Milatuzumab (hLL1, anti-CD74) showed low toxicity; however, efficacy needs to be further assessed [175, 264, 265]. BAX69 is an antibody particularly raised against oxidized MIF (oxMIF) which has been studied in clinical and preclinical cancer trials thus far [175, 265, 266]. To date, very little is known about the redox-dependent isoform of MIF and its biological properties and more research is needed in this field [267]. However, it has been reported that oxMIF might be the disease related isoform which has been shown to be upregulated in tumor cells of CRC patients [265, 266]. Thiele *et al.* proposed that oxidation of MIF results in a conformational change of the protein [268]. Based on these data, it could be speculated that the conformational change of MIF due its oxidation increases its dependency on HSP90 superchaperone binding, resulting in stabilization of MIF in colorectal cancer cells. As most other studies in this research area, we did not distinguish between reduced and oxidized MIF. Consequently, it would be of interest to differentiate the two and to find out if oxMIF is the isoform that is more dependent on the HSP90 superchaperone support.

More recently, the use of nanobodies against MIF has been investigated in the context of endotoxic shock [175, 269]. Nanobodies are camelid-derived single-domain antigen-binding antibody fragments [269, 270]. Compared to conventional monoclonal antibodies, nanobodies have been shown to have better solubility and tissue penetration, as well as lower immunogenicity [269]. Hence, the use of nanobodies might also be of interest for targeting oxidized MIF in preclinical and potential clinical studies in order to increase the efficacy of anti-MIF therapy in colorectal cancer.

In conclusion, post-translational modifications such as oxidation of MIF might provide an explanation for the functional switch of MIF from a pro-inflammatory cytokine during tumor initiation, to a tumor promoting protein in established tumors.

Our study confirms that MIF can serve as a biomarker in colorectal cancer. Due to the lack of successful clinical studies so far, a combination of different cancer treatments might be of interest [265]. We hypothesize that the combination of HSP90 inhibitors and anti-MIF or anti-CD74 therapies could provide a novel approach to target colorectal cancer cells in individual patients. Of note, we have previously shown that mutp53$^{R248Q/W}$ is also a cancer relevant HSP90 client, driving tumor growth and invasion in CRC [56]. Hence, in those tumors harboring the stabilized mutp53$^{R248Q/W}$ variant HSP90 inhibition would concomitantly result in a degradation of MIF and

mutp53$^{R248Q/W}$. This effect might be a promising basis for novel treatment strategies, using biomarkes in order to increase the efficacy of cancer therapy.

4.2 MUTP53$^{R248Q/W}$ PROMOTES MIGRATION IN CRC AND PDAC

Since decades, researchers from all over the world have been trying to investigate the role of the tumor suppressor p53 in cancer. As 'guardian of the genome', p53 is mutated in a majority of cancers providing a selection advantage for cells [188, 190, 201, 221]. Over time it became evident, that different mutants of p53 must be considered as individual proteins, harboring different functions [204, 213]. The exact biological function of mutp53 variants is dependent on the mutation itself as well as newly arising complex interactions with other proteins [204, 210, 224] (**section 2.3.3**).

In a previous study in colorectal cancer, we showed that the interaction of mutp53$^{R248Q/W}$ with pSTAT3 drives proliferation and invasion of cancer cells [56] (**section 2.3.4**). Based on these results, we proceeded to investigate the impact of mutp53^{R248W} in PDAC. A panel of different PDAC cell lines revealed high levels of stabilized mutp53^{R248W} in MIA-PACA-2, mutp53^{C176S} in PA-TU-8902 and mutp53^{R282W} in PA-TU-8988T cells (**Manuscript Figure 1A, B**). Treatment of PDAC cells with second generation HSP90 inhibitors Ganetespib and Onalespib resulted in reduced mutp53 levels in all cell lines except BXPC-3 cells harboring mutp53^{Y220C} (**Manuscript Figure 2A**). In PANC-1, MIA-PACA-2, PA-TU-8902 and PA-TU-8988T cells, HSP90 inhibitor treatment resulted in reduced cell confluency (**Manuscript Figure 2B**). These data reveal that all mutants except Y220C are targetable using HSP90 inhibitors.

As we have previously shown that stabilized mutp53 variants bind to pSTAT3 in colorectal cancer cells [56], we aimed to investigate if this also occurred in PDAC. Therefore, we performed co-immunoprecipitations in different PDAC cell lines. Strongest interaction was observed between mutp53 and pSTAT3 in MIA-PACA-2 and PA-TU-8988T cells (**Manuscript Figure 4B-D**). Of note, the interaction of mutp53 and pSTAT3 was independent of the levels of pSTAT3; even upon pSTAT3 induction in MIA-PACA-2, PANC-1 and BXPC-3 cells, strongest interaction was only observed between mutp53^{R248W} (MIA-PACA-2 cells) and pSTAT3 (**Manuscript Figure 4H**). This confirmed our results in CRC, indicating that specific variants of stabilized mutp53 predict new complex formations to drive tumorigenesis.

In CRC, mutp53$^{R248Q/W}$ – pSTAT3 complexes drive migration and invasion [56]. To evaluate if p53 mutants also acquire such new and specific functions in PDAC, we depleted single p53 mutants in different PDAC cells. Importantly, a depletion of mutp53 only diminished migration in MIA-PACA-2 cells harboring mutp53^{R248W} (**Manuscript Figure 3A, F**). It as to why the PA-TU-8988T cells, which showed a strong binding between p53^{R282W} and pSTAT3 failed to have a GOF on migration remains speculative. Possible explanations will be discussed in the following sections in more detail.

Furthermore, an ablation of mutp53 only resulted in reduced pSTAT3 levels in MIA-PACA-2 cells but not in any other tested cell lines (**Manuscript Figure 4E and S2B**), suggesting that only the specific mutp53^{R248W} regulates the activity of STAT3. Concomitantly, the absence of pSTAT3 reduced migration of MIA-PACA-2 cells but not PA-TU-8988T or PANC-1 cells (**Manuscript Figure 5A-D**). Finally, clinical data revealed that R248 missense mutations of p53 decrease overall patient survival compared to other p53 mutations (**Manuscript Figure 5E**). In sum, these data suggest that mutp53^{R248W} drives migration of PDAC cells *via* its complex formation with pSTAT3 in a similar manner to that observed in CRC [56] (**Figure 10**).
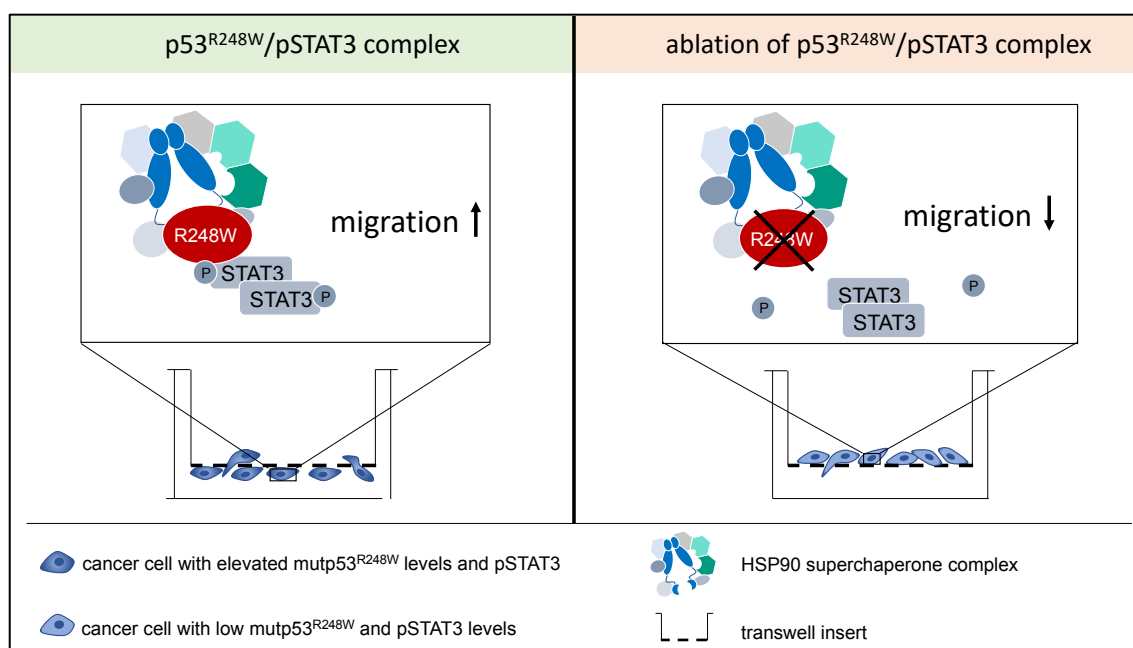
Figure 10: Migratory potential of PDAC cells depends on mutp53^{R248W} and pSTAT3 complex formation. In PDAC cells mutp53^{R248W} is stabilized by the HSP90 superchaperone complex. Depletion of mutp53^{R248W} reduces pSTAT3 levels and results in decreased migration of PDAC cells. Ablation of STAT3 only diminishes migration of mutp53^{R248W} harboring cells.

4.2.1 Distinct complex formation of mutp53 variants

The current study confirms the importance of mutp53^{R248W} – pSTAT3 complex formation on migration in PDAC and the regulatory impact of mutp53^{R248W} on STAT3 activity, which was already observed in colorectal cancer *in vivo* and *in vitro* [56]. To date, the only existing PDAC cell line harboring the R248 mutation of p53 is the MIA-PACA-2 cell line. Options to overcome this issue would be:

(I) Altering the endogenous alleles using targeted homologous recombination (e.g., CRISPR/Cas9) to generate R248W mutations in other cell lines. This approach enables the study of proteins under normal regulatory control elements [271, 272].

(II) Generation of isogenic cell lines, by altering the endogenous alleles using homologous recombination. Analyzing different mutation in one genetic cell background helps to exclude effects from other cell-specific mutations and alterations [272, 273].

In colorectal cancer, Sur *et al.* made use of this approach to study the physiological function of mutp53^{R248W} independent of plasmid overexpression induced effects [271]. Furthermore, CRISPR/Cas9 technology helps to maintain the gene copy number [273], which might be of tremendous importance in the case of stabilized proteins. Because of that, we propose the use of CRISPR/Cas9 or other approaches using homologous recombination technology in isogenic cell line models to better understand the impact of different single nucleotide polymorphisms on the function of the protein under isogenic conditions.

Although our current study shows that the specific variant mutp53^{R248W} regulates pSTAT3 in PDAC, further research is needed to investigate the underlying mechanism. One possible explanation for increased pSTAT3 levels in the presence of mutp53^{R248W} could be the displacement of the phosphatase SHP2, as observed in CRC [56]. However, we cannot exclude that other phosphatases known to regulate STAT3 activity might also be involved [274].

As displayed in **section 2.3.3**, mutp53 has been described to exert its gain of tumorigenic functions *via* interaction with other proteins such as the transcription factor

pSTAT3 [56, 210] (**Figure 6**). However, the exact underlying mechanism and the interacting proteins are highly dependent on the cellular context [204, 210]. Stabilization of mutp53 through the HSP90 complex is a prerequisite for GOF in cancer cells [56, 221, 222] (**Figure 3**). The presence of certain co-chaperones or post-translational modifications of the HSP90 chaperone complex are known to define its interaction with client proteins [23, 75]. Therefore, different co-chaperones and modifications of the HSP90 superchaperone complex might also have an impact on interaction partners of mutp53 [210]. In the current study, we did not elaborate on any further interaction partners of mutp53^{R248W} in PDAC. Given that many proteins have been described to interact with different mutants of p53 [204, 210, 224, 233], we cannot exclude that other proteins might also be part of the complex (hetero TF complex formation), leading to mutp53^{R248W}-dependent migration in PDAC. This finding is further supported by the fact that STAT3 is reported to form hetero transcription factor (TF) complexes with other proteins such as other STAT isoforms [275], NF-κB [276] or NFATc1 [277] in cancer.

Based on our current study, we cannot state whether mutp53^{R248W} binds to pSTAT3 homodimers or hetero TF complexes [277] and/or whether this interaction supports the recruitment of additional co-factors that drive the transcriptional program [278]. However, the formation of hetero TF complexes might provide an explanation for binding of mutp53 to pSTAT3 in various PDAC cells (**Manuscript Figures 4B-D**), without regulating migration (**Manuscript Figure 3A-H**). One such example is the PA-TU-8988T cell line, which showed strong binding of mutp53^{R282W} to pSTAT3 (**Manuscript Figure 4D**). However, reduced phosphorylation levels upon mutp53 ablation and diminished migration were not observed (**Manuscript Figures 3C, H and 4E**). STAT3 is known to be involved in many of the hallmarks of cancer, such as angiogenesis, proliferation and inflammation to promote tumor progression [279, 280]. To date, very little is known about the exact interaction partners of mutp53^{R282W}. These results again suggest that mutp53^{R282W} might be part of a hetero TF complex, together with other proteins and transcription factors, resulting in a gain-of-function other than migration.

Further examples for hetero TF complexes have been proposed for mutp53^{R273H} and mutp53^{R175H}. Cooks *et al.* have previously reported that mutp53^{R273H} in PANC-1 cells supports activation of NF-κB to promote inflammation-associated cancer progression

[281]. The authors hypothesize that this effect could be due to a direct protein-protein interaction as observed for other mutp53 variants [281]. In this context, mutp53^{R175H} and the corresponding murine mutp53^{R172H} were also reported to enhance NF-κB activity [282, 283]. Murine mutp53^{R172H} was shown to physically interact with NF-κB p65 [283] and both homologs were found to colocalize with the transcription factor on some of its promotor sites, regulating the transcriptional outcome [283, 284]. Interestingly, besides strong interaction of mutp53 to pSTAT3 in MIA-PACA-2 cells, we found low binding in PANC-1, BXPC-3 and CAPAN-1 cells (**Manuscript Figures 4B, C**). One explanation for the minor co-precipitation of pSTAT3 in PANC-1 could be the formation of hetero TF complexes between mutp53^{R273H} and NF-κB together with pSTAT3; this might be triggering inflammatory processes instead of migration in PDAC cells. Nevertheless, since levels of phosphorylated STAT3 were not affected after mutp53 ablation in PANC-1 cells, binding of mutp53^{R273H} to pSTAT3 might not result in a direct displacement of phosphatases to regulate STAT3 activity (**Manuscript Figure S2B**).

To exploit the exact gain-of-function mechanism of the different mutp53 variants, intensive research is required. Binding of mutp53 to pSTAT3 does not necessarily result in a gain-of-function on migration. It is more likely that the exact composition of the complex and the participation of other proteins and transcription factors might define which tumorigenic function is gained. Because of this vast complexity and heterogeneity, it is important to further investigate the underlying mechanism of each p53 mutant in a context-specific manner.

4.2.2 Stabilized mutp53 as potential therapeutic target

Since *TP53* is mutated in the majority of cancers, resulting in its accumulation especially in cancer cells compared to normal cells [285], several efforts have been made in different cancer entities to specifically target mutp53 in tumor cells e.g. *via* HSP90 inhibition [56, 85, 226].

To investigate whether mutp53 is also a potential drug target in PDAC, we treated different PDAC cells with the two HSP90 inhibitors Gantespib and Onalespib. Interestingly, HSP90 inhibition results in destabilization of the mutp53 protein in all analyzed PDAC cells except BXPC-3 cells (**Manuscript Figure 2A**). However, the

positive control AKT also failed to be degraded upon inhibitor treatment in BXPC-3 cells. These data suggest a resistance mechanism towards HSP90 inhibition. As previously shown in CRC, that resistance towards Ganetespib correlates with the expression of UDP glucuronosyltransferase 1A (UGT1A) [286]. UGT1A belongs to a superfamily of proteins involved in the biotransformation and excretion of various compounds and proteins [286, 287]. An overexpression of UGT1A in BXPC-3 cells could provide an explanation for the resistance towards both HSP90 inhibitors.

As in our current PDAC study, many other studies have also shown that different mutp53 proteins are stabilized by the HSP90 chaperone machinery, resulting in elevated mutp53 levels in cancer cells [56, 85, 214, 229, 288]. In addition, Parrales *et al.* showed that mutp53 can be targeted by interference with the mevalonate pathway, using the small molecule inhibitor Statin [289]. An intermediate of this pathway (mevalonate-5-phosphate) contributes to the inhibition of the ubiquitin ligase CHIP by promoting the interaction between HSP40 and mutp53 [289, 290]. Inhibition of this intermediate results in an increased CHIP-mediated degradation of mutp53 [289, 290]. Interestingly, one of the investigated cell lines in their study is the BXPC-3 cell line harboring the conformational mutant mutp53^{Y220C} [290]. The fact that mutp53^{Y220C} was not targetable using HSP90 inhibitors (**Manuscript Figure 2A**) could also be explained, by HSP90-independent stabilization *via* interaction with other co-chaperones such as HSP40 [290]. Taken together these results highlight that the entire HSP machinery is essential for stabilization of mutp53 which is required for its gain-of-function activities.

It has been demonstrated that high levels of stabilized mutp53 are a prerequisite for the gain of new tumorigenic functions [221, 222]. However, some controversies exist in the literature concerning the exact mechanism that leads to elevated mutp53 levels. It is important to note that mutation-induced unstable conformations of some mutant p53 proteins such as R248Q, R273H, R175H, R282W and Y220C, might contribute to an aggregation of these mutants, either amongst themselves and/or with other proteins [217, 291, 292], independent of HSP90. Mutations-induced conformational changes of p53 can expose an aggregation-prone sequence within the hydrophopic core of DNA binding domain resulting in oligomerization [218]. These prion-like aggregates were shown to interact and thereby modulate the transcriptional activity of other proteins such as remaining WTp53 as well as p53-family members such as p63 and p73 and

[217, 219, 220, 293]. BXPC-3 cells display the Y220C mutation of p53, which was described to form oligomeric structures [291]. Therefore, further studies are needed to elucidate whether higher concentrations of the HSP90 inhibitors are able to induce degradation of mutp53 in these cells at all. Treatment with Statins to inhibit the mevalonate pathway could provide some evidence whether mutp53^{Y220C} is stabilized in a HSP40-dependent manner in PDAC [290]. Altogether, this would help to understand if mutp53^{Y220C} is a client of HSP90/HSP40 in pancreatic cancer cells or if moderately elevated levels of mutp53 in these cells are due to self-aggregation of the protein. Co-immunoprecipitation of mutp53^{Y220C} and HSP90/HSP40 would help to further elucidate whether this mutant in BXPC-3 cells is a client of HSPs or not.

In contrast, we confirmed mutp53^{R248W}, mutp53^{R282W} and mutp53^{R273H} to be clients of the HSP90 chaperone machinery in PDAC (**Manuscript Figure 2A**). In fact, cancer cells might even have an equilibrium of HSP90-stabilized and aggregated proteins, resulting in the gain of new tumorigenic functions *via* interaction of mutp53 with other proteins to form complexes in general [217]. The exact mechanism might be highly dependent on the cellular and molecular context. Of note, small molecules, such as ReACp53 or PRIMA-1, targeting these prion-like heterogeneous aggregates of mutp53 have been applied to preclinical and clinical trials [228, 291, 294]. This approach focuses on personalized drugs in order to change the conformation of different p53 mutants, leading to their disaggregation or the restoration of wildtype p53 functions (reactivators) [228, 291].

Further investigation of the transient and dynamic nature of these complexes is necessary to obtain a better understanding of the different mutp53 GOFs [291]. In the current study we provided first evidence that most of the p53 mutants (except Y220C) can serve as potential biomarkers for HSP90 inhibitor treatment. Given the plethora of HSP90 clients, simultaneous inhibition of cancer-relevant clients can help to overcome possible therapy induced resistance mechanisms by targeting more than one tumor driving mechanisms [19, 235].

Apart from the strategies discussed above to target mutp53 itself (HSP90 inhibitors, Statins, p53 reactivators), it would also be possible to target mutp53 through targeting its interaction partners to disrupt hetero TF complexes. Hence, in the context of mutp53^{R248W}, it would be of particular interest to target pSTAT3. In this context, our study revealed that siRNA-mediated knockdown or inhibition of STAT3 using Stattic,

resulted in diminished migration specifically in mutp53^{R248W} harboring MIA-PACA-2 cells (**Manuscript Figure 5A, B, D**). Additionally, MIA-PACA-2 cells were most susceptible towards Stattic treatment compared to other PDAC cells (**Manuscript Figure 5C**). However, Stattic was tested in several other preclinical trials, but is not considered a potent therapeutic candidate, due to diverse off-target effects and lacking efficacy *in vivo* [295-297]. In contrast BBI608 (Napabucasin), a small molecule shown to inhibit stemness pathways such as the STAT3 signaling pathway [298] has achieved orphan status by the FDA for treatment of gastric and pancreatic cancers [279, 299]. Unfortunately, phase III clinical trial for both cancers were discontinued due to futility [298, 300]. In contrast, mutp53^{R273H} might form hetero TF complexes with NF-κB and other cofactors such as pSTAT3 (**Manuscript Figure 4B**) causing a GOF on inflammation rather than migration [281]. In that case, a modulator of inflammatory pathways might be more relevant Interestingly, the triterpenoid bardoxolone methyl (RTA 402 or CDDO-Me) was found to inhibit both: STAT3 and NF-κB pathways [301-304]. First clinical evaluations for advanced solid tumors showed low toxicity and promising anti-tumor efficacy [303].

Using inhibitors for the specific hetero TF complexes based on specific biomarkers might be an important step towards personalized medicine, helping to increase success rates of pancreatic cancer treatments. A combination of novel HSP90 inhibitors (**section 2.1.3**) together with mutp53 variant-specific STAT3/NF-κB inhibitors (BBI608, RTA 402) could provide a good treatment option to selectively target tumor cells and prevent acquisition of resistance [19, 235].

4.2.3 Mutp53 and the PDAC tumor microenvironment

In the past couple of years, it became more evident that mutp53 can influence the crosstalk between cancer cells and the components of the tumor microenvironment [305]. It is thought that the interaction of mutp53 variants with different transcription factors (e.g., NF-κB, pSTAT3, **see section 4.2.1**) can trigger a pro-tumorigenic response of stromal cells either by specific secretion of soluble bioactive mediators (e.g. cytokines, angiogenic factors) or the transcription of proteins which are necessary for interaction between tumor and stromal cells [305-307]. In that way, mutp53 can

regulate the exact composition of the cancer secretome in order to acquire new tumorigenic functions and to promote tumor progression [305].

PDAC is histologically characterized by a very high stromal content (approx. 90% of the tumor bulk), also contributing to the broad heterogeneity and plasticity of the disease as well as therapeutic resistance [178, 179]. Because of that, it is especially important for further studies to take the tumor microenvironment into consideration. A recent publication from Butera $et\ al.$ investigated the impact of different mutp53 proteins on the tumor secretome [308]. They found that mutp53^{R175H} and mutp53^{R273H} can alter the cancer secretome to promote anti-apoptotic and hyperproliferative responses as well as chemoresistance of PDAC cells [308]. Interestingly, closer analysis of the exact composition of secreted proteins revealed a vast interaction network with several proteins, including HSP90 [308]. This is in line with our study presenting mutp53^{R273H} as a HSP90 client in PDAC (**Manuscript Figure 2A**). Taken together, HSP90-stabilized mutp53^{R273H} in PDAC cells, might lead to the formation of hetero TF complexes with NF-κB, pSTAT3 and potential other cofactors to promote inflammatory processes and to regulate the cancer secretome [281, 308]. Thus, mutp53^{R273H} in PANC-1 cells might constitute a GOF on inflammation, apoptosis or chemoresistance instead of migration.

Since PDAC is a cancer entity with high desmoplastic reaction, the interaction of the tumor microenvironment (predominantly cancer-associated fibroblasts, CAFs) and cancer cells has to be taken into account [309]. Models like patient-derived xenograft and 3D organoid co-cultures harboring different p53 mutations could allow a crosstalk between stromal and cancer cells, mimicking the broad tumor heterogeneity in human PDAC patients [309, 310]. $In\ vivo$ studies and $in\ vitro$ co-cultures with stromal compartments of the tumor microenvironment can help to clarify the impact of different mutants on the composition of the secretome, which might help to better understand this broad heterogeneity.

In the context of tumor microenvironment, tumor associated macrophages have been extensively studied and are suggested to significantly contribute to tumor progression [170, 311]. Cooks $et\ al.$ propose that mutp53 in colorectal cancer cells, promotes increased secretion of miR-1246 containing exosomes [311]. Uptake of these exosomes by macrophages results in a phenotypic shift towards M2

(immunosuppressive, tumor-promoting) contributing to the progression and metastasis of cancer [307, 311].

In sum, the current study investigates the role of different p53 mutants in PDAC, showing that different mutations are differentially stabilized and that only the HSP90-stabilized R248W mutant has a GOF on migration. Again, these data further emphasize the necessity to investigate the role of mutp53 in a mutant variant and context-specific manner. Additionally, it highlights that different mutants of p53 can have different GOFs which might be due to different interaction partners and the formation of hetero TF complexes. However, intensive research is needed to fully understand the underlying GOF mechanism and the clinical potential in cancer entities with inadequate therapeutic approaches, such as PDAC.

4.3 CONCLUSION

In our studies, we aimed to investigated HSP90-stabilized proteins as therapeutic targets in cancer.

We show that mutp53^{R248W} is an important HSP90 client in pancreatic ductal adenocarcinoma driving migration *via* hijacking of pSTAT3 (**Manuscript, section 3.2**). Our data provide first evidence that the mutp53^{R248W} variant is a cancer-relevant HSP90 client in PDAC and that its ablation reduces migration of cancer cells. However, further research is necessary to elaborate on the exact mechanism of action. Additional experimental models could be deployed, to better understand the complexity and the impact of stabilized mutp53 variants in cancer cells on the interaction with other compartments of the tumor bulk (e.g., cancer-associated fibroblasts or immune cells).

Furthermore, our data highlight MIF as a cancer-relevant HSP90 client in colorectal cancer which can serve as target for cancer therapy (**Publication, section 3.1**). These data are in line with different studies suggesting MIF as a potential target in other models for intestinal cancer [111, 149] and other cancer entities [57, 112, 312]. So far, little is known about the exact mechanism leading to the stabilization of MIF through the HSP90 chaperone machinery. The oxidation of MIF might provide an explanation but needs to be further analyzed. Our findings, that MIF is dispensable for normal but not for cancer cells make it an interesting target for cancer therapy. In normal cells,

other pro-inflammatory cytokines might be able take over the function after MIF depletion. In contrast, tumor cells are addicted to tumorigenic function of HSP90-stabilized MIF. Thus, the combination of novel HPS90 inhibitors and anti-MIF or anti-CD74 treatments can provide an opportunity to better disrupt cancer cells.

In this respect, it might also be of interest to investigate whether MIF can serve as potential target in PDAC. Two studies have proven that MIF promotes tumor aggressiveness, metastasis and invasion in PDAC [312, 313]. Thus, elevated MIF levels were also a predictor for worse prognosis for PDAC patients [312, 314]. Especially in a stromal dense cancer entity like PDAC [179], investigating the impact of MIF especially on the regulation and activation of macrophages and their contribution to tumor angiogenesis might be of interest. Therapeutically, it would be interesting to understand if MIF can serve as a cancer-relevant HSP90 client also in PDAC.

To date, none of the tested HSP90 inhibitors have passed clinical validation and achieved FDA approval [14, 91]. Nevertheless, the vast plethora of clients and the specific higher affinity of inhibitors to tumoral Hsp90 make it a preferable target for cancer therapies [21, 68, 79]. Simultaneous inhibition of cancer-relevant HSP90 clients can also help to overcome resistance mechanism [19, 235]. To improve the clinical outcome of HSP90 inhibitors, it is important to investigate possible cancer-relevant HSP90 clients that could help to increase efficacy of these inhibitors. Additionally, a combination treatment of HSP90 inhibitors and compounds against specific biomarkers such as MIF, mutp53 or mutp53-specific hetero TF complexes could be of interest to improve the success of cancer therapy.

5   REFERENCES

1.   National Cancer Institute, *Cancer Statistics*. 2020 [cited 15.12.2020]; Available from: https://www.cancer.gov/about-cancer/understanding/statistics.

2.   Sung H, Ferlay J, Siegel RL, Laversanne M, Soerjomataram I, et al., *Global cancer statistics 2020: GLOBOCAN estimates of incidence and mortality worldwide for 36 cancers in 185 countries.* CA Cancer J Clin, 2021. DOI: 10.3322/caac.21660

3.   *The global challenge of cancer*. Nature Cancer, 2020. **1**, 1-2 DOI: 10.1038/s43018-019-0023-9.

4.   Cagan R and Meyer P, *Rethinking cancer: current challenges and opportunities in cancer research.* Dis Model Mech, 2017. **10**(4): p. 349-352. DOI: 10.1242/dmm.030007

5.   Wong CH, Siah KW, and Lo AW, *Estimation of clinical trial success rates and related parameters.* Biostatistics, 2019. **20**(2): p. 273-286. DOI: 10.1093/biostatistics/kxx069

6.   Dietlein F, Weghorn D, Taylor-Weiner A, Richters A, Reardon B, et al., *Identification of cancer driver genes based on nucleotide context.* Nat Genet, 2020. **52**(2): p. 208-218. DOI: 10.1038/s41588-019-0572-y

7.   Hanahan D and Weinberg RA, *The hallmarks of cancer.* Cell, 2000. **100**(1): p. 57-70. DOI: 10.1016/s0092-8674(00)81683-9

8.   Greenman C, Stephens P, Smith R, Dalgliesh GL, Hunter C, et al., *Patterns of somatic mutation in human cancer genomes.* Nature, 2007. **446**(7132): p. 153-8. DOI: 10.1038/nature05610

9.   Loeb LA, Loeb KR, and Anderson JP, *Multiple mutations and cancer.* Proc Natl Acad Sci U S A, 2003. **100**(3): p. 776-81. DOI: 10.1073/pnas.0334858100

10.   Chakravarthi BV, Nepal S, and Varambally S, *Genomic and Epigenomic Alterations in Cancer.* Am J Pathol, 2016. **186**(7): p. 1724-35. DOI: 10.1016/j.ajpath.2016.02.023

11.   Senft D and Ronai ZA, *Adaptive Stress Responses During Tumor Metastasis and Dormancy.* Trends Cancer, 2016. **2**(8): p. 429-442. DOI: 10.1016/j.trecan.2016.06.004

12.   Xu W, Trepel J, and Neckers L, *Ras, ROS and proteotoxic stress: a delicate balance.* Cancer Cell, 2011. **20**(3): p. 281-2. DOI: 10.1016/j.ccr.2011.08.020

13.   Ruggero D, *Translational control in cancer etiology.* Cold Spring Harb Perspect Biol, 2013. **5**(2). DOI: 10.1101/cshperspect.a012336

14.   Jaeger AM and Whitesell L, *HSP90: Enabler of Cancer Adaptation.* Annual Review of Cancer Biology, 2019. **3**(1): p. 275-297. DOI: 10.1146/annurev-cancerbio-030518-055533

15.   Guang MHZ, Kavanagh EL, Dunne LP, Dowling P, Zhang L, et al., *Targeting Proteotoxic Stress in Cancer: A Review of the Role that Protein Quality Control*

Pathways Play in Oncogenesis. Cancers (Basel), 2019. **11**(1). DOI: 10.3390/cancers11010066

16. Whitesell L and Lindquist SL, *HSP90 and the chaperoning of cancer.* Nat Rev Cancer, 2005. **5**(10): p. 761-72. DOI: 10.1038/nrc1716

17. Miyata Y, Nakamoto H, and Neckers L, *The therapeutic target Hsp90 and cancer hallmarks.* Curr Pharm Des, 2013. **19**(3): p. 347-65. DOI: 10.2174/138161213804143725

18. Acquaviva J, Smith DL, Jimenez JP, Zhang C, Sequeira M, et al., *Overcoming acquired BRAF inhibitor resistance in melanoma via targeted inhibition of Hsp90 with ganetespib.* Mol Cancer Ther, 2014. **13**(2): p. 353-63. DOI: 10.1158/1535-7163.MCT-13-0481

19. Jhaveri K and Modi S, *HSP90 inhibitors for cancer therapy and overcoming drug resistance.* Adv Pharmacol, 2012. **65**: p. 471-517. DOI: 10.1016/B978-0-12-397927-8.00015-4

20. Jhaveri K and Modi S, *Ganetespib: research and clinical development.* Onco Targets Ther, 2015. **8**: p. 1849-58. DOI: 10.2147/OTT.S65804

21. Picard, D., *HSP90 INTERACTORS.* 2021 [cited 31.03.2021]; Available from: https://www.picard.ch/downloads/Hsp90interactors.pdf.

22. Lindquist S and Craig EA, *The heat-shock proteins.* Annu Rev Genet, 1988. **22**: p. 631-77. DOI: 10.1146/annurev.ge.22.120188.003215

23. Taipale M, Jarosz DF, and Lindquist S, *HSP90 at the hub of protein homeostasis: emerging mechanistic insights.* Nat Rev Mol Cell Biol, 2010. **11**(7): p. 515-28. DOI: 10.1038/nrm2918

24. Csermely P, Schnaider T, Soti C, Prohaszka Z, and Nardai G, *The 90-kDa molecular chaperone family: structure, function, and clinical applications. A comprehensive review.* Pharmacol Ther, 1998. **79**(2): p. 129-68. DOI: 10.1016/s0163-7258(98)00013-8

25. Ritossa F, *A new puffing pattern induced by temperature shock and DNP in drosophila.* Experientia, 1962. **18**(12): p. 571-573. DOI: 10.1007/BF02172188

26. Bakthisaran R, Tangirala R, and Rao Ch M, *Small heat shock proteins: Role in cellular functions and pathology.* Biochim Biophys Acta, 2015. **1854**(4): p. 291-319. DOI: 10.1016/j.bbapap.2014.12.019

27. De Maio A, *Heat shock proteins: facts, thoughts, and dreams.* Shock, 1999. **11**(1): p. 1-12. DOI: 10.1097/00024382-199901000-00001

28. Li Z and Srivastava P, *Heat-shock proteins.* Curr Protoc Immunol, 2004. **Appendix 1**: p. Appendix 1T. DOI: 10.1002/0471142735.ima01ts58

29. Li J, Richter K, and Buchner J, *Mixed Hsp90-cochaperone complexes are important for the progression of the reaction cycle.* Nat Struct Mol Biol, 2011. **18**(1): p. 61-6. DOI: 10.1038/nsmb.1965

30. Geller R, Taguwa S, and Frydman J, *Broad action of Hsp90 as a host chaperone required for viral replication.* Biochim Biophys Acta, 2012. **1823**(3): p. 698-706. DOI: 10.1016/j.bbamcr.2011.11.007

31. Picard D, *Heat-shock protein 90, a chaperone for folding and regulation.* Cell Mol Life Sci, 2002. **59**(10): p. 1640-8. DOI: 10.1007/pl00012491

32. Lai BT, Chin NW, Stanek AE, Keh W, and Lanks KW, *Quantitation and intracellular localization of the 85K heat shock protein by using monoclonal and polyclonal antibodies.* Mol Cell Biol, 1984. **4**(12): p. 2802-10. DOI: 10.1128/mcb.4.12.2802

33. Sreedhar AS, Kalmar E, Csermely P, and Shen YF, *Hsp90 isoforms: functions, expression and clinical importance.* FEBS Lett, 2004. **562**(1-3): p. 11-5. DOI: 10.1016/s0014-5793(04)00229-7

34. Perdew GH, Hord N, Hollenback CE, and Welsh MJ, *Localization and characterization of the 86- and 84-kDa heat shock proteins in Hepa 1c1c7 cells.* Exp Cell Res, 1993. **209**(2): p. 350-6. DOI: 10.1006/excr.1993.1320

35. Richter K, Muschler P, Hainzl O, and Buchner J, *Coordinated ATP hydrolysis by the Hsp90 dimer.* J Biol Chem, 2001. **276**(36): p. 33689-96. DOI: 10.1074/jbc.M103832200

36. Wayne N and Bolon DN, *Dimerization of Hsp90 is required for in vivo function. Design and analysis of monomers and dimers.* J Biol Chem, 2007. **282**(48): p. 35386-95. DOI: 10.1074/jbc.M703844200

37. Nemoto T, Ohara-Nemoto Y, Ota M, Takagi T, and Yokoyama K, *Mechanism of dimer formation of the 90-kDa heat-shock protein.* Eur J Biochem, 1995. **233**(1): p. 1-8. DOI: 10.1111/j.1432-1033.1995.001_1.x

38. Schopf FH, Biebl MM, and Buchner J, *The HSP90 chaperone machinery.* Nat Rev Mol Cell Biol, 2017. **18**(6): p. 345-360. DOI: 10.1038/nrm.2017.20

39. Li J, Soroka J, and Buchner J, *The Hsp90 chaperone machinery: conformational dynamics and regulation by co-chaperones.* Biochim Biophys Acta, 2012. **1823**(3): p. 624-35. DOI: 10.1016/j.bbamcr.2011.09.003

40. Hernandez MP, Chadli A, and Toft DO, *HSP40 binding is the first step in the HSP90 chaperoning pathway for the progesterone receptor.* J Biol Chem, 2002. **277**(14): p. 11873-81. DOI: 10.1074/jbc.M111445200

41. Johnson BD, Schumacher RJ, Ross ED, and Toft DO, *Hop modulates Hsp70/Hsp90 interactions in protein folding.* J Biol Chem, 1998. **273**(6): p. 3679-86. DOI: 10.1074/jbc.273.6.3679

42. Hoter A, El-Sabban ME, and Naim HY, *The HSP90 Family: Structure, Regulation, Function, and Implications in Health and Disease.* Int J Mol Sci, 2018. **19**(9). DOI: 10.3390/ijms19092560

43. Wang H, Tan MS, Lu RC, Yu JT, and Tan L, *Heat shock proteins at the crossroads between cancer and Alzheimer's disease.* Biomed Res Int, 2014. **2014**: p. 239164. DOI: 10.1155/2014/239164

44. Lanneau D, Wettstein G, Bonniaud P, and Garrido C, *Heat shock proteins: cell protection through protein triage.* ScientificWorldJournal, 2010. **10**: p. 1543-52. DOI: 10.1100/tsw.2010.152

45. Zuehlke A and Johnson JL, *Hsp90 and co-chaperones twist the functions of diverse client proteins.* Biopolymers, 2010. **93**(3): p. 211-7. DOI: 10.1002/bip.21292

46. Scroggins BT, Robzyk K, Wang D, Marcu MG, Tsutsumi S, et al., *An acetylation site in the middle domain of Hsp90 regulates chaperone function.* Mol Cell, 2007. **25**(1): p. 151-9. DOI: 10.1016/j.molcel.2006.12.008

47. Riggs DL, Cox MB, Cheung-Flynn J, Prapapanich V, Carrigan PE, et al., *Functional specificity of co-chaperone interactions with Hsp90 client proteins.* Crit Rev Biochem Mol Biol, 2004. **39**(5-6): p. 279-95. DOI: 10.1080/10409230490892513

48. Sahasrabudhe P, Rohrberg J, Biebl MM, Rutz DA, and Buchner J, *The Plasticity of the Hsp90 Co-chaperone System.* Mol Cell, 2017. **67**(6): p. 947-961 e5. DOI: 10.1016/j.molcel.2017.08.004

49. Akerfelt M, Morimoto RI, and Sistonen L, *Heat shock factors: integrators of cell stress, development and lifespan.* Nat Rev Mol Cell Biol, 2010. **11**(8): p. 545-55. DOI: 10.1038/nrm2938

50. Prodromou C, *Mechanisms of Hsp90 regulation.* Biochem J, 2016. **473**(16): p. 2439-52. DOI: 10.1042/BCJ20160005

51. Vabulas RM, Raychaudhuri S, Hayer-Hartl M, and Hartl FU, *Protein folding in the cytoplasm and the heat shock response.* Cold Spring Harb Perspect Biol, 2010. **2**(12): p. a004390. DOI: 10.1101/cshperspect.a004390

52. Neef DW, Jaeger AM, Gomez-Pastor R, Willmund F, Frydman J, et al., *A direct regulatory interaction between chaperonin TRiC and stress-responsive transcription factor HSF1.* Cell Rep, 2014. **9**(3): p. 955-66. DOI: 10.1016/j.celrep.2014.09.056

53. Zou J, Guo Y, Guettouche T, Smith DF, and Voellmy R, *Repression of heat shock transcription factor HSF1 activation by HSP90 (HSP90 complex) that forms a stress-sensitive complex with HSF1.* Cell, 1998. **94**(4): p. 471-80. DOI: 10.1016/s0092-8674(00)81588-3

54. Gomez-Pastor R, Burchfiel ET, and Thiele DJ, *Regulation of heat shock transcription factors and their roles in physiology and disease.* Nat Rev Mol Cell Biol, 2018. **19**(1): p. 4-19. DOI: 10.1038/nrm.2017.73

55. Luo W, Sun W, Taldone T, Rodina A, and Chiosis G, *Heat shock protein 90 in neurodegenerative diseases.* Mol Neurodegener, 2010. **5**: p. 24. DOI: 10.1186/1750-1326-5-24

56. Schulz-Heddergott R, Stark N, Edmunds SJ, Li J, Conradi LC, et al., *Therapeutic Ablation of Gain-of-Function Mutant p53 in Colorectal Cancer Inhibits Stat3-Mediated Tumor Growth and Invasion.* Cancer Cell, 2018. **34**(2): p. 298-314 e7. DOI: 10.1016/j.ccell.2018.07.004

57. Schulz R, Marchenko ND, Holembowski L, Fingerle-Rowson G, Pesic M, et al., *Inhibiting the HSP90 chaperone destabilizes macrophage migration inhibitory factor and thereby inhibits breast tumor progression.* J Exp Med, 2012. **209**(2): p. 275-89. DOI: 10.1084/jem.20111117

58. McDowell CL, Bryan Sutton R, and Obermann WM, *Expression of Hsp90 chaperone [corrected] proteins in human tumor tissue.* Int J Biol Macromol, 2009. **45**(3): p. 310-4. DOI: 10.1016/j.ijbiomac.2009.06.012

59. Pick E, Kluger Y, Giltnane JM, Moeder C, Camp RL, et al., *High HSP90 expression is associated with decreased survival in breast cancer.* Cancer Res, 2007. **67**(7): p. 2932-7. DOI: 10.1158/0008-5472.CAN-06-4511

60.   Yano M, Naito Z, Tanaka S, and Asano G, *Expression and roles of heat shock proteins in human breast cancer.* Jpn J Cancer Res, 1996. **87**(9): p. 908-15. DOI: 10.1111/j.1349-7006.1996.tb02119.x

61.   Zhang S, Guo S, Li Z, Li D, and Zhan Q, *High expression of HSP90 is associated with poor prognosis in patients with colorectal cancer.* PeerJ, 2019. **7**: p. e7946. DOI: 10.7717/peerj.7946

62.   Kim K, Lee HW, Lee EH, Park MI, Lee JS, et al., *Differential expression of HSP90 isoforms and their correlations with clinicopathologic factors in patients with colorectal cancer.* Int J Clin Exp Pathol, 2019. **12**(3): p. 978-986.

63.   Gress TM, Muller-Pillasch F, Weber C, Lerch MM, Friess H, et al., *Differential expression of heat shock proteins in pancreatic carcinoma.* Cancer Res, 1994. **54**(2): p. 547-51.

64.   Ogata M, Naito Z, Tanaka S, Moriyama Y, and Asano G, *Overexpression and localization of heat shock proteins mRNA in pancreatic carcinoma.* J Nippon Med Sch, 2000. **67**(3): p. 177-85. DOI: 10.1272/jnms.67.177

65.   Walczak A, Gradzik K, Kabzinski J, Przybylowska-Sygut K, and Majsterek I, *The Role of the ER-Induced UPR Pathway and the Efficacy of Its Inhibitors and Inducers in the Inhibition of Tumor Progression.* Oxid Med Cell Longev, 2019. **2019**: p. 5729710. DOI: 10.1155/2019/5729710

66.   Takayama S, Reed JC, and Homma S, *Heat-shock proteins as regulators of apoptosis.* Oncogene, 2003. **22**(56): p. 9041-7. DOI: 10.1038/sj.onc.1207114

67.   Seo YH, *Small Molecule Inhibitors to Disrupt Protein-protein Interactions of Heat Shock Protein 90 Chaperone Machinery.* J Cancer Prev, 2015. **20**(1): p. 5-11. DOI: 10.15430/JCP.2015.20.1.5

68.   Workman P, *Altered states: selectively drugging the Hsp90 cancer chaperone.* Trends Mol Med, 2004. **10**(2): p. 47-51. DOI: 10.1016/j.molmed.2003.12.005

69.   Kamal A, Boehm MF, and Burrows FJ, *Therapeutic and diagnostic implications of Hsp90 activation.* Trends Mol Med, 2004. **10**(6): p. 283-90. DOI: 10.1016/j.molmed.2004.04.006

70.   Dai C, *The heat-shock, or HSF1-mediated proteotoxic stress, response in cancer: from proteomic stability to oncogenesis.* Philos Trans R Soc Lond B Biol Sci, 2018. **373**(1738). DOI: 10.1098/rstb.2016.0525

71.   Kamal A, Thao L, Sensintaffar J, Zhang L, Boehm MF, et al., *A high-affinity conformation of Hsp90 confers tumour selectivity on Hsp90 inhibitors.* Nature, 2003. **425**(6956): p. 407-10. DOI: 10.1038/nature01913

72.   Mahalingam D, Swords R, Carew JS, Nawrocki ST, Bhalla K, et al., *Targeting HSP90 for cancer therapy.* Br J Cancer, 2009. **100**(10): p. 1523-9. DOI: 10.1038/sj.bjc.6605066

73.   Hanahan D and Weinberg RA, *Hallmarks of cancer: the next generation.* Cell, 2011. **144**(5): p. 646-74. DOI: 10.1016/j.cell.2011.02.013

74.   Vahid S, Thaper D, and Zoubeidi A, *Chaperoning the Cancer: The Proteostatic Functions of the Heat Shock Proteins in Cancer.* Recent Pat Anticancer Drug Discov, 2017. **12**(1): p. 35-47. DOI: 10.2174/1574892811666161102125252

75. Trepel J, Mollapour M, Giaccone G, and Neckers L, *Targeting the dynamic HSP90 complex in cancer.* Nat Rev Cancer, 2010. **10**(8): p. 537-49. DOI: 10.1038/nrc2887

76. Schulz R, Streller F, Scheel AH, Ruschoff J, Reinert MC, et al., *HER2/ErbB2 activates HSF1 and thereby controls HSP90 clients including MIF in HER2-overexpressing breast cancer.* Cell Death Dis, 2014. **5**: p. e980. DOI: 10.1038/cddis.2013.508

77. Mimnaugh EG, Chavany C, and Neckers L, *Polyubiquitination and proteasomal degradation of the p185c-erbB-2 receptor protein-tyrosine kinase induced by geldanamycin.* J Biol Chem, 1996. **271**(37): p. 22796-801. DOI: 10.1074/jbc.271.37.22796

78. He S, Zhang C, Shafi AA, Sequeira M, Acquaviva J, et al., *Potent activity of the Hsp90 inhibitor ganetespib in prostate cancer cells irrespective of androgen receptor status or variant receptor expression.* Int J Oncol, 2013. **42**(1): p. 35-43. DOI: 10.3892/ijo.2012.1698

79. Neckers L and Lee YS, *Cancer: the rules of attraction.* Nature, 2003. **425**(6956): p. 357-9. DOI: 10.1038/425357a

80. Schulz R and Moll UM, *Targeting the heat shock protein 90: a rational way to inhibit macrophage migration inhibitory factor function in cancer.* Curr Opin Oncol, 2014. **26**(1): p. 108-13. DOI: 10.1097/CCO.0000000000000036

81. Kim YS, Alarcon SV, Lee S, Lee MJ, Giaccone G, et al., *Update on Hsp90 inhibitors in clinical trial.* Curr Top Med Chem, 2009. **9**(15): p. 1479-92. DOI: 10.2174/156802609789895728

82. Jhaveri K, Ochiana SO, Dunphy MP, Gerecitano JF, Corben AD, et al., *Heat shock protein 90 inhibitors in the treatment of cancer: current status and future directions.* Expert Opin Investig Drugs, 2014. **23**(5): p. 611-28. DOI: 10.1517/13543784.2014.902442

83. Parimi S and Tsang RY, *Hsp90 inhibitors in oncology: ready for prime time?* Curr Oncol, 2014. **21**(5): p. e663-7. DOI: 10.3747/co.21.2163

84. Do K, Speranza G, Chang LC, Polley EC, Bishop R, et al., *Phase I study of the heat shock protein 90 (Hsp90) inhibitor onalespib (AT13387) administered on a daily for 2 consecutive days per week dosing schedule in patients with advanced solid tumors.* Invest New Drugs, 2015. **33**(4): p. 921-30. DOI: 10.1007/s10637-015-0255-1

85. Alexandrova EM, Yallowitz AR, Li D, Xu S, Schulz R, et al., *Improving survival by exploiting tumour dependence on stabilized mutant p53 for treatment.* Nature, 2015. **523**(7560): p. 352-6. DOI: 10.1038/nature14430

86. Shimamura T, Perera SA, Foley KP, Sang J, Rodig SJ, et al., *Ganetespib (STA-9090), a nongeldanamycin HSP90 inhibitor, has potent antitumor activity in in vitro and in vivo models of non-small cell lung cancer.* Clin Cancer Res, 2012. **18**(18): p. 4973-85. DOI: 10.1158/1078-0432.CCR-11-2967

87. Graham B, Curry J, Smyth T, Fazal L, Feltell R, et al., *The heat shock protein 90 inhibitor, AT13387, displays a long duration of action in vitro and in vivo in non-small cell lung cancer.* Cancer Sci, 2012. **103**(3): p. 522-7. DOI: 10.1111/j.1349-7006.2011.02191.x

88.   Lee H, Saini N, Howard EW, Parris AB, Ma Z, et al., *Ganetespib targets multiple levels of the receptor tyrosine kinase signaling cascade and preferentially inhibits ErbB2-overexpressing breast cancer cells.* Sci Rep, 2018. **8**(1): p. 6829. DOI: 10.1038/s41598-018-25284-0

89.   Kryeziu K, Bruun J, Guren TK, Sveen A, and Lothe RA, *Combination therapies with HSP90 inhibitors against colorectal cancer.* Biochim Biophys Acta Rev Cancer, 2019. **1871**(2): p. 240-247. DOI: 10.1016/j.bbcan.2019.01.002

90.   He S, Smith DL, Sequeira M, Sang J, Bates RC, et al., *The HSP90 inhibitor ganetespib has chemosensitizer and radiosensitizer activity in colorectal cancer.* Invest New Drugs, 2014. **32**(4): p. 577-86. DOI: 10.1007/s10637-014-0095-4

91.   Park HK, Yoon NG, Lee JE, Hu S, Yoon S, et al., *Unleashing the full potential of Hsp90 inhibitors as cancer therapeutics through simultaneous inactivation of Hsp90, Grp94, and TRAP1.* Exp Mol Med, 2020. **52**(1): p. 79-91. DOI: 10.1038/s12276-019-0360-x

92.   Eskew JD, Sadikot T, Morales P, Duren A, Dunwiddie I, et al., *Development and characterization of a novel C-terminal inhibitor of Hsp90 in androgen dependent and independent prostate cancer cells.* BMC Cancer, 2011. **11**: p. 468. DOI: 10.1186/1471-2407-11-468

93.   Butler LM, Ferraldeschi R, Armstrong HK, Centenera MM, and Workman P, *Maximizing the Therapeutic Potential of HSP90 Inhibitors.* Mol Cancer Res, 2015. **13**(11): p. 1445-51. DOI: 10.1158/1541-7786.MCR-15-0234

94.   Neckers L, Blagg B, Haystead T, Trepel JB, Whitesell L, et al., *Methods to validate Hsp90 inhibitor specificity, to identify off-target effects, and to rethink approaches for further clinical development.* Cell Stress Chaperones, 2018. **23**(4): p. 467-482. DOI: 10.1007/s12192-018-0877-2

95.   Bickel D and Gohlke H, *C-terminal modulators of heat shock protein of 90kDa (HSP90): State of development and modes of action.* Bioorg Med Chem, 2019. **27**(21): p. 115080. DOI: 10.1016/j.bmc.2019.115080

96.   Marmol I, Sanchez-de-Diego C, Pradilla Dieste A, Cerrada E, and Rodriguez Yoldi MJ, *Colorectal Carcinoma: A General Overview and Future Perspectives in Colorectal Cancer.* Int J Mol Sci, 2017. **18**(1). DOI: 10.3390/ijms18010197

97.   Ferlay J, Colombet M, Soerjomataram I, Mathers C, Parkin DM, et al., *Estimating the global cancer incidence and mortality in 2018: GLOBOCAN sources and methods.* Int J Cancer, 2019. **144**(8): p. 1941-1953. DOI: 10.1002/ijc.31937

98.   Bray F, Ferlay J, Soerjomataram I, Siegel RL, Torre LA, et al., *Global cancer statistics 2018: GLOBOCAN estimates of incidence and mortality worldwide for 36 cancers in 185 countries.* CA Cancer J Clin, 2018. **68**(6): p. 394-424. DOI: 10.3322/caac.21492

99.   Bosman FT, *Chapter 5.5: Colorectal Cancer*, in *World Cancer Report 2014*, B.W.W.C.P. Steward, Editor. 2014, International Agency for Research on Cancer, World Health Organization. p. 392 ff. ISBN: 978-92-832-0443-5

100.   Vogelstein B, Fearon ER, Hamilton SR, Kern SE, Preisinger AC, et al., *Genetic alterations during colorectal-tumor development.* N Engl J Med, 1988. **319**(9): p. 525-32. DOI: 10.1056/NEJM198809013190901

101. Fearon ER and Vogelstein B, *A genetic model for colorectal tumorigenesis.* Cell, 1990. **61**(5): p. 759-67. DOI: 10.1016/0092-8674(90)90186-i

102. Xie J and Itzkowitz SH, *Cancer in inflammatory bowel disease.* World J Gastroenterol, 2008. **14**(3): p. 378-89. DOI: 10.3748/wjg.14.378

103. Tanaka T, Kohno H, Suzuki R, Yamada Y, Sugie S, et al., *A novel inflammation-related mouse colon carcinogenesis model induced by azoxymethane and dextran sodium sulfate.* Cancer Sci, 2003. **94**(11): p. 965-73. DOI: 10.1111/j.1349-7006.2003.tb01386.x

104. Rosenberg DW, Giardina C, and Tanaka T, *Mouse models for the study of colon carcinogenesis.* Carcinogenesis, 2009. **30**(2): p. 183-96. DOI: 10.1093/carcin/bgn267

105. De Robertis M, Massi E, Poeta ML, Carotti S, Morini S, et al., *The AOM/DSS murine model for the study of colon carcinogenesis: From pathways to diagnosis and therapy studies.* J Carcinog, 2011. **10**: p. 9. DOI: 10.4103/1477-3163.78279

106. Chassaing B, Aitken JD, Malleshappa M, and Vijay-Kumar M, *Dextran sulfate sodium (DSS)-induced colitis in mice.* Curr Protoc Immunol, 2014. **104**: p. 15 25 1-15 25 14. DOI: 10.1002/0471142735.im1525s104

107. Kuipers EJ, Grady WM, Lieberman D, Seufferlein T, Sung JJ, et al., *Colorectal cancer.* Nat Rev Dis Primers, 2015. **1**: p. 15065. DOI: 10.1038/nrdp.2015.65

108. Walter FM, Emery JD, Mendonca S, Hall N, Morris HC, et al., *Symptoms and patient factors associated with longer time to diagnosis for colorectal cancer: results from a prospective cohort study.* Br J Cancer, 2016. **115**(5): p. 533-41. DOI: 10.1038/bjc.2016.221

109. Xu X, Wang B, Ye C, Yao C, Lin Y, et al., *Overexpression of macrophage migration inhibitory factor induces angiogenesis in human breast cancer.* Cancer Lett, 2008. **261**(2): p. 147-57. DOI: 10.1016/j.canlet.2007.11.028

110. Meyer-Siegler K and Hudson PB, *Enhanced expression of macrophage migration inhibitory factor in prostatic adenocarcinoma metastases.* Urology, 1996. **48**(3): p. 448-52. DOI: 10.1016/S0090-4295(96)00207-5

111. He XX, Chen K, Yang J, Li XY, Gan HY, et al., *Macrophage migration inhibitory factor promotes colorectal cancer.* Mol Med, 2009. **15**(1-2): p. 1-10. DOI: 10.2119/molmed.2008.00107

112. Hira E, Ono T, Dhar DK, El-Assal ON, Hishikawa Y, et al., *Overexpression of macrophage migration inhibitory factor induces angiogenesis and deteriorates prognosis after radical resection for hepatocellular carcinoma.* Cancer, 2005. **103**(3): p. 588-98. DOI: 10.1002/cncr.20818

113. Calandra T and Roger T, *Macrophage migration inhibitory factor: a regulator of innate immunity.* Nat Rev Immunol, 2003. **3**(10): p. 791-800. DOI: 10.1038/nri1200

114. Roger T, David J, Glauser MP, and Calandra T, *MIF regulates innate immune responses through modulation of Toll-like receptor 4.* Nature, 2001. **414**(6866): p. 920-4. DOI: 10.1038/414920a

115. Nishihira J, *Macrophage migration inhibitory factor (MIF): its essential role in the immune system and cell growth.* J Interferon Cytokine Res, 2000. **20**(9): p. 751-62. DOI: 10.1089/10799900050151012

116. David JR, *Delayed hypersensitivity in vitro: its mediation by cell-free substances formed by lymphoid cell-antigen interaction.* Proc Natl Acad Sci U S A, 1966. **56**(1): p. 72-7. DOI: 10.1073/pnas.56.1.72

117. Calandra T, Bernhagen J, Mitchell RA, and Bucala R, *The macrophage is an important and previously unrecognized source of macrophage migration inhibitory factor.* J Exp Med, 1994. **179**(6): p. 1895-902. DOI: 10.1084/jem.179.6.1895

118. Bloom BR and Shevach E, *Requirement for T cells in the production of migration inhibitory factor.* J Exp Med, 1975. **142**(5): p. 1306-11. DOI: 10.1084/jem.142.5.1306

119. Suzuki M, Sugimoto H, Nakagawa A, Tanaka I, Nishihira J, et al., *Crystal structure of the macrophage migration inhibitory factor from rat liver.* Nat Struct Biol, 1996. **3**(3): p. 259-66. DOI: 10.1038/nsb0396-259

120. Sun HW, Bernhagen J, Bucala R, and Lolis E, *Crystal structure at 2.6-A resolution of human macrophage migration inhibitory factor.* Proc Natl Acad Sci U S A, 1996. **93**(11): p. 5191-6. DOI: 10.1073/pnas.93.11.5191

121. Rosengren E, Bucala R, Aman P, Jacobsson L, Odh G, et al., *The immunoregulatory mediator macrophage migration inhibitory factor (MIF) catalyzes a tautomerization reaction.* Mol Med, 1996. **2**(1): p. 143-9.

122. Morand EF, Leech M, and Bernhagen J, *MIF: a new cytokine link between rheumatoid arthritis and atherosclerosis.* Nat Rev Drug Discov, 2006. **5**(5): p. 399-410. DOI: 10.1038/nrd2029

123. Asare Y, Schmitt M, and Bernhagen J, *The vascular biology of macrophage migration inhibitory factor (MIF). Expression and effects in inflammation, atherogenesis and angiogenesis.* Thromb Haemost, 2013. **109**(3): p. 391-8. DOI: 10.1160/TH12-11-0831

124. Zernecke A, Bernhagen J, and Weber C, *Macrophage migration inhibitory factor in cardiovascular disease.* Circulation, 2008. **117**(12): p. 1594-602. DOI: 10.1161/CIRCULATIONAHA.107.729125

125. Petralia MC, Battaglia G, Bruno V, Pennisi M, Mangano K, et al., *The Role of Macrophage Migration Inhibitory Factor in Alzheimer's Disease: Conventionally Pathogenetic or Unconventionally Protective?* Molecules, 2020. **25**(2). DOI: 10.3390/molecules25020291

126. Florez-Sampedro L, Soto-Gamez A, Poelarends GJ, and Melgert BN, *The role of MIF in chronic lung diseases: looking beyond inflammation.* Am J Physiol Lung Cell Mol Physiol, 2020. **318**(6): p. L1183-L1197. DOI: 10.1152/ajplung.00521.2019

127. Leng L, Metz CN, Fang Y, Xu J, Donnelly S, et al., *MIF signal transduction initiated by binding to CD74.* J Exp Med, 2003. **197**(11): p. 1467-76. DOI: 10.1084/jem.20030286

128. Bernhagen J, Krohn R, Lue H, Gregory JL, Zernecke A, et al., *MIF is a noncognate ligand of CXC chemokine receptors in inflammatory and*

atherogenic cell recruitment. Nat Med, 2007. **13**(5): p. 587-96. DOI: 10.1038/nm1567

129. Alampour-Rajabi S, El Bounkari O, Rot A, Muller-Newen G, Bachelerie F, et al., *MIF interacts with CXCR7 to promote receptor internalization, ERK1/2 and ZAP-70 signaling, and lymphocyte chemotaxis.* FASEB J, 2015. **29**(11): p. 4497-511. DOI: 10.1096/fj.15-273904

130. Jankauskas SS, Wong DWL, Bucala R, Djudjaj S, and Boor P, *Evolving complexity of MIF signaling.* Cell Signal, 2019. **57**: p. 76-88. DOI: 10.1016/j.cellsig.2019.01.006

131. Xie L, Qiao X, Wu Y, and Tang J, *beta-Arrestin1 mediates the endocytosis and functions of macrophage migration inhibitory factor.* PLoS One, 2011. **6**(1): p. e16428. DOI: 10.1371/journal.pone.0016428

132. Schwartz V, Kruttgen A, Weis J, Weber C, Ostendorf T, et al., *Role for CD74 and CXCR4 in clathrin-dependent endocytosis of the cytokine MIF.* Eur J Cell Biol, 2012. **91**(6-7): p. 435-49. DOI: 10.1016/j.ejcb.2011.08.006

133. Tillmann S, Bernhagen J, and Noels H, *Arrest Functions of the MIF Ligand/Receptor Axes in Atherogenesis.* Front Immunol, 2013. **4**: p. 115. DOI: 10.3389/fimmu.2013.00115

134. Shi X, Leng L, Wang T, Wang W, Du X, et al., *CD44 is the signaling component of the macrophage migration inhibitory factor-CD74 receptor complex.* Immunity, 2006. **25**(4): p. 595-606. DOI: 10.1016/j.immuni.2006.08.020

135. Sampey AV, Hall PH, Mitchell RA, Metz CN, and Morand EF, *Regulation of synoviocyte phospholipase A2 and cyclooxygenase 2 by macrophage migration inhibitory factor.* Arthritis Rheum, 2001. **44**(6): p. 1273-80. DOI: 10.1002/1529-0131(200106)44:6<1273::AID-ART219>3.0.CO;2-8

136. Mitchell RA, Metz CN, Peng T, and Bucala R, *Sustained mitogen-activated protein kinase (MAPK) and cytoplasmic phospholipase A2 activation by macrophage migration inhibitory factor (MIF). Regulatory role in cell proliferation and glucocorticoid action.* J Biol Chem, 1999. **274**(25): p. 18100-6. DOI: 10.1074/jbc.274.25.18100

137. Lang T, Foote A, Lee JP, Morand EF, and Harris J, *MIF: Implications in the Pathoetiology of Systemic Lupus Erythematosus.* Front Immunol, 2015. **6**: p. 577. DOI: 10.3389/fimmu.2015.00577

138. Mitchell RA, Liao H, Chesney J, Fingerle-Rowson G, Baugh J, et al., *Macrophage migration inhibitory factor (MIF) sustains macrophage proinflammatory function by inhibiting p53: regulatory role in the innate immune response.* Proc Natl Acad Sci U S A, 2002. **99**(1): p. 345-50. DOI: 10.1073/pnas.012511599

139. Kleemann R, Hausser A, Geiger G, Mischke R, Burger-Kentischer A, et al., *Intracellular action of the cytokine MIF to modulate AP-1 activity and the cell cycle through Jab1.* Nature, 2000. **408**(6809): p. 211-6. DOI: 10.1038/35041591

140. Bucala R, *Signal transduction. A most interesting factor.* Nature, 2000. **408**(6809): p. 146-7. DOI: 10.1038/35041654

141. Claret FX, Hibi M, Dhut S, Toda T, and Karin M, *A new group of conserved coactivators that increase the specificity of AP-1 transcription factors.* Nature, 1996. **383**(6599): p. 453-7. DOI: 10.1038/383453a0

142. Tomoda K, Kubota Y, and Kato J, *Degradation of the cyclin-dependent-kinase inhibitor p27Kip1 is instigated by Jab1.* Nature, 1999. **398**(6723): p. 160-5. DOI: 10.1038/18230

143. Tomoda K, Yoneda-Kato N, Fukumoto A, Yamanaka S, and Kato JY, *Multiple functions of Jab1 are required for early embryonic development and growth potential in mice.* J Biol Chem, 2004. **279**(41): p. 43013-8. DOI: 10.1074/jbc.M406559200

144. Fan H, Kao W, Yang YH, Gu R, Harris J, et al., *Macrophage migration inhibitory factor inhibits the antiinflammatory effects of glucocorticoids via glucocorticoid-induced leucine zipper.* Arthritis Rheumatol, 2014. **66**(8): p. 2059-70. DOI: 10.1002/art.38689

145. Bucala R and Donnelly SC, *Macrophage migration inhibitory factor: a probable link between inflammation and cancer.* Immunity, 2007. **26**(3): p. 281-5. DOI: 10.1016/j.immuni.2007.03.005

146. Conroy H, Mawhinney L, and Donnelly SC, *Inflammation and cancer: macrophage migration inhibitory factor (MIF)--the potential missing link.* QJM, 2010. **103**(11): p. 831-6. DOI: 10.1093/qjmed/hcq148

147. Meyer-Siegler KL, Bellino MA, and Tannenbaum M, *Macrophage migration inhibitory factor evaluation compared with prostate specific antigen as a biomarker in patients with prostate carcinoma.* Cancer, 2002. **94**(5): p. 1449-56. DOI: 10.1002/cncr.10354

148. Morris KT, Nofchissey RA, Pinchuk IV, and Beswick EJ, *Chronic macrophage migration inhibitory factor exposure induces mesenchymal epithelial transition and promotes gastric and colon cancers.* PLoS One, 2014. **9**(6): p. e98656. DOI: 10.1371/journal.pone.0098656

149. Wilson JM, Coletta PL, Cuthbert RJ, Scott N, MacLennan K, et al., *Macrophage migration inhibitory factor promotes intestinal tumorigenesis.* Gastroenterology, 2005. **129**(5): p. 1485-503. DOI: 10.1053/j.gastro.2005.07.061

150. Sun B, Nishihira J, Suzuki M, Fukushima N, Ishibashi T, et al., *Induction of macrophage migration inhibitory factor by lysophosphatidic acid: relevance to tumor growth and angiogenesis.* Int J Mol Med, 2003. **12**(4): p. 633-41.

151. Ogawa H, Nishihira J, Sato Y, Kondo M, Takahashi N, et al., *An antibody for macrophage migration inhibitory factor suppresses tumour growth and inhibits tumour-associated angiogenesis.* Cytokine, 2000. **12**(4): p. 309-14. DOI: 10.1006/cyto.1999.0562

152. Nalbantoglu I, Blanc V, and Davidson NO, *Characterization of Colorectal Cancer Development in Apc (min/+) Mice.* Methods Mol Biol, 2016. **1422**: p. 309-27. DOI: 10.1007/978-1-4939-3603-8_27

153. Skinner HD, Zheng JZ, Fang J, Agani F, and Jiang BH, *Vascular endothelial growth factor transcriptional activation is mediated by hypoxia-inducible factor 1alpha, HDM2, and p70S6K1 in response to phosphatidylinositol 3-kinase/AKT signaling.* J Biol Chem, 2004. **279**(44): p. 45643-51. DOI: 10.1074/jbc.M404097200

154. Triner D and Shah YM, *Hypoxia-inducible factors: a central link between inflammation and cancer.* J Clin Invest, 2016. **126**(10): p. 3689-3698. DOI: 10.1172/JCI84430

155. Shachar I, Cohen S, Marom A, and Becker-Herman S, *Regulation of CLL survival by hypoxia-inducible factor and its target genes.* FEBS Lett, 2012. **586**(18): p. 2906-10. DOI: 10.1016/j.febslet.2012.07.016

156. Zhu G, Tang Y, Geng N, Zheng M, Jiang J, et al., *HIF-alpha/MIF and NF-kappaB/IL-6 axes contribute to the recruitment of CD11b+Gr-1+ myeloid cells in hypoxic microenvironment of HNSCC.* Neoplasia, 2014. **16**(2): p. 168-79. DOI: 10.1593/neo.132034

157. Bozzi F, Mogavero A, Varinelli L, Belfiore A, Manenti G, et al., *MIF/CD74 axis is a target for novel therapies in colon carcinomatosis.* J Exp Clin Cancer Res, 2017. **36**(1): p. 16. DOI: 10.1186/s13046-016-0475-z

158. Lee CY, Su MJ, Huang CY, Chen MY, Hsu HC, et al., *Macrophage migration inhibitory factor increases cell motility and up-regulates alphavbeta3 integrin in human chondrosarcoma cells.* J Cell Biochem, 2012. **113**(5): p. 1590-8. DOI: 10.1002/jcb.24027

159. O'Reilly C, Doroudian M, Mawhinney L, and Donnelly SC, *Targeting MIF in Cancer: Therapeutic Strategies, Current Developments, and Future Opportunities.* Med Res Rev, 2016. **36**(3): p. 440-60. DOI: 10.1002/med.21385

160. Lue H, Thiele M, Franz J, Dahl E, Speckgens S, et al., *Macrophage migration inhibitory factor (MIF) promotes cell survival by activation of the Akt pathway and role for CSN5/JAB1 in the control of autocrine MIF activity.* Oncogene, 2007. **26**(35): p. 5046-59. DOI: 10.1038/sj.onc.1210318

161. Noe JT and Mitchell RA, *MIF-Dependent Control of Tumor Immunity.* Front Immunol, 2020. **11**: p. 609948. DOI: 10.3389/fimmu.2020.609948

162. Gordon-Weeks AN, Lim SY, Yuzhalin AE, Jones K, and Muschel R, *Macrophage migration inhibitory factor: a key cytokine and therapeutic target in colon cancer.* Cytokine Growth Factor Rev, 2015. **26**(4): p. 451-61. DOI: 10.1016/j.cytogfr.2015.03.002

163. Sang N, Stiehl DP, Bohensky J, Leshchinsky I, Srinivas V, et al., *MAPK signaling up-regulates the activity of hypoxia-inducible factors by its effects on p300.* J Biol Chem, 2003. **278**(16): p. 14013-9. DOI: 10.1074/jbc.M209702200

164. Oda S, Oda T, Nishi K, Takabuchi S, Wakamatsu T, et al., *Macrophage migration inhibitory factor activates hypoxia-inducible factor in a p53-dependent manner.* PLoS One, 2008. **3**(5): p. e2215. DOI: 10.1371/journal.pone.0002215

165. Swamy MV, Herzog CR, and Rao CV, *Inhibition of COX-2 in colon cancer cell lines by celecoxib increases the nuclear localization of active p53.* Cancer Res, 2003. **63**(17): p. 5239-42.

166. Choi EM, Kim SR, Lee EJ, and Han JA, *Cyclooxygenase-2 functionally inactivates p53 through a physical interaction with p53.* Biochim Biophys Acta, 2009. **1793**(8): p. 1354-65. DOI: 10.1016/j.bbamcr.2009.05.006

167. Yaddanapudi K, Putty K, Rendon BE, Lamont GJ, Faughn JD, et al., *Control of tumor-associated macrophage alternative activation by macrophage migration*

inhibitory factor. J Immunol, 2013. **190**(6): p. 2984-93. DOI: 10.4049/jimmunol.1201650

168. Mitchell RA and Yaddanapudi K, *Stromal-dependent tumor promotion by MIF family members.* Cell Signal, 2014. **26**(12): p. 2969-78. DOI: 10.1016/j.cellsig.2014.09.012

169. Owen JL and Mohamadzadeh M, *Macrophages and chemokines as mediators of angiogenesis.* Front Physiol, 2013. **4**: p. 159. DOI: 10.3389/fphys.2013.00159

170. Erreni M, Mantovani A, and Allavena P, *Tumor-associated Macrophages (TAM) and Inflammation in Colorectal Cancer.* Cancer Microenviron, 2011. **4**(2): p. 141-54. DOI: 10.1007/s12307-010-0052-5

171. Russo R, Matrone N, Belli V, Ciardiello D, Valletta M, et al., *Macrophage Migration Inhibitory Factor Is a Molecular Determinant of the Anti-EGFR Monoclonal Antibody Cetuximab Resistance in Human Colorectal Cancer Cells.* Cancers (Basel), 2019. **11**(10). DOI: 10.3390/cancers11101430

172. Cheon SK, Kim HP, Park YL, Jang JE, Lim Y, et al., *Macrophage migration inhibitory factor promotes resistance to MEK blockade in KRAS mutant colorectal cancer cells.* Mol Oncol, 2018. **12**(8): p. 1398-1409. DOI: 10.1002/1878-0261.12345

173. Fingerle-Rowson G, Kaleswarapu DR, Schlander C, Kabgani N, Brocks T, et al., *A tautomerase-null macrophage migration-inhibitory factor (MIF) gene knock-in mouse model reveals that protein interactions and not enzymatic activity mediate MIF-dependent growth regulation.* Mol Cell Biol, 2009. **29**(7): p. 1922-32. DOI: 10.1128/MCB.01907-08

174. Kok T, Wasiel AA, Cool RH, Melgert BN, Poelarends GJ, et al., *Small-molecule inhibitors of macrophage migration inhibitory factor (MIF) as an emerging class of therapeutics for immune disorders.* Drug Discov Today, 2018. **23**(11): p. 1910-1918. DOI: 10.1016/j.drudis.2018.06.017

175. Cavalli E, Ciurleo R, Petralia MC, Fagone P, Bella R, et al., *Emerging Role of the Macrophage Migration Inhibitory Factor Family of Cytokines in Neuroblastoma. Pathogenic Effectors and Novel Therapeutic Targets?* Molecules, 2020. **25**(5). DOI: 10.3390/molecules25051194

176. Grasso C, Jansen G, and Giovannetti E, *Drug resistance in pancreatic cancer: Impact of altered energy metabolism.* Crit Rev Oncol Hematol, 2017. **114**: p. 139-152. DOI: 10.1016/j.critrevonc.2017.03.026

177. Orth M, Metzger P, Gerum S, Mayerle J, Schneider G, et al., *Pancreatic ductal adenocarcinoma: biological hallmarks, current status, and future perspectives of combined modality treatment approaches.* Radiat Oncol, 2019. **14**(1): p. 141. DOI: 10.1186/s13014-019-1345-6

178. Smigiel JM, Parameswaran N, and Jackson MW, *Targeting Pancreatic Cancer Cell Plasticity: The Latest in Therapeutics.* Cancers (Basel), 2018. **10**(1). DOI: 10.3390/cancers10010014

179. Hessmann E, Buchholz SM, Demir IE, Singh SK, Gress TM, et al., *Microenvironmental Determinants of Pancreatic Cancer.* Physiol Rev, 2020. **100**(4): p. 1707-1751. DOI: 10.1152/physrev.00042.2019

180. Collisson EA, Sadanandam A, Olson P, Gibb WJ, Truitt M, et al., *Subtypes of pancreatic ductal adenocarcinoma and their differing responses to therapy.* Nat Med, 2011. **17**(4): p. 500-3. DOI: 10.1038/nm.2344

181. Bailey P, Chang DK, Nones K, Johns AL, Patch AM, et al., *Genomic analyses identify molecular subtypes of pancreatic cancer.* Nature, 2016. **531**(7592): p. 47-52. DOI: 10.1038/nature16965

182. Moffitt RA, Marayati R, Flate EL, Volmar KE, Loeza SG, et al., *Virtual microdissection identifies distinct tumor- and stroma-specific subtypes of pancreatic ductal adenocarcinoma.* Nat Genet, 2015. **47**(10): p. 1168-78. DOI: 10.1038/ng.3398

183. Martens S, Lefesvre P, Nicolle R, Biankin AV, Puleo F, et al., *Different shades of pancreatic ductal adenocarcinoma, different paths towards precision therapeutic applications.* Ann Oncol, 2019. **30**(9): p. 1428-1436. DOI: 10.1093/annonc/mdz181

184. Morris JPt, Wang SC, and Hebrok M, *KRAS, Hedgehog, Wnt and the twisted developmental biology of pancreatic ductal adenocarcinoma.* Nat Rev Cancer, 2010. **10**(10): p. 683-95. DOI: 10.1038/nrc2899

185. Heßmann E, *The Molecular Frame of Pancreatic Carcinogenesis.* 2014: IntechOpen.

186. Guo J, Xie K, and Zheng S, *Molecular Biomarkers of Pancreatic Intraepithelial Neoplasia and Their Implications in Early Diagnosis and Therapeutic Intervention of Pancreatic Cancer.* Int J Biol Sci, 2016. **12**(3): p. 292-301. DOI: 10.7150/ijbs.14995

187. Cicenas J, Kvederaviciute K, Meskinyte I, Meskinyte-Kausiliene E, Skeberdyte A, et al., *KRAS, TP53, CDKN2A, SMAD4, BRCA1, and BRCA2 Mutations in Pancreatic Cancer.* Cancers (Basel), 2017. **9**(5). DOI: 10.3390/cancers9050042

188. Lane DP, *Cancer. p53, guardian of the genome.* Nature, 1992. **358**(6381): p. 15-6. DOI: 10.1038/358015a0

189. Lane DP and Crawford LV, *T antigen is bound to a host protein in SV40-transformed cells.* Nature, 1979. **278**(5701): p. 261-3. DOI: 10.1038/278261a0

190. Zilfou JT and Lowe SW, *Tumor suppressive functions of p53.* Cold Spring Harb Perspect Biol, 2009. **1**(5): p. a001883. DOI: 10.1101/cshperspect.a001883

191. Moll UM and Slade N, *p63 and p73: roles in development and tumor formation.* Mol Cancer Res, 2004. **2**(7): p. 371-86.

192. Lane DP and Benchimol S, *p53: oncogene or anti-oncogene?* Genes Dev, 1990. **4**(1): p. 1-8. DOI: 10.1101/gad.4.1.1

193. Vousden KH and Lane DP, *p53 in health and disease.* Nat Rev Mol Cell Biol, 2007. **8**(4): p. 275-83. DOI: 10.1038/nrm2147

194. Reed SM and Quelle DE, *p53 Acetylation: Regulation and Consequences.* Cancers (Basel), 2014. **7**(1): p. 30-69. DOI: 10.3390/cancers7010030

195. Moll UM and Petrenko O, *The MDM2-p53 interaction.* Mol Cancer Res, 2003. **1**(14): p. 1001-8.

196. Momand J, Zambetti GP, Olson DC, George D, and Levine AJ, *The mdm-2 oncogene product forms a complex with the p53 protein and inhibits p53-*

mediated transactivation. Cell, 1992. **69**(7): p. 1237-45. DOI: 10.1016/0092-8674(92)90644-r

197. Kamada R, Toguchi Y, Nomura T, Imagawa T, and Sakaguchi K, *Tetramer formation of tumor suppressor protein p53: Structure, function, and applications.* Biopolymers, 2016. **106**(4): p. 598-612. DOI: 10.1002/bip.22772

198. Wu L and Levine AJ, *Differential regulation of the p21/WAF-1 and mdm2 genes after high-dose UV irradiation: p53-dependent and p53-independent regulation of the mdm2 gene.* Mol Med, 1997. **3**(7): p. 441-51.

199. Vousden KH and Lu X, *Live or let die: the cell's response to p53.* Nat Rev Cancer, 2002. **2**(8): p. 594-604. DOI: 10.1038/nrc864

200. Hollstein M, Sidransky D, Vogelstein B, and Harris CC, *p53 mutations in human cancers.* Science, 1991. **253**(5015): p. 49-53. DOI: 10.1126/science.1905840

201. Vogelstein B, Lane D, and Levine AJ, *Surfing the p53 network.* Nature, 2000. **408**(6810): p. 307-10. DOI: 10.1038/35042675

202. Sabapathy K and Lane DP, *Therapeutic targeting of p53: all mutants are equal, but some mutants are more equal than others.* Nat Rev Clin Oncol, 2018. **15**(1): p. 13-30. DOI: 10.1038/nrclinonc.2017.151

203. Kandoth C, McLellan MD, Vandin F, Ye K, Niu B, et al., *Mutational landscape and significance across 12 major cancer types.* Nature, 2013. **502**(7471): p. 333-339. DOI: 10.1038/nature12634

204. Freed-Pastor WA and Prives C, *Mutant p53: one name, many proteins.* Genes Dev, 2012. **26**(12): p. 1268-86. DOI: 10.1101/gad.190678.112

205. Brosh R and Rotter V, *When mutants gain new powers: news from the mutant p53 field.* Nat Rev Cancer, 2009. **9**(10): p. 701-13. DOI: 10.1038/nrc2693

206. Hollstein M, Hergenhahn M, Yang Q, Bartsch H, Wang ZQ, et al., *New approaches to understanding p53 gene tumor mutation spectra.* Mutat Res, 1999. **431**(2): p. 199-209. DOI: 10.1016/s0027-5107(99)00162-1

207. Bullock AN, Henckel J, and Fersht AR, *Quantitative analysis of residual folding and DNA binding in mutant p53 core domain: definition of mutant states for rescue in cancer therapy.* Oncogene, 2000. **19**(10): p. 1245-56. DOI: 10.1038/sj.onc.1203434

208. Sabapathy K, *The Contrived Mutant p53 Oncogene - Beyond Loss of Functions.* Front Oncol, 2015. **5**: p. 276. DOI: 10.3389/fonc.2015.00276

209. Alexandrova EM, Mirza SA, Xu S, Schulz-Heddergott R, Marchenko ND, et al., *p53 loss-of-heterozygosity is a necessary prerequisite for mutant p53 stabilization and gain-of-function in vivo.* Cell Death Dis, 2017. **8**(3): p. e2661. DOI: 10.1038/cddis.2017.80

210. Muller PA and Vousden KH, *p53 mutations in cancer.* Nat Cell Biol, 2013. **15**(1): p. 2-8. DOI: 10.1038/ncb2641

211. Bullock AN, Henckel J, DeDecker BS, Johnson CM, Nikolova PV, et al., *Thermodynamic stability of wild-type and mutant p53 core domain.* Proc Natl Acad Sci U S A, 1997. **94**(26): p. 14338-42. DOI: 10.1073/pnas.94.26.14338

212. Baugh EH, Ke H, Levine AJ, Bonneau RA, and Chan CS, *Why are there hotspot mutations in the TP53 gene in human cancers?* Cell Death Differ, 2018. **25**(1): p. 154-160. DOI: 10.1038/cdd.2017.180

213. Walerych D, Lisek K, and Del Sal G, *Mutant p53: One, No One, and One Hundred Thousand.* Front Oncol, 2015. **5**: p. 289. DOI: 10.3389/fonc.2015.00289

214. Li D, Marchenko ND, Schulz R, Fischer V, Velasco-Hernandez T, et al., *Functional inactivation of endogenous MDM2 and CHIP by HSP90 causes aberrant stabilization of mutant p53 in human cancer cells.* Mol Cancer Res, 2011. **9**(5): p. 577-88. DOI: 10.1158/1541-7786.MCR-10-0534

215. Blagosklonny MV, Toretsky J, Bohen S, and Neckers L, *Mutant conformation of p53 translated in vitro or in vivo requires functional HSP90.* Proc Natl Acad Sci U S A, 1996. **93**(16): p. 8379-83. DOI: 10.1073/pnas.93.16.8379

216. Ano Bom AP, Rangel LP, Costa DC, de Oliveira GA, Sanches D, et al., *Mutant p53 aggregates into prion-like amyloid oligomers and fibrils: implications for cancer.* J Biol Chem, 2012. **287**(33): p. 28152-62. DOI: 10.1074/jbc.M112.340638

217. Wawrzynow B, Zylicz A, and Zylicz M, *Chaperoning the guardian of the genome. The two-faced role of molecular chaperones in p53 tumor suppressor action.* Biochim Biophys Acta Rev Cancer, 2018. **1869**(2): p. 161-174. DOI: 10.1016/j.bbcan.2017.12.004

218. Xu J, Reumers J, Couceiro JR, De Smet F, Gallardo R, et al., *Gain of function of mutant p53 by coaggregation with multiple tumor suppressors.* Nat Chem Biol, 2011. **7**(5): p. 285-95. DOI: 10.1038/nchembio.546

219. Silva JL, De Moura Gallo CV, Costa DC, and Rangel LP, *Prion-like aggregation of mutant p53 in cancer.* Trends Biochem Sci, 2014. **39**(6): p. 260-7. DOI: 10.1016/j.tibs.2014.04.001

220. de Oliveira GAP, Petronilho EC, Pedrote MM, Marques MA, Vieira T, et al., *The Status of p53 Oligomeric and Aggregation States in Cancer.* Biomolecules, 2020. **10**(4). DOI: 10.3390/biom10040548

221. Oren M and Rotter V, *Mutant p53 gain-of-function in cancer.* Cold Spring Harb Perspect Biol, 2010. **2**(2): p. a001107. DOI: 10.1101/cshperspect.a001107

222. Mantovani F, Collavin L, and Del Sal G, *Mutant p53 as a guardian of the cancer cell.* Cell Death Differ, 2019. **26**(2): p. 199-212. DOI: 10.1038/s41418-018-0246-9

223. Bellazzo A, Sicari D, Valentino E, Del Sal G, and Collavin L, *Complexes formed by mutant p53 and their roles in breast cancer.* Breast Cancer (Dove Med Press), 2018. **10**: p. 101-112. DOI: 10.2147/BCTT.S145826

224. Kim MP and Lozano G, *Mutant p53 partners in crime.* Cell Death Differ, 2018. **25**(1): p. 161-168. DOI: 10.1038/cdd.2017.185

225. Liu X, Wilcken R, Joerger AC, Chuckowree IS, Amin J, et al., *Small molecule induced reactivation of mutant p53 in cancer cells.* Nucleic Acids Res, 2013. **41**(12): p. 6034-44. DOI: 10.1093/nar/gkt305

226. Schulz-Heddergott R and Moll UM, *Gain-of-Function (GOF) Mutant p53 as Actionable Therapeutic Target.* Cancers (Basel), 2018. **10**(6). DOI: 10.3390/cancers10060188

227. Bykov VJ, Issaeva N, Shilov A, Hultcrantz M, Pugacheva E, et al., *Restoration of the tumor suppressor function to mutant p53 by a low-molecular-weight compound.* Nat Med, 2002. **8**(3): p. 282-8. DOI: 10.1038/nm0302-282

228. Soragni A, Janzen DM, Johnson LM, Lindgren AG, Thai-Quynh Nguyen A, et al., *A Designed Inhibitor of p53 Aggregation Rescues p53 Tumor Suppression in Ovarian Carcinomas.* Cancer Cell, 2016. **29**(1): p. 90-103. DOI: 10.1016/j.ccell.2015.12.002

229. Muller P, Hrstka R, Coomber D, Lane DP, and Vojtesek B, *Chaperone-dependent stabilization and degradation of p53 mutants.* Oncogene, 2008. **27**(24): p. 3371-83. DOI: 10.1038/sj.onc.1211010

230. Xu J, Wang J, Hu Y, Qian J, Xu B, et al., *Unequal prognostic potentials of p53 gain-of-function mutations in human cancers associate with drug-metabolizing activity.* Cell Death Dis, 2014. **5**: p. e1108. DOI: 10.1038/cddis.2014.75

231. Graziano F and Cascinu S, *Prognostic molecular markers for planning adjuvant chemotherapy trials in Dukes' B colorectal cancer patients: how much evidence is enough?* Ann Oncol, 2003. **14**(7): p. 1026-38. DOI: 10.1093/annonc/mdg284

232. Roman-Rosales AA, Garcia-Villa E, Herrera LA, Gariglio P, and Diaz-Chavez J, *Mutant p53 gain of function induces HER2 over-expression in cancer cells.* BMC Cancer, 2018. **18**(1): p. 709. DOI: 10.1186/s12885-018-4613-1

233. Ahn JH, Kim TJ, Lee JH, and Choi JH, *Mutant p53 stimulates cell invasion through an interaction with Rad21 in human ovarian cancer cells.* Sci Rep, 2017. **7**(1): p. 9076. DOI: 10.1038/s41598-017-08880-4

234. Klemke L, De Oliveira T, Witt D, Winkler N, Bohnenberger H, et al., *Hsp90-stabilized MIF supports tumor progression via macrophage recruitment and angiogenesis in colorectal cancer.* Cell Death Dis, 2021. **12**(2): p. 155. DOI: 10.1038/s41419-021-03426-z

235. Schulz-Heddergott R and Moll UM, *HSP90-Stabilized MIF in Oncogenesis and Cell Growth Control*, in *MIF Family Cytokines in Innate Immunity and Homeostasis*, R. Bucala and J. Bernhagen, Editors. 2017, Springer International Publishing: Cham. p. 21-42. ISBN: 978-3-319-52354-5

236. Nishihira J, Ishibashi T, Fukushima T, Sun B, Sato Y, et al., *Macrophage migration inhibitory factor (MIF): Its potential role in tumor growth and tumor-associated angiogenesis.* Ann N Y Acad Sci, 2003. **995**: p. 171-82. DOI: 10.1111/j.1749-6632.2003.tb03220.x

237. Fan H, Hall P, Santos LL, Gregory JL, Fingerle-Rowson G, et al., *Macrophage migration inhibitory factor and CD74 regulate macrophage chemotactic responses via MAPK and Rho GTPase.* J Immunol, 2011. **186**(8): p. 4915-24. DOI: 10.4049/jimmunol.1003713

238. White ES, Strom SR, Wys NL, and Arenberg DA, *Non-small cell lung cancer cells induce monocytes to increase expression of angiogenic activity.* J Immunol, 2001. **166**(12): p. 7549-55. DOI: 10.4049/jimmunol.166.12.7549

239. Chesney JA and Mitchell RA, *25 Years On: A Retrospective on Migration Inhibitory Factor in Tumor Angiogenesis.* Mol Med, 2015. **21 Suppl 1**: p. S19-24. DOI: 10.2119/molmed.2015.00055

240. Kanzler I, Tuchscheerer N, Steffens G, Simsekyilmaz S, Konschalla S, et al., *Differential roles of angiogenic chemokines in endothelial progenitor cell-induced angiogenesis.* Basic Res Cardiol, 2013. **108**(1): p. 310. DOI: 10.1007/s00395-012-0310-4

241. Cui J, Zhang F, Wang Y, Liu J, Ming X, et al., *Macrophage migration inhibitory factor promotes cardiac stem cell proliferation and endothelial differentiation through the activation of the PI3K/Akt/mTOR and AMPK pathways.* Int J Mol Med, 2016. **37**(5): p. 1299-309. DOI: 10.3892/ijmm.2016.2542

242. Girard E, Strathdee C, Trueblood E, and Queva C, *Macrophage migration inhibitory factor produced by the tumour stroma but not by tumour cells regulates angiogenesis in the B16-F10 melanoma model.* Br J Cancer, 2012. **107**(9): p. 1498-505. DOI: 10.1038/bjc.2012.392

243. Weber C, Kraemer S, Drechsler M, Lue H, Koenen RR, et al., *Structural determinants of MIF functions in CXCR2-mediated inflammatory and atherogenic leukocyte recruitment.* Proc Natl Acad Sci U S A, 2008. **105**(42): p. 16278-83. DOI: 10.1073/pnas.0804017105

244. Martin C, Burdon PC, Bridger G, Gutierrez-Ramos JC, Williams TJ, et al., *Chemokines acting via CXCR2 and CXCR4 control the release of neutrophils from the bone marrow and their return following senescence.* Immunity, 2003. **19**(4): p. 583-93. DOI: 10.1016/s1074-7613(03)00263-2

245. Kruger P, Saffarzadeh M, Weber AN, Rieber N, Radsak M, et al., *Neutrophils: Between host defence, immune modulation, and tissue injury.* PLoS Pathog, 2015. **11**(3): p. e1004651. DOI: 10.1371/journal.ppat.1004651

246. Hu CT, Guo LL, Feng N, Zhang L, Zhou N, et al., *MIF, secreted by human hepatic sinusoidal endothelial cells, promotes chemotaxis and outgrowth of colorectal cancer in liver prometastasis.* Oncotarget, 2015. **6**(26): p. 22410-23. DOI: 10.18632/oncotarget.4198

247. el Marjou F, Janssen KP, Chang BH, Li M, Hindie V, et al., *Tissue-specific and inducible Cre-mediated recombination in the gut epithelium.* Genesis, 2004. **39**(3): p. 186-93. DOI: 10.1002/gene.20042

248. Kim H, Kim M, Im SK, and Fang S, *Mouse Cre-LoxP system: general principles to determine tissue-specific roles of target genes.* Lab Anim Res, 2018. **34**(4): p. 147-159. DOI: 10.5625/lar.2018.34.4.147

249. Djudjaj S, Martin IV, Buhl EM, Nothofer NJ, Leng L, et al., *Macrophage Migration Inhibitory Factor Limits Renal Inflammation and Fibrosis by Counteracting Tubular Cell Cycle Arrest.* J Am Soc Nephrol, 2017. **28**(12): p. 3590-3604. DOI: 10.1681/ASN.2017020190

250. Brocks T, Fedorchenko O, Schliermann N, Stein A, Moll UM, et al., *Macrophage migration inhibitory factor protects from nonmelanoma epidermal tumors by regulating the number of antigen-presenting cells in skin.* FASEB J, 2017. **31**(2): p. 526-543. DOI: 10.1096/fj.201600860R

251. McClelland M, Zhao L, Carskadon S, and Arenberg D, *Expression of CD74, the receptor for macrophage migration inhibitory factor, in non-small cell lung*

cancer. Am J Pathol, 2009. **174**(2): p. 638-46. DOI: 10.2353/ajpath.2009.080463

252. Binsky I, Haran M, Starlets D, Gore Y, Lantner F, et al., *IL-8 secreted in a macrophage migration-inhibitory factor- and CD74-dependent manner regulates B cell chronic lymphocytic leukemia survival.* Proc Natl Acad Sci U S A, 2007. **104**(33): p. 13408-13. DOI: 10.1073/pnas.0701553104

253. Wynn TA and Vannella KM, *Macrophages in Tissue Repair, Regeneration, and Fibrosis.* Immunity, 2016. **44**(3): p. 450-462. DOI: 10.1016/j.immuni.2016.02.015

254. Wang J, *Neutrophils in tissue injury and repair.* Cell Tissue Res, 2018. **371**(3): p. 531-539. DOI: 10.1007/s00441-017-2785-7

255. Wilgus TA, Roy S, and McDaniel JC, *Neutrophils and Wound Repair: Positive Actions and Negative Reactions.* Adv Wound Care (New Rochelle), 2013. **2**(7): p. 379-388. DOI: 10.1089/wound.2012.0383

256. Li J, Tan J, Martino MM, and Lui KO, *Regulatory T-Cells: Potential Regulator of Tissue Repair and Regeneration.* Front Immunol, 2018. **9**: p. 585. DOI: 10.3389/fimmu.2018.00585

257. Liu Y, Wang L, Kikuiri T, Akiyama K, Chen C, et al., *Mesenchymal stem cell-based tissue regeneration is governed by recipient T lymphocytes via IFN-gamma and TNF-alpha.* Nat Med, 2011. **17**(12): p. 1594-601. DOI: 10.1038/nm.2542

258. Pellowe AS, Sauler M, Hou Y, Merola J, Liu R, et al., *Endothelial cell-secreted MIF reduces pericyte contractility and enhances neutrophil extravasation.* FASEB J, 2019. **33**(2): p. 2171-2186. DOI: 10.1096/fj.201800480R

259. Pantouris G, Syed MA, Fan C, Rajasekaran D, Cho TY, et al., *An Analysis of MIF Structural Features that Control Functional Activation of CD74.* Chem Biol, 2015. **22**(9): p. 1197-205. DOI: 10.1016/j.chembiol.2015.08.006

260. Farr L, Ghosh S, Jiang N, Watanabe K, Parlak M, et al., *CD74 Signaling Links Inflammation to Intestinal Epithelial Cell Regeneration and Promotes Mucosal Healing.* Cell Mol Gastroenterol Hepatol, 2020. **10**(1): p. 101-112. DOI: 10.1016/j.jcmgh.2020.01.009

261. Baugh JA, Gantier M, Li L, Byrne A, Buckley A, et al., *Dual regulation of macrophage migration inhibitory factor (MIF) expression in hypoxia by CREB and HIF-1.* Biochem Biophys Res Commun, 2006. **347**(4): p. 895-903. DOI: 10.1016/j.bbrc.2006.06.148

262. Cheng B, Wang Q, Song Y, Liu Y, Liu Y, et al., *MIF inhibitor, ISO-1, attenuates human pancreatic cancer cell proliferation, migration and invasion in vitro, and suppresses xenograft tumour growth in vivo.* Sci Rep, 2020. **10**(1): p. 6741. DOI: 10.1038/s41598-020-63778-y

263. Meyer-Siegler KL, Iczkowski KA, Leng L, Bucala R, and Vera PL, *Inhibition of macrophage migration inhibitory factor or its receptor (CD74) attenuates growth and invasion of DU-145 prostate cancer cells.* J Immunol, 2006. **177**(12): p. 8730-9. DOI: 10.4049/jimmunol.177.12.8730

264. Haran M, Mirkin V, Braester A, Harpaz N, Shevetz O, et al., *A phase I-II clinical trial of the anti-CD74 monoclonal antibody milatuzumab in frail patients with*

refractory chronic lymphocytic leukaemia: A patient based approach. Br J Haematol, 2018. **182**(1): p. 125-128. DOI: 10.1111/bjh.14726

265. Mahalingam D, Patel MR, Sachdev JC, Hart LL, Halama N, et al., *Phase I study of imalumab (BAX69), a fully human recombinant antioxidized macrophage migration inhibitory factor antibody in advanced solid tumours.* Br J Clin Pharmacol, 2020. **86**(9): p. 1836-1848. DOI: 10.1111/bcp.14289

266. Schinagl A, Thiele M, Douillard P, Volkel D, Kenner L, et al., *Oxidized macrophage migration inhibitory factor is a potential new tissue marker and drug target in cancer.* Oncotarget, 2016. **7**(45): p. 73486-73496. DOI: 10.18632/oncotarget.11970

267. Schindler L, Dickerhof N, Hampton MB, and Bernhagen J, *Post-translational regulation of macrophage migration inhibitory factor: Basis for functional fine-tuning.* Redox Biol, 2018. **15**: p. 135-142. DOI: 10.1016/j.redox.2017.11.028

268. Thiele M, Kerschbaumer RJ, Tam FW, Volkel D, Douillard P, et al., *Selective Targeting of a Disease-Related Conformational Isoform of Macrophage Migration Inhibitory Factor Ameliorates Inflammatory Conditions.* J Immunol, 2015. **195**(5): p. 2343-52. DOI: 10.4049/jimmunol.1500572

269. Sparkes A, De Baetselier P, Brys L, Cabrito I, Sterckx YG, et al., *Novel half-life extended anti-MIF nanobodies protect against endotoxic shock.* FASEB J, 2018. **32**(6): p. 3411-3422. DOI: 10.1096/fj.201701189R

270. Harmsen MM and De Haard HJ, *Properties, production, and applications of camelid single-domain antibody fragments.* Appl Microbiol Biotechnol, 2007. **77**(1): p. 13-22. DOI: 10.1007/s00253-007-1142-2

271. Sur S, Pagliarini R, Bunz F, Rago C, Diaz LA, Jr., et al., *A panel of isogenic human cancer cells suggests a therapeutic approach for cancers with inactivated p53.* Proc Natl Acad Sci U S A, 2009. **106**(10): p. 3964-9. DOI: 10.1073/pnas.0813333106

272. Antonova E, Glazova O, Gaponova A, Eremyan A, Zvereva S, et al., *Successful CRISPR/Cas9 mediated homologous recombination in a chicken cell line.* F1000Res, 2018. **7**: p. 238. DOI: 10.12688/f1000research.13457.2

273. Vartanian S, Bentley C, Brauer MJ, Li L, Shirasawa S, et al., *Identification of mutant K-Ras-dependent phenotypes using a panel of isogenic cell lines.* J Biol Chem, 2013. **288**(4): p. 2403-13. DOI: 10.1074/jbc.M112.394130

274. Igelmann S, Neubauer HA, and Ferbeyre G, *STAT3 and STAT5 Activation in Solid Cancers.* Cancers (Basel), 2019. **11**(10). DOI: 10.3390/cancers11101428

275. Wu CJ, Sundararajan V, Sheu BC, Huang RY, and Wei LH, *Activation of STAT3 and STAT5 Signaling in Epithelial Ovarian Cancer Progression: Mechanism and Therapeutic Opportunity.* Cancers (Basel), 2019. **12**(1). DOI: 10.3390/cancers12010024

276. Lee H, Herrmann A, Deng JH, Kujawski M, Niu G, et al., *Persistently activated Stat3 maintains constitutive NF-kappaB activity in tumors.* Cancer Cell, 2009. **15**(4): p. 283-93. DOI: 10.1016/j.ccr.2009.02.015

277. Baumgart S, Chen NM, Siveke JT, Konig A, Zhang JS, et al., *Inflammation-induced NFATc1-STAT3 transcription complex promotes pancreatic cancer*

initiation by KrasG12D. Cancer Discov, 2014. **4**(6): p. 688-701. DOI: 10.1158/2159-8290.CD-13-0593

278. Qin JJ, Yan L, Zhang J, and Zhang WD, *STAT3 as a potential therapeutic target in triple negative breast cancer: a systematic review.* J Exp Clin Cancer Res, 2019. **38**(1): p. 195. DOI: 10.1186/s13046-019-1206-z

279. Zou S, Tong Q, Liu B, Huang W, Tian Y, et al., *Targeting STAT3 in Cancer Immunotherapy.* Mol Cancer, 2020. **19**(1): p. 145. DOI: 10.1186/s12943-020-01258-7

280. Siveen KS, Sikka S, Surana R, Dai X, Zhang J, et al., *Targeting the STAT3 signaling pathway in cancer: role of synthetic and natural inhibitors.* Biochim Biophys Acta, 2014. **1845**(2): p. 136-54. DOI: 10.1016/j.bbcan.2013.12.005

281. Cooks T, Pateras IS, Tarcic O, Solomon H, Schetter AJ, et al., *Mutant p53 prolongs NF-kappaB activation and promotes chronic inflammation and inflammation-associated colorectal cancer.* Cancer Cell, 2013. **23**(5): p. 634-46. DOI: 10.1016/j.ccr.2013.03.022

282. Weisz L, Damalas A, Liontos M, Karakaidos P, Fontemaggi G, et al., *Mutant p53 enhances nuclear factor kappaB activation by tumor necrosis factor alpha in cancer cells.* Cancer Res, 2007. **67**(6): p. 2396-401. DOI: 10.1158/0008-5472.CAN-06-2425

283. Schneider G, Henrich A, Greiner G, Wolf V, Lovas A, et al., *Cross talk between stimulated NF-kappaB and the tumor suppressor p53.* Oncogene, 2010. **29**(19): p. 2795-806. DOI: 10.1038/onc.2010.46

284. Dell'Orso S, Fontemaggi G, Stambolsky P, Goeman F, Voellenkle C, et al., *ChIP-on-chip analysis of in vivo mutant p53 binding to selected gene promoters.* OMICS, 2011. **15**(5): p. 305-12. DOI: 10.1089/omi.2010.0084

285. Hanel W, Marchenko N, Xu S, Yu SX, Weng W, et al., *Two hot spot mutant p53 mouse models display differential gain of function in tumorigenesis.* Cell Death Differ, 2013. **20**(7): p. 898-909. DOI: 10.1038/cdd.2013.17

286. Landmann H, Proia DA, He S, Ogawa LS, Kramer F, et al., *UDP glucuronosyltransferase 1A expression levels determine the response of colorectal cancer cells to the heat shock protein 90 inhibitor ganetespib.* Cell Death Dis, 2014. **5**: p. e1411. DOI: 10.1038/cddis.2014.378

287. Angstadt AY, Hartman TJ, Lesko SM, Muscat JE, Zhu J, et al., *The effect of UGT1A and UGT2B polymorphisms on colorectal cancer risk: haplotype associations and gene-environment interactions.* Genes Chromosomes Cancer, 2014. **53**(6): p. 454-66. DOI: 10.1002/gcc.22157

288. Li D, Marchenko ND, and Moll UM, *SAHA shows preferential cytotoxicity in mutant p53 cancer cells by destabilizing mutant p53 through inhibition of the HDAC6-Hsp90 chaperone axis.* Cell Death Differ, 2011. **18**(12): p. 1904-13. DOI: 10.1038/cdd.2011.71

289. Parrales A, Thoenen E, and Iwakuma T, *The interplay between mutant p53 and the mevalonate pathway.* Cell Death Differ, 2018. **25**(3): p. 460-470. DOI: 10.1038/s41418-017-0026-y

290. Parrales A, Ranjan A, Iyer SV, Padhye S, Weir SJ, et al., *DNAJA1 controls the fate of misfolded mutant p53 through the mevalonate pathway.* Nat Cell Biol, 2016. **18**(11): p. 1233-1243. DOI: 10.1038/ncb3427

291. Silva JL, Cino EA, Soares IN, Ferreira VF, and G APdO, *Targeting the Prion-like Aggregation of Mutant p53 to Combat Cancer.* Acc Chem Res, 2018. **51**(1): p. 181-190. DOI: 10.1021/acs.accounts.7b00473

292. Zhang Y, Coillie SV, Fang JY, and Xu J, *Gain of function of mutant p53: R282W on the peak?* Oncogenesis, 2016. **5**: p. e196. DOI: 10.1038/oncsis.2016.8

293. Kehrloesser S, Osterburg C, Tuppi M, Schafer B, Vousden KH, et al., *Intrinsic aggregation propensity of the p63 and p73 TI domains correlates with p53R175H interaction and suggests further significance of aggregation events in the p53 family.* Cell Death Differ, 2016. **23**(12): p. 1952-1960. DOI: 10.1038/cdd.2016.75

294. Yue X, Zhao Y, Xu Y, Zheng M, Feng Z, et al., *Mutant p53 in Cancer: Accumulation, Gain-of-Function, and Therapy.* J Mol Biol, 2017. **429**(11): p. 1595-1606. DOI: 10.1016/j.jmb.2017.03.030

295. Kolosenko I, Yu Y, Busker S, Dyczynski M, Liu J, et al., *Identification of novel small molecules that inhibit STAT3-dependent transcription and function.* PLoS One, 2017. **12**(6): p. e0178844. DOI: 10.1371/journal.pone.0178844

296. Debnath B, Xu S, and Neamati N, *Small molecule inhibitors of signal transducer and activator of transcription 3 (Stat3) protein.* J Med Chem, 2012. **55**(15): p. 6645-68. DOI: 10.1021/jm300207s

297. Spitzner M, Roesler B, Bielfeld C, Emons G, Gaedcke J, et al., *STAT3 inhibition sensitizes colorectal cancer to chemoradiotherapy in vitro and in vivo.* Int J Cancer, 2014. **134**(4): p. 997-1007. DOI: 10.1002/ijc.28429

298. Kawazoe A, Kuboki Y, Bando H, Fukuoka S, Kojima T, et al., *Phase 1 study of napabucasin, a cancer stemness inhibitor, in patients with advanced solid tumors.* Cancer Chemother Pharmacol, 2020. **85**(5): p. 855-862. DOI: 10.1007/s00280-020-04059-3

299. Boston Biomedical, Inc., *Boston Biomedical Announces Orphan Drug Designation for Napabucasin in Pancreatic Cancer*. 2016 [cited 20.04.2021]; Available from: https://www.prnewswire.com/news-releases/boston-biomedical-announces-orphan-drug-designation-for-napabucasin-in-pancreatic-cancer-300361932.html.

300. Boston Biomedical, Inc., *Boston Biomedical, Inc. Announces Update on Phase 3 CanStem111P Study of Napabucasin in Patients with Metastatic Pancreatic Cancer Following Interim Analysis*. 2019 [cited 20.04.2021]; Available from: https://www.prnewswire.com/news-releases/boston-biomedical-inc-announces-update-on-phase-3-canstem111p-study-of-napabucasin-in-patients-with-metastatic-pancreatic-cancer-following-interim-analysis-300879064.html.

301. Ling X, Konopleva M, Zeng Z, Ruvolo V, Stephens LC, et al., *The novel triterpenoid C-28 methyl ester of 2-cyano-3, 12-dioxoolen-1, 9-dien-28-oic acid inhibits metastatic murine breast tumor growth through inactivation of STAT3 signaling.* Cancer Res, 2007. **67**(9): p. 4210-8. DOI: 10.1158/0008-5472.CAN-06-3629

302. Duan Z, Ames RY, Ryan M, Hornicek FJ, Mankin H, et al., *CDDO-Me, a synthetic triterpenoid, inhibits expression of IL-6 and Stat3 phosphorylation in multi-drug resistant ovarian cancer cells.* Cancer Chemother Pharmacol, 2009. **63**(4): p. 681-9. DOI: 10.1007/s00280-008-0785-8

303. Hong DS, Kurzrock R, Supko JG, He X, Naing A, et al., *A phase I first-in-human trial of bardoxolone methyl in patients with advanced solid tumors and lymphomas.* Clin Cancer Res, 2012. **18**(12): p. 3396-406. DOI: 10.1158/1078-0432.CCR-11-2703

304. Ahmad R, Raina D, Meyer C, Kharbanda S, and Kufe D, *Triterpenoid CDDO-Me blocks the NF-kappaB pathway by direct inhibition of IKKbeta on Cys-179.* J Biol Chem, 2006. **281**(47): p. 35764-9. DOI: 10.1074/jbc.M607160200

305. Capaci V, Mantovani F, and Del Sal G, *Amplifying Tumor-Stroma Communication: An Emerging Oncogenic Function of Mutant p53.* Front Oncol, 2020. **10**: p. 614230. DOI: 10.3389/fonc.2020.614230

306. Stein Y, Aloni-Grinstein R, and Rotter V, *Mutant p53-a potential player in shaping the tumor-stroma crosstalk.* J Mol Cell Biol, 2019. **11**(7): p. 600-604. DOI: 10.1093/jmcb/mjz071

307. Pavlakis E and Stiewe T, *p53's Extended Reach: The Mutant p53 Secretome.* Biomolecules, 2020. **10**(2). DOI: 10.3390/biom10020307

308. Butera G, Brandi J, Cavallini C, Scarpa A, Lawlor RT, et al., *The Mutant p53-Driven Secretome Has Oncogenic Functions in Pancreatic Ductal Adenocarcinoma Cells.* Biomolecules, 2020. **10**(6). DOI: 10.3390/biom10060884

309. Sperb N, Tsesmelis M, and Wirth T, *Crosstalk between Tumor and Stromal Cells in Pancreatic Ductal Adenocarcinoma.* Int J Mol Sci, 2020. **21**(15). DOI: 10.3390/ijms21155486

310. Garcia PL, Miller AL, and Yoon KJ, *Patient-Derived Xenograft Models of Pancreatic Cancer: Overview and Comparison with Other Types of Models.* Cancers (Basel), 2020. **12**(5). DOI: 10.3390/cancers12051327

311. Cooks T, Pateras IS, Jenkins LM, Patel KM, Robles AI, et al., *Mutant p53 cancers reprogram macrophages to tumor supporting macrophages via exosomal miR-1246.* Nat Commun, 2018. **9**(1): p. 771. DOI: 10.1038/s41467-018-03224-w

312. Wang D, Wang R, Huang A, Fang Z, Wang K, et al., *Upregulation of macrophage migration inhibitory factor promotes tumor metastasis and correlates with poor prognosis of pancreatic ductal adenocarcinoma.* Oncol Rep, 2018. **40**(5): p. 2628-2636. DOI: 10.3892/or.2018.6703

313. Yang S, He P, Wang J, Schetter A, Tang W, et al., *A Novel MIF Signaling Pathway Drives the Malignant Character of Pancreatic Cancer by Targeting NR3C2.* Cancer Res, 2016. **76**(13): p. 3838-50. DOI: 10.1158/0008-5472.CAN-15-2841

314. Funamizu N, Hu C, Lacy C, Schetter A, Zhang G, et al., *Macrophage migration inhibitory factor induces epithelial to mesenchymal transition, enhances tumor aggressiveness and predicts clinical outcome in resected pancreatic ductal adenocarcinoma.* Int J Cancer, 2013. **132**(4): p. 785-94. DOI: 10.1002/ijc.27736

6   ACKNOWLEDGEMENTS

Starting my PhD in 2017, I can now look back on 3.5 years of constructive collaborations, great experiences and lots of memories. In this regard I would like to express my special thanks to those who accompanied me on my way:

To begin with, I would like to thank my supervisor PD Dr. Ramona Schulz-Heddergott for the great opportunity to work in her group during my PhD. I am very thankful for her constant support, insightful feedback and guidance throughout my projects. Her commitment for the team and for science is inspiring.

I also take this opportunity, to thank Prof. Matthias Dobbelstein for giving me the opportunity to be part of his Institute of Molecular Oncology. I am grateful for the valuable input and advice I got during our regular jour fixes and seminars.

Furthermore, I would like to extend my gratitude to my TAC members Prof. Holger Reichardt and Prof. Argyris Papantonis for fruitful scientific discussions during the thesis advisory committee meetings. Additionally, I thank Prof. Heidi Hahn, Dr. Shiv Singh and Dr. Nico Posnien for being members of the extended examination board.

Many thanks also to all past and present members of the 3rd floor of GZMB and especially the Molecular Oncology for generating such a cheerful, productive and interactive working environment. In particular I would like to thank the best PhD buddy I could imagine: Valentina Manzini. From the very beginning, we were going through all phases of everyday PhD life together. I am very grateful for her constant encouragement, our vivid discussions and the friendship we have. I would also like to thank Dr. Josephine Choo for always giving great advice throughout my PhD and for spreading joy in the lab. Furthermore, I would like to thank Nadine Winkler and Tamara Isermann for their constant support, our collaboration and the great team spirit we have had. I really appreciated the daily work with all members of the MolOnkol in the past couple of years.

7   AFFIDAVIT

Herewith I declare that the PhD Thesis entitled "HSP90-stabilized proteins as therapeutic targets in cancer" was written independently and with no other sources and aids than quoted.

_____

Luisa Klemke

Göttingen, April 2021